

**Order Number 9016883**

**Limestone dissolution in modeling of slurry scrubbing for flue  
gas desulfurization**

**Gage, Cynthia Lee, Ph.D.**

**The University of Texas at Austin, 1989**

**Copyright ©1989 by Gage, Cynthia Lee. All rights reserved.**

**U·M·I**  
300 N. Zeeb Rd.  
Ann Arbor, MI 48106

**LIMESTONE DISSOLUTION IN MODELING OF SLURRY  
SCRUBBING FOR FLUE GAS DESULFURIZATION**

By

Cynthia Lee Gage, B.S., M.S.

DISSERTATION

Presented to the Faculty of the Graduate School of  
The University of Texas at Austin  
in Partial Fulfillment  
of the Requirements  
for the Degree of

DOCTOR OF PHILOSOPHY

The University of Texas at Austin  
December 1989

**Limestone Dissolution in Modeling of Slurry Scrubbing  
for Flue Gas Desulfurization**

**Approved by  
Supervisory Committee**

Gary Rochelle  
J. N. Rodu  
Peter John  
James R. Zei  
Jim B. Rahn

Copyright  
by  
Cynthia Lee Gage  
1989



**To my loving son, Kelly**

## ACKNOWLEDGEMENTS

I wish to thank Dr. Gary Rochelle for his guidance, patience, and enthusiastic interest over the past years. I appreciate the fact that he adopted me after Dr. Vasilakos left and that he allowed me to continue my research in an environmental area. Thanks also to my committee members whose courses have been challenging and whose assistance has been invaluable. I would also like to recognize the significant modeling work of Pui K. Chan. His untimely death left our group without a valued friend and colleague. I am glad that I was able to restore his work and to contribute to its potential use and profitability. Thanks also to Pat Terry and Jim Jarvis at Radian who provided me with additional data.

A special thank you goes to all my friends in the Rochelle gang whose personalities gave research an interesting twist. Those from the past include: Cindy Gleason - everyone else's mother and my very good friend, Jim Critchfield - political cartoonist and rose distributor, Paul Chu - my adopted brother, Rob Sheily - midnight computer jock, Wojciech Jozewicz - Polish penny pincher, Will and Dana White - fellow Margaritaville residents, Joe Peterson - FGD dance partner, and Rosa Ruiz-Alsop - shopper extraordinaire. I have also enjoyed the many conversations and the company of other group members: David and Kathy Glasscock, Dave and Te Austgen, Dave Trempe, Steve Beaudoin, Lynn McGuire, Jerry Toman, Todd Carey, and Charlotte Stromblad.

Thanks also to my loving family, especially my mother, Barbara, and my grandfather, Bob Sippel, for their continued emotional and occasional financial support. Most importantly I want to thank my son, Kelly, who has always inspired and encouraged me. It started when he was in kindergarten and wanted to help me with my differential equations homework and has continued to the present with his kibitzing and editing assistance on my dissertation.

Finally I am grateful for the financial support of my research by the EPA, EPRI/Radian, and other FGD various donors.

# **Limestone Dissolution in Modeling of Slurry Scrubbing for Flue Gas Desulfurization**

Publication No. \_\_\_\_\_

Cynthia Lee Gage, Ph.D.  
The University of Texas, 1989

Supervising Professor: Gary T. Rochelle

Batch limestone dissolution experiments were carried out in a pH stat apparatus at 55°C with CO<sub>2</sub> sparging and dissolved sulfite. Particle size distribution, utilization, sulfite in solution, limestone type, and the approach to calcite equilibrium were all found to contribute to the limestone reactivity.

In the absence of sulfite limestone dissolution was controlled solely by mass transfer. For a given stone under mass transfer control, film thickness was found to be independent of pH. The dissolution rate in the presence of sulfite was controlled by a combined surface kinetics/mass transfer regime. SEM micrographs supported this conclusion. A surface rate correlation was developed which accounted for observed inhibition by an inverse dependence on calcium sulfite concentration at the limestone surface. While the form of the rate expression was applicable to all stones, the surface rate constant was stone dependent. A computer code which accounted for mass transfer with surface kinetics was tested against experimental observations of four limestone types. Changes in pH and the concentrations of calcium, carbonate, sulfite, sulfate, and adipic acid were accurately modeled.

An overall slurry scrubber model was expanded to predict limestone reactivity from particle size and solution effects. This model predicts scrubber performance and hold tank compositions from the chemistry of the limestone slurry process. Additional subroutines were written to predict particle size distributions from sieve data using the log gamma density function. The expanded model was tested against a limestone type and grind study which investigated utilizations of four limestone types at ten different grinds.

The expanded Slurry Scrubber Model was able to predict both SO<sub>2</sub> removal and hold tank compositions of the limestone study. The effects of limestone type were handled through changes in the surface rate parameter. Within a given type the effects of grind and utilization were well modeled. Additionally the model indicated that for three runs at very low utilizations of the Fredonia stone, the limestone may have partially blinded. The Slurry Scrubber Model was also able to predict the relatively constant removal observed for Georgia Coarse even though utilization was changed by 12%.

## Table of Contents

Acknowledgments . . . . .	v
Abstract . . . . .	vi
Table of Contents . . . . .	viii
List of Figures . . . . .	xi
List of Tables . . . . .	xiii
<b>Chapter 1: Background of Research . . . . .</b>	<b>1</b>
1.1 Overview of Limestone Scrubbing . . . . .	1
1.1.1 The SO <sub>2</sub> Regulations . . . . .	1
1.1.2 Wet FGD Commercial Applications . . . . .	3
1.1.3 Limestone FGD Process . . . . .	4
1.1.4 Limestone Preparation Systems . . . . .	7
1.2 Previous Work on Limestone Dissolution and Modeling . . . . .	9
1.2.1 Particle Size Distributions and Type and Grind . . . . .	9
1.2.2 Limestone Dissolution . . . . .	11
1.2.3 Modeling of the FGD Process . . . . .	15
1.3 Scope of Investigation . . . . .	18
<b>Chapter 2: Prediction of Particle Size Distributions . . . . .</b>	<b>20</b>
2.1 Introduction . . . . .	20
2.2 Theory . . . . .	20
2.2.1 Log Gamma Model . . . . .	21
2.2.2 Method of Moments . . . . .	25
2.3 Results . . . . .	26
2.3.1 Experimental Alphas and Betas . . . . .	27
2.3.2 Predicted Particle Size Distributions . . . . .	28
2.3.3 Statistical and Error Analysis . . . . .	38

2.4 Summary . . . . .	42
2.5 Notation . . . . .	43
<b>Chapter 3: The Effect of Sulfite on Limestone Reactivity . . . . .</b>	<b>44</b>
3.1 Introduction . . . . .	44
3.2 Theory . . . . .	45
3.2.1 Film Theory . . . . .	45
3.2.2 Mass Transfer Model . . . . .	46
3.3 Experimental Apparatus and Procedure . . . . .	49
3.3.1 Batch Reagent Experiments . . . . .	49
3.3.2 Experimental Methods of Previous Work . . . . .	55
3.4 Results . . . . .	56
3.4.1 SEM Observations . . . . .	63
3.4.2 Film Thickness . . . . .	67
3.4.3 Effects of Sulfite . . . . .	73
3.4.4 Surface Kinetics Rate Expression . . . . .	78
3.4.5 Surface Area Changes . . . . .	81
3.4.6 Temperature Effects . . . . .	86
3.4.7 Statistical and Error Analysis . . . . .	87
3.5 Summary . . . . .	93
3.6 Notation . . . . .	94
<b>Chapter 4: Limestone Reactivity and Slurry Scrubber Performance . . . . .</b>	<b>95</b>
4.1 Introduction . . . . .	95
4.2 Theory . . . . .	95
4.2.1 Particle Size Effects in the Mass Transfer Regime . . . . .	95
4.2.2 Film Theory for Mass Transfer . . . . .	99
4.2.3 Average Film Thickness . . . . .	99
4.3 Pilot Plant Conditions . . . . .	101
4.3.1 Modeling Approach . . . . .	101
4.4 Results . . . . .	103
4.4.1 Batch Experiments. . . . .	103

4.4.2 Limestone Type and Grind Studies	110
Fredonia Limestone	111
Georgia Marble Limestone	117
Longview Limestone	120
Stoneman Limestone	123
General Discussion	125
4.4.3 CaSO <sub>3</sub> Dissolution	130
4.4.4 Parameter Analysis	133
4.5 Summary	137
4.6 Notation	138
 Chapter 5: Conclusions and Recommendations	 139
5.1 Particle Size Predictions	139
5.2 Effects of Sulfite	140
5.3 Slurry Scrubber Modeling	141
5.4 Recommendations for Future Work	142
5.4.1 Experimental Work	142
5.4.2 Modeling	143
 Appendix A: Experimental Data	 145
 Appendix B: Analytical Procedures	 170
B.1 Iodometric Titration	170
B.2 EDS Analysis	171
B.3 Coulter Counter Procedure and Data	172
 Appendix C: Slurry Scrubber Model Documentation	 176
C.1 Introduction	176
C.2 Individual Subroutine Documentation	190
C.3 Input Requirements	273
C.4 Common Block Cross Reference Sheet	279
 References	 281

## List of Figures

Fig. No.	Title	Page
1.1	Influence of Sulfur in Coal on Required SO <sub>2</sub> Removal . . . . .	2
1.2	Limestone FGD Flow Diagram . . . . .	5
1.3	Limestone Grinding Flow Diagram . . . . .	8
2.1	Effect of $\beta$ on Log Gamma Density Function . . . . .	22
2.2	Effect of $\alpha$ on Log Gamma Density Function . . . . .	23
2.3	Effect of D <sub>100</sub> on Log Gamma Density Function . . . . .	24
2.4	Cumulative Density Function for Two Fixed Values of $\alpha$ . . . . .	31
2.5	Cumulative Distribution for Georgia Marble Fine . . . . .	32
2.6	Cumulative Distribution for Stoneman Coarse . . . . .	33
2.7	Cumulative Distribution for Fredonia Coarse . . . . .	34
2.8	Cumulative Distribution for Limestone 588 . . . . .	36
2.9	Longview Coarse Predicted Curves - Effect of Sieve Selection . . . . .	37
3.1	pH Stat Apparatus . . . . .	51
3.2	Experimental Reactor . . . . .	52
3.3	SEM Photograph: Reagent Limestone . . . . .	65
3.4	SEM Photograph: Reagent Dissolution - Mass Transfer Regime . . . . .	65
3.5	SEM Photograph: Reagent Dissolution - Surface Kinetics Regime . . . . .	66
3.6	SEM Photograph: Edwards Limestone . . . . .	68
3.7	SEM Photograph: Iceland Spar . . . . .	68
3.8	SEM Photograph: Edwards Limestone in 6mM SO <sub>3</sub> , 30% Dissolved . . . . .	69
3.9	SEM Photograph: Iceland Spar in 6 mM SO <sub>3</sub> , 50% Dissolved . . . . .	69
3.10	EDS Analysis of Inhibited Limestone Particle . . . . .	70
3.11	EDS Analysis of Calcium Sulfite Particle . . . . .	71
3.12	Effect of Sulfite on Reagent 1 Limestone . . . . .	74
3.13	Parity Plot for HSTC and Monteagle Limestones . . . . .	76
3.14	Test of Combined Model as Function of CaSO <sub>3</sub> Saturation . . . . .	77
3.15	SEM Photograph: Reagent in 6 mM SO <sub>3</sub> , 10% Dissolved . . . . .	83
3.16	SEM Photograph: Reagent in 6 mM SO <sub>3</sub> , 25% Dissolved . . . . .	83
3.17	SEM Photograph: Reagent in 6 mM SO <sub>3</sub> , 55% Dissolved . . . . .	84



3.18	SEM Photograph: Reagent in 6 mM SO <sub>3</sub> , 75% Dissolved	. . .	84
3.19	Normalized Fluxes for Reagent 1 Limestone	. . .	85
3.20	CaCO <sub>3</sub> Activity at the Surface of HSTC Limestone	. . .	88
4.1	Fraction Remaining of Reagent 1 Limestone: No Sulfite	. . .	105
4.2	Fraction Remaining of Fredonia Limestone with Sulfite	. . .	107
4.3	Fraction Remaining of Georgia Limestone with Sulfite	. . .	108
4.4	Parity Plot for SO <sub>2</sub> Removals from the Slurry Scrubber Model	. . .	126
4.5	SO <sub>2</sub> Dependence on Limestone Reactivity	. . .	129
4.6	Effect of CaSO <sub>3</sub> Reactivity on Scrubber Performance	. . .	131
4.7	Relationship between Dissolved Solids	. . .	132
4.8	Comparison of Solids Reactivity	. . .	135

## List of Tables

Table No.	Title	Page
1.1	Comparison of Largest FGD Using Countries . . . . .	3
1.2	U.S. Power Plant FGD Systems . . . . .	4
2.1	Calculated Alphas and Betas for 1980-81 Stones . . . . .	28
2.2	Calculated Alphas and Betas for 1988-98 Stones . . . . .	29
2.3	Comparison of Measured Values of $d_{100}$ to Predicted Values . . . . .	39
2.4	Statistical Parameters for the Log Gamma Parameters . . . . .	40
3.1	Reagent 1 Limestone Particle Size Distributions . . . . .	53
3.2	Limestone Characteristics . . . . .	56
3.3	Results with Reagent 1 Calcite . . . . .	58
3.4	Results with HSTC Limestone . . . . .	59
3.5	Results with Monteagle Limestone . . . . .	60
3.6	Results with Reagent 2 Calcite . . . . .	61
3.7	Rate Constants and Film Thicknesses for All Limestones . . . . .	64
3.8	Sulfite Effects on the BET Surface Area of Reagent 1 Calcite . . . . .	81
3.9	Statistical Parameters from Regression on $\text{CaCO}_3\text{-CaSO}_3$ . . . . .	90
3.10	Statistical Parameters from Regression on Driving Force . . . . .	91
3.11	Statistical Parameters from Regression on Surface Rate Constant . . . . .	92
4.1	Surface Rate Constants for EPA Stones . . . . .	110
4.2	Wet Sieve Summary for Fredonia Grinds . . . . .	112
4.3	Hold Tank and Scrubber Performance: Fredonia Coarse . . . . .	113
4.4	Hold Tank and Scrubber Performance: Fredonia Extra Coarse . . . . .	114
4.5	Hold Tank and Scrubber Performance: Fredonia Fine . . . . .	115
4.6	Hold Tank and Scrubber Performance: Fredonia Feedbelt . . . . .	116
4.7	Wet Sieve Summary for Georgia Marble Grinds . . . . .	118
4.8	Hold Tank and Scrubber Performance: Georgia Fine . . . . .	118
4.9	Hold Tank and Scrubber Performance: Georgia Coarse . . . . .	119
4.10	Wet Sieve Summary for Longview Grinds . . . . .	121
4.11	Hold Tank and Scrubber Performance: Longview Fine . . . . .	121
4.12	Hold Tank and Scrubber Performance: Longview Coarse . . . . .	122

4.13	Wet Sieve Summary for Stoneman Grinds . . . . .	123
4.14	Hold Tank and Scrubber Performance: Stoneman Fine . . . . .	124
4.15	Hold Tank and Scrubber Performance: Stoneman Coarse . . . . .	125
4.16	Slurry Scrubber Model Parameter Sensitivities . . . . .	136
A.1	Reagent 1 Experiments: Raw Data . . . . .	146
A.2	Edwards Experiments . . . . .	155
A.3	As-Ground Experiments . . . . .	157
A.4	Screened Experiments . . . . .	161
A.5	Zero Sulfite Experiments . . . . .	164
A.6	Solution Compositions of Flouride Study . . . . .	168
A.7	Dissolution Rates of Reagent 1 Calcite: Flouride Study . . . . .	168
A.8	Type and Grind Limestone Compositions . . . . .	169
A.9	Other Limestone Compositions . . . . .	169
B.1	Coulter Counter Data . . . . .	173
C.1	Slurry Scrubber Model Diffusivities . . . . .	188

## **Chapter 1**

### **Background of Research**

#### **1.1 Overview of Limestone Scrubbing**

Sulfur dioxide has long been recognized as a human health hazard and as a precursor of acid rain. More recently researchers have noted that SO<sub>2</sub> in the stratosphere can support the surface reactions which create ozone depletion (Monastersky, 1988). As a result of these problems, SO<sub>2</sub> is one of the species controlled by the Clean Air Act.

Sulfur dioxide is produced by many sources including sulfuric acid and sulfur recovery process equipment and primary smelters of copper, zinc, and lead. The primary emission sources, though, are coal and oil-fired boilers used by electric power utilities.

Flue Gas Desulfurization (FGD) processes are used to achieve the SO<sub>2</sub> emissions guidelines set by the federal and state governments. These technologies are classified by whether the absorbent is or is not regenerable. Additionally the by-products of the process may be a useable product or a waste solid which must be processed for landfill. Limestone slurry scrubbing is a non-regenerable process which can produce gypsum as a useable product or calcium sulfite as a waste solid.

##### **1.11 The SO<sub>2</sub> Regulations**

With the passage of the Clean Air Act in 1970 the federal government was empowered to set and enforce air quality standards. The first regulations for SO<sub>2</sub> emissions were the New Source Performance Standards (NSPS) which placed a ceiling

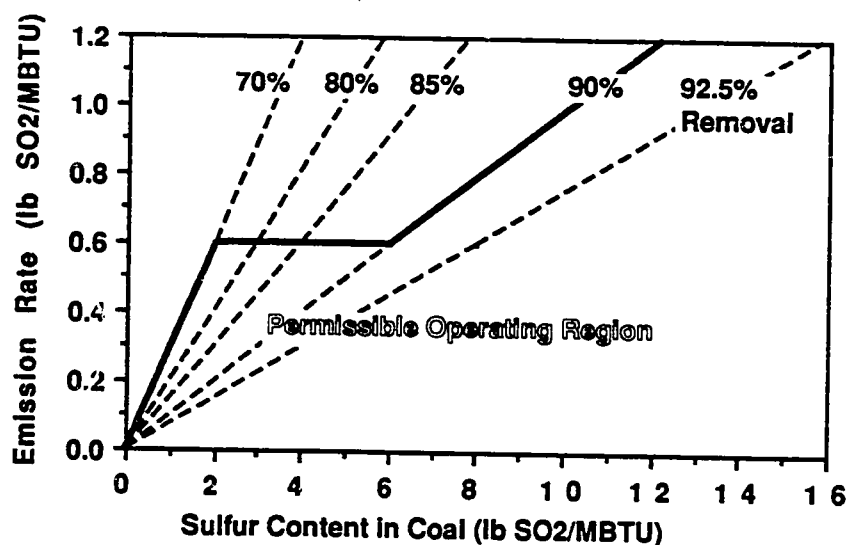


**Figure 1.1: Influence of Sulfur in Coal on Required SO<sub>2</sub> Removal Efficiency**  
(From Henzel et al., 1982)

of 1.2 lbs SO<sub>2</sub>/MBTU on the emissions of coal fired boilers. This restriction proved advantageous for low sulfur coal mines because combustion of these coals often produced emissions which were already within the regulation. This advantage was lost in 1977 when the regulations were modified by the Revised NSPS which took affect on all coal-fired boilers built after September 1978. The new restrictions require a minimum of 70% SO<sub>2</sub> removal from all coal-fired emissions and have a sliding scale removal rate which is dependent on the sulfur content of the coal. These new restrictions are shown graphically in Figure 1.1. The revised standards also require continuous monitoring of emissions to show compliance on a 30 day rolling average. This additional restriction requires that the scrubber system correct for changes in the SO<sub>2</sub> emission rate. Variations in the emission rate occur for many reasons including differences in the sulfur content of the coal and differences in the utility demand.

### 1.12 Wet FGD Commercial Applications

Of the many FGD technologies which are available, the lime/limestone slurry systems are the most commonly used. This is the result of several factors. First, there is a large body of operating experience available for these systems. Secondly, these systems have high design removal capability. Limestone systems, for example, are capable of 95% removal. A third factor is based on economics. Capital costs for these systems may be up to 25% of the cost of the total facility and operating costs run 1-7% of boiler capacity (Baviello, 1982). While these costs may seem high, lime/limestone systems are nonregenerable absorbents, and therefore have lower capital, operating, and maintenance costs than the more expensive regenerable systems. A recent study by the United Kingdom's electric utilities compared the economics of coal cleaning, limestone boiler injection, and the FGD technologies. Based on their research, wet limestone scrubbing with oxidation of the product to salable gypsum was determined to be the most cost effective (Kyte, 1988).

Worldwide, the largest users of FGD are Japan, West Germany, and the United States. As of November 1986, Japan had 130 wet lime/limestone units in operation and West Germany had 115 (Ando and Sedman, 1986; Ellison and Sedman, 1987). Table 1.1 compares the usages and end products of the three major countries in

<b>Table 1.1: Comparison of Largest FGD-Using Countries</b> (From Weiier and Ellison, 1988)			
	Japan	West Germany	U.S.A.
Total Electric Utility FGD (MW)	39,000	38,000	56,000
Wet FGD (MW)	38,220	34,200	51,520
Throwaway Waste (%)	3	8	86
Useable Gypsum (%)	70	87	10

Table 1.2: U.S. Power Plant Flue Gas Desulfurization Systems (From Melia et al., 1987)			
	Number of Systems		
	Operational	Under Construction	Planned
Limestone Scrubbing	62	10	8
Lime Scrubbing	39	0	2
Dry Lime	12	3	1
Sodium Carbonate Scrubbing	6	1	2
Sodium Carbonate (Dual Alkali)	5	1	--
Sodium Sulfite Scrubbing	7	--	--
Magnesia Scrubbing	3	--	--
Dry Sodium Carbonate	1	--	--

1988. This table clearly shows the difference between the United States and other foreign FGD users. In general, foreign users convert the by-product of lime/limestone systems to saleable gypsum while the United States produces a waste product for landfill.

In the United States, FGD applications have increased from 22 units in 1975 to 135 units in late 1986. Of these units, 112 are wet systems and 13 are dry. Table 1.2 lists a breakdown of the FGD technologies in operation at that time and those under construction or planned.

### 1.13 Limestone FGD Process

Figure 1.2 shows a flow chart for a simple limestone slurry scrubbing process. In this system incoming flue gas is pretreated to remove particulates in an electrostatic precipitator or a fabric filter. Typically the flue gas from the boiler contains 500-5000 ppm of sulfur dioxide. Within the scrubber  $\text{SO}_2$  absorbs into an aqueous solution and

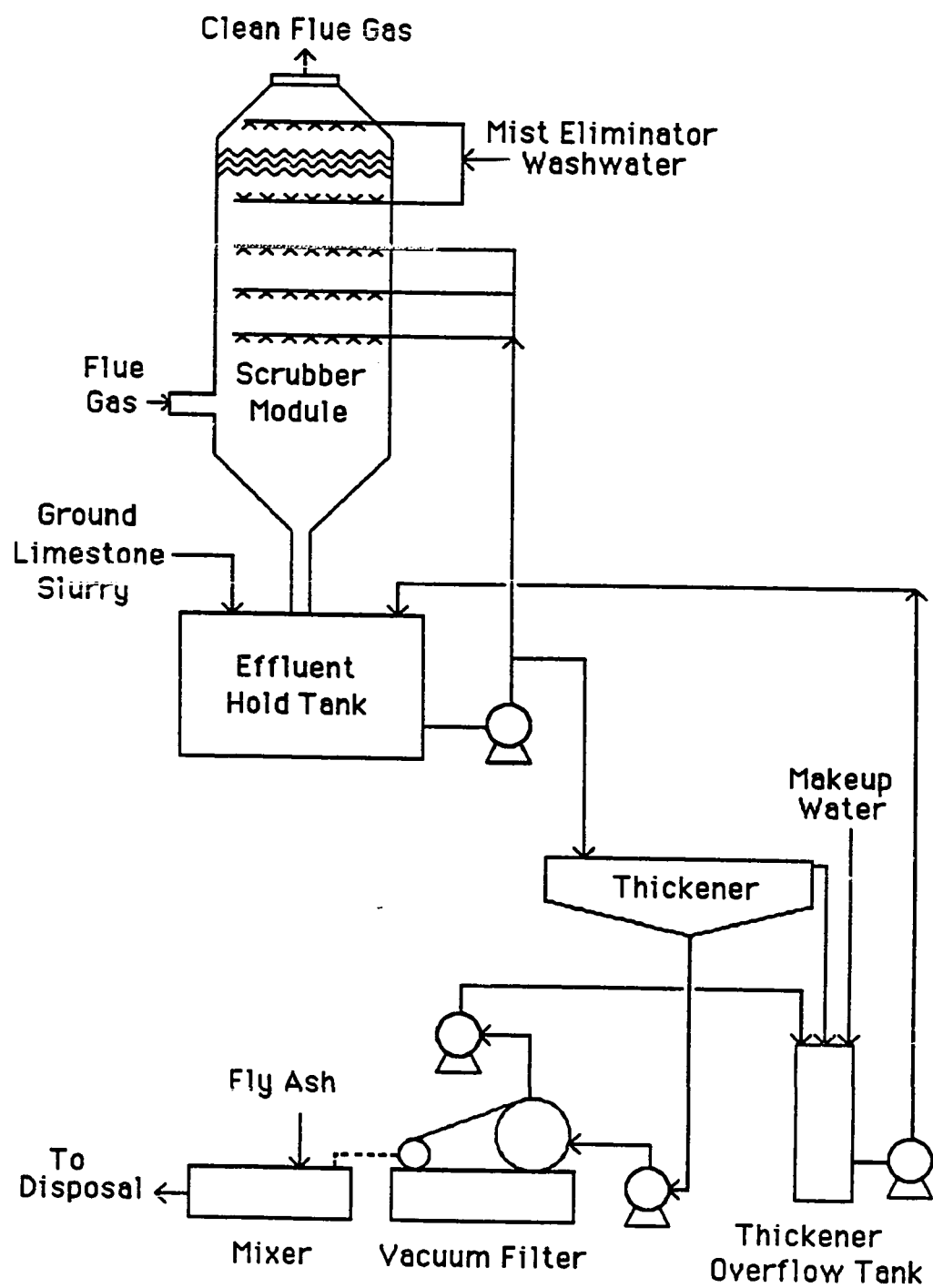
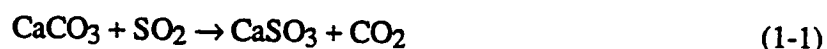


**Figure 1.2: Limestone FGD Flow Diagram**



reacts chemically with dissolved limestone. The spent liquor is collected in a hold tank where crystallization of the products and dissolution of make-up limestone occurs. Liquor from the hold tank is recycled to the scrubber and a side stream is taken off to a thickener where solids are concentrated. This concentrated solution is further dewatered in a vacuum filter and the final solids are stabilized with flyash to form a claylike material which can be sent to a landfill.

Equation (1-1) gives the overall chemistry of a wet limestone scrubbing system.



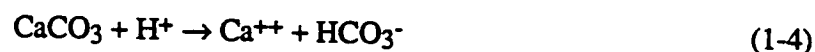
This reaction can be separated into simplified steps which show what happens in the different phases of the system. At the gas-liquid interface,  $\text{SO}_2$  absorption occurs through Equation (1-2).



In the bulk liquid of the scrubber or hold tank, bisulfite reacts with dissolved limestone through Equation (1-3).



And at the solid surface, limestone dissolves through Equation (1-4).



The sum of Equations (1-2) through (1-4) gives the overall chemistry of a limestone scrubbing system. Research has shown that the rate limiting mechanisms of limestone scrubbing are (Rochelle, 1977; 1982)

- 1) gas phase mass transfer to the interface,
- 2) liquid phase mass transfer of dissolved species to the bulk, and
- 3) dissolution of the limestone.

As a result of these limitations, it is important to optimize the design of both the scrubber and the hold tank.

There are several scrubber designs which are used in FGD processes. These include spray, venturi, static and mobile packed beds, and sieve trays. The most commonly used scrubber is the spray tower which is an empty tower containing 1 to 6 spray headers, thus offering simplicity of design. These scrubbers require high liquid-to-gas flowrates in order to provide sufficient absorption efficiency for  $\text{SO}_2$ . Because there are solids present in the scrubber's liquid phase, there is a possibility for plugging or scaling to occur if the hold tank is designed improperly.

A hold tank is usually a single stirred tank which must provide sufficient liquid residence time to allow for precipitation of the waste solids and dissolution of the limestone. Typically 8-10 minutes of liquid residence time is sufficient to relieve the calcium sulfite and gypsum supersaturations (Henzel et al., 1982). The recycle from the hold tank should contain 8-16% solids in order to provide seed crystals in the scrubber. The pH exiting the hold tank is a direct indication of the amount of limestone which has dissolved. Higher pH values indicate higher concentrations of excess limestone and, while this enhances  $\text{SO}_2$  absorption, it also increases the chances of scaling from precipitation of calcium sulfite. Scaling results because excess limestone dissolves in the scrubber while  $\text{SO}_2$  is absorbing. This results in supersaturated solutions and precipitation of the calcium sulfite. At low pH, scaling can result from calcium sulfate (gypsum) precipitation. As the solution passes through the scrubber, oxidation of sulfite to sulfate occurs and the solution becomes supersaturated with respect to gypsum. Scaling has been shown to occur at gypsum saturations of 1.35 and higher (Kohl and Riesenfeld, 1985). Additionally, lower pH values indicate less excess limestone and less capacity for  $\text{SO}_2$  absorption. Therefore there is a trade-off between  $\text{SO}_2$  absorption, pH, and reliable scrubber operation.

#### 1.14 Limestone Preparation Systems

Researchers have shown that finer grinds of limestone require less limestone to be fed for a given  $\text{SO}_2$  removal (Henzel et al., 1982). This occurs because a reduction in particle size increases the surface area per mass and therefore increases the rate of dissolution. Typical desired grinding ranges are 70-90% less than 325 mesh (44 microns). The recent trend has been to use even finer grinds. Because finer grinds

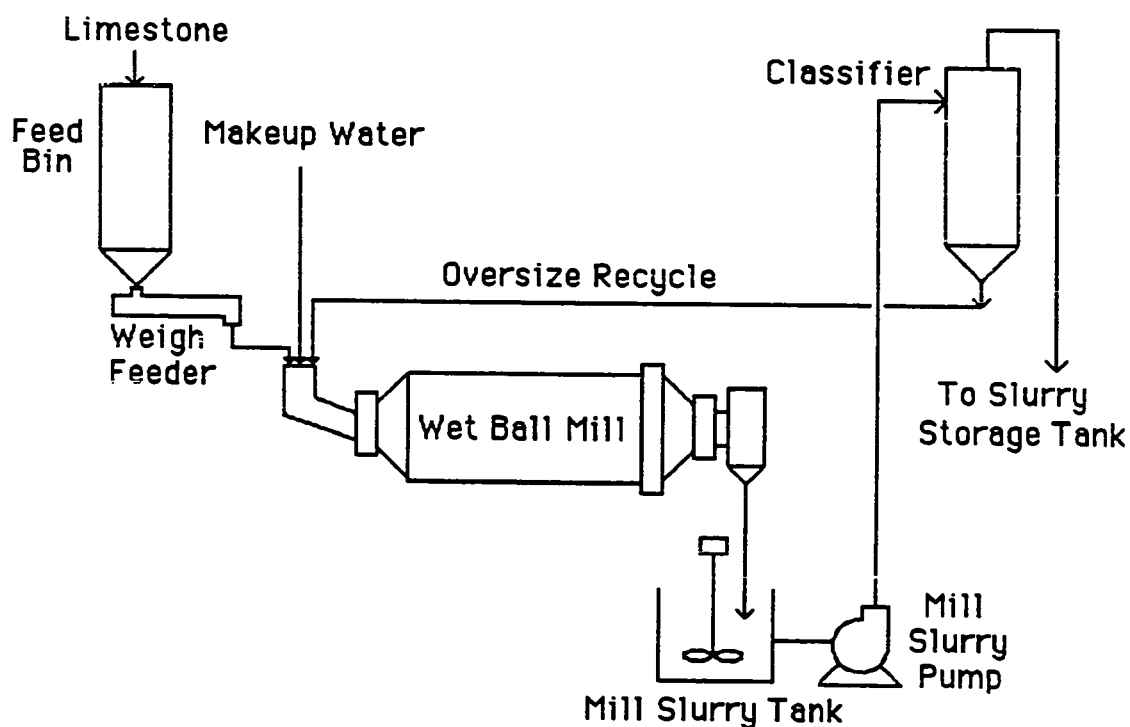


**Figure 1.3: Limestone Grinding Flow Diagram**

require less limestone, the additional grinding proves to be less costly than the excess limestone required when coarser grinds are used (Stewart et al., 1985).

Figure 1.3 shows a flow diagram for wet grinding of limestone solids. A preweighed amount of limestone is added continuously with water to a ball mill. As the mill rotates the limestone rock is crushed between the balls. The ground slurry is pumped to a cyclone or classifier where larger particles settle out and are returned to the mill for further grinding. The fine particles remain suspended in the water and leave through the overflow. This slurry which contains 40-60% solids is then sent to a storage tank for eventual use in the scrubber.

The characterization of the ground particle size distribution includes the mean particle size and the shape of the distribution curve. These parameters are determined by the grinding process. The mean particle size is controlled by the residence time in the ball mill, and the shape of the curve is determined by the recycle rate from the classifier.

## **1.2 Previous Work on Limestone Dissolution and Modeling**

Prediction of limestone dissolution is an important step in determining scrubber performance of flue gas desulfurization (FGD) processes. Accurate predictions, in turn, require an understanding of the factors which affect the dissolution process, especially those factors representative of scrubbing systems. The most common term used to describe the potential performance of limestone is "reactivity". Reactivity has implications of the dissolution rate. A limestone with a faster dissolution rate is considered to be "more reactive" than one with a slower rate. Reactivity is affected by both particle size and solution composition.

### **1.2.1 Particle Size Distributions and Type and Grind**

The prediction of limestone dissolution rates requires knowledge of the complete distribution of particle sizes. When measurements are not available, particle size distributions can be predicted using cumulative density functions found in probability analysis. The most commonly used distributions for this purpose are the log-normal and the gamma distributions (Randolph, 1971). Both of these density functions are two parameter models which have a lower particle size bound of zero. However, neither distribution limits the maximum particle size, and thus unreasonably large particles are predicted. It is possible to truncate the log-normal distribution to account for the finite size range of crushed limestone. The model then has four adjustable parameters.

Recently other probability density functions have been used for the prediction of particle size distributions created by comminution processes. Von Tress et al. (1985) used the beta distribution to represent calcite distributions. Their work predicted

particle size distributions from measured dissolution data. This was a three parameter model which required the dissolution rate constant and the maximum and minimum particle sizes before the complete distribution could be approximated.

Shultz and Crouse (1973) developed a log-gamma density function which has the advantage of limiting maximum particle size. This model has three parameters, one of which is the maximum particle size. In their development one parameter was fixed by assuming that each particle broke into two new particles. They successfully applied the model to distributions of stones crushed in a ball mill.

Toprac (1981) applied the three parameter log gamma model successfully to the prediction of limestone dissolution rates in batch systems. By performing a rigorous analysis on four stones he fixed the value of one parameter. His work resulted in a restrictive empirical correlation for the remaining two parameters which required knowledge of the sizes corresponding to specific screenings of 50 and 90 cumulative percent. In some cases the resulting correlation predicts a maximum particle size which can be ten to twenty times greater than the measured value.

There have been a few studies performed to determine the impact of particle size on limestone dissolution and scrubber performance. Barton and Vatanatham (1975) studied the neutralization rate of sulfuric acid from screened limestones. They modeled the dissolution by a shrinking particle model which depends on the initial particle size. Kim et al. (1975) measured the dissolution rate of an industrial limestone screened to 3 different sizes. Based on the amount of limestone dissolved after five hours, they established that both the dissolution rate and the utilization were proportional to the geometrical surface area.

Drehmel (1971) studied particle size and limestone type effects of 10 screened limestones. He measured the dissolution rates in  $\text{H}_2\text{SO}_3$  and the  $\text{SO}_2$  removal efficiencies in a batch scrubber. For a given particle size, he found a factor of five difference in dissolution rates between the 10 types of limestones. For a given type, dissolution rates increased as particle size decreased. In the scrubber experiments he found that calcites performed better than dolomites.

Shah (1972) tested fourteen limestones in a pilot plant venturi scrubber. He found that finer grinds (< 325 mesh) within a given type yielded higher SO<sub>2</sub> removals than coarse grinds (<200 mesh). For a fixed grind, scrubber performance also varied among the limestone types with SO<sub>2</sub> removals ranging from 30 to 80%.

Borgwardt et al. (1979) studied type and grind effects of three limestones in a bench-scale turbulent contact absorber(TCA). When screened to the same size each limestone type required a different utilization to give the same scrubber performance. Within a limestone type, a reduction in particle size yielded better scrubber performance at a given utilization. They concluded that scrubber performance depended on both the limestone type and the grind.

Toprac (1981; Toprac and Rochelle, 1982) used the same limestones as Borgwardt and measured dissolution rates in a batch pH stat apparatus with HCl. Using a Coulter Counter apparatus he measured the complete distributions of the limestones and found significant differences between stones which had been ground to the same sieve size. He then used the measured particle size distributions in a mass transfer model and correctly predicted the order of reactivity between limestone types studied in the TCA experiments. He concluded that scrubber performance was a function of particle size only and did not depend on limestone type.

Chang et al. (1985) measured type and grind effects of five limestones on the pilot plant performance of a dual alkali scrubbing system. They concurred with Borgwardt in finding that coarser grinds required higher excess limestone to yield equivalent pH and SO<sub>2</sub> removal. Additionally they noted that chemical/physical analyses (wet screening, BET, SEM, and solution composition differences) could not explain the observed differences in the pilot plant. An important conclusion from their work was that when testing limestone for reactivity, titrating with NaHSO<sub>3</sub> was better than HCl in giving the order of reactivity seen in the pilot plant process.

### 1.22 Limestone Dissolution

The dissolution rate of limestone particles in acid systems has been previously treated as a mass transfer process (Berner and Morse, 1974; Lund et al., 1974; King

and Liu, 1933; Sjöberg and Rickard 1984 and 1985; Toprac and Rochelle, 1982; Uchida et al., 1974). All of these systems were aqueous acid/ $\text{CO}_2$  systems which contained none of the other species present in FGD systems. The general conclusion was that for systems with low partial pressures of  $\text{CO}_2$  and with pH less than 5, the dissolution rate of limestone is diffusion controlled. Additional researchers (Chan and Rochelle, 1982; Wallin and Bjerle, 1989) found that in systems of high partial pressures of  $\text{CO}_2$ , the rate could be modelled as a mass transfer process with the finite homogeneous reaction of aqueous  $\text{CO}_2$  to hydrogen ion and bicarbonate.

Only a few systems have been studied in which dissolution was thought to be controlled by a combined regime of mass transfer and surface kinetics. Most of these experiments (Lund et al., 1974; Compton and Daly, 1983; Rickard and Sjöberg, 1983; and Sjöberg and Rickard, 1984) were performed with a rotating disk apparatus using the results of Levich (1972). Levich's development integrated the convective diffusion equations for a spinning disk when a first order kinetic rate is applicable at the surface. In this development the mass transfer contribution was easily separated from the overall rate.

Lund et al. (1974) studied limestone dissolution in HCl solutions at temperatures of  $-15.6^\circ\text{C}$  to  $25^\circ\text{C}$  using the rotating disk apparatus. Only at very low temperatures did they find dissolution to be controlled by mixed mass transfer and surface kinetics. They calculated the surface concentrations by integrating the convective diffusion equations and postulated a rate limiting step of the adsorption of  $\text{H}^+$  onto the surface.

Compton and Daly (1983) measured the dissolution rate of Iceland Spar at  $25^\circ\text{C}$  with varying partial pressures of  $\text{CO}_2$  using a rotating disk. They varied pH between 3 and 6.2 and found contributions of surface kinetics in buffered systems at conditions close to equilibrium to calcite (pH 6.11 with 0.091 or 0.167 atm  $\text{CO}_2$ ). Bjerle and Rochelle (1984) using a pH stat apparatus also noted surface kinetics limitations for plane surfaces of limestones at conditions near equilibrium (pH 4.8 with  $\text{CO}_2$  sparging).

Rickard and Sjöberg (1983) and Sjöberg and Rickard (1984) used the rotating disk apparatus and found a mixed mass transfer/surface kinetic controlled regime at 25°C and pH 8.3. Their rate expression was linear in the driving force between the equilibrium and surface concentrations of dissolved calcite. The surface rate constant was dependent on the stone type. The surface kinetics contribution approached lower pH values as the temperature increased.

Several species are known to adsorb or precipitate onto calcite and may therefore inhibit dissolution rates. Kitano et al. (1976) studied adsorption of 100 µg of zinc or copper ions onto calcite in 50 mls of pure water or artificial sea water. Copper uptake was found to be greater than zinc with 100% uptake of copper occurring at all calcite loadings in the artificial sea water. Additionally, they found that the adsorbed ions could not be removed by washing with water. Clark et al. (1985) studied precipitation of ferric oxides onto calcite in  $\text{Fe}(\text{ClO}_4)_2$  solutions sparged with air and 20%  $\text{CO}_2$ . The precipitation rate was found to be controlled by the oxidation rate of  $\text{Fe}^{+2}$  to  $\text{Fe}^{+3}$ .

Phosphate adsorption/precipitation has been studied by several investigators (Freeman and Rowell, 1981; House and Donaldson, 1985; Giannimaras and Koutsoukos, 1987). SEM micrographs taken by Freeman and Rowell have shown corym growths on calcite exposed to phosphate concentrations as low as 0.3 mM. An important conclusion from their work was that no decrease in the solubility product of calcite occurred as a result of phosphate adsorption. This was also noted by House and Donaldson who found that the solution composition was determined by calcite rather than by a calcium phosphate phase.

The effect of potential inhibitors on the limestone dissolution process has been measured by some researchers. Morse (1974) measured limestone dissolution rates in the presence of phosphates at 25°C and at pH values close to equilibrium with calcite. He found that the rate was inhibited with phosphate concentrations as low as 0.5 µM.

Barton and Vatanatham (1976) observed a ten-fold increase in the time required for limestone to neutralize sulfuric acid when  $\text{Fe}^{+2}$ ,  $\text{Fe}^{+3}$ , or  $\text{Al}^{+3}$  was present in solution. Rochelle et al. (1983) measured rate reductions of limestone dissolution in



$\text{Mg}^{+2}$ ,  $\text{Mn}^{+2}$ , and  $\text{Fe}^{+2}$ . In 100 mM magnesium, a 60% reduction in rate was noted at pH 6.5 with  $\text{N}_2$  sparging. Manganese at a concentration of 10 mM had a much stronger effect with an 85% rate reduction at the same conditions. The maximum effect from 1 mM  $\text{Fe}^{+2}$  was a 50% reduction in the dissolution rate at pH 4.0 with  $\text{CO}_2$  sparging.

Erga and Terjesen (1956) and Terjesen et al. (1961) measured inhibition of the dissolution rate of calcite in the presence of metal ions. Copper and scandium were found to be inhibitors at very low concentrations (less than  $10^{-6}$  moles/l). Magnesium was found to inhibit to a lesser extent. They expressed the empirical dissolution rate in terms of an apparent equilibrium reached in the presence of the inhibitor. For all the metal ions studied, the apparent equilibrium was less than the ideal value and depended on the specific inhibitor and its concentration. They also concluded that the effectiveness of inhibition increased with decreasing solubility of the metal carbonate.

Nestaas and Terjesen (1969) also studied the effect of scandium ions on the dissolution rate of limestone using radioactive  $\text{Sc}^{+3}$  as a tracer. They also saw an approach to an apparent equilibrium which was less than the measured value in the absence of inhibitors. The amount of scandium on the surface was determined by collecting the limestone solids, measuring the radioactivity, and correcting for the scandium in solution around the solids. They proposed that scandium adsorbed onto active sites (or "kinks") of the limestone thus blocking the dissolution at one "kink". The empirical dissolution rate expression was written as linear relationships to the bulk calcium bicarbonate concentration and to the scandium surface concentration. Although this correlation lead to the concept of an apparent equilibrium, the experimental evidence contradicted it. The theory requires the inhibitor to desorb when bulk concentrations of  $\text{Ca}[\text{HCO}_3]_2$  exceed the apparent equilibrium, however this phenomenon was not observed.

Mori et al. (1981) studied the effect of thirteen FGD solution species (separately and combined) on the dissolution rate of an industrial limestone screened to < 325 mesh. Only the combination of  $\text{Al}^{+3}$  and  $\text{F}^-$  was found to reduce the rate. In 3 mM fluoride and 1.3 mM aluminum the limestone dissolution rate was one-tenth its value in the absence of these species. For 5 mM  $\text{F}^-$  and 1.3 mM  $\text{Al}^{+3}$ , limestone dissolution

stopped. SEM micrographs of the treated limestone showed small particles containing Ca, Al and F covering the limestone. For FGD processes an important feature of their work was to show that limestone reactivity could not be recovered by washing with water. Farmer and Jarvis (1987) and Jarvis et al. (1988) also measured significant rate reductions in  $\text{Al}^{+3}$  and  $\text{F}^-$  even at conditions far from equilibrium to calcite. They estimated that inhibition would occur for F to Al ratios of 2 to 4. Additionally they showed in a bench scale FGD apparatus that limestone inhibition could occur in systems which initially contained precipitated fluoride if fly ash was also present. Inhibition occurred when aluminum was leached from the fly ash and the fluoride redissolved.

In another FGD application, Chan and Rochelle (1982) quantified inhibition by sulfite in concentrations greater than 1 mM at conditions far from equilibrium to calcite. Measured rates were significantly less than values predicted by a mass transfer model which accounted for the buffering effect of sulfite/bisulfite. At some conditions rates measured in sulfite were less than the zero sulfite rates. They successfully modeled the inhibition as a shift in surface equilibrium from the calcite solubility product to a mixed calcium sulfite/carbonate solid solution.

Jarvis et al. (1988) studied FGD solution effects on ten different limestone types. Solution species which were tested included pH,  $\text{Ca}^{++}$ ,  $\text{Mg}^{++}$ ,  $\text{Na}^+$ ,  $\text{SO}_3^-$ ,  $\text{SO}_4^-$ ,  $\text{CO}_3^-$ ,  $\text{Fe}^{+++}$ ,  $\text{Al}^{+++}$ ,  $\text{F}^-$ , and adipic acid. Of the species studied, magnesium and adipic acid were found to be minor inhibitors while sulfite and aluminum fluoride complexes were noted to be significant inhibitors to the limestone dissolution rate. Additionally the magnitude of sulfite inhibition was found to be dependent on limestone type. Another important conclusion of their work was that the  $\text{CO}_2$  hydrolysis reaction was insignificant in FGD systems where other buffer species such as sulfite are present.

### 1.23 Modeling of the FGD Process

Computer modeling of FGD systems falls into three categories: equipment design parameters and economics, database performance information, and process simulation. The first two categories cover two specialized models (Laeske et al.,

1982). The first model is the TVA/Bechtel lime/limestone scrubbing computer model. This program calculates the major design parameters and costs of lime/limestone systems. Output from the model includes pond size parameters, equipment sizes and costs, capital costs, etc. The second model is the PEDCO FGD information system. This program maintains design and performance information on operating FGD systems.

Process simulation has been studied by several investigators. Performance data in 10 MW scrubbers have been correlated by McMichael et al. (1976) and Head (1977). Additionally hold tank data have also been correlated by McMichael et al. (1977).

Early scrubber simulations were performed on venturi scrubbers. These models were based more on fluid dynamics than scrubber chemistry and involved the use of accepted empirical correlations for many of the parameters. Wen and Uchida (1972) integrated gas and liquid velocities,  $\text{SO}_2$  concentration, water evaporation, and temperature across the length of the scrubber. These researchers treated absorption of  $\text{SO}_2$  into alkali solutions as a physical mechanism only. Dissolution of solids in the scrubber was neglected.

Epstein et al. (1972) also developed a hydrodynamic model for venturi scrubbers using many of the same approaches as Wen and Uchida. Their model, however, assumed that  $\text{SO}_2$  absorption was enhanced by a pseudo-second order chemical reaction with dissolved reagent. This reaction was accounted for by addition of a correction term to the liquid side mass transfer coefficient.

An early effort in modeling the chemistry of the process was limited to gas/liquid/solid equilibria (Lowell et al., 1970). This model contained the database information to determine activity coefficients and equilibrium constants for FGD species. Bechtel then fitted scrubber data to this model in order to monitor gypsum saturation at the scrubber outlet (Epstein, 1975; Henzel, 1982). Thus the original model coded by Radian became the Bechtel-Modified Radian Equilibrium Program, BMREP.

In 1981 Radian extended their equilibrium model to make it more general by writing the Species Distribution Model, SDM (Faist et al., 1981; Faist et al., 1982). This program satisfies multiphase equilibrium by minimizing the Gibbs free energy of all species.

For systems with high ionic strengths, Taylor (1984) developed the binary parameters necessary to determine the activity coefficients of FGD species. These parameters are applicable to the local composition model developed by Chen et al. (1982). Taylor's program is a submodel extension for SDM.

The chemistry of scrubber operations was addressed by Rochelle and King (1977), who integrated the  $\text{SO}_2$  mass transfer rate over the changing gas-phase concentration assuming constant dissolved alkalinity and no  $\text{SO}_2$  back pressure. Mehta (1982) integrated  $\text{SO}_2$  gas/liquid mass transfer and  $\text{CaCO}_3$  dissolution as a function of changing gas and solution composition (Mehta and Rochelle, 1983). His model for  $\text{SO}_2$  mass transfer includes both gas and liquid phase resistance and simulated liquid phase transfer by approximate surface renewal theory with equilibrium reactions (Chang and Rochelle, 1982; Weems, 1981).  $\text{CaCO}_3$  dissolution was modeled by mass transfer with equilibrium reactions using film theory (Chan and Rochelle, 1982; Rochelle et al., 1983). Solution equilibria were calculated by the Bechtel-Modified Radian Equilibrium program, BMREP.

Chan and Rochelle extended Mehta's work by adding gas/liquid mass transfer of  $\text{CO}_2$  and  $\text{O}_2$ . Chan also expanded the scrubber model to include solids balances on each stage. This work included routines to predict  $\text{CaSO}_3$  dissolution by mass transfer with equilibrium reactions as well as routines for the crystallization of  $\text{CaSO}_3$  (Tseng, 1983). The number of species in the scrubber were reduced by defining pseudospecies as the sum of the parent species and all associated ion pairs. With appropriate system parameters for specific industrial scrubbers the model correctly predicted  $\text{SO}_2$  removal in the presence of chloride (Chan and Rochelle, 1983). Later Chan simulated the hold tank as an additional scrubber stage in order to predict scrubber inlet concentrations for a given limestone reactivity. Gas phase mass transfer of  $\text{SO}_2$  was assumed to be negligible in the hold tank.

Presently Radian is also developing a wet scrubber program in conjunction with EPRI, the Electric Power Research Institute (Jarvis et al., 1988). When completed, FGDPRIISM will predict the effects of process changes on many of the operations of wet FGD systems. This program will include unit operations modules for the absorber, hold tank, and thickener.

### 1.3 Scope of Investigation

As shown in Table 1.2, the dominant FGD technology is limestone slurry scrubbing. In the slurry process limestone dissolution is a rate limiting step in the performance of scrubber systems. The rate of dissolution affects not only the solution alkalinity from the hold tank, but also the additional capacity which could be used in the scrubber. As a result it is important to determine those factors which affect limestone reactivity. Therefore the objective of this work is to understand and model the role of limestone type and grind on the performance of limestone slurry scrubbers.

To achieve this goal, the following subtasks were performed. Limestone dissolution was measured at conditions representative of an FGD hold tank. Batch experiments were performed using reagent calcite at 55°C in a pH stat apparatus. Equilibrium to calcite was approached by sparging with CO<sub>2</sub> and by varying pH. Relative saturation to calcium sulfite was varied from 0 to 2.5 which encompasses all saturations typical of FGD systems. An empirical correlation based on the theory of surface kinetics was developed to predict the dissolution rate at these conditions. This correlation was tested against other batch dissolution experiments performed by Radian using industrial limestones (Jarvis et al., 1988) and against previous work done at conditions typical of FGD scrubbers (Chan and Rochelle, 1982).

Subroutines were written to predict limestone reactivity as a function of limestone grind and utilization using the approach of Toprac and Rochelle (1982). Since limestone grind data are not usually available at industrial sites, subroutines were written to predict the particle size distribution from sieve data. A new mathematical approach was taken in using the log-gamma distribution for this purpose.

The slurry scrubber model written by Chan at the University of Texas was decoded and documented. Each subroutine was documented extensively to give usage, calling sequence, algorithmic techniques, and step by step programming details (Appendix C). The model was then expanded to predict particle size distributions, limestone reactivity from particle size effects, and to account for sulfite effects on reactivity.

The complete slurry scrubber model was then tested against a limestone type and grind study sponsored by the EPA (Borgwardt et al., 1980). This work studied four limestone types at ten different grinds in a turbulent contact absorber. Each grind was tested at 2 to 4 utilizations.

## **Chapter 2**

### **Prediction of Particle Size Distributions**

#### **2.1 Introduction**

Since the limestone dissolution mass transfer model accounts for the effects of particle size distribution as well as solution composition, a method is required to predict distributions when complete measurements cannot be made. For industrial applications it is common that the only data available relative to limestone particle size distributions are two or three sieve measurements. And because limestone utilization and scrubber performance are improved when particle size is reduced, limestone is often ground in a ball-mill to sizes which are difficult to measure using the wet sieving technique. The ground particles are then sized in a classifier, and the larger particles are returned to the mill. Typically limestone distributions are reported as percents less than 200 and 325 mesh (74 and 44 microns, respectively). Thus a prediction method is required which needs only two sieve measurements and which will not predict infinitely large particles. The log-gamma density function fits these requirements if one parameter can be fixed.

#### **2.2 Theory**

The log-gamma density function is a three parameter model which has been used by previous investigators to predict particle size distributions from comminution processes (Shultz, 1973, and Toprac, 1981). The cumulative distribution for the log-gamma model is found by integrating the density function. The resulting continuous

function can be related to the discrete particle size distributions through the method of moments.

### 2.2.1 Log Gamma Model

The particle size distributions are predicted from the log-gamma density function. This probability function is given by Equation (2-1).

$$f(W) = \frac{W^{\alpha-1} \exp(-W/\beta)}{\beta^{\alpha} \Gamma(\alpha)} \quad (2-1)$$

where  $W = 3 \ln(d_{100}/d)$ .

The parameters required to describe the function are  $\alpha$ ,  $\beta$ , and  $d_{100}$ , the maximum particle size. Physically  $\beta$  and  $\alpha$  are related to the mode and frequency of breakage, respectively. The maximum particle size is dependent on the oversize recycle in the hydroclone. The effect of the three parameters on the shape of the density function are shown in Figures 2.1 through Figures 2.3. For fixed  $\alpha$  and  $d_{100}$  the density function becomes flatter when  $\beta$  increases and the peak in the curve shifts to smaller diameters as shown in Figure 2.1. When  $\alpha$  increases with fixed  $\beta$  the curve becomes skewed to smaller diameters as shown in Figure 2.2. As  $d_{100}$  increases, the distribution spreads out as would be expected and the location of the peak shifts to larger diameters. However the peak shift is lesser for larger values of  $\alpha$  as shown in Figure 2.3. As  $\alpha$  approaches large values the log gamma distribution approaches the log normal distribution.

When the value of the parameters are known, the volume fraction within a size interval is found by integrating the density function between the two diameters which bound the interval. If  $\alpha$  is an integer, Equation (2-1) can be integrated analytically. The bounds on the integration are given by Equations (2-2) and (2-3).

$$d = d_{\min} \quad P(d) = 1 \quad (2-2)$$

$$d = d_{100} \quad P(d) = 0 \quad (2-3)$$



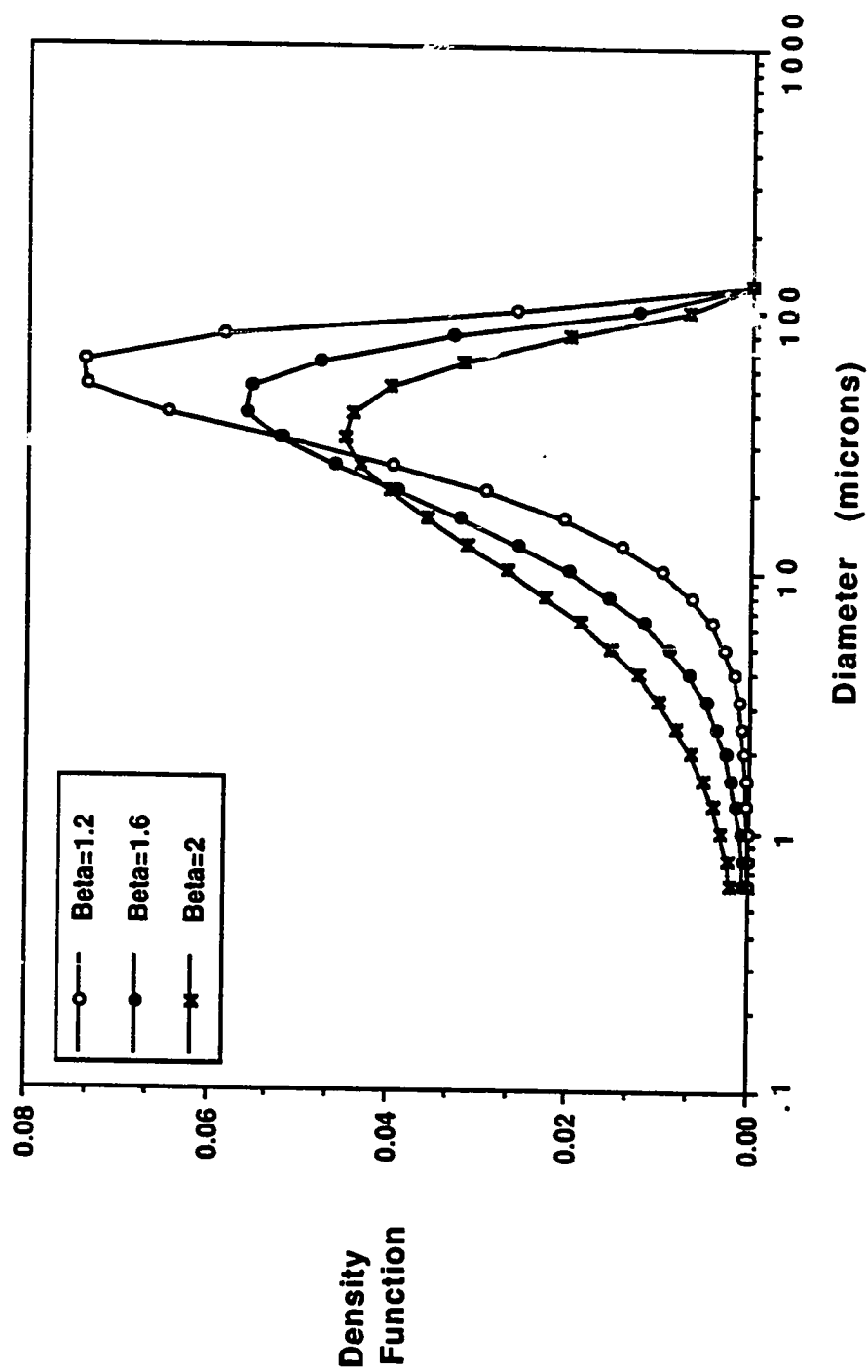


Figure 2.1: Effect of Beta on the Log Gamma Density Function for Alpha = 3 and D100 = 128 Microns

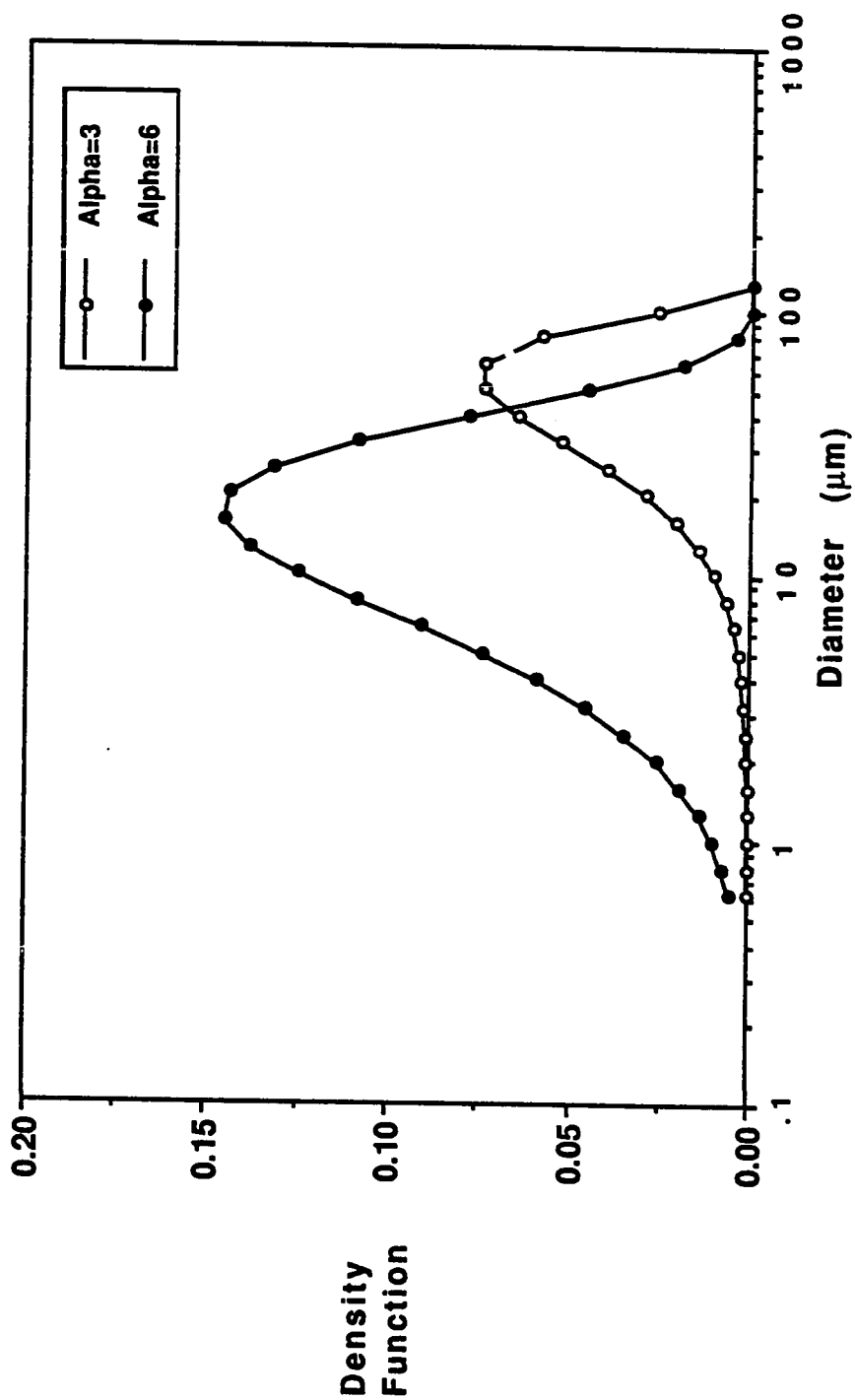


Figure 2.2: Effect of Alpha on the Log Gamma Density Function for Beta = 1.2 and D100 = 128 Microns

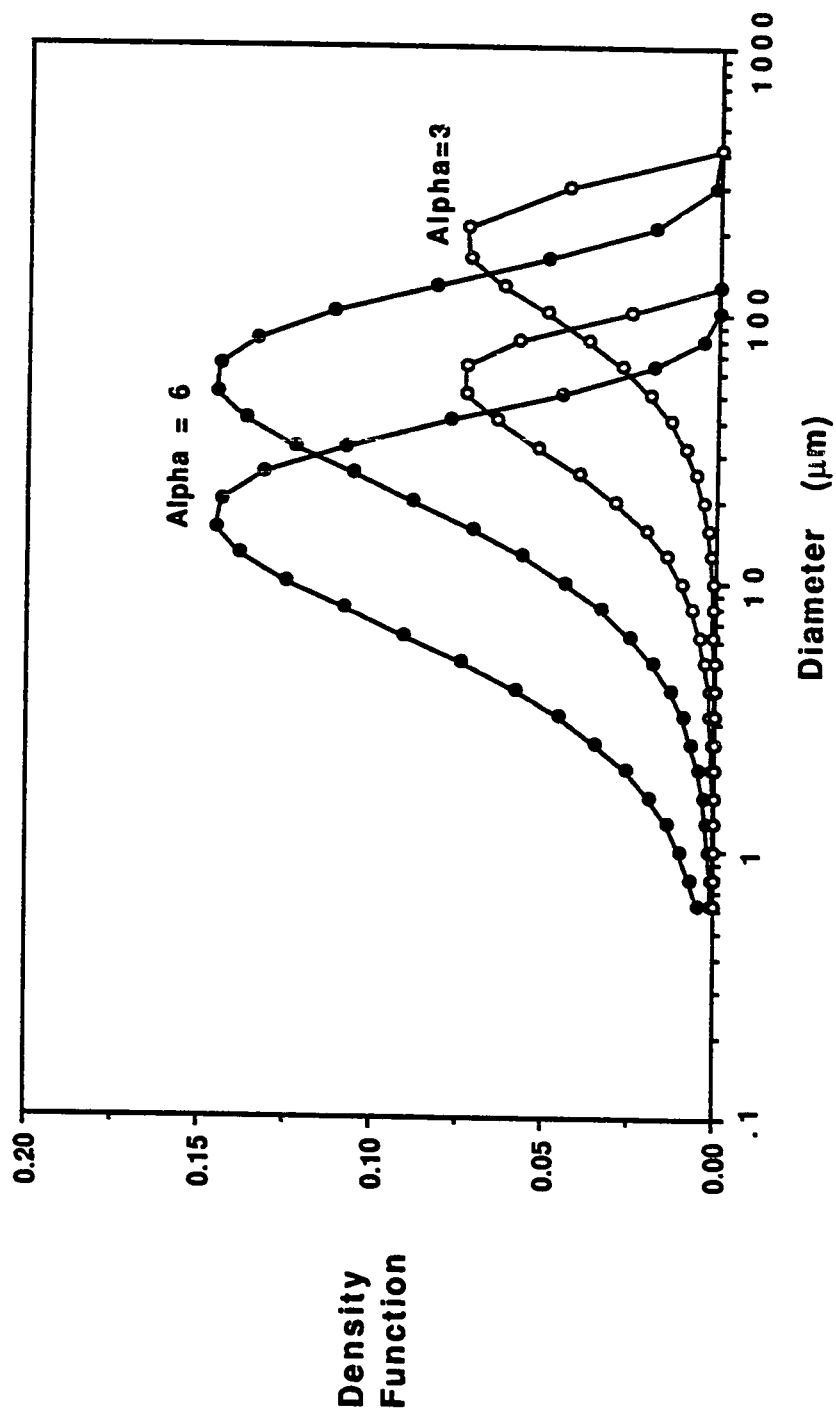


Figure 2.3: Effect of D100 on Log Gamma Density Function for Two Alphas when Beta = 1.2

Letting  $Y = \frac{W}{\beta}$  the resulting polynomial in  $\alpha$  is given by Equation (2-4).

$$P(Y) = \frac{e^{-Y} Y^{\alpha-1}}{(\alpha-1)!} \left[ 1 + \frac{\alpha-1}{Y} + \frac{(\alpha-1)(\alpha-2)}{Y^2} + \dots + \frac{(\alpha-1)(\alpha-2)\dots(2)(1)}{Y^{\alpha-1}} \right] \quad (2-4)$$

### 2.2.2 Method of Moments

There are experimental apparatuses, such as the Coulter Counter, which can measure complete particle size distributions. These distributions are discrete, not continuous, but the resulting data can be used to calculate the parameters  $\alpha$  and  $\beta$ . (The third parameter,  $d_{100}$ , is known from the measured distribution.) The technique which is used is called the method of moments. The moments of a continuous density function are found by differentiating the moment generating function. For the log-gamma function the definition of the moment generating function, MGF, is given in Equation (2-5).

$$MGF(t) = \int_0^{\infty} \exp(tW) \frac{W^{\alpha-1} \exp(-W/\beta)}{\beta^{\alpha} \Gamma(\alpha)} dW \quad (2-5)$$

By combining the exponential terms and letting  $\theta = \frac{1-\beta t}{\beta}$ , Equation (2-5) becomes Equation (2-6).

$$MGF(t) = \frac{1}{\beta^{\alpha} \theta^{\alpha}} \int_0^{\infty} \frac{\theta^{\alpha}}{\Gamma(\alpha)} W^{\alpha-1} \exp(-\theta W) dW \quad (2-6)$$

The integrand of Equation (2-6) is just the cumulative gamma density function with parameters  $\theta$  and  $\alpha$ , and when integrated over the limits equals one. Then substitution of the definition for  $\theta$  gives the final expression for the moment generating function (Equation 2-7).

$$MGF(t) = \left[ \frac{1}{1-\beta t} \right]^{\alpha} \quad (2-7)$$

The first moment of the log-gamma density function is found by evaluating the first derivative of Equation (2-7) at  $t = 0$ . This value is set equal to the first moment of the discrete function, the measured particle size distribution. This procedure is repeated for the second moment which is found from the second derivative of Equation (2-7) evaluated at  $t = 0$ . For the log gamma density function these two expressions are given by Equations (2-8) and (2-9).

$$\alpha\beta = \sum_i W_i \phi(W_i) \quad (2-8)$$

$$\alpha(\alpha+1)\beta^2 = \sum_i W_i^2 \phi(W_i) \quad (2-9)$$

where  $\phi(W_i)$  is the discrete distribution dependent on the diameter.

The right hand side of Equation (2-8) is the mean of the log gamma density function as well as the first moment. The variance of the log gamma function is related to the first and second moments through Equation (2-10).

$$\text{Var} = \alpha(\alpha+1)\beta^2 - (\alpha\beta)^2 = \alpha\beta^2 \quad (2-10)$$

### 2.3 Results

The use of a three parameter model to predict a limestone particle size distribution required that three sieve measurements are known. If one of the log gamma parameters can be fixed for all limestone grinds the number of sieve measurements needed to calculate the distribution can be reduced. The selection of this fixed parameter required that values were known of  $\alpha$  and  $\beta$  which represent industrial crushed limestones.

These unknown log gamma parameters were regressed from the distributions of 19 limestones, and then a model was developed to predict particle size distributions. This model assumes a fixed value for  $\alpha$  and uses the cumulative density function to

regress  $\beta$  and  $d_{100}$  from two sieve measurements. Then the complete distribution was calculated using these parameters in the log gamma density function.

### 2.3.1 Experimental Alphas and Betas

The method of moments can be applied to known limestone particle size distributions in order to determine the applicable  $\alpha$  and  $\beta$  of the given grind. Since the independent parameter ( $W_i$ ) of the log-gamma function depends on the maximum particle size, Equations (2-8) and (2-10) can be simplified for measured particle size distributions to Equations (2-11) and (2-12).

$$\alpha\beta = 3 \ln d_{100} - 3 \sum_i \ln(d_i)p_i \quad (2-11)$$

$$\alpha\beta^2 = 9 \{ \sum_i [\ln(d_i)]^2 p_i - [\sum_i \ln(d_i)p_i]^2 \} \quad (2-12)$$

For a given differential size distribution these equations can be used to regress the values of  $\alpha$  and  $\beta$  when  $d_{100}$  is known.

Equations (2-11) and (2-12) were coded into a computer program, FINDAB. This model calculates the values of  $\alpha$  and  $\beta$  for limestones whose differential particle sizes are measured on a Coulter Counter or similar particle size analyzer. FINDAB was used to calculate the log gamma parameters for 12 stones which were used in 1980-1981 and for 7 stones which were used in 1988-1989. Particle size distributions of the early limestones were measured and reported by Toprac (1981). The particle size distributions for the 1988-89 stones were measured as part of this work. With the exception of the Ashgrove and Maysville stones, the 1980-81 limestones were used in an EPA sponsored study of limestone type and grind effects on scrubber performance. In preparation for the EPA study these stones were ground in a dry roller mill and classified by a rotating classifier. The Ashgrove and Maysville stones were commercially ground stones used at other facilities. The 1988-89 stones were commercially ground in wet ball mills and sent as raw slurry samples.

The  $\alpha$  and  $\beta$  values regressed from the particle size distributions of all 19 stones are shown in Tables 2-1 and 2-2. Also shown in these tables are the cumulative

percents less than 40.3  $\mu\text{m}$ , approximately 325 mesh, which is indicative of the fineness of the grind. There are clear differences between the two limestone groups. For the earlier stones, the value for  $\beta$  was found to range from 1.0 to 2.5 and  $\alpha$  was bounded between 2.5 and 5.4. For the later stones,  $\beta$  ranged from 0.9 to 1.5 and  $\alpha$  ranged from 5 to 7.2. These differences probably occur because of differences in grinding times. The later stones are finer than the earlier ones. Finer grinding cause more limestone to be recycled to the mill, thus a given particle spends longer in the mill

**Table 2.1: Calculated Alphas and Betas for 1980-81 Stones Using Particle Size Distributions from Toprac (1981)**

	% < 40.3 $\mu\text{m}$	Alpha	Beta
Ashgrove	98.7	3.718	1.049
Maysville	94.2	4.026	1.305
Georgia Fine	81.1	3.727	1.165
Stoneman Fine	78.7	2.494	2.045
Longview Fine	80.0	3.651	1.765
Fredonia Feedbelt	85.2	5.336	1.554
Fredonia Fine	88.3	4.067	1.943
Longview Coarse	63.0	3.017	2.539
Georgia Coarse	47.7	4.113	1.592
Stoneman Coarse	49.9	3.517	2.061
Fredonia Coarse	51.7	3.775	2.374
Fredonia Extra Coarse	50.3	<u>3.581</u>	<u>2.379</u>
(Mean Parameters)		3.752	1.814

than is required to produce coarser grinds. This increased time in the mill is reflected by the larger  $\alpha$  values of the 1988-89 stones. This result is expected since  $\alpha$  is related to the frequency (time) of breakage, and higher  $\alpha$  values skew the curve to smaller diameters indicating finer grinds.

The parameters in this work can be compared to the values deduced by Shultz and Crouse (1973) for crushed stones in a ball mill. In their work  $\beta$  was fixed at 0.5, and  $\alpha$  increased from 0.3 to 2.5 as grinding times increased from 1/3 to 8 minutes. For the limestones studied in this work the mean  $\beta$  decreased from 1.8 to 1.2, while the mean  $\alpha$  increased from 3.7 to 6.2 as grinding times increased. Typically limestone grinding times are from 30-60 minutes.

<b>Table 2.2: Calculated Alphas and Betas for 1988-89 Stones</b>			
	<b>% &lt; 40.3 <math>\mu</math>m</b>	<b>Alpha</b>	<b>Beta</b>
Radian	93.6	6.813	0.906
Limestone 587	89.5	5.572	1.258
Limestone 588	83.9	5.028	1.340
HSTC1	88.9	6.330	1.360
HSTC2	86.3	5.509	1.474
Limestone 585	89.2	6.854	1.123
Limestone County	84.8	<u>7.204</u>	<u>1.152</u>
(Mean Parameters)		6.187	1.230



### 2.3.2 Predicted Particle Size Distributions

Based on the experimental mean  $\alpha$  values, the probability density function was integrated analytically for values of  $\alpha = 4$  and  $\alpha = 6$  (Figure 2-4). A sieve measurement set includes a particle size and the weight fraction of the total sample which is less than that size. Given two sets of sieve measurements, a curve from Figure 2-4 can be used to get two values of  $Y$  from which the unknown parameters  $\beta$  and  $d_{100}$  can be found. Once  $\beta$  and  $d_{100}$  are regressed from sieve measurements, they are used with the fixed  $\alpha$  value to calculate the complete particle size distribution curve. Two computer programs, PPSD and PPSD6, were written to predict the required parameters and complete distributions for fixed  $\alpha$  of 4 and 6, respectively. These programs require two sets of sieve measurements as input.

Figures 2.5 to 2.7 show comparisons for three 1980-81 stones between the measured particle size distributions and the predictions by the log gamma density function. Predicted distributions were found using a fixed  $\alpha$  value of 4 and two sieve measurements (Chang et al., 1982a) to estimate the unknown parameters of  $d_{100}$  and  $\beta$ . For Georgia Marble fine the parameters were estimated from wet sieve data of 98.6% < 74 microns and 84.1% < 44 microns (200 and 325 mesh, respectively). From Figure 2.4 using the two sieve measurements, two points were located on the cumulative curve of  $\alpha = 4$ . These points are:

$$\text{When } d = 74 \mu\text{m with } P(Y) = 0.986, \quad \frac{3}{\beta} \ln \left[ \frac{d_{100}}{d} \right] = 0.918$$

$$\text{When } d = 44 \mu\text{m with } P(Y) = 0.841, \quad \frac{3}{\beta} \ln \left[ \frac{d_{100}}{d} \right] = 2.094$$

Using these relationships,  $\beta$  was calculated to be 1.3256 and  $d_{100}$  was 111 microns. In a computer code the two abscissa values can be calculated using an iterative numerical technique with Equation (2-4) and the sieve measurements.

This procedure was repeated for Stoneman coarse and Fredonia Extra Coarse. For Stoneman coarse the parameters were estimated from 96.4% < 149 microns (120 mesh) and 52.9% < 44 microns. For this stone  $\beta$  was 1.5842 and  $d_{100}$  was 285

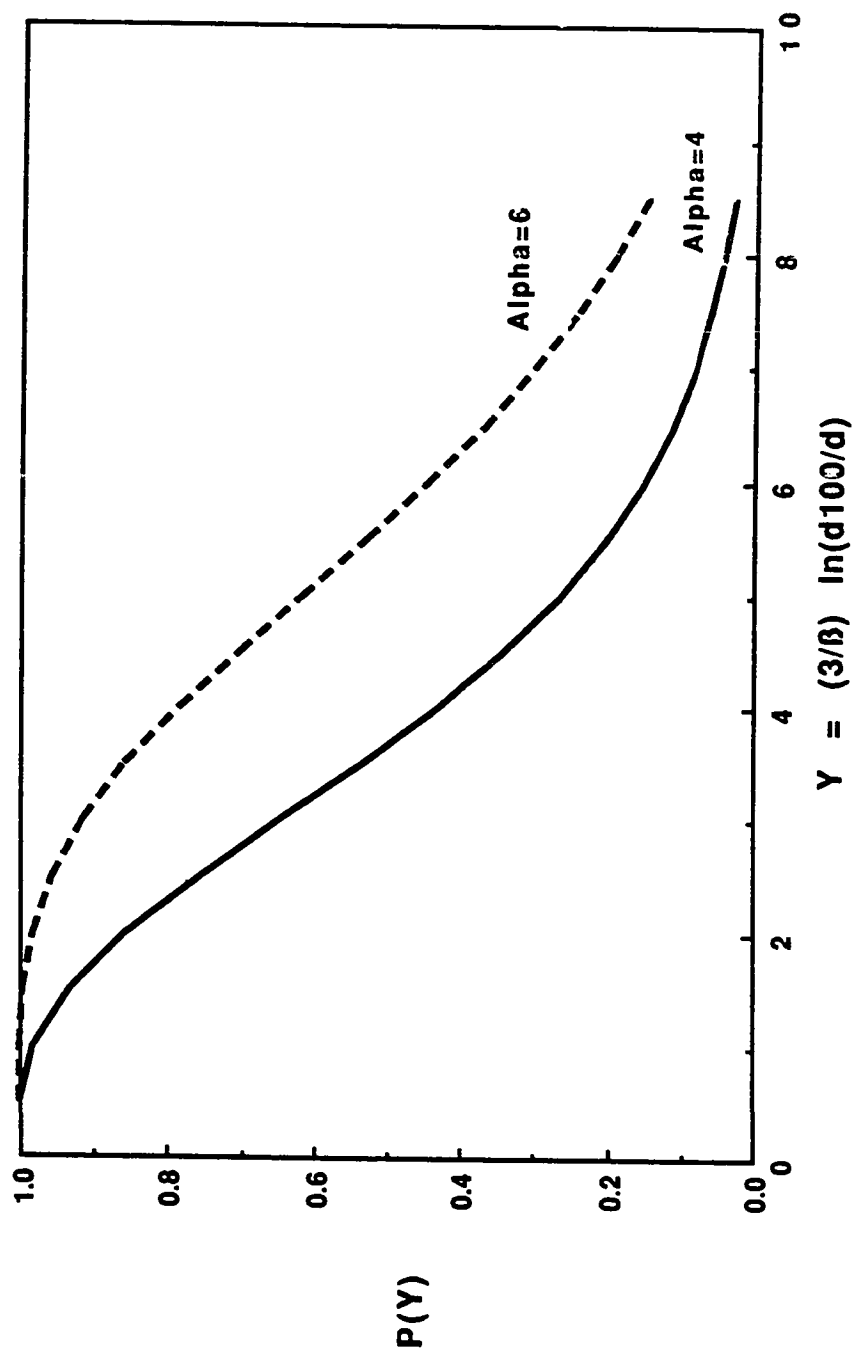


Figure 2.4: Cumulative Log Gamma Density Function  
for Two Fixed Values of Alpha

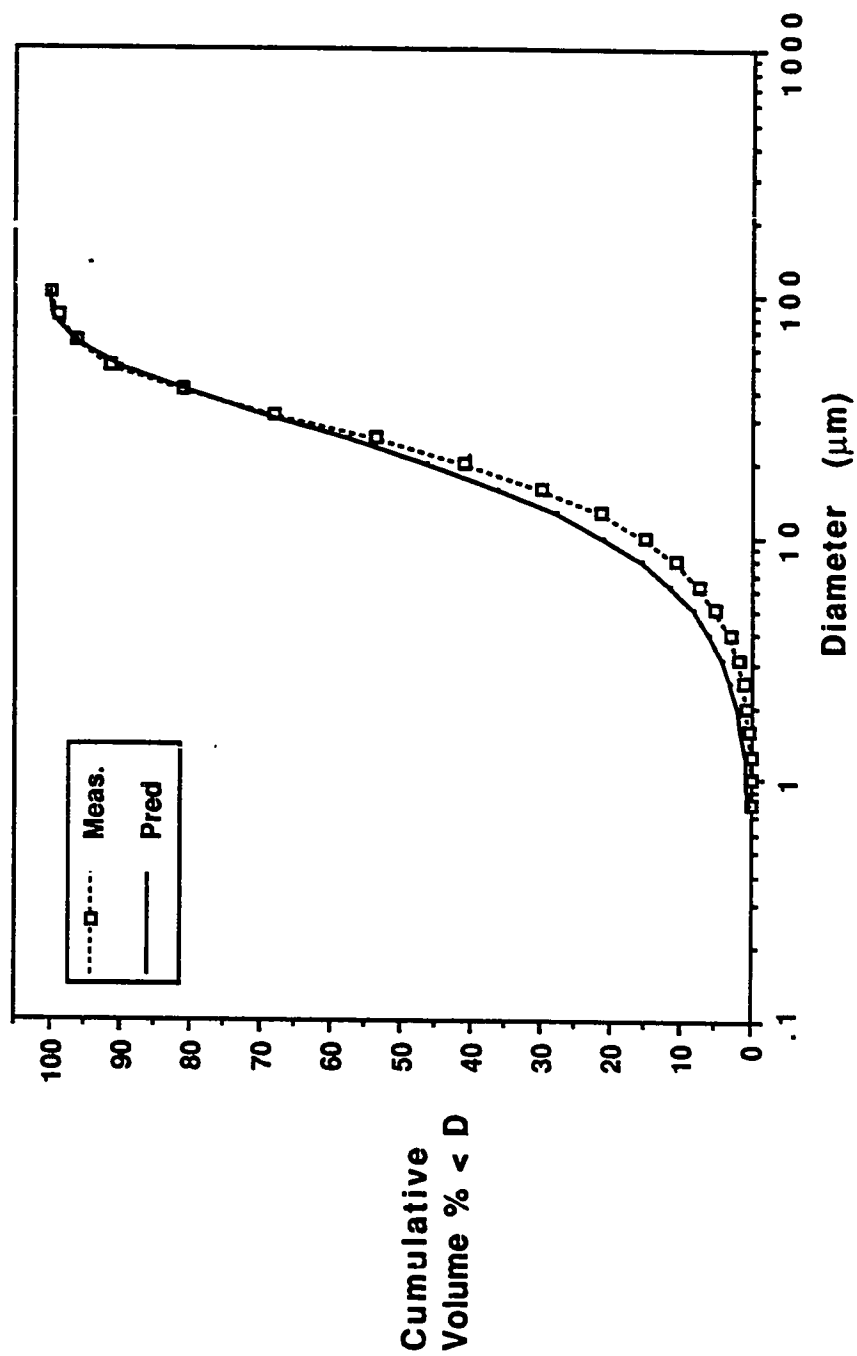


Figure 2.5: Cumulative Distribution for Georgia Marble Fine  
 Predicted uses  $D_{100} = 111$  microns,  $Beta = 1.3256$  and  $Alpha = 4$

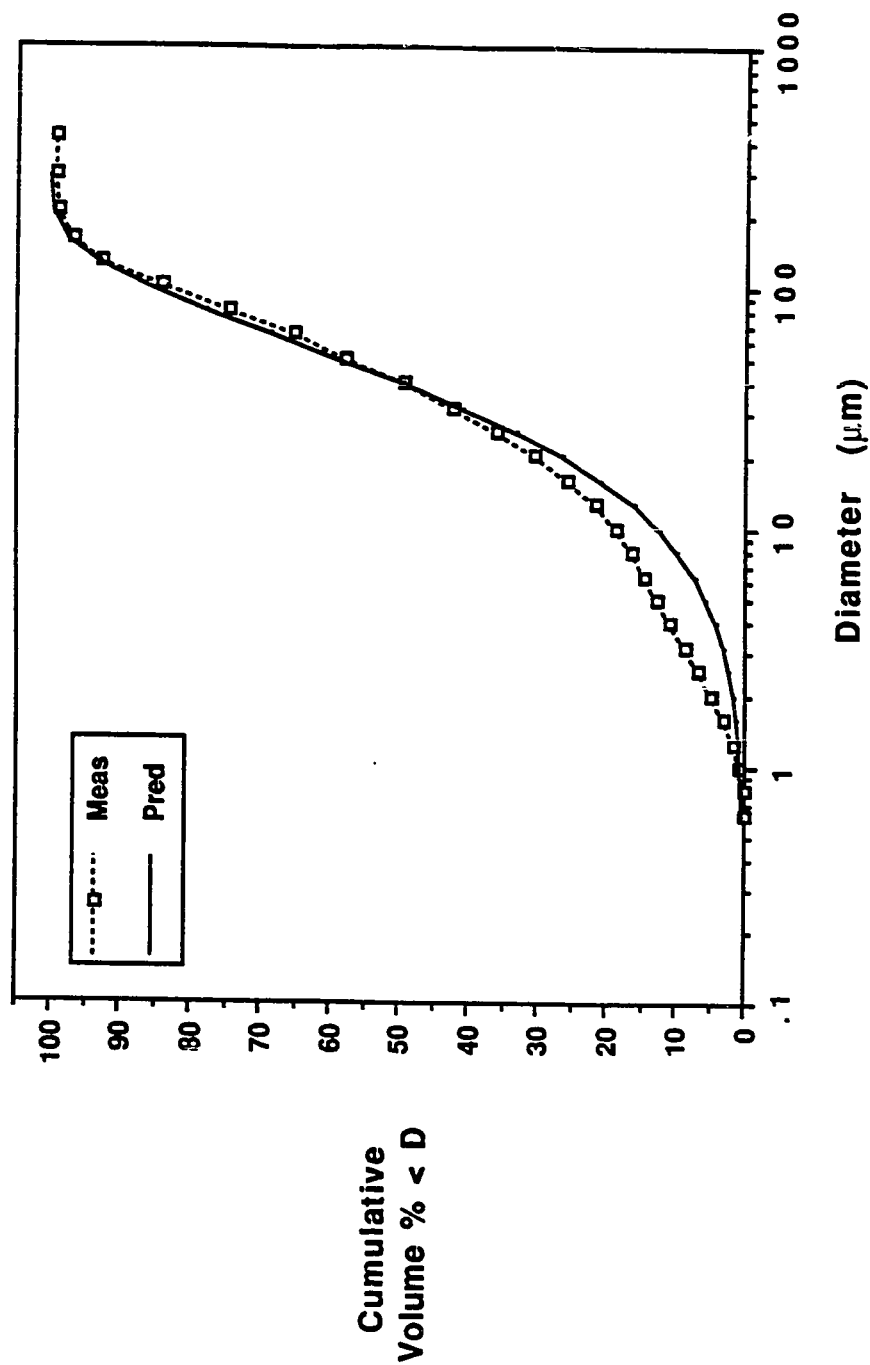


Figure 2.6: Cumulative Distribution for Stoneman Coarse  
 Predicted uses D100 = 285 microns, Beta = 1.5842, and Alpha = 4

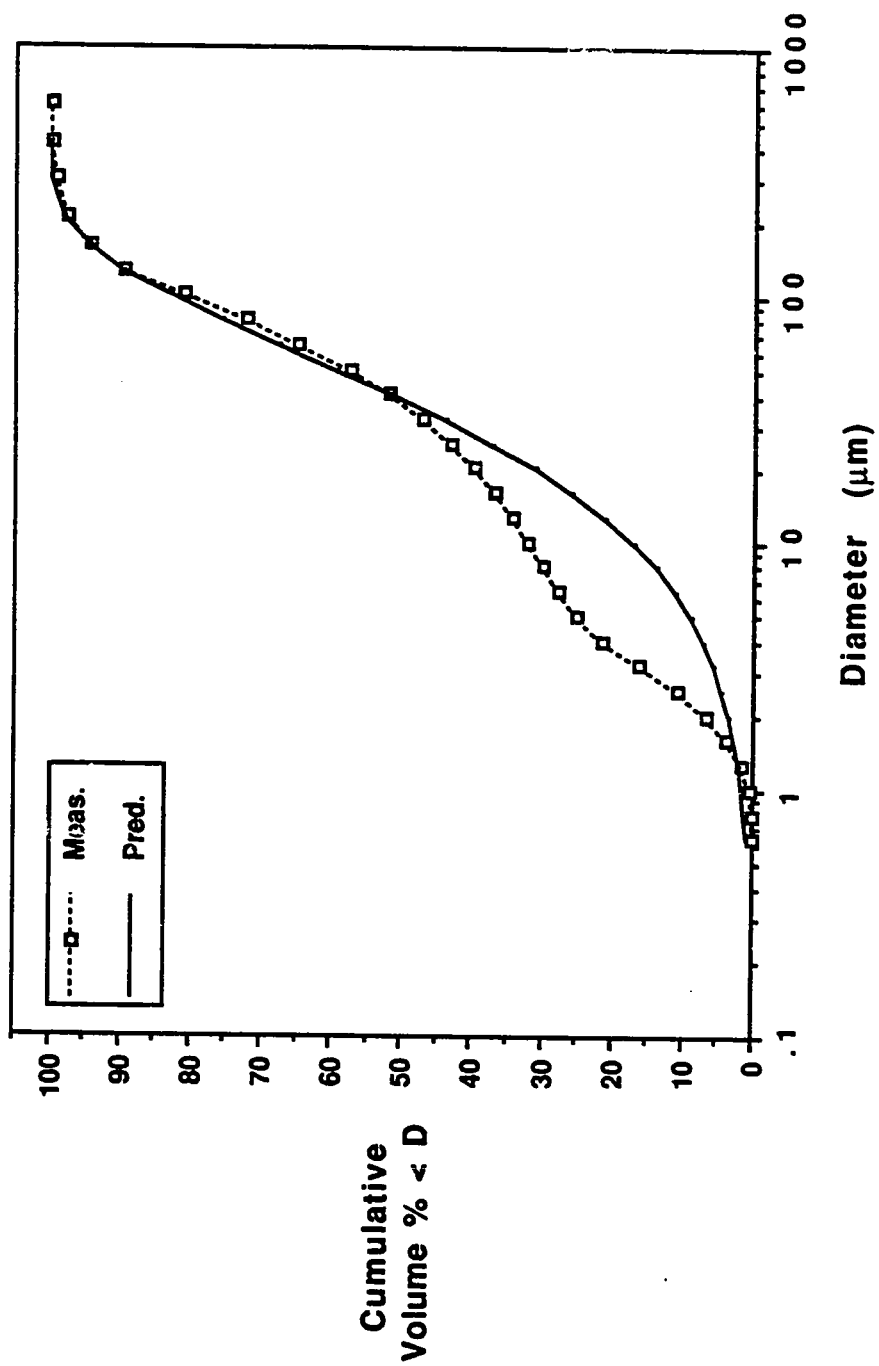


Figure 2.7: Cumulative Distribution for Fredonia Coarse  
 Predicted uses  $D_{100}=396$  microns,  $\text{Beta} = 1.9014$  and  $\text{Alpha} = 4$

microns. For Fredonia extra coarse the parameters were estimated from 92.9% < 149 microns and 54.4% < 44 microns. Using these measurements  $\beta$  was 1.9014 and  $d_{100}$  was 396 microns.

Once  $\beta$  and  $d_{100}$  are known, the complete distribution can be calculated using  $\alpha = 4$  in Equation (2-4). The predicted distributions are shown in Figures 2.5 to 2.7. These curves show that the log gamma function can predict the large end (> 40 microns) of the stones better than the fine ends (< 40 microns). This fit occurs because the sieve measurements used to determine  $\beta$  and  $d_{100}$  represent the larger end of the grind. Additionally since limestone grinds are formed from fresh and recycled material, some distributions become bimodal. However the log gamma distribution can fit only one of the peaks, and it is preferable to fit the large end because at high utilizations it is the larger sizes which remain to determine the dissolution rate.

Figure 2.8 shows predicted and measured distributions for a 1987-88 stone. Since sieve data were not available, predictions were made using the cumulative percent less than 40 and 80 microns which are approximate equivalent to 325 and 200 mesh, respectively. Figure 2.9 shows predicted distributions for Limestone 588 using cumulative data of 98.7% < 80.6 microns and 83.9% < 40.3 microns. Using these data sets when  $\alpha = 4$ ,  $\beta = 1.7196$  and  $d_{100} = 134$  microns. When  $\alpha = 6$ ,  $\beta = 1.1919$  and  $d_{100} = 171$  microns. It is apparent from this graph that even though the mean for this group was 6, either  $\alpha$  value will do an adequate job of estimating the finer ground limestones. This is a result of the insensitivity of the distributions to  $\alpha$  and is explained in the next section. Although  $\alpha = 4$  would be expected to move the peak to larger diameters relative to  $\alpha = 6$ , this effect was counteracted by the differences in the  $\beta$  values. The  $\beta$  for  $\alpha = 4$  was larger than the  $\beta$  for  $\alpha = 6$  resulting in a shift back to smaller diameters. Additionally  $d_{100}$  is better fit using an  $\alpha$  value of 4. The measured value was 128 microns, and the predicted values were 134  $\mu\text{m}$  for  $\alpha = 4$  compared to 171  $\mu\text{m}$  for  $\alpha = 6$ .

Figure 2.9 shows the effect of sieve choices on the predicted distributions for Longview Coarse. Three sets of sieve measurements were used: 93.9% < 149  $\mu\text{m}$ , 70.9% < 74  $\mu\text{m}$ , and 58.2% < 44  $\mu\text{m}$ . These sets were used in three pairs to generate the curves in Figure 2.9. When the 149 and 74  $\mu\text{m}$  pair is used,  $d_{100} = 353$   $\mu\text{m}$  and  $\beta$

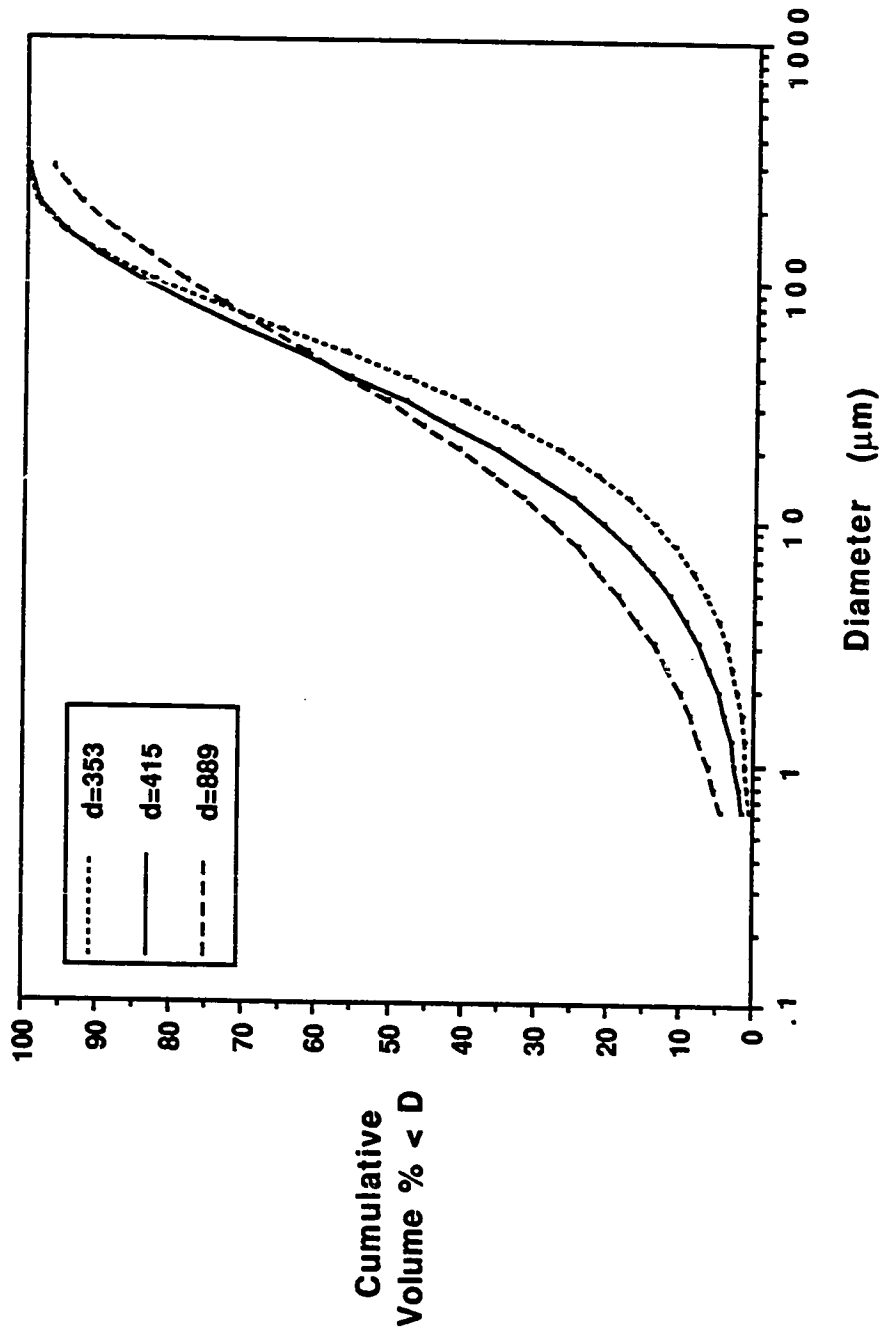


Figure 2.9: Longview Coarse Predicted Curves  
Effect of Sieve Selections for Alpha = 4

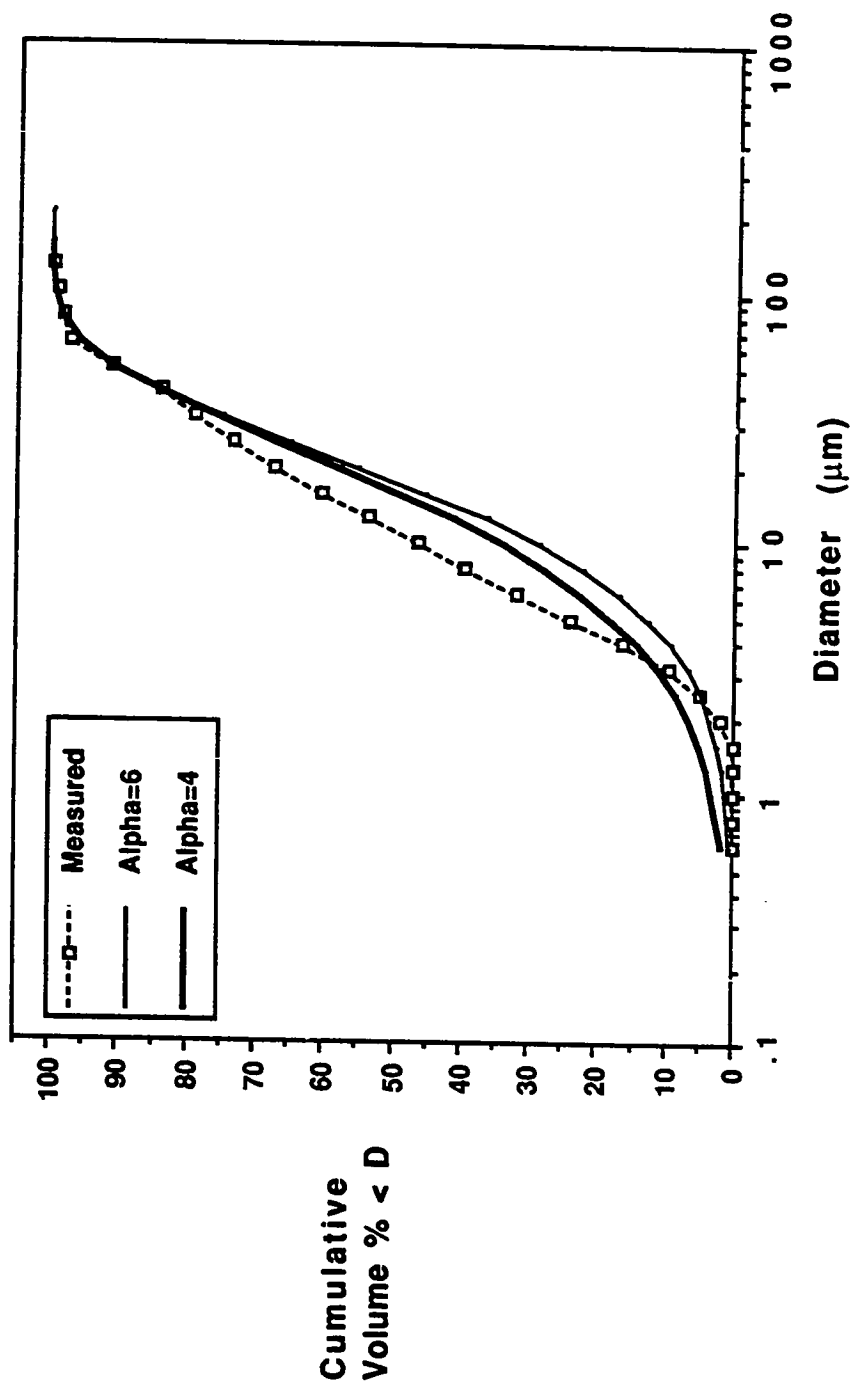


Figure 2.8: Cumulative Distributions for Limestone 588  
Effect of Alpha on Predicted Distribution



= 1.7204. When the 149 and 44  $\mu\text{m}$  pair is used,  $d_{100} = 415 \mu\text{m}$  and  $\beta = 2.0445$ . When the 74 and 44  $\mu\text{m}$  pair is used,  $d_{100} = 889 \mu\text{m}$  and  $\beta = 2.7394$ . From Figure 2.9 it is apparent that the first two pairs can do a good job of predicting the cumulative distribution. However the last pair (74 and 44  $\mu\text{m}$ ) does not fit as well. This is because the regressed  $d_{100}$  was about three times the measured value. As a result of this analysis, it seems important that one of the sieve measurements be in the 90-99% range.

The log gamma density function was used by Toprac (1981) to calculate limestone particle size distributions. His approach was to fix  $\beta$  and use empirical correlations to relate  $\alpha$  and  $d_{100}$  to the ratio of  $d_{90}$  to  $d_{50}$ , the diameters through which 90% and 50% pass, respectively. When this method is compared to the fixed  $\alpha$  approach, the new method proves to be better and has several advantages. For example, Table 2.3 compares the maximum particle sizes predicted by the fixed  $\alpha$  method for  $\alpha = 4$  and the empirical correlations derived by Toprac. It is apparent that the fixed  $\alpha$  method is superior to Toprac's method in determining  $d_{100}$ . The fixed  $\alpha$  method has the advantage of analytical integration whereas Toprac's method requires numerical integration. Additionally the fixed  $\alpha$  method has the advantage of being able to use any two sieve measurements while Toprac's method requires the two specific diameters through which 90% and 50% of the material passes. In general the present method would be expected to perform better because the fixed  $\alpha$  method uses the cumulative log gamma function itself to determine the unknown parameters from sieve data, while Toprac's method uses empirical correlations to determine his unknown parameters.

### 2.3.3 Statistical and Error Analysis

Since the slurry scrubber model will use the mean  $\alpha$  parameters to calculate distributions from sieve data, there are several statistical questions to be answered. First, between the two stone groups are the  $\alpha$  and  $\beta$  values statistically different? Then, if they are different, within a group is the actual  $\alpha$  value an integer? Assuming a normal distribution for the within-group means and variances, Table 2.4 lists the statistical parameters needed for the analysis of variance.

**Table 2.3: Comparison of the Measured Values of  $d_{100}$  to Values Predicted by the Fixed  $\alpha$  and Toprac Methods for 1980-81 Limestones**

	Meas.	Fixed $\alpha$	Toprac
Georgia Fine	101.6	111	84
Stoneman Fine	101.6	106	88
Longview Fine	128	121	198
Fredonia Feedbelt	161	162	860
Fredonia Fine	210	187	2571
Longview Coarse	297	353	1934
Georgia Coarse	420	305	255
Stoneman Coarse	420	284	257
Fredonia Coarse	595	395	436
Fredonia Extra Coarse	595	532	650

The first tests are the between-group comparisons. From Table 2.4 it is readily apparent that the mean  $\alpha$  values are different, however it is not as clear for the mean  $\beta$  values, thus a t-test is required. The hypothesis for this test is that the means for the  $\beta$  values are the same. For 17 degrees of freedom at a 5% level of significance, the hypothesis will be rejected if the t value is greater than 1.74. Since this test requires the variances, the between group variances must be compared and pooled. Using the F test with eleven and six degrees of freedom and a significance level of 1%, the between-group variances are considered to be estimates of the same variance if F is less than 7.79. ( $F = 4.03$  at 5% level of significance.) For the  $\beta$  variances from Table 2.4, F is calculated to be 6.94. The pooled variance is 0.17, and the resulting t-value becomes

6.756. Thus the hypothesis is rejected and the between-group  $\beta$  values are statistically different.

It has been shown that using integer values for  $\alpha$  reduces the numerical complexity of the analysis. This requires a within-group test for the mean. For the 1981-82 stones the hypothesis is  $\mu_0 = 4$ . For the one-tailed t-test with 11 degrees of freedom, this mean is rejected at a 5% level of significance if the t-value is greater than 1.80. The calculated t-value is 1.27, thus the hypothesis is not rejected. For the 87-88 stones the hypothesis is  $\mu_0 = 6$  which with 6 degrees of freedom would be rejected if the t-test value is greater than 1.94. The calculated t-value for these stones is 0.60, and therefore this hypothesis cannot be rejected either. The result of these statistical tests is to validate the choice of integer values for  $\alpha$  in the log gamma model.

The error associated with the prediction of the log gamma density parameters occurs from the inaccuracies in the Coulter Counter measurements. Once the counter is calibrated, the diameters of any channel are exact, however the volume percent in any channel can only be determined to  $\pm 10\%$  of the measured value. The effect of this inaccuracy on the log gamma parameters is found using Equations (2-11) and (2-12).

<b>Table 2.4: Statistical Parameters for the Log Gamma Parameters</b>					
	<b>Alpha</b>		<b>Beta</b>		<b>Number of</b>
	<b>Mean</b>	<b>Variance</b>	<b>Mean</b>	<b>Variance</b>	<b>Data Sets</b>
1981-82 Stones	3.752	0.458	1.814	0.243	12
1987-88 Stones	6.187	0.679	1.230	0.035	7

Solving Equation (2-11) for  $\alpha$  in terms of  $\beta$  yields Equation (2-13).

$$\alpha = \frac{3 \ln d_{100} - 3 \sum_i \ln(d_i) p_i}{\beta} \quad (2-13)$$

$\beta$  can be solved for in terms of the Coulter Counter data by ratioing (2-12) over (2-11).

$$\alpha = \frac{9 \{ \sum_i [\ln(d_i)]^2 p_i - [\sum_i \ln(d_i) p_i]^2 \}}{3 \ln d_{100} - 3 \sum_i \ln(d_i) p_i} \quad (2-14)$$

Taking the derivations of Equations (2-13) and (2-14) with respect to  $p_i$ , the Coulter Counter measurements, yields the corresponding errors in  $\alpha$  and  $\beta$  as shown in Equations (2-15) and (2-16).

$$d\alpha = \frac{[3B-A]\Delta\beta - 3\beta C}{\beta^2} \quad (2-15)$$

$$d\beta = \frac{9D(A-3B) + 9C(3B^2+3E-2AB)}{A^2-6AB+9B^2} \quad (2-16)$$

where

$$A = 3 \ln d_{100}$$

$$B = \sum_i (\ln d_i) p_i$$

$$C = \sum_i (\ln d_i) \Delta p_i$$

$$D = \sum_i (\ln d_i)^2 \Delta p_i$$

$$E = \sum_i (\ln d_i)^2 p_i$$

Using these derivatives, it was found that  $\alpha$  was not very sensitive to errors in the particle size measurements. A 10% error in the Coulter Counter measurements gives less than 0.1% error in  $\alpha$ . In reverse, this result says that the prediction of the particle size distribution will be very sensitive to small changes in  $\alpha$ . This helps to justify the method of fixing  $\alpha$ . The parameter  $\beta$  was more sensitive to errors in the

measurements. A 10% Coulter Counter error gives about 9% error in  $\beta$ . However this error is less than the standard error of the mean for  $\beta$ .

These sensitivity results also help to explain why the fixed  $\alpha$  method is superior to Toprac's method. Since there is a greater uncertainty in the value of  $\beta$ , fixing  $\beta$  could cause the selection of  $\alpha$  to be very inaccurate, thus resulting in an inadequate particle size distribution. It is better to fix  $\alpha$  since appropriate values for this parameter were well established by the method of moments. Once  $\alpha$  is fixed,  $\beta$  can be selected to give a better fit.

## 2.4 Summary

The log gamma density function was successfully applied to the prediction of limestone particle size distributions. This model had three unknown parameters:  $\alpha$ ,  $\beta$ , and  $d_{100}$ . The method of moments was used to regress the parameters for the model when the particle size distributions including  $d_{100}$  were known. Two groups of stones were regressed to find mean values of the log gamma parameters. For stones ground by a dry roller mill,  $\alpha = 3.75$  and  $\beta = 1.81$  and for stones ground in a wet ball mill  $\alpha = 6.19$  and  $\beta = 1.23$ . These differences were a result of the variabilities in the fineness of the grinds between the two mill types. Statistical analysis indicated that the  $\alpha$  means could be adequately represented by assuming integer values of 4 and 6.

A new method was proposed for predicting complete distributions from sieve data by fixing  $\alpha$ . Several important advantages result from the fixed  $\alpha$  method compared to the older fixed  $\beta$  method. By assuming that  $\alpha$  was an integer, the log gamma density function could be integrated analytically and the resulting cumulative function could be used to determine the remaining unknown parameters. The fixed  $\beta$  method required numerical integration and empirical correlations to determine its two unknown parameters. Sensitivity analysis also supported fixing  $\alpha$  over  $\beta$ . A comparison of the two methods also demonstrated that the common unknown parameter,  $d_{100}$ , was modeled more accurately using the fixed  $\alpha$  method. Despite the

differences in the  $\alpha$  means, particle size distributions from both dry roller mills and wet ball mills could be predicted by the log gamma model using sieve data with  $\alpha = 4$ .

## 2.5 Nomenclature

$d$  = diameter, microns

$d_{100}$  = maximum particle size, microns

$p_i$  = measured volume fraction for particle size  $i$

$W$  = random variable for log gamma density function

$t$  = time, seconds

### Greek letters

$\alpha$  = log gamma parameter, unitless

$\beta$  = log gamma parameter, unitless

$\Gamma(\alpha)$  = gamma function evaluated at  $\alpha$

## Chapter 3

### The Effect of Sulfite on Limestone Reactivity

#### 3.1 Introduction

Prediction of limestone dissolution is an important step in determining scrubber performance of flue gas desulfurization (FGD) processes. Accurate predictions, in turn, require an understanding of the factors which affect the dissolution process, particularly those factors representative of scrubbing systems. Most of the previous work on measurement of limestone dissolution rates has been done in aqueous acid systems with varying partial pressures of  $\text{CO}_2$ . The work has shown that at  $\text{pH} < 4$  the dissolution rate is controlled by mass transfer of  $\text{H}^+$  to the surface. Chan and Rochelle (1982) used mass transfer with homogeneous chemical reactions to predict measured dissolution rates at higher pH when  $\text{CO}_2$  is present. In these aqueous systems Toprac and Rochelle (1982) have shown that there is no effect of limestone type. Other researchers have interpreted some experiments as having dissolution rates with surface kinetics contributions. The present work indicates that when sulfite is present in these aqueous systems, limestone dissolution rates are inhibited. This effect has been successfully modeled using surface kinetics combined with mass transfer and a dependence on limestone type.

### 3.2 Theory

#### 3.2.1 Film Theory

This predictive model for limestone dissolution uses film theory to describe the mass transfer. For spherical particles the dissolution flux is given by Equation (3-1).

$$\text{Flux} = \frac{\rho}{\pi d^2 N_p} \frac{dV}{dt} = \frac{-D\Delta C}{\delta} \quad (3-1)$$

When using film theory for the mass transfer development, the ratio,  $(D/\delta)$ , is equivalent to the mass transfer coefficient.

Since the area at any time is well defined for monodispersed limestones, Equation (3-1) can be used directly to calculate either  $\delta$  or  $\Delta C$  from experimental data when the other variable and the rate are known. The film thickness,  $\delta$ , can be expressed as a function of the particle size when the mass transfer coefficient is determined through empirical correlations for mass transfer from a sphere.

For polydispersed stones the equivalent flux using film theory can be calculated using an "average" film thickness,  $\delta_{ave}$  as shown in Equation (3-2).

$$\text{Flux} = \frac{\rho V_{tot}}{\sum \pi d_i^2 N_{p_i}} \frac{dF}{dt} = \frac{-D\Delta C}{\delta_{ave}} \quad (3-2)$$

Unfortunately this equation can not be used directly since the total area at any time depends on the rate of dissolution, the total elapsed time, and the number of particles for each size. Thus a method must be developed to determine the area from the measured dissolution.

Polydispersed stones have been previously modeled by Chan and Rochelle (1982) and by Toprac and Rochelle (1982). In both studies the total rate of dissolution was expressed using the initial particle size distribution and the slope of the total fraction remaining versus time curve. Using a similar approach here, Equation (3-1) can be integrated for a single particle of initial size  $d_{0i}$  to give



$$d_i = d_{oi} \left(1 - \frac{\omega t}{d_{oi}}\right) \quad (3-3)$$

The parameter  $\omega t$  is found by iteration using Equation (3-4) until the desired utilization (or total fraction remaining) is reached.

$$U = 1 - F = 1 - \sum \phi_i \left(1 - \frac{\omega t}{d_{oi}}\right)^3 \quad (3-4)$$

The number of particles for any initial volume,  $V_{oi}$ , can also be written in terms of the particle size distribution by Equation (3-5).

$$N_{pi} = \frac{V_{tot}\phi_i}{V_{oi}} \quad (3-5)$$

Once  $\omega t$  is found for a given utilization using Equation (3-4), Equations (3-5) and (3-3) can be used to find the area available from each size fraction. These areas are then added to give the total area needed by Equation (3-2).

### 3.2.2 Mass Transfer Model

Since prediction of limestone dissolution rates requires knowledge of the surface concentrations, a chemical mass transfer model has been written to predict DAC. This model is a mass transfer extension to the Bechtel Modified Radian Equilibrium (BMREP) program (Epstein, 1975). BMREP is a computer code which solves the set of equilibrium and mass balance expressions applicable to an FGD system. The thermodynamic database of this model comes from the work of Lowell et al. (1970) who amassed (or measured) the temperature dependent parameters for the equilibrium constants of 41 chemical reactions. Lowell and his coworkers also assembled the temperature dependent parameters needed for the extended Debye-Huckel expression which predicts activity coefficients. The BMREP database was used as written with the exception of the temperature dependent parameters for  $\text{CaHCO}_3^+$ ,  $\text{CaCO}_3^0$ , and calcite solubility. These parameters were updated to the values given by Plummer and Busenberg (1982) as given in Equations (3-6) through (3-8). Additionally the model has been modified to assure charge balance in the bulk solution.

$$\log K_{\text{CaHCO}_3^+} = 1209.120 + 0.31294T - \frac{34765.05}{T} - 478.782\log T \quad (3-6)$$

$$\log K_{\text{CaCO}_3^0} = -1228.732 - 0.299444T + \frac{35512.75}{T} + 485.818\log T \quad (3-7)$$

$$\log K_c = -171.9065 - 0.077993T + \frac{2839.319}{T} + 71.595\log T \quad (3-8)$$

BMREP is used to calculate activity coefficients, concentrations, and equilibrium constants of the 41 FGD species. Then the mass transfer extension is called to calculate limestone surface species and reactivity. The model assumes equilibrium in the bulk and at the surface of the limestone dependent on the applicable boundary condition. Diffusivities used in the model were those values at 25°C given by Tseng (1986) and Chan (1982) (Appendix C). These values were corrected for temperature using the Stokes-Einstein relationship (Equation (3-9)).

$$D_{T^{\circ}\text{C}} = D_{25^{\circ}\text{C}} \frac{T^{\circ}\text{K}}{298^{\circ}\text{K}} \frac{\mu_{25^{\circ}\text{C}}}{\mu_{T^{\circ}\text{C}}} \quad (3-9)$$

The number of variables required by the model is reduced by defining pseudoconcentrations, pseudodiffusivities, and pseudoequilibrium constants from the rigorous data. Pseudoconcentrations are calculated from the equilibrium concentrations found by the rigorous model. A pseudoconcentration is defined as the sum of the ion pairs with their parent species. For example, the pseudoconcentration of bicarbonate is given by Equation (3-10).

$$[\text{HCO}_3^-]_p = [\text{HCO}_3^-] + [\text{CaHCO}_3^+] + [\text{MgHCO}_3^+] + [\text{NaHCO}_3^0] \quad (3-10)$$

Pseudodiffusivities and pseudoequilibrium constants are found from the pseudoconcentrations. The bicarbonate pseudodiffusivity is given by Equation (3-11).

$$D_{\text{HCO}_3} = \frac{\sum D_i [\text{HCO}_3^-]_i}{\sum [\text{HCO}_3^-]_i} \quad (3-11)$$

Here the summation over  $i$  is for the same species as given in Equation (3-10). The pseudoequilibrium constant for bicarbonate is determined from the bulk pseudoconcentrations. This constant is given by Equation (3-12).

$$K_{\text{HCO}_3^-} = \frac{[\text{H}^+]_p [\text{CO}_3^{2-}]_p}{[\text{HCO}_3^-]_p} \quad (3-12)$$

Once the bulk pseudoconditions are calculated, the mass transfer model uses film theory to converge on the surface concentrations. This model is subject to several flux constraints. Since sulfite and sulfate are not consumed or produced at the limestone surface, the net flux of each these species must be zero as shown in Equations (3-13) and (3-14).

$$D_{\text{HSO}_3}([\text{HSO}_3^-]_s - [\text{HSO}_3^-]_b) + D_{\text{SO}_3}([\text{SO}_3^{2-}]_s - [\text{SO}_3^{2-}]_b) = 0 \quad (3-13)$$

$$D_{\text{HSO}_4}([\text{HSO}_4^-]_s - [\text{HSO}_4^-]_b) + D_{\text{SO}_4}([\text{SO}_4^{2-}]_s - [\text{SO}_4^{2-}]_b) = 0 \quad (3-14)$$

In these equations and all future expressions the pseudoconcentration subscript has been dropped in order to simplify notation. All future concentrations will imply pseudoconcentrations unless otherwise noted.

Since FGD limestone dissolves in a highly ionic environment, the potential gradient at the surface is very small. The mass transfer model neglects this gradient and requires the charge flux to be zero between the surface and bulk (Equation (3-15)).

$$\begin{aligned} & D_{\text{Ca}}([\text{Ca}^{++}]_s - [\text{Ca}^{++}]_b) + D_{\text{HCO}_3}([\text{HCO}_3^-]_s - [\text{HCO}_3^-]_b) + \\ & D_{\text{CO}_3}([\text{CO}_3^{2-}]_s - [\text{CO}_3^{2-}]_b) + D_{\text{HSO}_3}([\text{HSO}_3^-]_s - [\text{HSO}_3^-]_b) + \\ & D_{\text{SO}_3}([\text{SO}_3^{2-}]_s - [\text{SO}_3^{2-}]_b) + D_{\text{HSO}_4}([\text{HSO}_4^-]_s - [\text{HSO}_4^-]_b) + \\ & D_{\text{SO}_4}([\text{SO}_4^{2-}]_s - [\text{SO}_4^{2-}]_b) + D_{\text{H}}([\text{H}^+]_s - [\text{H}^+]_b) + D_{\text{OH}}([\text{OH}^-]_s - [\text{OH}^-]_b) + \\ & D_{\text{Cl}}([\text{Cl}^-]_s - [\text{Cl}^-]_b) = 0 \end{aligned} \quad (3-15)$$

Additional cations, such as  $Mg^{++}$  or  $Na^+$ , and additional anions, such as adipate, are also included in the charge flux expression. Note that with a zero charge flux, charge balance at the surface is not explicitly satisfied.

The total calcium flux must equal the total carbonate flux (Equation (3-16)).

$$D_{Ca}([Ca^{++}]_s - [Ca^{++}]_b) = D_{HCO_3}([HCO_3^-]_s - [HCO_3^-]_b) + D_{CO_3}([CO_3^{=}]_s - [CO_3^{=}]_b) \quad (3-16)$$

The boundary condition which is satisfied at the limestone surface depends on the species present in the bulk solution. In the absence of sulfite species, the boundary condition is given by Equation (3-17), the solubility product of calcium carbonate.

$$[Ca^{++}]_s [CO_3^{=}]_s = K_{sp}(\text{calcite}) \quad (3-17)$$

It will be shown in the results section that in the presence of sulfite, limestone dissolves under a combined regime where resistances from both mass transfer and surface kinetics affect the overall rate. The form of the surface kinetics rate expression is written in terms of activities and is given by Equation (3-18).

$$\text{Flux} = k_c \frac{(CaCO_3^o_{eq} - CaCO_3^o_s)^{0.5}}{CaSO_3^o_s \cdot CaCO_3^o_s} \quad (3-18)$$

Therefore when sulfite is present, the boundary condition is the continuity of flux at the surface. In this case the calcium flux from the surface must equal the flux determined by the surface kinetic rate of Equation (3-18).

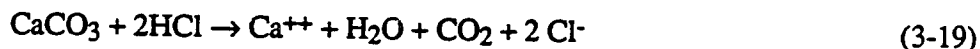
The bisection technique is used to iterate on the surface concentrations. The approach assumes a hydrogen ion concentration at the surface and then calculates the concentrations of other species using equilibrium constants and the flux expressions (Equations 3-13, 3-14, and 3-15). Calcium and carbonate fluxes are calculated and the appropriate boundary condition is selected (either Equation 3-17 or 3-18). The calculated surface conditions are compared to the selected boundary condition, and the

assumed hydrogen ion concentration is updated. This procedure is repeated until convergence is reached when the appropriate boundary condition is satisfied.

### 3.3 Experimental Apparatus and Procedure

#### 3.3.1 Batch Reagent Experiments

Limestone dissolution rates were measured in a batch mode using a pH stat apparatus consisting of a Fisher Model 360 electrometer and Model 395 Burette Dispenser (Figure 3.1). The basic stoichiometry used in this apparatus is given in Equation (3-19).



Experiments were performed in a batch slurry reactor with mechanical stirring. The reactor was a 700 ml jacketed beaker covered with a # 22 rubber stopper. Details of the reactor are shown in Figure 3.2. Solution temperature was controlled at  $55^\circ\text{C} \pm 0.5$  by water recirculation from an external bath. Agitation was provided by a three-blade propellor at 700 rpm which was sufficient to maintain suspension of the solids. Presaturated  $\text{CO}_2$  was sparged through the reactor solution during the experiments at a rate of 315 cc/min. All experiments were performed in a background solution of 0.1 M  $\text{CaCl}_2$  to provide constant ionic strength and to reduce changes in solution concentration as the limestone dissolved. The acid titrant was 1.00 N HCl. Experimental pH varied from 4.8 to 5.3.

Most experiments used reagent grade limestone (Reagent 1) whose particle size distribution was measured with a Model TAIL Coulter Counter (Table 3.1). To prevent the limestone from dissolving during the particle size measurements, four weight percent  $\text{CaCl}_2$  was used as the electrolyte.

Corning rugged bulb combination electrodes (Model No. X-EL) were used to measure pH. These electrodes were reconditioned every two weeks by replacing the reference electrode solution and treating the electrode for one hour in warm dilute acid solution. This procedure reduced electrode errors by preventing clogging of the

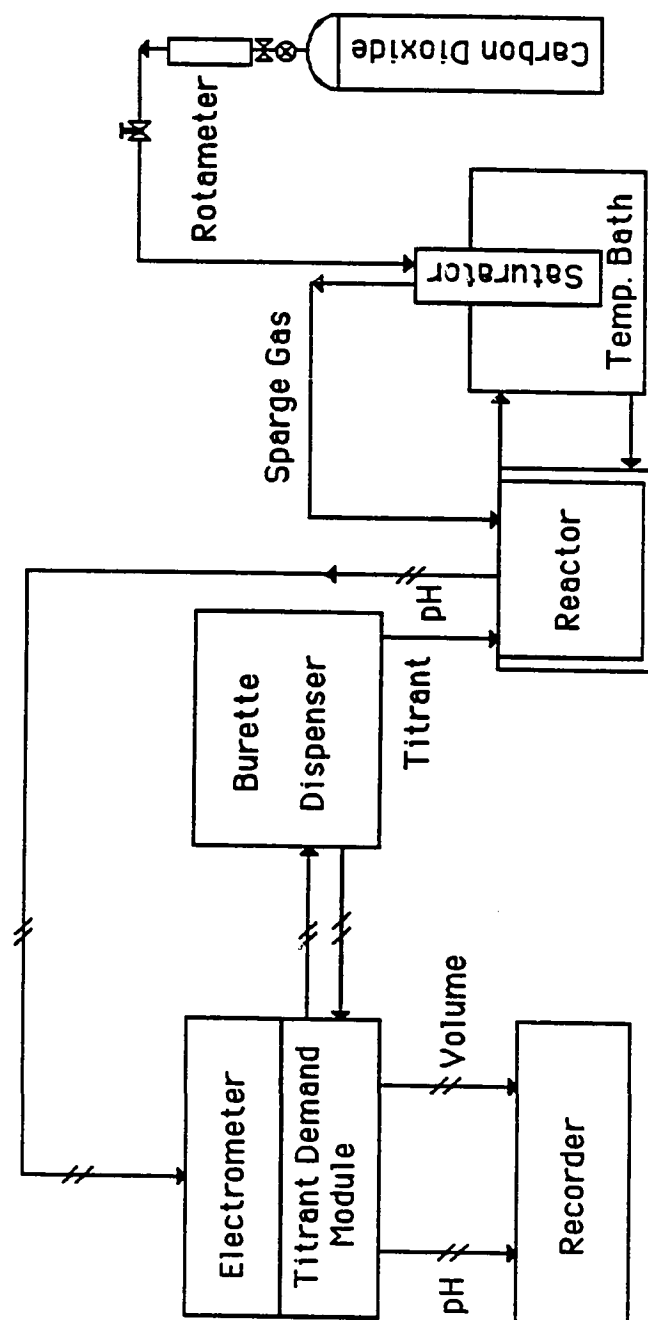


Figure 3.1: pH Stat Apparatus

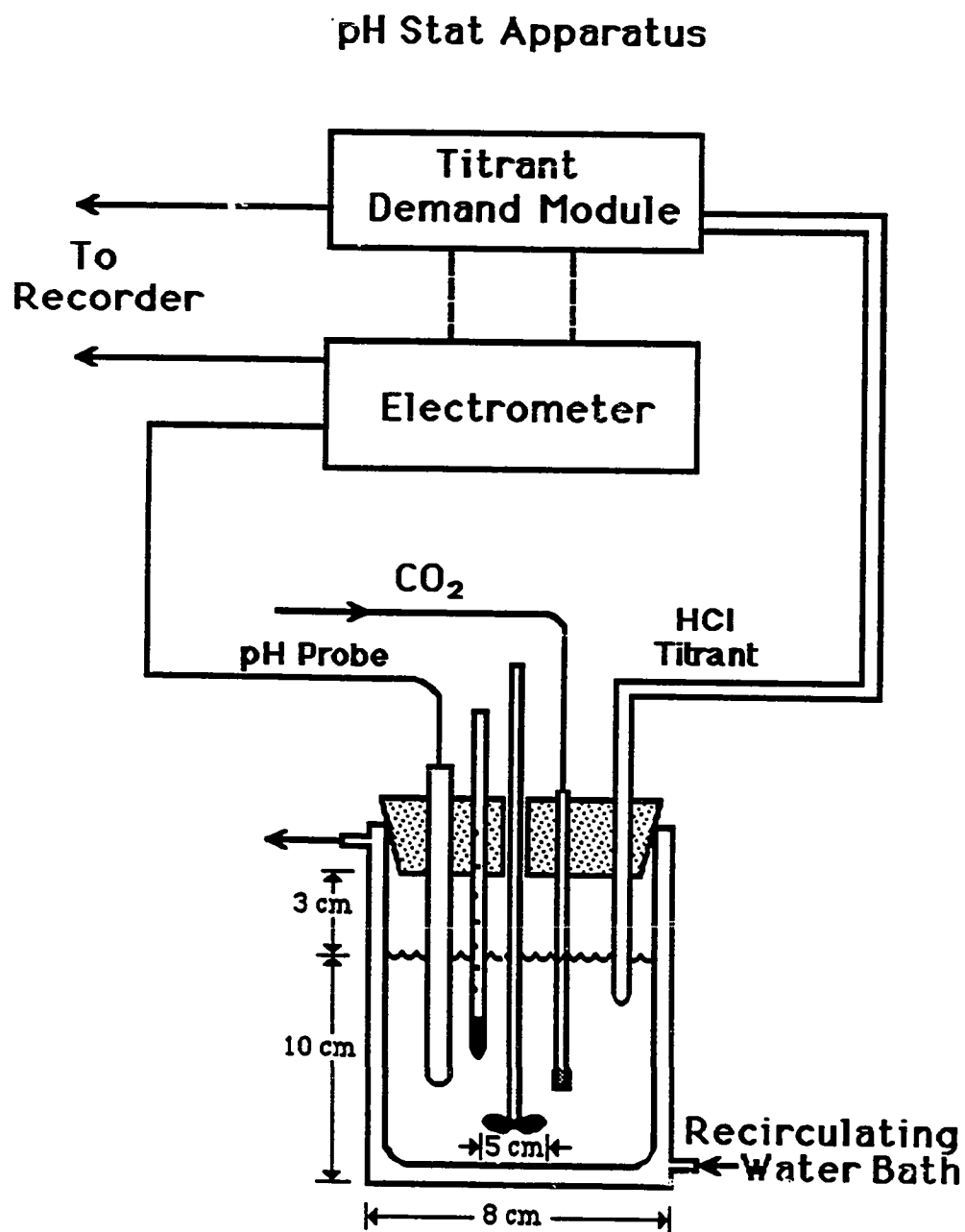


Figure 3.2: Experimental Reactor

**Table 3.1 Reagent 1 Particle Size Distribution**

<b>Diameter Microns</b>	<b>Differential Volume %</b>	<b>Cumulative Volume % &gt; D</b>
6.35	0.0	100.0
8.00	0.4	100.0
10.08	0.5	99.6
12.7	1.1	99.1
16.0	2.7	98.0
20.2	8.8	95.3
25.4	22.7	86.5
32.0	38.5	63.8
40.3	20.6	25.3
50.8	3.2	4.7
64.0	0.6	1.5
80.6	0.5	0.9
101.6	0.3	0.4
128.0	0.1	0.1
161.0	0.0	0.0

reference junction and by replacing adsorbed  $\text{Na}^+$  with  $\text{H}^+$  on the pH electrode tip. Electrodes were calibrated at 56°C before each experiment using a pH 5.06 buffer at the same ionic strength as the experiments (0.01N adipic acid- sodium hydroxide in 0.1M  $\text{CaCl}_2$ ).

Sulfate is a typical species present in scrubbing systems and is a known inhibitor for calcium sulfite crystallization. Therefore sodium sulfate was added to the solution to give sulfate concentrations ranging from 0 to 12 mM. Calcium sulfite saturations (CSS) were varied from 0 to 2.5 by addition of 0.5M sodium sulfite solution. Sulfite concentrations were monitored during the experiments by collecting and filtering approximately 2 ml of solution. This fluid was added to a preweighed aliquot of 0.1N iodine and reweighed to determine actual sample size. The sulfite concentration was then calculated by back titration with 0.01N sodium thiosulfate. Calcium sulfite saturation was calculated by ratioing the product of calcium and sulfite



concentrations over the solubility constant measured by Tseng (1986). This value is  $2.474 \times 10^{-7} \text{ M}^2$  at  $55^\circ\text{C}$  and is equivalent to 0.55 times the BMREP value. Calcium carbonate saturation was calculated by ratioing the product of calcium and carbonate concentrations over the solubility constant calculated from Equation (3-7).

At the start of the experiment sodium sulfate was added to 500 ml of  $\text{CaCl}_2$  solution and the mixture was heated to temperature.  $\text{CO}_2$  was sparged through this solution for approximately thirty minutes to presaturate the solution and to strip off  $\text{O}_2$  which could react with dissolved  $\text{SO}_3$  to form sulfate. Once equilibrium was obtained, sodium sulfite was added to give the desired concentration. This concentration was checked by iodometric titration to confirm the starting value (Appendix B). An experimental run was initiated by adding 1 g of limestone. During the experiment pH was then held constant to within  $\pm 0.02$  units by automatic addition of titrant. Electrode millivolt signals and the titrant acid addition rate were continuously monitored on a strip chart recorder. The cumulative dissolution of  $\text{CaCO}_3$  was found directly from the titrant rate using the stoichiometry of Equation (3-19). For experiments lasting longer than 30 minutes, the sulfite concentration was checked after one half hour and then after each additional hour. When there was a drop in sulfite concentration because of oxidation to sulfate, additional sulfite was added as  $\text{Na}_2\text{SO}_3/\text{NaHSO}_3$  at the pH of the experiment. As a result sulfite concentrations averaged within 8% of the starting value throughout the duration of the experiment. The error in titrant demand occurring from the oxidation of sulfite to sulfate was calculated to be less than 0.1% at the worst conditions (pH 5.3 and 6 mM sulfite). At the end of a run, the sulfite concentration was checked again and the solution was filtered to collect the solids for SEM or BET analyses.

Dissolution experiments were also performed using samples of four industrial limestones which were provided to the University of Texas in 1981 from the EPA type and grind study performed in 1979 through 1981. Experiments were performed in the Jarvis apparatus (Section 3.3.3) with Fredonia, Georgia Marble, Longview, and Stoneman limestones. A portion of each stone was screened to give sizes between 325 and 400 mesh. These samples were dissolved at the same sulfite base conditions as the Jarvis experiments. Dissolution experiments were also performed with the as-ground

fine limestones at pH 5.8 with 5 mM dissolved carbonate and 2 mM sulfite. These experiments were used to determine the surface rate constants necessary for modeling the EPA type and grind study.

### 3.3.3 Experimental Methods of Previous Work

The rate model was also applied to work done by Chan and Rochelle (1982) and by Jarvis et al. (1988). Using work done by other researchers allows the model to be tested against a wide range of conditions representative of scrubbers and hold tanks. Table 3.2 lists the characteristics of the four limestones analyzed by the rate model. The particle size distributions were measured for all stones except Reagent 2 as part of the present work (Appendix B). The distribution summaries in this table are the cumulative percents less than the specified diameter. The mean diameters for the reagent stones are calculated from the volume percent size distributions. The industrial stones were wet screened between 325 and 400 mesh to give the listed sizes.

BET surface areas were also measured as part of the present work. Because of the low surface areas associated with limestones, krypton was used as the adsorbent gas. Measured surface areas were accurate to  $\pm 0.02 \text{ m}^2/\text{g}$ . (Nitrogen measurements were only accurate to  $\pm 0.9 \text{ m}^2/\text{g}$ .)

The work performed by Chan and Rochelle (1982) was done using reagent  $\text{CaCO}_3$  (Reagent 2) in a batch pH stat apparatus with  $\text{N}_2$  sparging. The particle size distribution of this limestone was reported by Chan (1982), but BET surface area was not measured. The bulk of the experimental work was done at  $25^\circ\text{C}$ , although one series was performed at  $55^\circ\text{C}$  and pH 5. Rates for these experiments were measured at 50% dissolution. These reagent experiments combine well with the present work by addressing the effect of sulfite in a very low saturation of  $\text{CaCO}_3$  and by providing extensive data at  $25^\circ\text{C}$ .

Table 3.2: Limestone Characteristics				
Source	Reagent 1 Fisher (1988)	Reagent 2 Fisher (1981)	HSTC Beachville, On	Monteagle Tiftonia, Tn
Mg(Wt. %)	0.01	---	0.2	0.6
BET Area (m <sup>2</sup> /g)	0.22	---	0.27	2.23
PSD (μm)				
% < 6.35	0.0	1.6	0.0	0.0
% < 12.7	0.9	69.6	0.0	0.2
% < 25.4	13.5	99.8	1.1	2.0
% < 50.8	95.3	100	95.1	89.1
% < 80.6	99.0	100	99.3	99.6
Mean diameter	32.4	10.3	41.5	41.5

The experimental work done by Jarvis et al. (1988) involved the dissolution of the industrial limestones which were screened and collected to give particles between 325-400 mesh. The pH-stat apparatus used was a 2 liter sealed reactor operating in a batch mode for the solids and flow-through for the liquid. The bulk of their work was done at 50°C on two stones (HSTC and Monteagle) by varying CaCO<sub>3</sub> saturation at two fixed CaSO<sub>3</sub> saturations. For most experiments total dissolved carbonate was fixed at 2mM. Dissolution rates of eight other screened stones were measured at pH 5.5 in the absence and presence (CSS =1.6) of sulfite. In this work, initial rates were reported. These experiments test the applicability of the combined mass transfer and surface kinetics model on industrial limestones.

### 3.4 Results and Discussion

The results from the four major limestones are shown in Tables 3.3 to 3.6 and discussed in the next sections. The tables include the bulk solution concentrations, the measured dissolution fluxes, the calculated surface activities, and the fluxes predicted by the combined mass transfer and surface kinetics model. The measured fluxes were calculated from the measured absolute rates with spherical areas based on the particle size distributions. The surface activities were calculated from the mass transfer model by iterating on surface concentrations to satisfy the measured fluxes. The predicted fluxes were calculated from the mass transfer model using the surface kinetics rate expression as the boundary condition. In analyzing the results of batch limestone dissolution experiments the variables of interest relative to FGD systems are pH, CSS, and CCS (calcium carbonate saturation). For this work presented in Table 3.3, pH varied from 4.8 to 5.3, CSS varied from 0 to 2.8, and CCS varied from 0.02 to 0.26. Within these ranges, the measured flux for reagent  $\text{CaCO}_3$  varied from  $9.32 \times 10^{-10}$  to  $1.53 \times 10^{-8}$  gmol per  $\text{cm}^2\text{-sec}$ . Saturation to gypsum (calcium sulfate dihydrate) was 0.9 and the total area at 50% dissolution was  $2820 \text{ cm}^2$  ( $5640 \text{ cm}^2/\text{g}$ ).

For the industrial stones (Jarvis et al., 1988) presented in Tables 3.4 and 3.5, pH varied from 4.5 to 6.1, CSS varied from 0 to 1.9, and CCS varied from 0.01 to 0.25. The measured fluxes ranged from  $2.9 \times 10^{-10}$  to  $1.38 \times 10^{-8}$  gmole per  $\text{cm}^2\text{-sec}$  for HSTC limestone and from  $5.1 \times 10^{-10}$  to  $2.22 \times 10^{-8}$  gmole per  $\text{cm}^2\text{-sec}$  for Monteaule limestone. Gypsum saturation was 1.1 and the initial total area was  $510 \text{ cm}^2$  ( $535.4 \text{ cm}^2/\text{g}$ ).

For the work of Chan and Rochelle (1982) presented in Table 3.6, pH varied from 4.5 to 6.0, CSS varied from 0 to 7.2, and CCS was always less than 0.01. Within these ranges, the measured flux for reagent  $\text{CaCO}_3$  varied from  $3.4 \times 10^{-10}$  to  $9.08 \times 10^{-9}$ . Gypsum saturation was 0 and total area at 50% dissolution was  $8300 \text{ cm}^2$  ( $16,600 \text{ cm}^2/\text{g}$ ).

For reagent calcites (this work and Chan and Rochelle) which are polydispersed, the measured fluxes were taken at the time required for the cumulative dissolution to reach 50%. The flux was calculated using Equation (3-2). For the

**Table 3.3: Results with Reagent 2 Limestone**  
**At 55°C, 0.1M CaCl<sub>2</sub>, 0.01M Na<sub>2</sub>SO<sub>4</sub> and 0.85 atm CO<sub>2</sub>**

<b>Bulk Solution (M)</b>		<b>Surface Solution (M)<sup>†</sup></b>		<b>Flux (gmol/cm<sup>2</sup>-s)*</b>	
<b>pH</b>	<b>[SO<sub>3</sub><sup>=</sup>] (x10<sup>3</sup>)</b>	<b>aCaSO<sub>3</sub><sup>0</sup> (x10<sup>3</sup>)</b>	<b>aCaCO<sub>3</sub><sup>0</sup> (x10<sup>7</sup>)</b>	<b>Measured (x10<sup>9</sup>)</b>	<b>Predicted<sup>^</sup> (x10<sup>9</sup>)</b>
4.8	0.0	---	74.2	12.42	11.62
4.8	0.6	0.27	12.3	14.43	15.40
4.8	1.0	0.36	9.93	15.27	16.01
4.8	4.9	0.93	4.72	15.22	15.33
4.8	9.7	1.50	3.70	13.64	12.81
4.8	14.7	1.99	3.05	10.13	10.89
4.8	14.7	2.05	3.25	12.34	10.89
4.8	20.0	2.57	2.88	9.97	9.40
5.0	0.0	---	74.2	5.59	6.23
5.0	5.0	1.04	7.47	5.82	6.47
5.1	0.0	---	74.2	4.77	5.00
5.1	2.0	0.57	13.6	5.99	6.32
5.2	0.0	---	74.2	3.74	4.13
5.2	1.0	0.43	28.5	7.35	6.64
5.2	3.0	0.92	18.6	5.12	4.69
5.2	3.0	0.93	18.7	5.27	4.69
5.2	4.8	1.33	16.1	2.58	2.84
5.3	0.0	---	74.2	2.80	2.96
5.3	1.0	0.41	34.0	4.23	3.98
5.3	2.3	0.78	26.8	2.60	2.65
5.3	5.6	1.76	24.2	1.30	1.33
5.3	6.1	1.90	23.9	0.93	1.25
5.3	6.3	1.97	24.0	1.09	1.21

<sup>†</sup> Activities calculated using the measured fluxes and  $\delta = 3.4 \mu\text{m}$ .

\* Measured fluxes at 50% dissolution with 2820 cm<sup>2</sup> total area (5640 cm<sup>2</sup>/g).

<sup>^</sup> Fluxes predicted using  $k_c = 2.407 \times 10^{-12} \text{ M}^{5/2}\text{-cm/s}$  and  $\delta = 3.4 \mu\text{m}$ .

Table 3.4: Results with HSTC Limestone (Jarvis et al., 1988)

Bulk Solution (M)			Surface Solution (M) <sup>†</sup>		Flux(gmol/cm <sup>2</sup> /s) <sup>~</sup>	
pH	[SO <sub>3</sub> =] (x10 <sup>3</sup> )	Other (x10 <sup>3</sup> )	aCaSO <sub>3</sub> <sup>0</sup> (x10 <sup>3</sup> )	aCaCO <sub>3</sub> <sup>0</sup> (x10 <sup>7</sup> )	Measured (x10 <sup>9</sup> )	Predicted <sup>^</sup> (x10 <sup>9</sup> )
4.5	0.0	Base*	---	70.7	7.60	7.58
4.5	30	Base	1.63	0.61	13.77	14.32
5.0	0.0	Base	---	70.7	2.87	2.81
5.0	8.5	Base	1.25	1.22	6.66	7.81
5.0	17	Base	2.04	1.04	7.26	7.23
5.5	0.0	Base	---	70.7	1.09	1.06
5.5	0.75	Base	0.36	6.87	2.61	3.52
5.5	3	Base	0.98	4.39	3.38	3.42
5.5	6	Base	1.63	3.23	2.55	2.75
5.5	6	Base	1.66	3.40	2.90	2.75
5.8	0.0	Base	---	70.7	0.34	0.59
5.8	2	Base	0.89	10.3	1.64	1.58
5.8	3.75	Base	1.49	8.28	1.04	1.14
6.1	0.0	Base	---	70.7	0.27	0.31
6.1	1.25	Base	0.69	24.1	0.47	0.69
6.1	2.5	Base	1.33	22.5	0.41	0.42
5.0	17	8 CO <sub>3</sub> =	1.83	1.66	5.30	5.14
5.5	6	8 CO <sub>3</sub> =	1.53	0.98	1.63	1.03
5.5	6	100 Mg <sup>++</sup>	0.76	3.32	3.62	3.72
5.5	3	0 SO <sub>4</sub> =	1.09	5.42	4.02	3.13
5.5	6	0 SO <sub>4</sub> =	1.74	3.67	2.70	2.46
5.5	3	6 Adipic	0.74	3.27	4.07	5.19
5.5	6	6 Adipic	1.47	3.23	4.25	3.57
5.7	1.5	**	0.94	28.5	0.56	0.46
5.7	2	**	1.24	27.7	0.50	0.40
5.8	15	5 Ca <sup>++</sup>	1.36	1.76	8.44	7.30
5.8	30	5 Ca <sup>++</sup>	1.90	1.15	7.36	7.16
6.1	2.5	100 Mg <sup>++</sup>	0.88	18.7	0.31	0.73

<sup>†</sup> Activities calculated using the measured fluxes and  $\delta = 9.3 \mu\text{m}$ .

<sup>~</sup> Measured fluxes are initial rates with 510 cm<sup>2</sup> total area (535.4 cm<sup>2</sup>/g).

<sup>^</sup> Fluxes predicted using  $k_c = 5.93 \times 10^{-13} \text{ M}^{5/2}\text{-cm per sec}$  and  $\delta = 9.3 \mu\text{m}$ .

\* Base conditions: 50°C, 0.04 M Ca<sup>++</sup>, 0.015M Mg<sup>++</sup>, 0.027M Na<sup>+</sup>, 0.015 SO<sub>4</sub>=, 0.002M CO<sub>3</sub>=, and 0.0962M Cl<sup>-</sup>.

\*\* 144 mM Ca<sup>++</sup> and 3 mM CO<sub>3</sub>=

Table 3.5: Results with Monteagle Limestone (Jarvis et al., 1988)

Bulk Solution (M)			Surface Solution (M) <sup>†</sup>		Flux (gmol/cm <sup>2</sup> -s) <sup>~</sup>	
pH	[SO <sub>3</sub> <sup>=</sup> ]	Other	aCaSO <sub>3</sub> <sup>o</sup>	aCaCO <sub>3</sub> <sup>o</sup>	Measured	
Predicted <sup>^</sup>		(x10 <sup>3</sup> )	(x10 <sup>3</sup> )	(x10 <sup>3</sup> )	(x10 <sup>7</sup> )	(x10 <sup>9</sup> )
(x10 <sup>9</sup> )						
4.5	0.0	Base*	---	70.7	9.91	9.92
4.5	30	Base	1.84	0.84	22.21	22.80
5.0	0.0	Base	---	70.7	3.95	3.68
5.0	8.5	Base	1.49	1.96	12.92	12.84
5.0	17	Base	2.34	1.60	14.05	12.16
5.5	0.0	Base	---	70.7	1.31	1.39
5.5	0.75	Base	0.44	10.0	4.80	5.62
5.5	3	Base	1.21	7.07	8.25	6.09
5.5	3	Base	1.03	4.88	5.22	6.09
5.5	6	Base	1.67	3.47	4.00	5.27
5.5	6	Base	1.63	3.23	3.32	5.27
5.5	6	Base	1.67	3.50	3.97	5.27
5.8	0.0	Base	---	70.7	8.75	7.66
5.8	2	Base	1.02	14.0	4.39	3.09
5.8	3.75	Base	1.58	9.79	2.93	2.42
6.1	0.0	Base	---	70.7	0.48	0.39
6.6	1.25	Base	0.75	29.5	1.69	1.42
6.1	2.5	Base	1.36	23.9	1.05	0.96
5.0	17	8 CO <sub>3</sub> <sup>=</sup>	1.96	1.90	8.58	9.28
5.5	6	100 Mg <sup>++</sup>	1.28	3.74	6.25	6.99
5.5	3	0 SO <sub>4</sub> <sup>=</sup>	1.17	6.42	6.59	5.65
5.8	2	6 Adipic	0.79	9.48	4.21	4.50
5.8	3.75	6 Adipic	1.45	9.16	4.40	3.04
5.8	15	5 Ca <sup>++</sup>	1.57	2.56	18.20	13.57
5.8	30	5 Ca <sup>++</sup>	1.96	1.32	12.99	13.64
6.1	2.5	100 Mg <sup>++</sup>	0.90	20.2	1.09	1.59

<sup>†</sup> Activities calculated using measured fluxes and  $\delta = 7.1 \mu\text{m}$ .

<sup>~</sup> Measured fluxes are initial rates with 510 cm<sup>2</sup> area (535.4 cm<sup>2</sup>/g).

<sup>^</sup> Fluxes predicted using  $k_c = 1.406 \times 10^{-12} \text{ M}^{5/2}\text{-cm per sec}$  and  $\delta = 7.1 \mu\text{m}$ .

\* Base conditions: 50°C, 0.04 M Ca<sup>++</sup>, 0.015M Mg<sup>++</sup>, 0.027M Na<sup>+</sup>, 0.015 SO<sub>4</sub><sup>=</sup>, 0.002M CO<sub>3</sub><sup>=</sup>, and 0.0962M Cl<sup>-</sup>.

Table 3.6: Results for Reagent 2 Limestone  
(Chan and Rochelle, 1982)  
Experiments at 25°C , 0.1M CaCl<sub>2</sub>, and N<sub>2</sub> Sparging

<u>Bulk Solution (M)</u>		<u>Surface Solution (M)<sup>†</sup></u>		<u>Flux (gmol/cm<sup>2</sup>-s)<sup>~</sup></u>	
pH	[SO <sub>3</sub> =] (x10 <sup>3</sup> )	aCaSO <sub>3</sub> <sup>o</sup> (x10 <sup>3</sup> )	aCaCO <sub>3</sub> <sup>o</sup> (x10 <sup>7</sup> )	Measured (x10 <sup>9</sup> )	Predicted <sup>^</sup> (x10 <sup>9</sup> )
4.5	0.0	---	55.5	4.87	4.87
4.5	0.9	0.43	1.43	7.02	7.18
4.5	3.0	0.75	0.70	7.55	7.96
4.5	5.8	1.22	0.69	9.08	8.14
4.5	8.7	1.45	0.53	8.83	8.08
4.5	27.0	2.90	0.34	9.07	7.33
4.5	38.0	3.41	0.22	7.28	6.97
5.0	0.0	---	55.5	1.36	1.64
5.0	0.9	0.50	0.96	3.39	4.48
5.0	3.2	1.19	0.74	4.41	4.82
5.0	6.3	1.89	0.56	4.41	4.52
5.0	13.2	3.19	0.31	3.13	3.86
5.0	20.0	4.34	0.16	1.56	3.43
5.5	0.0	---	55.5	0.74	0.68
5.5	1.0	0.78	2.03	2.60	2.86
5.5	1.8	1.35	2.81	3.97	2.85
5.5	2.6	1.73	2.21	3.89	2.70
5.5	5.8	2.85	0.33	0.85	2.19
5.75	0.0	---	55.5	0.54	0.49
5.75	1.0	0.82	2.02	1.69	2.14
5.75	1.7	1.30	1.90	1.93	2.07
5.75	3.5	2.32	0.97	1.23	1.74
6.0	0.0	---	55.5	0.36	0.35
6.0	1.0	0.85	2.02	0.90	1.51
6.0	1.7	1.10	1.06	0.46	1.47
6.0	3.1	2.32	0.83	0.34	1.19



Table 3.6(con't): Results for Reagent 2 Limestone  
(Chan and Rochelle, 1982)  
Experiments at 25°C , 0.1M CaCl<sub>2</sub>, and N<sub>2</sub> Sparging

<u>Bulk Solution (M)</u>		<u>Surface Solution (M)<sup>†</sup></u>		<u>Flux (gmol/cm<sup>2</sup>-s)<sup>~</sup></u>	
pH	[SO <sub>3</sub> <sup>=</sup> ] (x10 <sup>3</sup> )	aCaSO <sub>3</sub> <sup>o</sup> (x10 <sup>3</sup> )	aCaCO <sub>3</sub> <sup>o</sup> (x10 <sup>7</sup> )	Measured (x10 <sup>9</sup> )	Predicted <sup>^</sup> (x10 <sup>9</sup> )
5.0 *	0.0	---	74.2	3.94	3.94
5.0	0.7	0.33	2.26	5.58	7.17
5.0	2.8	0.99	2.25	8.54	7.37
5.0	5.8	1.58	1.80	8.88	6.62
5.0	11.1	2.39	0.87	5.58	5.66

<sup>†</sup> Activities calculated using measured fluxes and  $\delta = 7.3 \mu\text{m}$ .

<sup>~</sup> Measured fluxes at 50% dissolution with 8300 cm<sup>2</sup> area (16,600cm<sup>2</sup>/g).

<sup>^</sup> Fluxes predicted using  $k_c = 2.436 \times 10^{-13} \text{ M}^{5/2}\text{-cm per sec}$  and  $\delta = 7.3 \mu\text{m}$ .

\* This series performed at 55°C. Activities at 55°C calculated using  $\delta = 6.3 \mu\text{m}$ .

Fluxes at 55°C predicted using  $k_c = 2.244 \times 10^{-12} \text{ gmol}^{5/2}\text{-cm per liter}^{5/2}\text{-sec}$  and  $\delta = 6.3 \mu\text{m}$ .

industrial stones which were screened, the measured fluxes were calculated from the measured initial rates using Equation (3-1) and assuming a monodispersed stone of 41.5 microns in spherical diameter.

The measured fluxes from the zero sulfite cases were used with the mass transfer model to calculate apparent film thicknesses. In the absence of sulfite, limestone dissolution is controlled by mass transfer, thus the boundary condition in the mass transfer model is given by Equation (3-17). This condition along with the bulk solution compositions specifies the applicable driving forces. When these calculated driving forces are used with the measured rates, Equation (3-1) or (3-2) can be solved to give an estimate of the hypothetical film thickness around the particles. Once the film thickness was estimated, it was used with the sulfite experimental rates to calculate the surface activities shown in the Tables. The form of the kinetic rate expression was found by plotting surface concentrations against experimental rates. The surface rate constants and film thicknesses for all limestones are shown in Table 3.7.

#### 3.4.1 SEM Observations

SEM micrographs were taken of many of the partially dissolved limestones. Figures 3.3 to 3.5 show some of the typical features observed on the reagent calcite. All micrographs include a reference length of 10 microns. Figure 3.3 is a view of the undissolved reagent calcite. The crystals are fused blocky crystallites typical of precipitated calcite. Figure 3.4 is a micrograph of the reagent calcite at 55% dissolution in the absence of sulfite. In this environment dissolution is controlled by mass transfer, and the expected effect on the crystal shape is to round off the corners and edges. This result is clearly seen in the micrograph.

Figure 3.5 is a view of reagent calcite at 55% dissolution in the presence of 6.1 mM  $\text{SO}_3^{2-}$  at pH 5.3. From this micrograph it is clear that a different dissolution phenomenon is occurring when sulfite is present. Spikes and nodules were typical features seen in all the sulfite experiments at all pH values. The industrial limestones also produced these unusual surface features. It appears that some of the surfaces have been blocked from dissolving while opposing faces are eaten away towards the center.

**Table 3.7: Rate Constants and Film Thicknesses  
at 50°C for the Experimental Limestones\***

Stone	$k_c(\times 10^{13})^{\wedge}$	$\delta(\times 10^4)$ cm	BET area $m^2/g$	Mg wt %
Reagent 1**	24.07	3.4	0.227	0.01
Reagent 2***	2.44	7.3	---	--
HSTC	5.93	9.3	0.267	0.20
Monteagle	14.06	7.1	2.226	0.60
Maysville	17.50	9.0	1.174	1.7
Arapahoe	5.53	7.5	0.305	0.12
Iceland Spar	2.18	7.3	1.052	0.04
Edwards	4.63	9.7	0.837	0.10
Limestone B	12.71	8.1	1.062	0.10
Limestone C	5.74	8.1	1.188	0.0
Limestone D	8.93	9.3	1.502	3.1
Limestone A	4.70	8.1	1.946	0.19
Fredonia†	13.00	8.0	1.988	1.3
Georgia	3.77	3.8	0.915	1.1
Stoneman	8.15	--	1.910	4.6
Longview	6.58	--	---	--

\* Film thickness from measured fluxes at pH 5.5, CCS = 0.026, and CSS = 0.0. Rate constants from measured fluxes at pH 5.5, CCS = 0.026, and CSS = 1.6.

<sup>^</sup> Rate constant has units of  $M^{5/2}$ -cm per-sec.

\*\* For reagent calcite T= 55°C, pH = 5.3, CCS = 0.26, and CSS = 2.0.

\*\*\* For this reagent T=25°C, pH = 5.0, CCS = 0.0006, and CSS = 2.3.

† The last four limestones were run separately to provide the constants required for the Slurry Scrubber model. These stones were screened to 325-400 mesh. Film thicknesses come from measured fluxes at pH 5.0, CCS = 0.026, and CSS = 0.0. Rate constants from measured fluxes at pH 5.5, CCS = 0.026, and CSS = 1.6.



Figure 3.3 Reagent 1 Calcite - Raw Sample



Figure 3.4: Dissolved Reagent 1 - Mass Transfer Regime  
Exp. 67- pH 5.3, 0.1M  $\text{CaCl}_2$ , 0.85 atm  $\text{CO}_2$ , 55°C, 55% dissolved



Figure 3.5: Dissolved Reagent 1 - Surface Kinetics Regime  
Exp. 77- pH 5.3, 0.1M  $\text{CaCl}_2$ , 0.85 atm  $\text{CO}_2$ , 55°C, 6.1 mM  $\text{SO}_3$ , 55% dissolved

This observation of fast and slow dissolving sites supports the conclusion that in the presence of sulfite, limestone dissolution is controlled by surface reaction kinetics.

Figures 3.6 and 3.7 are micrographs of undissolved Edwards and Iceland Spar limestones. Figures 3.8 and 3.9 are these limestones after partial dissolution in the presence of sulfite. The spikes and nodules observed on reagent  $\text{CaCO}_3$  are also clearly seen on the industrial limestones. An important application of the SEM microscope is the Energy Dispersive Spectrographic analyzer(EDS). As the electron beam strikes the sample, x-rays are fluoresced. These x-rays are characteristic of the elements within the sample. In order to reduce interference, samples which are analyzed by EDS should not be coated. A coating of gold or palladium is typically applied to non-conducting samples such as limestone in order to improve picture quality and the imaging performance of the microscope.

The EDS analyzer was used to scan an uncoated sample of limestone exposed to sulfite. A sample was prepared by adding limestone to 6 mM sulfite at pH 5.3. The sample was allowed to dissolve to equilibrium pH. The limestone was then collected on a filter and rinsed with  $\text{CaCl}_2$  to remove traces of the sulfite solution from the surface. Figure 3.10 shows the result of the EDS scan. Using the ratio of x-ray counts from calcium and sulfur shows that 1 wt. percent of the sample is sulfur. This percentage is not strictly a surface representation because the x-rays are backscattered from a depth of a few microns. Therefore this percentage represents the amount within a thin shell at the surface. The chloride trace on the spectrogram is a result of the wash. Figure 3.11 shows the result of an EDS scan on a calcium sulfite particle. The x-ray counts from this sample show the expected 50-50 distribution for calcium and sulfur. A comparison of these scans helps to support the hypothesis that sulfite adsorbs onto the limestone surface as part of the inhibiting process.

#### 3.4.2 Film Thickness

If mass transfer controls the dissolution rate, the estimated film thickness should not depend on pH. This was found to be true, since for a given limestone, a

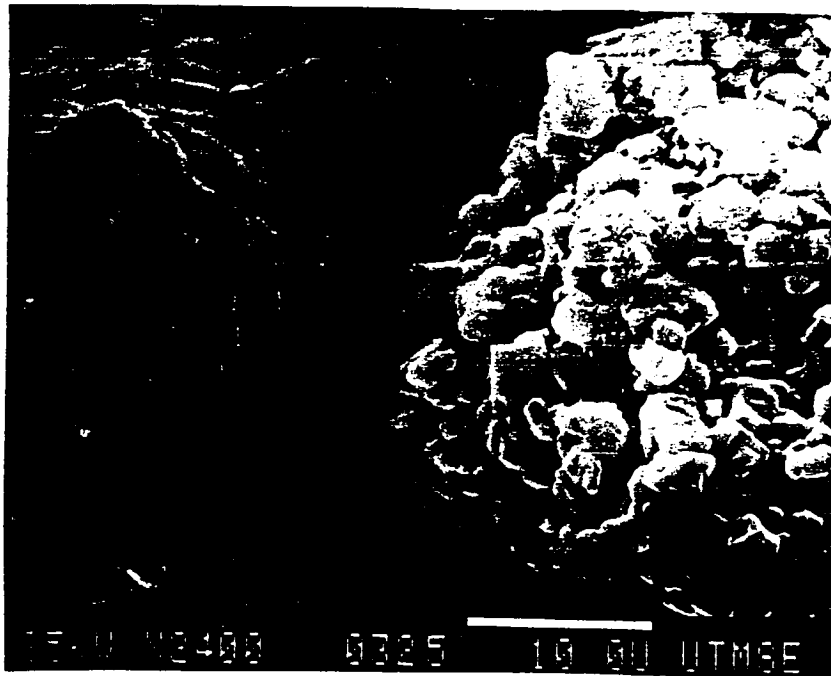


Figure 3.6: Edwards Limestone - Raw Sample



Figure 3.7: Iceland Spar - Raw Sample



Figure 3.8: Edwards Limestone in 6.1 mM  $\text{SO}_3$ , 30% dissolved  
Exp. 74 - pH 5.3, 0.1M  $\text{CaCl}_2$ , 0.85 atm  $\text{CO}_2$ , 55°C

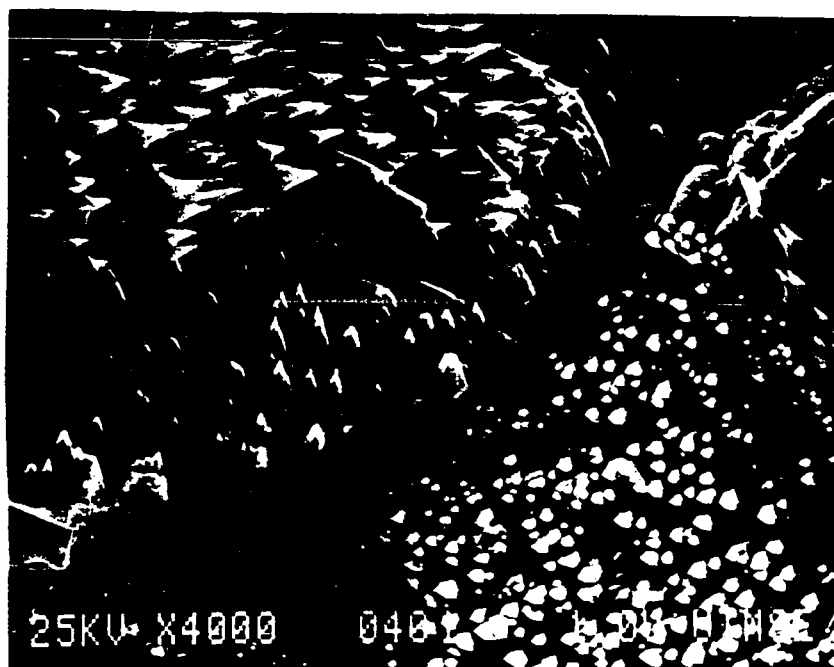


Figure 3.9: Iceland Spar in 6 mM  $\text{SO}_3$ , 50% dissolved  
Jarvis Exp. A4.1 - pH 5.5, Base Conditions, 50°C



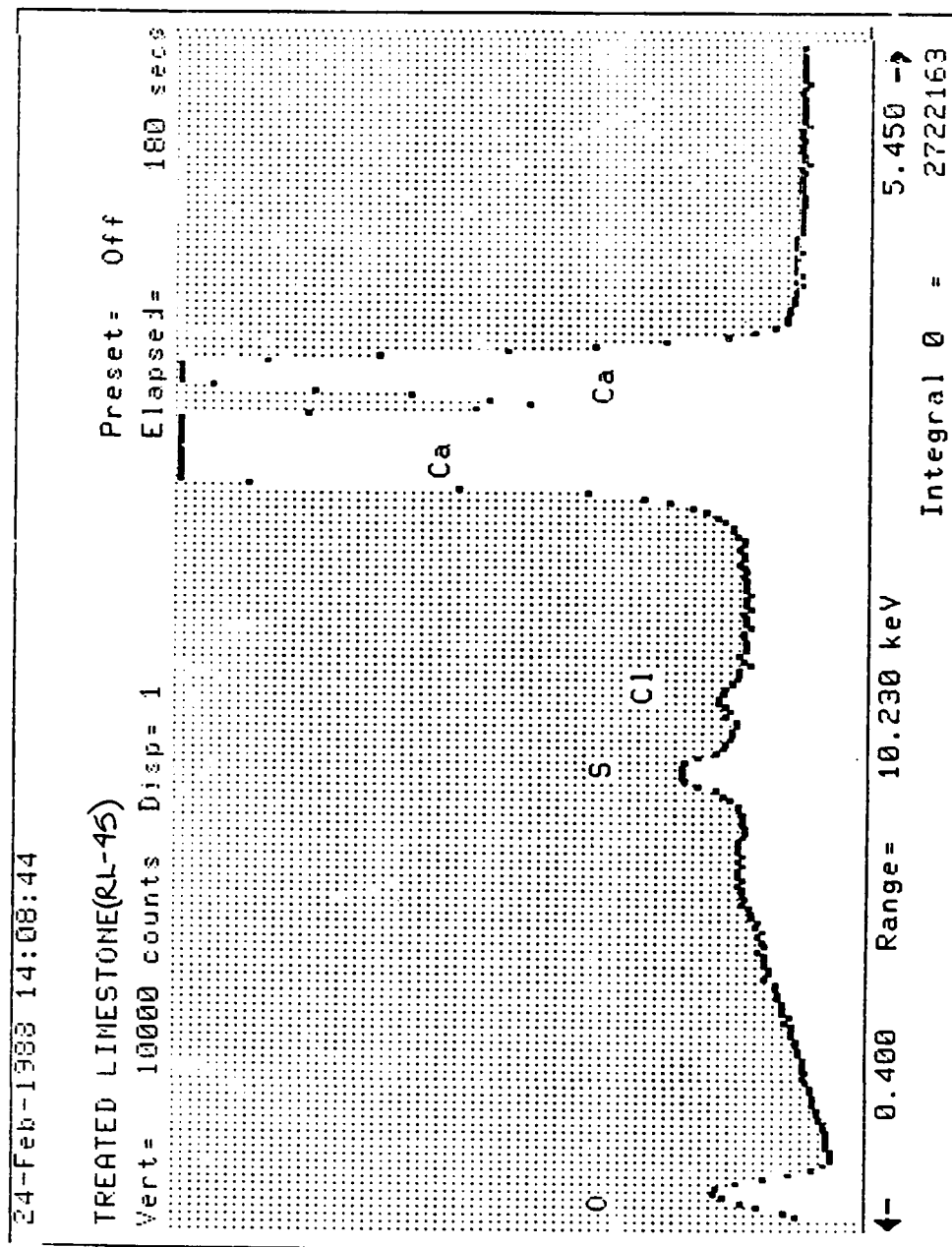


Figure 3.10: Energy Dispersive Spectrographic Analysis of a Limestone Particle Partially Dissolved in 6 mM Sulfite at pH 5.3.

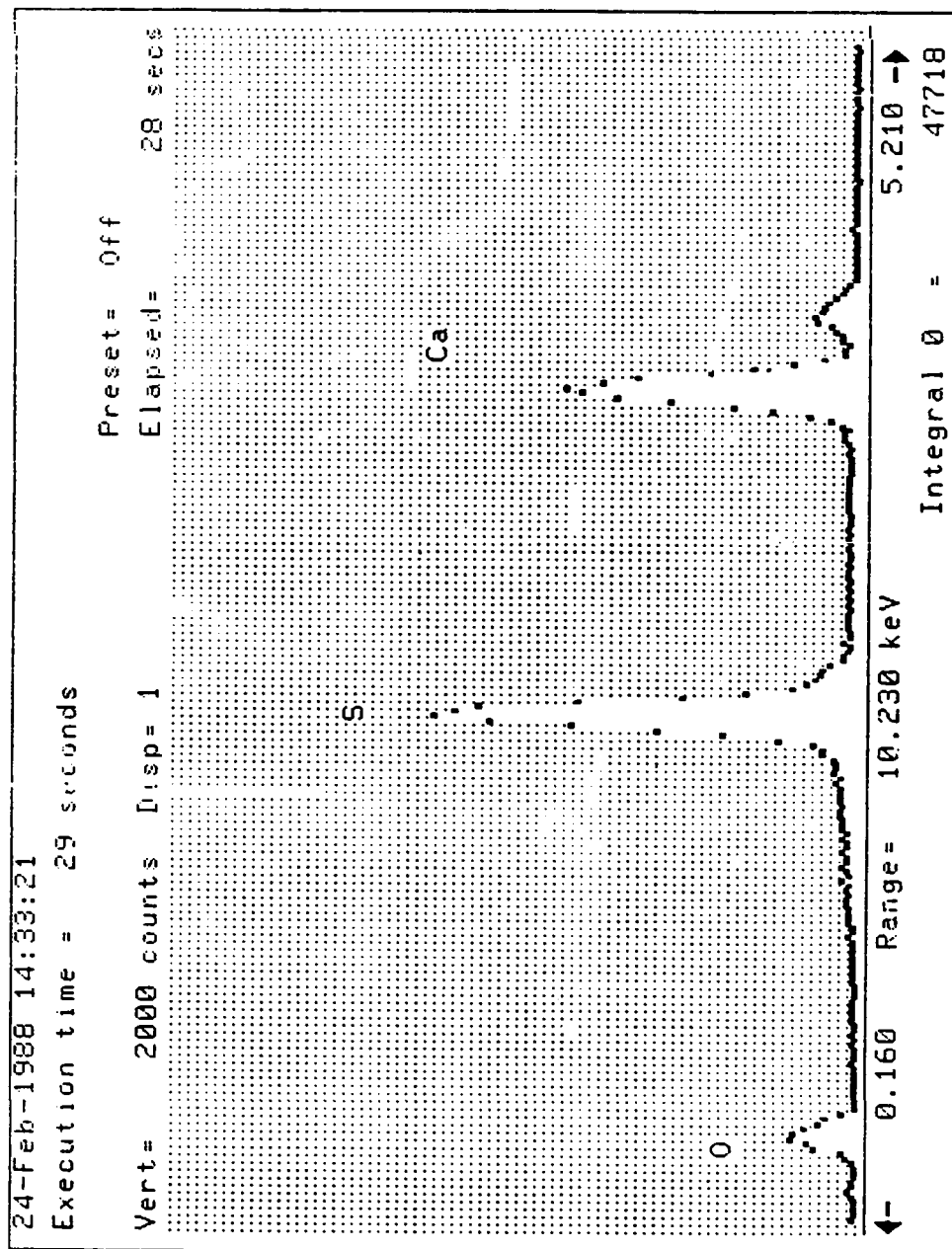


Figure 3.11: Energy Dispersive Spectrographic Analysis of a Calcium Sulfite Particle

single value of  $\delta$  predicted the measured rate to within 15%. The single exception was the HSTC case at pH 5.8 which Jarvis (1988) identified as an outlier.

The measured values of  $\delta$  ranged from 3.4 to 9.7  $\mu\text{m}$ . These data can be compared to values calculated from theory using the measured particle sizes. The theoretical calculations involve correlations for the mass transfer coefficient since the film thickness is inversely proportional to the mass transfer coefficient. In stagnant film theory where the Sherwood number is 2, the resulting mass transfer coefficient relationship gives film thicknesses equal to one-half the particle diameter. With this theory the predicted values of  $\delta$  range from 14 to 21  $\mu\text{m}$ . These values are from two to five times greater than the measured values. Film thickness can also be predicted using the mass transfer approach developed by Toprac and Rochelle (1982). Following their theory which developed a correlation for the mass transfer coefficient in agitated systems, the film thickness was derived and is given by Equation (3-20).

$$\delta = \frac{d}{2 + 1.612Bd} \quad (3-20)$$

In this equation B is a mass transfer enhancement factor accounting for the effects of agitation and the contribution of the  $\text{CO}_2$  hydrolysis reaction to limestone dissolution. In the absence of  $\text{CO}_2$ , Toprac (1981) estimated B to have a value of 400  $\text{cm}^{-1}$ . With  $\text{CO}_2$  sparging, B varied from 260 to 880  $\text{cm}^{-1}$  as pH increased from 4 to 5. B increases because as the hydrogen ion concentration decreases, the contribution of  $\text{CO}_2$  hydrolysis to limestone dissolution becomes more important. Using a B value of 400  $\text{cm}^{-1}$  on the limestones of this study, the calculated film thicknesses ranged from 7 to 9  $\mu\text{m}$ . At  $B = 880 \text{ cm}^{-1}$ ,  $\delta$  varied from 4 to 6  $\mu\text{m}$ . These values are in good agreement with the measured film thicknesses.

The measured film thicknesses can also be compared to the values determined by Sverdrup and Bjerle (1982) for dissolving calcite. These researchers measured mass transfer coefficients for screened calcite in a pH stat apparatus and concluded that dissolution was controlled by mass transfer of hydrogen ion. For screened limestones from 10 to 400 microns, the mass transfer coefficient was relatively constant, varying only from 0.55 to  $1.04 \times 10^{-3} \text{ m/s}$ . Using a hydrogen ion diffusion coefficient of  $9.3 \times$

$10^{-5}$  cm/s (Landolt-Bornstein, 1960) the corresponding film thicknesses are from 16 to 8  $\mu\text{m}$ , respectively. These values are on the same order as the film thicknesses measured in this work.

In this study the film thicknesses varied among the four limestones. Stone to stone variations could occur for several reasons. For reagent calcites, differences in particle size distribution will cause  $\delta_{\text{ave}}$  to vary. Also, as discussed previously,  $\text{CO}_2$  sparging will be expected to cause a change in  $\delta$  since the model does not explicitly account for the  $\text{CO}_2$  contribution to the rate. The work of Chan (Reagent 2) was performed in the absence of  $\text{CO}_2$ , and therefore the measured  $\delta$  would be larger than the present work (Reagent 1) which used  $\text{CO}_2$  sparging. Additionally the larger particles of the Reagent 1 calcite would require higher agitation to maintain suspension of the particles. Increases in agitation will cause decreases in  $\delta$ .

For the industrial stones which have the same diameter, the differences occur because of differences in the surface roughness. These stones have been screened to give the same spherical size, yet BET measurements show that the Monteagle stone has ten times the surface area as the HSTC stone (Table 3.2).

#### 3.4.3 Effects of Sulfite

Figure 3.12 shows measured and predicted rates for three of the pH values studied in this work. The data show that at low concentrations of sulfite and for a given pH, the dissolution rate is enhanced over the rate observed in the absence of sulfite. The experiments also indicated that at higher concentrations of sulfite, the rates become inhibited and in some cases are even lower than the zero sulfite rates. These phenomena concur with the observations made by Chan and Rochelle (1982). The ideal rate for pH 4.8 shown on Figure 3.12 is the rate calculated by assuming that mass transfer alone controls the dissolution. In this situation sulfite acts only as a buffer, and the limestone surface is saturated to calcite. It is clear from Figure 3.12 that mass transfer alone can not predict the observed rates because it does not account for the inhibiting effect of sulfite. The predicted rates shown for all three values of pH are those values calculated by the complete model including mass transfer and surface kinetics with the rate constants and film thicknesses listed in Table 3.7. The complete

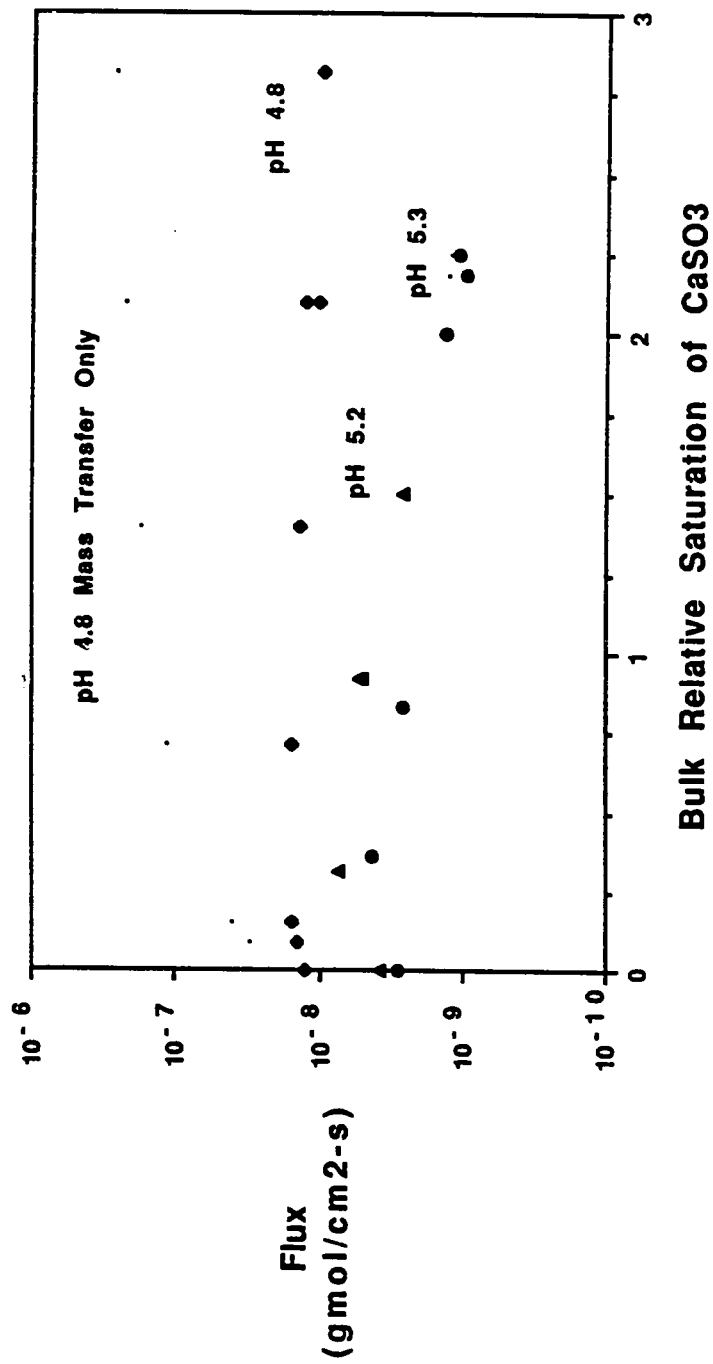


Figure 3.12: Effect of Sulfite on Fluxes of Reagent 1 Calcite in 0.1M  $\text{CaCl}_2$  and 10mM Sulfate at 55°C - Curves Predicted by Combined Rate Model

model does a good job of predicting the observed rates at all values of pH and sulfite concentrations. It accounts for both the buffering and inhibiting effects of sulfite.

Figure 3.13 shows a comparison of the measured fluxes and the model predictions for two industrial stones (HSTC and Monteagle). In general the complete model predicts the measured rates within 25% over two orders of magnitude in the rate. This shows that the model can account for changes in pH and concentrations of sulfite, sulfate, carbonate, calcium, and magnesium. However, the model does not do well for high magnesium at high pH. Magnesium is a known inhibitor of calcite dissolution (Terjesen et al., 1961; and Laslo and Chang, 1983). In the present form, the surface kinetics model cannot account for this inhibition. Additionally some variation is expected between the model and the measured rates because the sulfite concentrations used in the model were the nominal values since the actual measured concentrations were not reported.

The model was tested against the rates measured in sulfite solutions by Chan and Rochelle (1982). Table 3.6 gives the comparison between the measured and predicted rates. This table shows poor agreement for the experiments at pH 6 where the presence of small amounts of carbonate could significantly affect the dissolution rate. The concentration of this species was not monitored during the experiments and in modeling these experiments, the CO<sub>2</sub> partial pressure was set to 0.001 atm. If sparging were not adequate, this lack of carbonate concentration accuracy would be magnified at high pH resulting in overprediction of the rate. When the CO<sub>2</sub> partial pressure is set at 0.01 atm for the experiments at pH 6, the predicted rates are within 25% of the measured values.

Inadequacies in the model can be found by plotting the ratio of the predicted flux to the measured flux versus the independent variables. A valid model is indicated by random distribution of the data about one. Any trend in the data would indicate a poor model. Figure 3.14 compares the ratio of the predicted and measured fluxes with the calcium sulfite saturation for both reagent calcites. The Chan and Rochelle data sets at pH 6 were not included in this figure since there were recognized problems in modeling these data. For calcium sulfite saturations less than 3 a majority of the cases are predicted to within 25% of the measured rate. However for the reagent calcite of

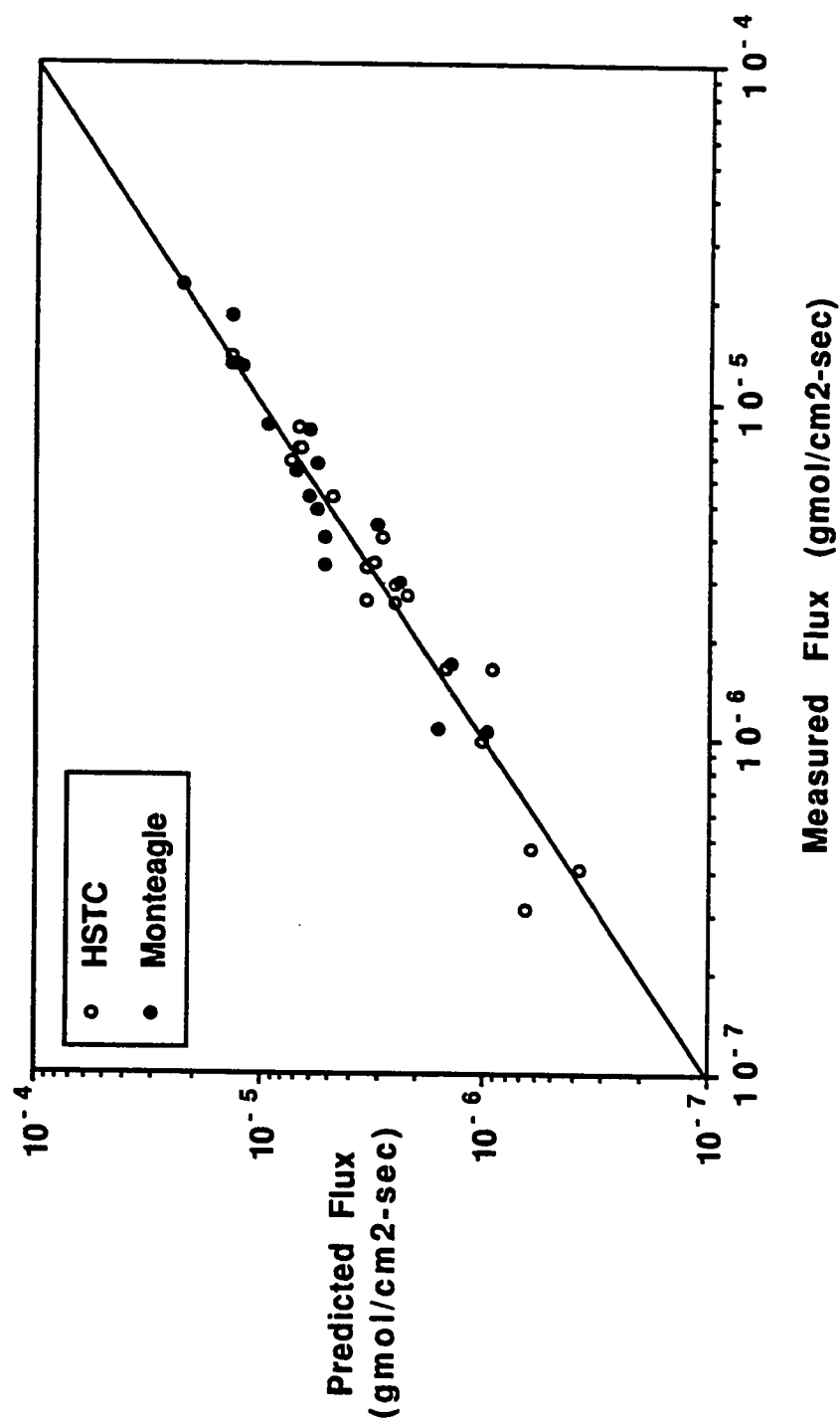


Figure 3.13: Parity Plot for HSTC and Monteagle Limestones  
Predicted Values from the Combined Rate Model

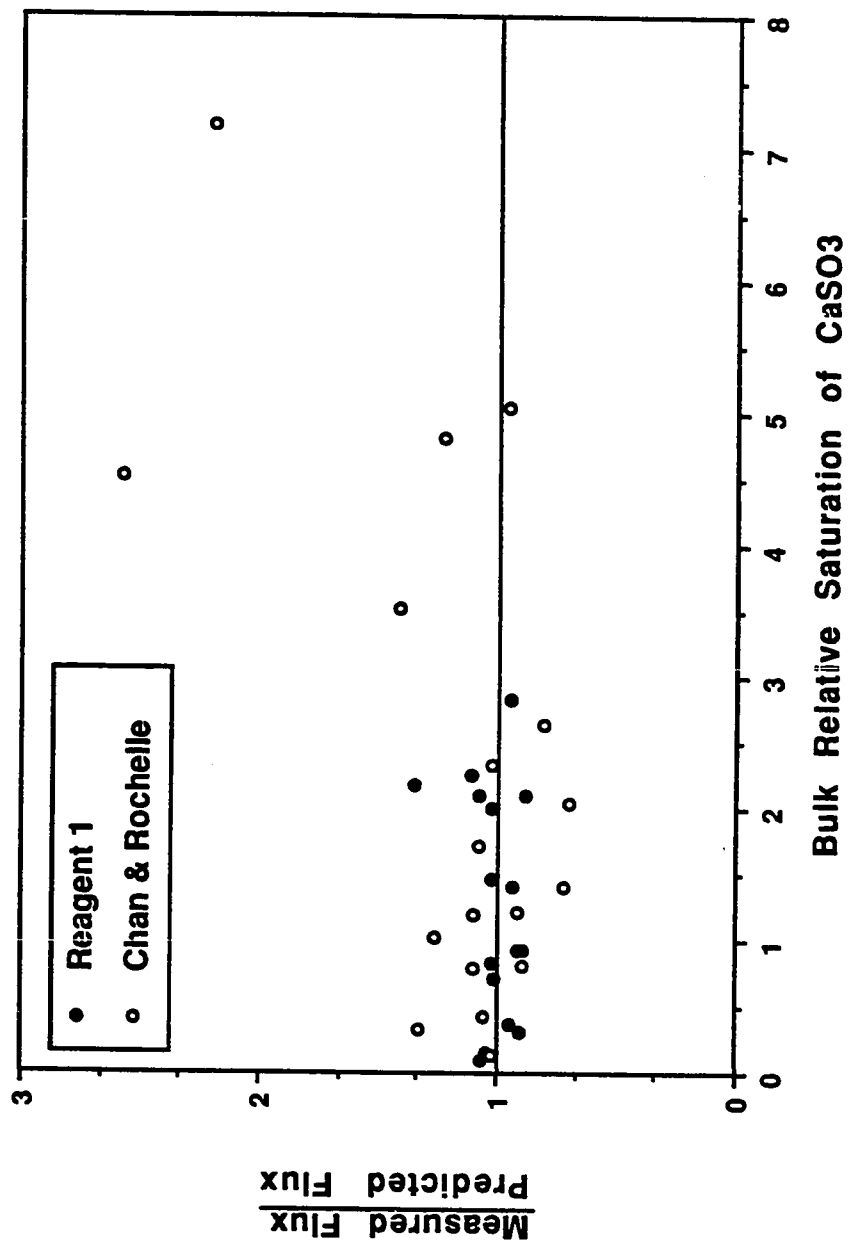


Figure 3.14: Test of Combined Model as a function of  $\text{CaSO}_3$  Saturation for Reagent Limestones



Chan and Rochelle, there is poor agreement at the high sulfite, high pH data where the saturation of  $\text{CaSO}_3$  is greater than 3. It could be that in these experiments calcium sulfite was crystallizing on the limestone and blinding it completely rather than causing the milder adsorption seen at lower saturations. Crystallization onto limestone would not be expected in scrubber systems where sulfite seed crystals exist to provide the surface area needed for crystallization. In the present work it was not possible to exceed a calcium sulfite saturation of 3 without significant crystallization of the calcium sulfite from the clear solution.

As discussed previously, the effect of sulfite on the dissolution of limestone is both to enhance and inhibit dissolution. The susceptibility to inhibition is represented in the value of the surface rate constant which itself is dependent on the limestone type. For a given bulk sulfite concentration, limestones with smaller rate constants will be more inhibited than limestones with higher constants. This limestone type dependence in the presence of sulfite is the primary cause of the observations of Chang et al. (1982b) who noted that titration of limestone with  $\text{NaHSO}_3$  was much better than titration with  $\text{HCl}$  in determining pilot plant reactivity. Since scrubbers always operate with dissolved sulfite, dissolution is controlled by the surface rate expression which has the type dependent constant. Logically, then, the best method to determine how a limestone might perform in a scrubber would be to conduct the titration with sulfite present in solution.

#### 3.4.4 Surface Kinetics Rate Expression

The combined model calculates rates by converging on the surface concentrations which satisfy both the mass transfer expression and the surface kinetics rate for a given film thickness and kinetics constant,  $k_c$ . The continuity of flux at the surface is the boundary condition with the surface kinetics rate as shown in Equation (3-18). This expression shows that sulfite inhibits the dissolution by forming  $\text{CaSO}_3$  which may be adsorbing onto the surface. The inclusion of this rate expression into the mass transfer model means that the limestone dissolution rate can be controlled by mass transfer, surface kinetics, or a mixture thereof. The absolute mass transfer rate is bounded between zero occurring when the surface concentrations equal the bulk values and a finite maximum value occurring when the surface is saturated to calcite. Within

these bounds, Equation (3-18) shows that surface kinetic resistance is significant in all but two situations. The first exception occurs when the surface concentration of the calcium sulfite ion pair approaches zero. When this happens the kinetic rate becomes infinitely fast, and then limestone dissolution is controlled by the finite mass transfer rate. The second exception occurs when the surface concentration of the calcium carbonate ion pair approaches its equilibrium value. In this case the surface rate is zero, and the dissolution rate is determined by finite mass transfer. The final exception is the case of a zero mass transfer rate. In this situation the limestone surface species equal their bulk values, and the dissolution is controlled entirely by the surface kinetics rate.

The surface kinetics rate applicable in sulfite solutions is different from the kinetics form found by other researchers using simple CO<sub>2</sub>/water systems. A direct comparison between expressions is difficult because of the presence of sulfite as an inhibitor. Most of the previous work which found a surface kinetics contribution had been done in CO<sub>2</sub>/water systems (Lund et al., 1974; Rickard and Sjöberg, 1983; and Sjöberg and Rickard, 1984) or in systems where a non-inhibiting buffer was present (Compton and Daly, 1983). In all of these cases, the Levich development was used for the experimental analyses. This development has a built in assumption of a first order surface kinetics rate expression. The sulfite rate correlation in this work was regressed from the measured data with no assumptions as to its potential form. The resulting equation shows a half-order dependence rather than first order. A common result, though, between the previous and present work is that the rate constant in the surface reaction is stone dependent.

The dissolution rate form in sulfite also differs from the forms of other inhibited systems which contained metal ions (Erga et al., 1956; Terjesen et al., 1961) or scandium ions (Nestaas and Terjesen, 1969). The rate form empirically determined by Nestaas and Terjesen is shown in Equation (3-21).

$$\frac{d[\text{Ca}(\text{HCO}_3)_2]}{dt} = k'([\text{Ca}(\text{HCO}_3)_2]_{\text{eq}} - [\text{Ca}(\text{HCO}_3)_2]) - k''[\text{Sc}^{+3}]_s \quad (3-21)$$

This rate form leads to an equivalent development of a driving force determined by a pseudoequilibrium constant (less than thermodynamic equilibrium) and the bulk concentrations. The pseudoequilibrium conclusion had been derived from the earlier work (Erga et al., 1956; Terjesen et al., 1961).

Although there are significant differences between the Nestaas rate form and the present rate expression, sulfite has effects similar to those of scandium. A plot of the dissolution rate against the surface concentration of scandium yielded a family of lines representing different bulk saturations of calcium bicarbonate, but each line producing approximately the same slope. If the reagent sulfite data is plotted in a similar manner with the rate against the surface concentration of  $\text{CaSO}_3$ , a family of lines results. Each line represents a different pH (or equivalently, a different bulk saturation of calcium carbonate) with approximately the same slope. Therefore, the scandium work could be expressed in a rate form similar to the one written for the sulfite work, and the analysis that scandium adsorbed onto the limestone could be extended to sulfite adsorption onto limestone.

The Nestaas and present models can also be compared to the previous reagent model of Chan and Rochelle (1982). In their work the rate of dissolution was also given by a driving force between pseudoequilibrium and the bulk conditions. However because their work was done with nitrogen sparging, the relative saturation to calcium carbonate was approximately zero at all pH values. Thus when compared to Nestaas model, their work would become a single line if the rate were plotted against the surface concentration. However since they never exceeded pseudoequilibrium in the bulk solution, they did not completely test the theoretical applicability of a pseudoequilibrium constant. The present work which studied different bulk relative saturations to calcium carbonate indicates that the value of the pseudoequilibrium constant would be dependent on the bulk saturation of calcium carbonate and sulfite. Thus a significant advantage to the present model over these pseudoequilibrium models is that Equation (3-18) will work with all bulk saturations of calcium carbonate, whereas the pseudoequilibrium models require a different pseudoconstant which must be measured experimentally for each different bulk saturation.

### 3.4.5 Surface Area Changes

The surface rate expression which is used in the model calculates the flux at a given conversion. For spherical particles, this theory results in a constant flux as conversion increases until the particles become small enough that film thickness is changing with conversion. However it was found experimentally that in the presence of sulfite the flux varied as conversion varied. The magnitude of the flux change was largest for the reagent calcite. Since the rate expression is applicable at the limestone surface it was hypothesized that the rate should be dependent on actual BET area rather than the assumed spherical area.

Sulfite has been shown to change the surface features of limestone. Therefore the effect of these changes on the BET surface area of reagent calcite was studied. Reagent calcite was dissolved at pH 5.3 in sulfite at a relative saturation of 2.5. Samples were collected at varying stages of dissolution. BET analyses and SEM micrographs were performed. Since low surface areas were expected, krypton was used as the BET adsorbent gas.

Table 3.8 and Figures 3.15 to 3.18 show the effects of sulfite on the BET surface area at 10%, 25%, 55%, and 70% dissolution. The total areas shown in Table 3.8 are the areas which would be available at the corresponding fraction remaining based on one g of initial limestone charge. For example, with one g of limestone as the initial charge, 0.75 g remain after 25% of the sample dissolves. The measured BET surface area at 25% dissolved was  $0.333 \text{ m}^2/\text{g}$ . Therefore the available surface area from 0.75 g would be  $0.250 \text{ m}^2$ . When limestone dissolution is controlled by mass transfer, it would be expected that the rate per spherical surface area would be relatively constant if the bulk solution concentration is constant. If, however, the dissolution is controlled by surface kinetics, the rate per BET surface area rather than spherical area should be constant.

To test this hypothesis, the five measured BET surface areas were correlated to give areas interpolated between 0 to 70% fraction dissolved. The rates per BET area and rates per spherical area were calculated and then normalized by the initial rates.

Figure 3.19 shows the normalized rates versus fraction dissolved. From this figure it is apparent that BET area does a better job of predicting a constant flux. The greatest deviations in the BET flux occur at less than 25% dissolved where the measured BET area showed a decrease. If this measurement were in error, then the correlation which was calculated using this point would be in error and could explain the deviations. Even though BET area was used, some of the limestone surface is inactive because of sulfite adsorption. However the active surface available for dissolution in the surface rate expression should be and is more closely correlated to BET rather than spherical area.

<b>Table 3.8: Sulfite Effects on the BET Surface Area of Reagent 1 Limestone</b>		
<b>% Dissolved</b>	<b>BET Area (m<sup>2</sup>/g)</b>	<b>Total Area (m<sup>2</sup>)</b>
0	0.221	0.221
10	0.173	0.156
25	0.333	0.250
55	0.654	0.294
70	0.461	0.138



Figure 3.15: Reagent 1 in 6.5 mM  $\text{SO}_3$ , 10% Dissolved  
Exp 77A - pH 5.3, 0.1M  $\text{CaCl}_2$ , 0.85 atm  $\text{CO}_2$ , 55°C

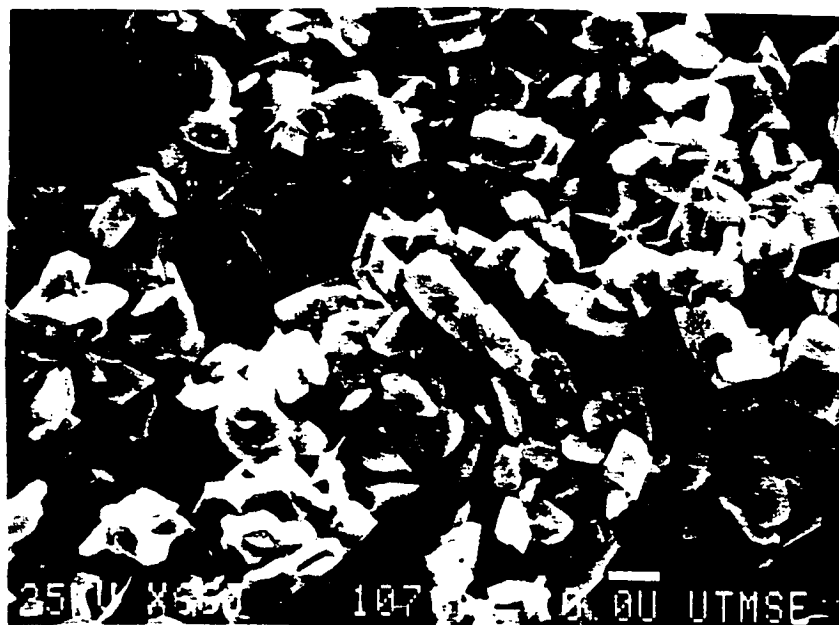


Figure 3.16: Reagent 1 in 6.1 mM  $\text{SO}_3$ , 25% Dissolved  
Exp 76A-pH 5.3, 0.1M  $\text{CaCl}_2$ , 0.85 atm  $\text{CO}_2$ , 55°C

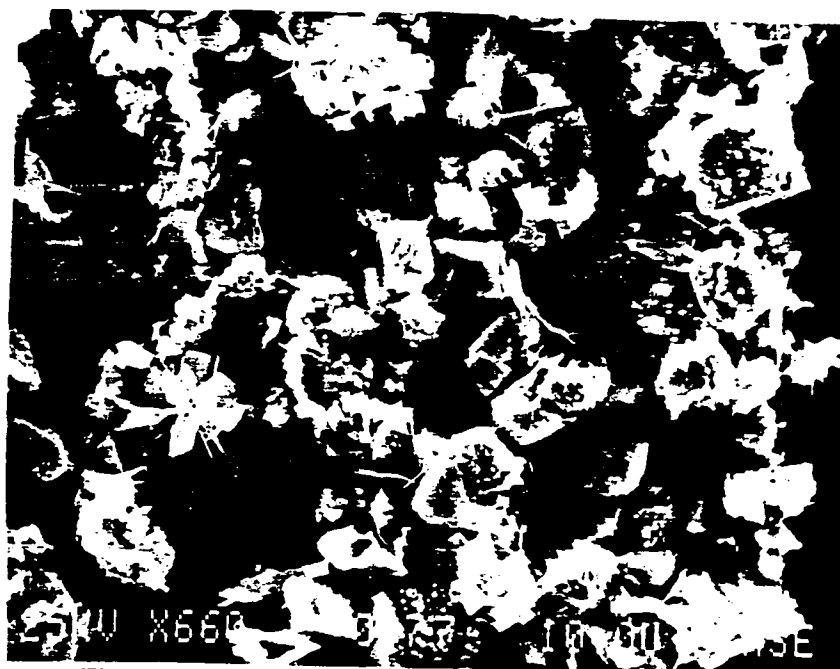


Figure 3.17: Reagent 1 in 6.1 mM  $\text{SO}_3$ , 55% Dissolved  
Exp 77 - pH 5.3, 0.1M  $\text{CaCl}_2$ , 0.85 atm  $\text{CO}_2$ , 55°C



Figure 3.18: Reagent 1 in 6.3 mM  $\text{SO}_3$ , 75% Dissolved  
Exp 76 - pH 5.3, 0.1M  $\text{CaCl}_2$ , 0.85 atm  $\text{CO}_2$ , 55°C

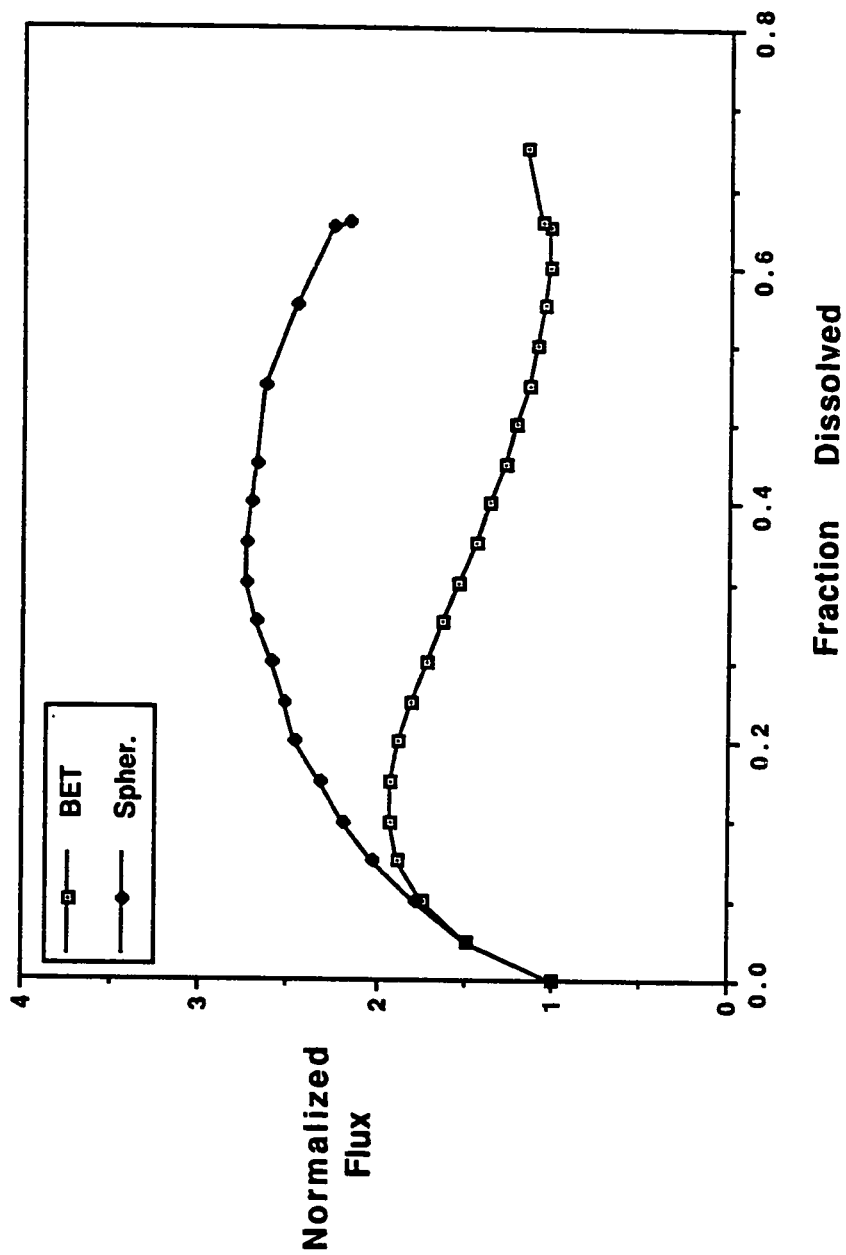


Figure 3.19: Normalized Fluxes for Reagent 1 Calcite Dissolved in 6 mM SO<sub>3</sub>. Fluxes Calculated with Spherical and BET Areas



The conclusion from the reagent calcite study that BET area gives an approximately constant flux confirms that in sulfite solution, limestone dissolution is controlled by a surface kinetics rate. This conclusion also explains an observation by Jarvis et al. (1988). They measured dissolution rates of the same limestone at three different initial sizes. When they determined the fluxes based on the appropriate spherical areas and normalized them by their respective initial rates, then a plot of these normalized rates versus fraction dissolved yielded a single curve. BET area is not expected to vary with particle size since it is dependent on surface roughness rather than diameter. Therefore changes in the BET area would explain the observation of a single curve.

As mentioned, the reagent calcite gave the largest changes in flux with changes in conversion. In fact reagent calcite showed an increase in flux with increasing conversion, while the industrial limestones showed a decrease in flux with increasing conversion. A BET surface area measurement on an industrial stone at 30% dissolved showed a corresponding decrease in available surface area rather than the increase in surface area observed for reagent calcite. This was also notable on the SEM micrographs of the Edwards stone which show significant surface roughness on the raw stone as well as the stone dissolved in sulfite. Reagent, however, became rougher as spikes formed on the initially smooth crystalline faces. Additionally the flux decreases for industrial stones were not as dramatic as the flux increase of reagent calcite. This suggests that the error associated with the assumption of spherical particles in determining conversion effects in the presence of sulfite may be within acceptable limits for the non-crystalline industrial stones.

#### 3.4.6 Temperature Effects

Using the present work and the work of Chan and Rochelle (1982), the effect of temperature on the surface rate constant of reagent calcite can be studied. With  $k_c$  at 55°C from the present work and  $k_c$  at 25°C from the work of Chan, the activation energy,  $E_a$ , of the surface rate constant is calculated to be 14.8 kcal/gmol. However if the data of Chan at both 25°C and 55°C is used, then  $E_a$  is 3.7 kcal/gmol.

The fact that the activation energy is sensitive to the particular limestone may indicate that the two reagent grade limestone are not equivalent. Comparison of the experimental rates show that the present Reagent 2 limestone was 5 times more reactive at 55°C than the Reagent 1 stone used by Chan. Other differences were shown in Table 3.2 where the mean diameter and the particle size distributions varied between these stones.

The sulfite effect on the HSTC stone was studied at three temperatures: 65°C, 50°C, and 35°C. The rate constants were regressed at all temperatures and the calculated  $E_a$  was 4.7 kcal/gmol. This value is comparable to the  $E_a$  of Chan. The standard error of this value, though, was very large. Since the constants at 65°C and 25°C were estimated from a single data measurement, any error in the rates would greatly affect the calculation of the rate constant and thus  $E_a$ . If the rate constants in the 25-55°C temperature range are used, then  $E_a$  is 11.9 kcal/gmol.

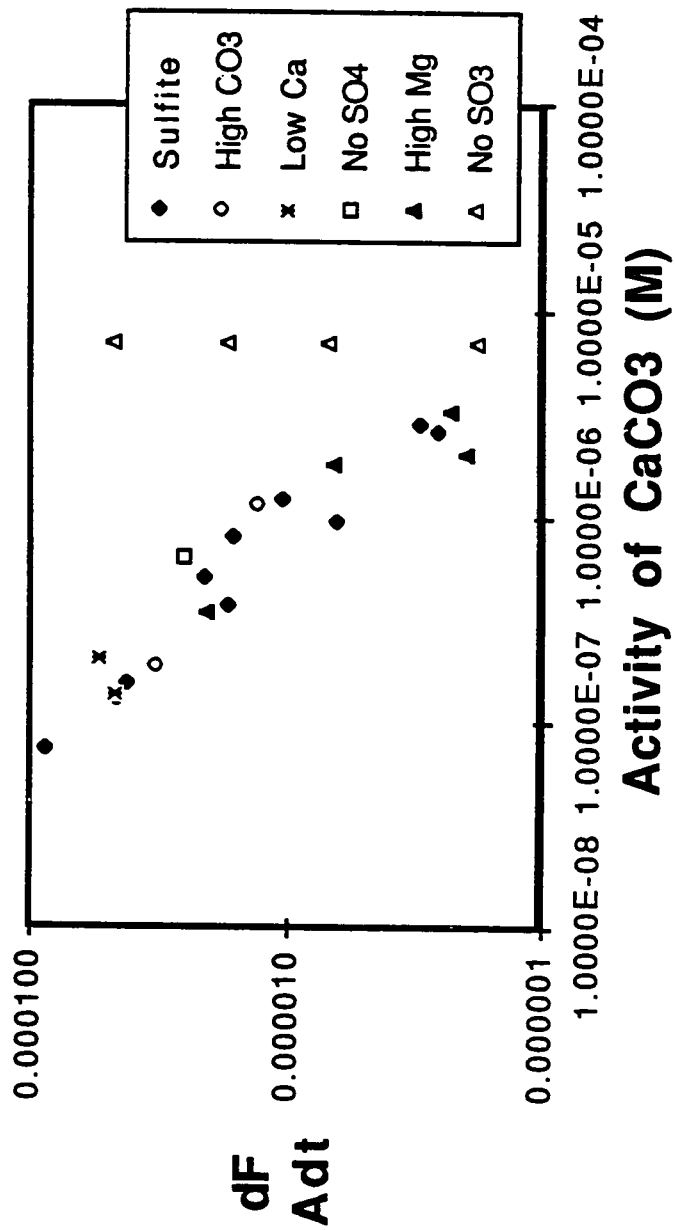
The interpretation of  $E_a$  for any limestone is complicated by the fact that the elementary steps of sulfite adsorption and reaction with calcite are not well understood. These elementary steps would have individual temperature dependencies and how these temperature expressions impact on the activation energy of the rate constant is not known at the present.

#### 3.4.7 Statistical and Error Analysis

The development of the surface rate correlation was performed as a step-wise regression. Initially the rate was plotted against the activity of  $\text{CaCO}_3$  at the surface. This result is shown in Figure 3.20 for the HSTC limestone. This figure suggested that the rate was inversely dependent on  $\text{CaCO}_3$  at the surface. The two sulfite saturations which were studied can be seen in the two lines formed on the plot. These results suggested a surface reaction rate of the form

$$\text{Rate} = b(\text{CaCO}_3 \cdot \text{CaSO}_3)^m \quad (3-22)$$

Figure 3.20: Fractional Rate vs Measured  $\text{CaCO}_3$  Activity at the Surface of HSTC Limestone



There are two possible ways to regress the exponent,  $m$ , of the  $\text{CaCO}_3\cdot\text{CaSO}_3$  activity variable. These methods depend on how the error in the rate is distributed. If the error is distributed normally (i.e. the error is independent of the value of the rate), then the model must be regressed by a non-linear iterative method using the form of Equation (3-22). However, if the errors in the rate are dependent on the value of the rate itself (i.e. the rate is  $\pm c\cdot\text{rate}$ , where  $c$  is a constant), then the expression can be transformed into logarithms. This results in transformed errors which are normally distributed. The transformed expression can be treated with a linear regression to determine the slope (exponent). This least squares method of linear regression assumes that the errors are normally distributed.

The latter is the case for the measurements of the dissolution rate. The measured rates are  $\pm 10\%$ , thus the errors are normally distributed in log space. In order to regress the surface rate correlation, the variables of interest were transformed into log space, thus

$$\log \text{ rate} = \log(b) + m \log(\text{CaCO}_3\cdot\text{CaSO}_3) \quad (3-23)$$

A linear regression was performed to determine the value of  $m$ , recognizing that the calculated slope is actually the exponent for the product of the activities at the surface.

The results of the regression and the statistical parameters for HSTC, Reagent, and Monteagle limestones are shown in Table 3.9. The  $t$ -values at an  $\alpha$  level of significance of 5% are the two-tailed values.

The first hypothesis to test is that the slope is zero (i.e. the rate is independent of the  $\text{CaCO}_3\cdot\text{CaSO}_3$  product at the surface). Comparing the calculated  $t$ -value to those from the  $t$ -table at the 5% level shows that this hypothesis can be easily rejected. In other words, the statistical evidence indicates a strong dependence of rate on the activities product.

Table 3.9 Statistical Parameters from the Regression of the Surface Rate Dependence on $\text{CaCO}_3\cdot\text{CaSO}_3$			
	HSTC	Reagent	Monteagle
Exponent (slope)	-1.005	-1.070	-0.974
Degrees of Freedom	18	14	19
Standard Error	0.078	0.068	0.118
t-value from data	12.849	15.653	8.259
t-value at $\alpha = 0.05$	2.101	2.145	2.131

The t-values at the 5% level can be used with the standard error to estimate the confidence intervals for each exponent. The intervals were found to be  $-1.005 \pm 0.164$  for HSTC,  $-1.070 \pm 0.146$  for Reagent, and  $-0.974 \pm 0.251$  for Monteagle. Since a single exponent will be used for all stones, the intervals overlap from -0.924 to -1.169, and this overlap helps to warrant the choice of -1.00.

Any desired form of the rate expression would require that the reaction at the surface become zero when the surface was saturated to calcite. This will occur if the rate expression has a driving force term, DF, of the form in Equation (3-24).

$$\text{DF} = (\text{CaCO}_{3\text{eq}} - \text{CaCO}_{3\text{s}})^n \quad (3-24)$$

In order to determine the exponent,  $n$ , of this term, the  $\text{CaCO}_3\cdot\text{CaSO}_3$  dependence was subtracted from the rate and the residual was plotted against the driving force expression in log space. Table 3.10 shows the regressed values of  $n$  and the calculated t-values for the three stones. Comparing the calculated t's to the values in Table 3.10 shows that for HSTC and Monteagle, the measured rates could be independent of the driving force term (i.e. the exponent could be zero). However for

<b>Table 3.10 Statistical Parameters from the Regression of the Surface Rate Dependence on the Driving Force</b>			
	<b>HSTC</b>	<b>Reagent</b>	<b>Monteagle</b>
Exponent	0.530	0.595	0.318
t-value from data	1.007	2.814	0.699
Significance level	30%	2%	50%

reagent calcite there is only a 2% chance that the exponent is zero. Along with the small values which were regressed for the exponents, this result indicates that the driving force dependence must be very weak. Since the surface rate is physically restricted to a zero rate at saturation to calcite, a zero exponent for the driving force term was rejected. Using an approximate average of the three exponents yields a square root dependence for the driving force term.

The final test involves the comparisons of the surface rate constants to evaluate whether they are statistically different. The parameters required for these tests are shown in Table 3.11. Since the rate expression was regressed by transforming to logarithms, the mean values in the table are the logarithms of the rate constants.

To compare the between stone means, the variances must first be compared. For three samples this requires three comparisons. The F test ratios of the variances are shown below along with the values from the F table which correspond to the 5% alpha test at the appropriate degrees of freedom.

$$F_{20,19} = \frac{0.0335}{0.0144} = 2.32 < 2.51$$

$$F_{20,15} = \frac{0.0335}{0.0207} = 1.62 < 2.76$$

$$F_{15,19} = \frac{0.0207}{0.0144} = 1.44 < 2.62$$

Since all these values are well within the limits, the variances can be combined to give a pooled variance of 0.0232. Using this value a t-test was performed for the three pairs of comparisons. The hypothesis is that within a limestone pair the rate constants are numerically equivalent. At 35 degrees of freedom, this hypothesis is rejected at the 5% level if calculated t's are less than 2.996. For the three necessary comparisons the calculated t values were 12.25, 7.88, and 4.97. Therefore the hypothesis is rejected, and the rate constants are uniquely different.

Using 95% confidence intervals and the standard errors calculated from the pooled variance, the estimates of the relative errors for the surface rate constants of the three limestones are all less than  $\pm 10\%$ . For Reagent 1,  $k_c = 2.406 \times 10^{-12} \pm 9.3\%$ ; for HSTC,  $k_c = 5.929 \times 10^{-13} \pm 8.3\%$ ; and for Monteagle  $k_c = 1.406 \times 10^{-12} \pm 9.9\%$ .

Table 3.11 Statistical Parameters from the Regression of the Surface Rate Constants			
	HSTC	Reagent	Monteagle
Mean	-12.227	-11.618	-11.852
Data sets	20	16	21
Variance	0.0144	0.0207	0.0335

### 3.5 Summary

In the absence of sulfite, limestone dissolution was controlled solely by mass transfer. For a given stone under mass transfer control, film thickness was found to be independent of pH.

The presence of sulfite in solution was found to have a dual effect on the dissolution of limestone. The sulfite/bisulfite pair acted as a buffer at the limestone interface by providing hydrogen ion consumed during the dissolution reaction. But sulfite also inhibited dissolution by adsorbing on the limestone. Because dissolution was enhanced, the rate in the presence of sulfite was controlled by a combined surface kinetics/mass transfer regime. The sulfite inhibition effect was accurately modeled in the surface kinetics expression by an inverse dependence on calcium sulfite concentration at the limestone surface. In modeling the dissolution rates, continuity of flux at the surface of the limestone was satisfied using the surface kinetics equation.

The surface rate expression did a good job of predicting the dissolution of limestone for a variety of stones and over a range of solutions compositions. Changes in the pH and the concentrations of calcium, carbonate, sulfite, sulfate, and adipic acid were accurately predicted. While the form of the rate expression was applicable to all stones, the rate constant was stone dependent. These individual rate constants could not be correlated to Mg content or to BET area.

When compared to other empirical rate models determined in inhibited systems, the present model was found to be superior since it did not require the experimental determination of solution dependent pseudoequilibrium constants.



### 3.6 Notation

$B$  = agitation enhancement factor,  $\text{cm}^{-2}$

$\Delta C$  = concentration driving force,  $\text{gmol}/\text{cm}^3$

$\text{CCS}$  = relative saturation of calcium carbonate

$\text{CSS}$  = relative saturation of calcium sulfite

$d$  = diameter of a spherical particle,  $\text{cm}$

$d_i$  = diameter of a particle from size fraction  $i$  at a given time,  $\text{cm}$

$d_{oi}$  = initial diameter of a spherical particle from size fraction  $i$ ,  $\text{cm}$

$D$  = diffusivity,  $\text{cm}^2/\text{sec}$

$f_i$  = volume fraction remaining from size fraction  $i$

$F$  = total fraction remaining

$k_c$  = surface kinetic rate constant,  $\text{M}^{5/2}\text{-cm}/\text{sec}$

$K_{sp}$  = solubility constant for calcium carbonate,  $\text{M}^2$

$M$  = Molarity,  $\text{gmol}/\text{l}$

$N_p$  = number of particles

$N_{pi}$  = number of particles from size fraction  $i$

$t$  = time,  $\text{sec}$

$U$  = utilization (moles dissolved per mole fed)

$V_{\text{tot}}$  = total initial volume of solids,  $\text{cm}^3$

$V_{oi}$  = initial volume of a particle from size fraction  $i$ ,  $\text{cm}^3$

#### Greek letters

$\delta$  = film thickness,  $\text{cm}$

$\phi_i$  = volume fraction of particles between size  $i$  and  $i+1$

$\rho$  = molar density of calcite,  $\text{gmol}/\text{cm}^3$

$\mu$  = absolute viscosity of water, poise

#### Subscripts

$b$  = bulk

$eq$  = equilibrium

$o$  = initial

$p$  = pseudo

$s$  = surface

## **Chapter 4**

### **Limestone Reactivity and Slurry Scrubber Performance**

#### **4.1 Introduction**

An important goal of this work is to test the Slurry Scrubber Model for Flue Gas Desulfurization in its predictions of scrubber performance. It is well known that the performance of a slurry scrubbing system is strongly dependent on the reactivity of the limestone. This reactivity has previously been thought to be only dependent on the limestone grind. This work now demonstrates that the limestone type will also contribute to the overall reactivity. In order to test this new conclusion, the Slurry Scrubber Model has been expanded to predict limestone reactivity. This resulting prediction accounts for the effects of limestone grind using the approach of Toprac and Rochelle (1982) and accounts for the effects of limestone type in the surface rate constant required by the rate expression applicable in sulfite solutions.

This chapter includes the additional theory needed to account for particle size effects on reactivity and on film thickness. Batch experiments show the applicability of this theory. Then the prediction of limestone reactivity is performed in the model and tested against a limestone type and grind study sponsored by EPA. This work studied SO<sub>2</sub> removal at different utilizations of four limestone types with ten different grinds.

#### **4.2 Theory**

##### **4.2.1 Particle Size Effects in the Mass Transfer Regime**

The dissolution rate of limestone particles has been previously treated as a mass

transfer process. When this regime is applicable the dissolution rate of a single particle is given by

$$\frac{dn}{dt} = -k_l \pi d^2 (C_s - C_b) \quad (4-1)$$

where the driving force for dissolution is the difference between concentrations at the surface,  $C_s$ , and in the bulk,  $C_b$ . When mass transfer controls the dissolution, the surface concentration is given by equilibrium to calcite.

The solid/liquid mass transfer coefficient,  $k_l$ , must be estimated from an empirical correlation. If a stagnant solution or small particles can be assumed then the coefficient can be estimated by setting the Sherwood number,  $N_{Sh}$ , equal to 2. However, if the system is agitated or there are large particles present, as in a FGD limestone system, then a more rigorous correlation is required. Toprac and Rochelle (1982) suggested the use of the Calderbank and Moo-Young correlation in superposition with the Sherwood number of 2. This two term expression for the mass transfer coefficient is

$$k_l = \frac{2D}{d} + \beta N_{Sc}^{-2/3} \quad (4-2)$$

where  $\beta$  = a term accounting for the agitation force imparted into the solution  
 $N_{Sc}$  = Schmidt number, involves diffusivity but not the particle size.

For spherical particles Equation (4-1) can be rewritten in terms of  $f$ , the fraction remaining, which is the ratio of the volume of the particle at any time to its initial volume. Then substituting Equation (4-2) into Equation (4-1) gives

$$\frac{df}{dt} = \frac{-k_m f^{1/3}}{V_o^{2/3}} - \frac{k_m B f^{2/3}}{V_o^{1/3}} \quad (4-3)$$

In this equation the mass transfer constant,  $k_m$ , is given by Equation (4-4).

$$k_m = \frac{6^{1/3} \pi^{2/3} 2D \Delta C}{\rho_m} \quad (4-4)$$

where  $\rho_m$  is the molar density of calcite and is equal to 0.027 gmol/cm<sup>3</sup>.

In Equation (4-3) B is the mass transfer enhancement factor occurring from agitation as shown in Equation (4-5).

$$B = 1.612\beta N_{Sc}^{-2/3} \quad (4-5)$$

If the bulk solution concentration does not change with time,  $k_m$  will be constant, and for a batch system Equation (4-3) can be integrated analytically to give Equation (4-6).

$$k_{mt} = \frac{3}{B^2} \left[ BV_o^{1/3}(1-f^{1/3}) + \ln \frac{1+BV_o^{1/3}f^{1/3}}{1+BV_o^{1/3}} \right] \quad (4-6)$$

This expression is the corrected version of the analytical expression reported by Toprac(1981; 1982). In his works the power of f in the first term was incorrectly reported as one when it should be 1/3.

Equation (4-6) relates the fraction remaining of a single particle of initial size  $V_o$  to the mass transfer constant and time. However in real systems limestone particle sizes are not uniformly distributed, therefore a rate expression equivalent to equation (4-3) must be written for each particle size fraction,  $f_i$ , with its unique  $V_{o,i}$ . The total fraction remaining, F, for a given  $k_{mt}$  in a batch system is then found by summing over the total particle size distribution.

$$F = 1 - U = \sum \phi_i f_i \quad (4-7)$$

The particle size distribution required by Equation (4-7) can be determined by one of two methods. If the complete distribution is well-defined by Coulter Counter or other measurements, the distribution can be used directly. If, however, only sieve measurements are known, then the complete distribution can be estimated from the sieve data using the methods developed in Chapter 2.

Equations (4-6) and (4-7) can be used in batch experiments to determine the mass transfer constant. Using the particle size distribution these equations will predict a curve of total fraction remaining versus  $k_{mt}$ . Then for a given bulk solution experiment

with a measured curve of fraction remaining versus time, the mass transfer constant,  $k_m$ , can be regressed. This measured  $k_m$  can be used with Equation (4-5) to determine surface conditions.

A similar approach is taken in the Slurry Scrubber Model for determining dissolution rates at a given fraction dissolved. However the scrubber stages are treated as CSTR not batch processes, therefore each  $f_i$  must be weighted by the CSTR residence time density function. A given utilization,  $U$ , is satisfied by converging on the  $k_m\tau$  parameter and then summing the weighted  $f_i$ 's over the particle size distribution.

$$F = \sum \phi_i \frac{1}{k_m\tau} \int_0^1 \frac{f_i \exp(-\frac{k_m t}{k_m\tau})}{\frac{df_i}{dt}} df_i \quad (4-8)$$

The final calculated reactivity is given by Equation (4-9).

$$K = \frac{U}{k_m\tau C_s(1-U)} \quad (4-9)$$

In this equation  $C_s$  is the total calcium solids concentration, gmol solid/liter of solution.

Equation (4-9) has been normalized by the  $\text{CaCO}_3$  solid concentration in order to approximate the changes in utilization by the changes in the limestone concentration. This normalized value, which is a constant throughout the scrubber system, can then be multiplied by the solids concentration of calcium carbonate at any point to calculate the point reactivity. In the hold tank and at each stage in the scrubber, the moles of limestone which dissolve are calculated using Equation (4-10).

$$\Delta\text{CaCO}_3 = K[\text{CaCO}_3]_{\text{solid}}\tau\text{DAC} \quad (4-10)$$

In a CSTR system, the residence time,  $\tau$ , in Equation (4-10) is either the liquor residence time in the hold tank or the residence time per stage in the scrubber. Since all scrubbers operate with sulfite in solution, DAC in Equation (4-10) is found by satisfying the surface rate expression given in Equation (3-17).

### 4.2.2 Film Theory for Mass Transfer

Another theory for mass transfer is based on the concept that a film exists around the particle through which the species must diffuse. If  $\delta$  represents this theoretical film layer then the mathematical relationship for the rate is given by Equation (4-11).

$$\frac{dn}{dt} = \pi d^2 \frac{D\Delta C}{\delta} \quad (4-11)$$

A comparison of Equation (4-11) to Equations (4-1) and (4-2) shows that these two models are equivalent when the film thickness is given by Equation (4-12).

$$\delta = \frac{d}{2+Bd} \quad (4-12)$$

### 4.2.3 Average Film Thickness

Because film thickness depends on the particle size as shown in Equation (4-12), each size fraction of a polydispersed stone will have a different film layer. As a result the surface kinetics rate given by Equation (3-17) will be faster for smaller diameters. In order to reduce the complexity, average film thicknesses can be used. The averaging factor for the film thickness is derived from the total dissolution rate shown in Equation (4-13).

$$\text{Total rate} = V_T \sum \phi_i \frac{a_i}{V_{oi}} \frac{D\Delta C_i}{\delta_i} \quad (4-13)$$

Again, as discussed with Equation (4-7), the particle size distribution which is also required for Equation (4-13) can be either measured directly or predicted from sieve data using the methods discussed in Chapter 2.

The total rate can also be found in terms of an average film thickness and concentration gradient as given in Equation (4-14).

$$\text{Total rate} = \frac{D(\Delta C)_{ave}}{\delta_{ave}} \sum V_T \phi_i \frac{6f_i}{d_i} \quad (4-14)$$

The summation in Equation (4-14) is the total area at any time in terms of the fraction remaining. Using Equations (4-13) and (4-14),  $\delta_{ave}$  can be found in terms of the individual film thicknesses and for a batch system is given by Equation (4-15).

$$\delta_{ave} = \frac{\sum \phi_i \frac{f_i}{d_i}}{\sum \phi_i \frac{f_i}{d_i \delta_i}} \quad (4-15)$$

For a CSTR system as required by the Slurry scrubber model, the average film thickness depends on the CSTR residence time function. For example the numerator of Equation (4-15) becomes

$$CSTR\left(\frac{f_i}{d_i}\right) = \frac{1}{k\tau} \int_0^{\infty} \frac{f_i}{d_i} e^{-(kt/k\tau)} dk \quad (4-16)$$

Using a similar expression for the denominator of Equation (4-15) and applying the definition in Equation (4-12), the average film thickness in a CSTR system is calculated in the Slurry Scrubber Model using Equation (4-17).

$$\frac{1}{\delta_{ave}} = \frac{2\sum \phi_i \int_1^0 \frac{e^{-(kt/k\tau)}}{-1-BV_i^{1/3}f_i^{1/3}} df_i}{\sum \phi_i d_{oi} \int_1^0 \frac{f_i^{1/3} e^{-(kt/k\tau)}}{-1-BV_i^{1/3}f_i^{1/3}} df_i} + 1.612B \quad (4-17)$$

For zero percent dissolved (all  $f_i = 1$ ), the average film thickness depends on the initial diameters of the smaller particles. As the solids dissolve ( $f_i \rightarrow 0$ ), the larger particles determine  $\delta_{ave}$ . In this case the first term becomes negligible, and the resulting film thickness is a constant as shown in Equation (4-18).

$$\delta_{ave} = \frac{1}{1.612B} \quad (4-18)$$

### 4.3 Pilot Plant Conditions

A limestone type and grind study was performed by EPA in 1979-1981 (Dempsey et al., March, 1979; August, 1979; September, 1979; November, 1979; December, 1980; and Chang et al., January, 1981; February, 1981; Borgwardt et al., 1980; Chang et al., 1982a). This program involved a comparison of four different stones at two degrees of fineness: 75% < 200 mesh (coarse grind) and 85% < 325 mesh (fine grind). Each grind was tested at steady state conditions for at least two utilizations in a single-loop turbulent contact limestone scrubber (TCA). The scrubber was six inches in diameter, 10 feet in height, and contained three beds of nitrile foam spheres. Hydrodynamic parameters were maintained at approximately constant conditions in order to determine type effects. The values of the constant parameters were:

Pressure drop = 8 in. of water  
Superficial gas velocity = 12.5 ft/sec  
Liquid-to-gas ratio = 50 gal/mcf  
Hold tank liquor residence time = 9 min.

No fly ash or chemical additives were used, and the hold tank operated without forced oxidation. Chloride concentration was maintained at 5000 ppm by addition of HCl to the flue gas.

SO<sub>2</sub> removal was measured using wet analysis on the gas and with an ultra-violet gas analyzer. The error in these measurements was estimated to be  $\pm 4\%$  (Borgwardt et al., 1979). Slurry solids and solutions were also collected and analyzed. Most grinds were run for an average of 180 hours - equivalent to 15 residence times for the solids. However Fredonia Extra Coarse only ran for 72 hours due to limited supplies (6 residence times).

#### 4.3.1 Modeling Approach

The EPA limestone study was simulated using the Slurry Scrubber Model. The TCA scrubber was modeled as a counter-current contactor with a total of 3 stages. Assuming that the scrubber pressure drop is equivalent to the liquid hold-up, the liquor



residence time was estimated to be 3 seconds per stage. Besides the fixed parameters shown above, this model also requires values for mass transfer coefficients,  $k_g$  and  $k_l$ , and for gas phase transfer units,  $N_g$ . Based on work done by Dempsey et al. (July, 1983) using the TCA scrubber, the following values were used in the model:

$$\frac{k_l}{k_g} = 200 \frac{\text{gmol-cm}}{\text{atm-l}}$$

$$N_g = 2.3 \text{ per stage}$$

Gas phase resistance in the scrubber was measured by absorption of  $\text{SO}_2$  into  $\text{Na}_2\text{CO}_3$  solutions. Liquid phase resistance was measured by  $\text{CO}_2$  absorption into  $\text{Na}_2\text{CO}_3/\text{NaHCO}_3$ . These values were also used by Chan and Rochelle (1983) in the modeling of high chloride scrubbers.

Since the hold tank is treated as an additional stage,  $L/G$  and liquid phase transfer units,  $N_l$ , are required by the model. (Gas phase resistances for  $\text{CO}_2$  and  $\text{O}_2$  are neglected.) Since no details were available for the hold tank,  $L/G$  was set to 45 l/gmol and  $N_l$  was set equal to 3. Values on the order of these would be expected in a natural oxidation system where "gas flow" occurs through entrained scrubber gases and through air flow across the surface of the tank. The resulting estimated gas flowrate is 225 times smaller than the scrubber gas flowrate.

Particle size distributions for the limestone grinds of the EPA study were taken from Coulter Counter work performed by Toprac (1982). Limestone surface rate constants were fixed for each limestone type but were not changed for different grinds within a given type. The calcium sulfite crystallization parameter,  $k_{\text{cry}}$ , was adjusted at each run to match the measured total sulfite in the hold tank. For most runs the calcium sulfite dissolution parameter was fixed at  $4.0 \times 10^4 \text{ sec M}^{-1}\text{cm}^{-2}$ . Since all runs operated under natural oxidation, only small amounts of gypsum are present. Therefore the gypsum crystallization parameter was fixed at 0.90 M for all runs.

The Slurry Scrubber Model also requires an enhancement factor to account for the increase in  $\text{O}_2$  absorption caused by its reaction with dissolved sulfite. Oxidation of sulfite to sulfate has a complicated effect on scrubber performance. In order to accurately account for these effects, the enhancement factor for  $\text{O}_2$  absorption was

adjusted at each run to match the measured sulfite oxidation. Values which were used ranged from 1 to 4. These values are well within the range of values observed by Ulrich (1983) and values used by Chan and Rochelle (1983) in scrubber simulation of chloride studies. The  $O_2$  absorption parameter was never set less than one (equivalent to physical absorption of  $O_2$ ).

As a check on the measured  $SO_2$  removals, material balances were calculated for each run using the measured feed rates and limestone utilization(U). Thus the  $SO_2$  removal based on a material balance is given by Equation (4-19).

$$SO_2 \text{ removal} = \frac{\text{moles } SO_2 \text{ absorbed}}{\text{moles } SO_2 \text{ fed}} = \frac{U * \text{moles limestone fed}}{\text{moles } SO_2 \text{ fed}} \quad (4-19)$$

The error associated with this number cannot be estimated since no error estimates were given for the four measured values required in this calculation.

## 4.4 Results

Chapter 3 demonstrated that the dissolution flux of limestone was controlled by a surface rate expression when sulfite was present. Measured dissolution fluxes at zero or 50% dissolved were well predicted for variations in pH and sulfite concentrations when limestone type was accounted for by an appropriate surface rate constant. The prediction of solution effects, however, addresses only part of the limestone reactivity parameter required to determine scrubber performance. In order to predict the total moles dissolved, a method is required to account for particle size distribution and utilization.

### 4.4.1 Batch Experiments

Before using a method for predicting reactivity in the Slurry Scrubber Model the applicability of the theory must be tested with batch experiments. Therefore some of the experiments discussed in Chapter 3 were analyzed to study particle size effects in the reactivity theory. Batch experiments in the absence of sulfite were studied with Reagent 1 limestone. Experiments with the as-ground limestones of the EPA study

were used to test the applicability of combined particle size and sulfite solution effects. The experimental methods and conditions used with these limestones were discussed in Section 3.3.1.

Using Reagent 1 limestone a theoretical curve of fraction remaining in a batch system versus time was generated using Equations (4-5) to (4-7). In the absence of sulfite, the surface of the limestone is in equilibrium with calcite. Thus at pH 4.8 and 55°C with CO<sub>2</sub> sparging, DAC equals  $3.954 \times 10^{-9} \text{ cm}^2\cdot\text{M/s}$ . At pH 5.3 DAC equals  $1.006 \times 10^{-9} \text{ cm}^2\cdot\text{M/sec}$ . These values determine  $k_m$  as given in Equation (4-5). With these values and using the reagent particle size distribution shown in Table 3.1, the time can be calculated required to reach a specified fraction remaining. Figure 4.1 shows the results of measured and predicted F against time for pH 4.8 and pH 5.3.

The agitation enhancement factor, B, used to develop these curves was  $0.1500 \mu\text{m}^{-1}$ . The predicted curves are within 8% of the measured values, well within the experimental errors of 10%. The shapes of the predicted curves is determined by the particle size distribution and the placement along the time axis is determined by DAC and B.

The value of B in this work is approximately twice the value determined by Toprac for CO<sub>2</sub> sparged systems at 25°C in pH 5 solutions. The present experiments were performed at 55°C which would affect the enhancement factor since it is a function of viscosity and diffusivity. And as discussed in Chapter 3 the enhancement factor also accounts for the contribution of the CO<sub>2</sub> finite rate reaction to limestone dissolution. This reaction rate would also vary with temperature. There would also be differences because of the method Toprac used to regress B. He estimated the value of  $k_m$  in Equation (4-5) by increasing the predicted DAC by 1.5. This would require smaller values of B with the particle size distributions in Equation (4-6) to match the predicted  $k_m$ .

As-ground limestones were studied to test the applicability of combined particle size and sulfite solution effects. In the presence of sulfite DAC is determined using the surface kinetics rate expression as shown in Equation (4-20).

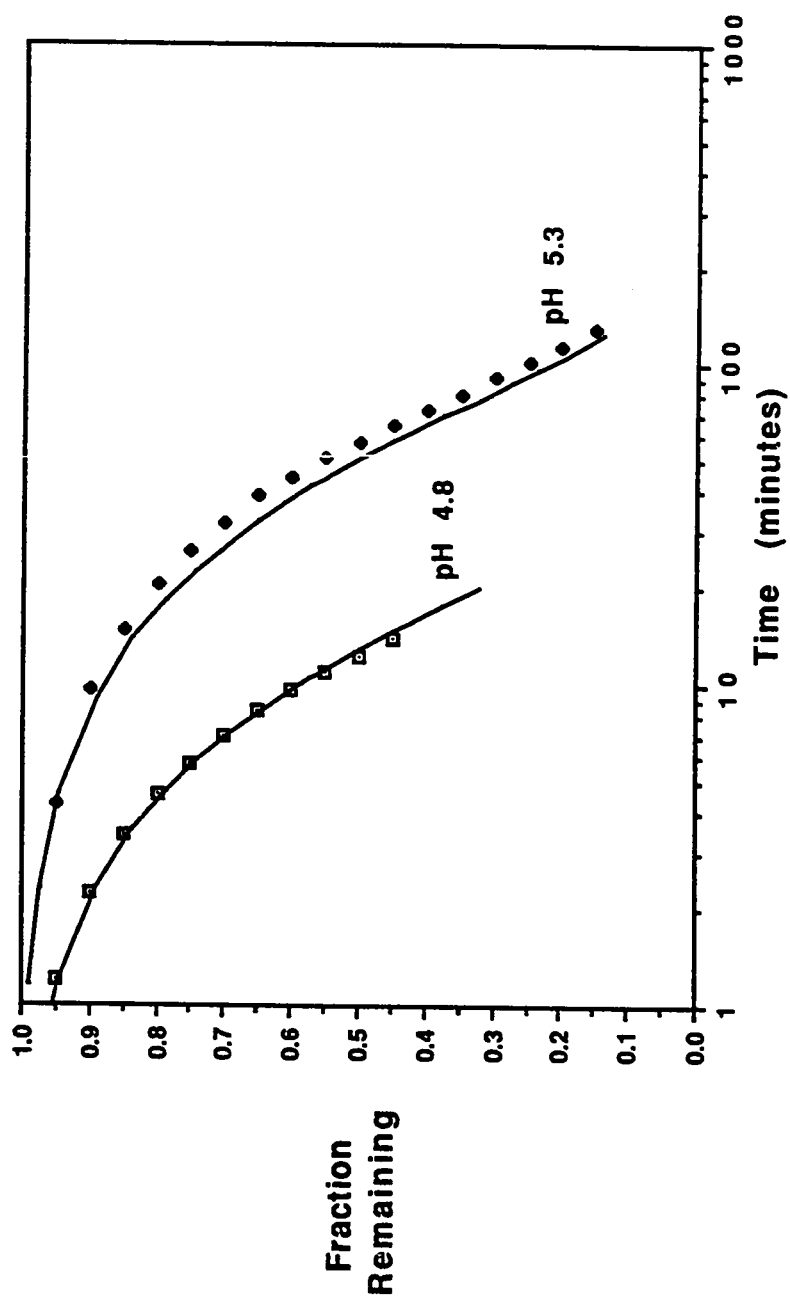


**Figure 4.1: Fraction Remaining of Reagent 1 Calcite  
Measured in 0.1M CaCl<sub>2</sub>, 0.85 atm CO<sub>2</sub> and at 55°C  
Fitted Curves using  $B = 0.1500 \mu\text{m}^{**}(-1)$**

$$D\Delta C = \delta_{ave} \frac{k_c(CaCO_{3eq} - CaCO_{3s})^{0.5}}{CaCO_{3s} \cdot CaCO_{3s}} \quad (4-20)$$

Here  $\delta_{ave}$  is found using Equation (4-18). Equation (4-20) is determined using the iterative method of the mass transfer model discussed in Chapter 3.

The value of mass transfer agitation enhancement factor, B, was estimated to be  $765 \text{ cm}^{-1}$ . This value comes from the fact that in acid solutions, the mass transfer rate is determined by the transfer rate of acid species to the limestone surface (Berner and Morse, 1974; Lund et al., 1974; Sjöberg and Rickard 1984, 1985; Wallin and Bjerle, 1989). Other researchers have noted that when acid species are present to enhance diffusion, the contribution of the finite rate reaction of  $\text{CO}_2$  to limestone dissolution can be neglected (Jarvis et al., 1988). Toprac (1981) found that in HCl solutions at  $25^\circ\text{C}$ , the enhancement factor  $B = 400 \text{ cm}^{-1}$ . In the present work with  $\text{HSO}_3^-$  as the dominant acid species at  $55^\circ\text{C}$ , his value was adjusted using Equation (4-21).

$$B = 400 \text{ cm}^{-1} \left[ \frac{D_{\text{HSO}_3^-} \text{ at } 55^\circ\text{C}}{D_{\text{H}^+} \text{ at } 25^\circ\text{C}} \right]^{-1/3} = 765 \text{ cm}^{-1} \quad (4-21)$$

Figures 4.2 and 4.3 show measured and predicted fraction remaining versus time for two limestones: Fredonia Fine and Georgia Marble Fine. The dissolution rates of the as-ground limestones were measured in the Jarvis (1988) apparatus at the conditions discussed in Chapter 3. The surface rate constants used to determine the complete curves were those values which predicted the correct time for 50% dissolved.

These predicted curves show a good fit after about 50% dissolved. The differences at high fraction remaining are probably a result of errors in the particle size measurement of the fines. When surface kinetics control dissolution, smaller particles will dissolve faster than larger ones. Thus at the start of an experiment the fraction remaining is strongly dependent on the measurement of the fines, which are the more difficult particles to measure. These differences will not cause problems with the modeling of the type and grind work in which utilizations varied from 50 to 90%. This is equivalent to the region in the fraction remaining curve of 0.5 to 0.1, respectively, which is well matched by the predictions. The good fit in this region supports the conclusion in Section 3.4.5 that the assumption of spherical particles in determining

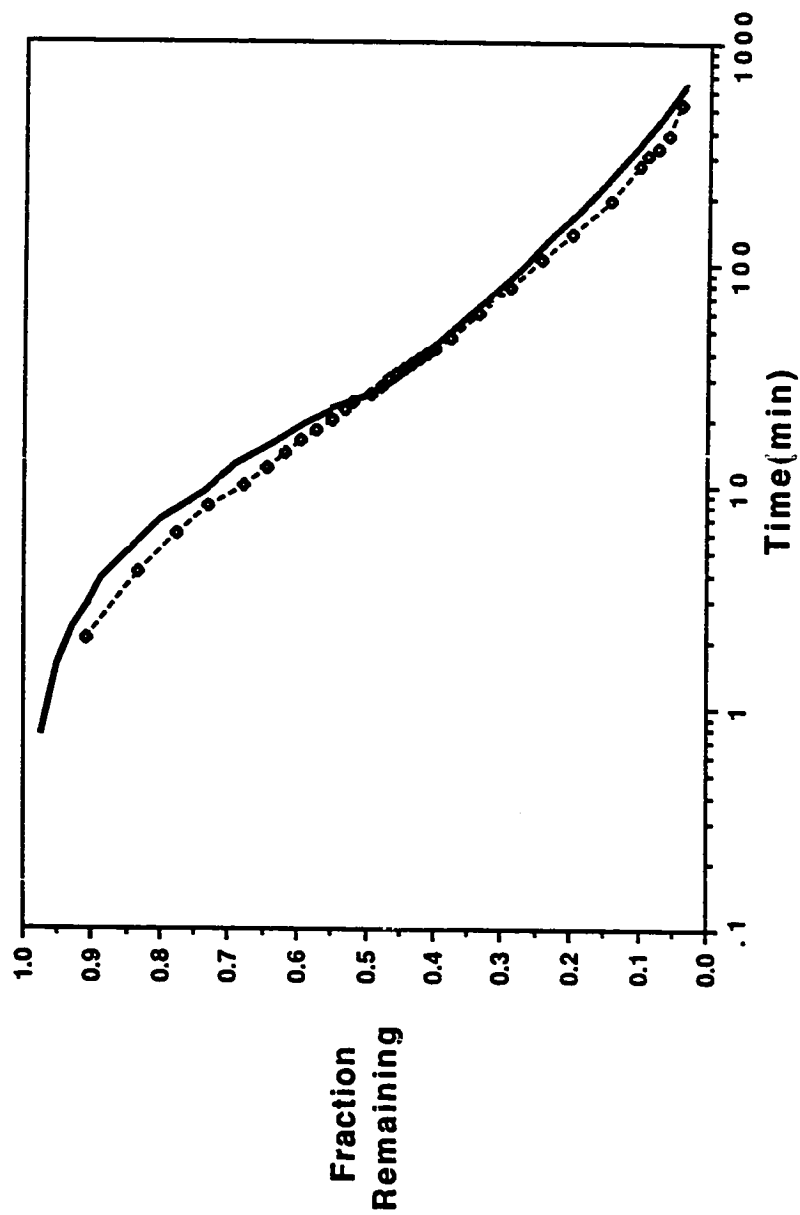


Figure 4.2: Fredonia Fine Dissolution in 2.8 mM SO<sub>3</sub>, pH 5.8 and 50°C  
Predicted Curve uses Measured PSD and  $k_c = 10^{**}(-11.80)$

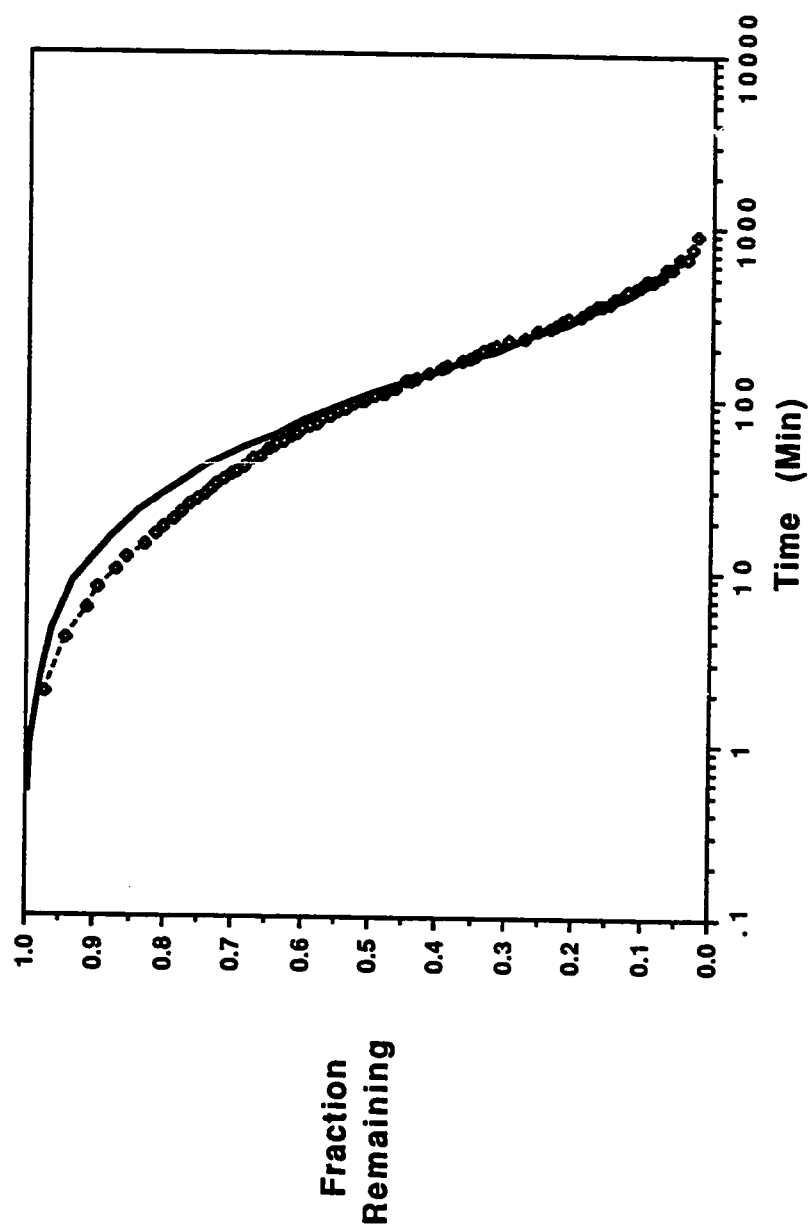


Figure 4.3: Georgia Marble Fine Dissolution in 3.3 mM SO<sub>3</sub>, pH 5.8 and 50°C. Predicted Curve uses Measured PSD and  $k_c = 10^{*(-11.86)}$

conversion of industrial stones gives acceptable results even in the presence of sulfite (i.e. BET surface area changes are not as significant as with the crystalline reagent).

As with the no sulfite experiments the shapes of the curves in Figures 4.2 and 4.3 were determined by the particle size distributions. The location of the curve along the time axis is fixed by the value of the rate constant,  $k_c$ . It was found that the enhancement factor,  $B$ , has no effect on the location of the curve when sulfite is present. This result confirms that in sulfite solutions, the dissolution of limestone is controlled by the surface rate rather than mass transfer. Additionally since  $B$  also represents the effect of the  $\text{CO}_2$  finite rate on dissolution, the lack of dependence on  $B$  confirms the results of Jarvis et al. (1988). The  $\text{CO}_2$  finite rate contribution is negligible in systems where bisulfite can act as a buffer.

These curves also demonstrate that with the appropriate surface rate constants and particle size distributions, the reactivity model can predict the relationship of fraction remaining with time. Table 4.1 shows the values of the surface rate constants for all four limestones as determined by three different methods. These methods include batch experiment measurement from initial rates of the screened stones, batch experiment measurement from the rate at 20% dissolved of the as-ground stones, and the values which were used in modeling of the EPA studies. The large errors associated with the experimental work indicate a severe problem with reproducibility. The modeled error came from sensitivity studies of the rate constant parameter.

Table 4.1 shows that there are significant differences between the values found by the experimental methods. The as-ground samples seem particularly bad since three of the stones appear to have the same reactivity while both screened and modeled show greater differences. Part of the as-ground problem may be a result of the very fast dissolution which occurs at the start of the experiments when there are many small particles present. Additionally the area calculation required to determine the flux at 20% dissolved may not be accurate. Unfortunately a significant portion of the available area depends on the smaller particles whose existence depends on the dissolution rate and the extent of time which has passed.



The values from the screened stones, however, yielded better estimates for use in the model. Part of the difference between the screened and modeled values comes from the differences in temperatures. The batch experiments were performed at 50°C, and the EPA studies were at 60°C. While rate constants decreased for three of the stones with the increase in temperature, it was necessary to increase the Fredonia value in the model. This indicates that either there were problems in measuring the dissolution of the Fredonia screened limestone (the sample actually contained fines rather than being screened to a narrow range) or that the temperature dependence of the rate constant is unique to each stone. If the latter is true, then for industrial applications it would be advisable to measure limestone dissolution at a temperature representative of scrubber conditions.

**Table 4.1: Surface Rate Constants for EPA Limestones - Screened and As-ground Values Measured in Batch Experiments; Modeled Values used in the Slurry Scrubber Model**

Limestone	Screened (325-400 mesh)	As-Ground Fine	Modeled
Fredonia	10-11.88 $\pm$ 13%	10-11.59 $\pm$ 22%	10-11.25 $\pm$ 25%
Longview	10-12.18 $\pm$ 43%	10-10.83 $\pm$ 50%	10-12.50 $\pm$ 25%
Georgia	10-12.42 $\pm$ 5%	10-11.64 $\pm$ 25%	10-12.70 $\pm$ 25%
Stoneman	10-12.09 $\pm$ 18%	10-11.63 $\pm$ 40%	10-12.65 $\pm$ 25%

#### 4.4.2 Limestone Type and Grind Studies

The computer code which was written to simulate batch experiments demonstrated that limestone reactivity could be modeled using a combined dependence on particle size distribution and limestone type surface kinetics. Therefore with appropriate modifications to account for a CSTR reactor (Equation 4-8 versus 4-7), this

approach was taken in the Slurry Scrubber Model. The agitation enhancement parameter,  $B$ , was fixed at  $765 \text{ cm}^{-1}$  for all type and grind studies. Then for each limestone type and utilization studied in the TCA system, the Slurry Scrubber Model was used to predict scrubber performance and hold tank conditions. This model requires the parameters discussed previously (Section 4.3.1) as well as the  $\text{SO}_2$  inlet concentration and initial estimates for solution and solids concentrations. The closed loop model for the scrubber and hold tank has two convergence loops. Scrubber performance is converged when the calculated  $\text{SO}_2$  inlet concentration matches the input value. The complete model convergence occurs when two consecutive hold tank solutions are equivalent within the required tolerance.

For a given limestone type the EPA study determined that  $\text{SO}_2$  removal improved with an increase in limestone fineness (Borgwardt et al., 1980). It was also noted that removal increases as utilization decreases. This is expected since for a given grind lower utilizations indicate more excess limestone and increased alkalinity. An interesting conclusion from their work was that Fredonia was much more reactive than Georgia Marble even though Fredonia had more impurities than Georgia Marble.

In modeling the type and grind study, the limestone dependent surface rate constant,  $k_c$ , was treated initially as an adjustable parameter. For each limestone type, one utilization was used to perform iterations on  $k_c$  which would give the measured removal. Then the rate constant was treated as a fixed parameter for all other utilizations and grinds of that particular stone.

#### Fredonia Limestones

The TCA scrubber was tested at four grinds of Fredonia Limestone. The wet sieve analyses of these grinds are summarized in Table 4.2. Tables 4.3 through 4.6 show measured and predicted scrubber performance values for all four grinds. These tables give the  $\text{SO}_2$  removals measured by UV, wet chemistry, and material balance. Hold tank solution compositions and make-per-pass (mpp) are shown in millimoles per liter (mM). These tables show the calcium sulfite saturation (CSS) at the measured values, as well as the error in the charge balance. This error is indicative of the errors in the measurement of solution compositions, since at equilibrium the solution should

be charge balanced. Also shown are the parameters which were specific for each run to give the measured oxidation (enhancement factor for oxygen absorption, EF) and hold tank sulfite concentration (calcium sulfite crystallization constant,  $k_{cry}$ ). The scrubber limestone reactivities which are determined from the particle sizes and the utilizations are also listed in the tables. The model results for all four grinds were predicted using a limestone rate constant of  $10^{-11.25}$ .

Table 4.2: Wet Sieve Summary for Fredonia Grinds			
Grind	% < 325 mesh	% < 200 mesh	% < 70 mesh
Feedbelt	88.6	97.4	99.9
Fine	84.1	95.3	98.1
Coarse	54.5	69.6	97.1
Extra Coarse	51.2	65.0	95.4

The results for the Fredonia Coarse grind are shown in Table 4.3. Using the appropriate rate constant and particle size distributions the Slurry Scrubber Model does a good job of predicting  $SO_2$  removal and make-per-pass. Solution compositions for most species are within 15% of the measured values. All measured pH values gave calcium sulfite saturations greater than one, and these values were also well matched by the computer model.

Table 4.4 shows the results for Fredonia Extra Coarse limestone. The  $SO_2$  removals and hold tank pH for this limestone were not predicted for either utilization. Make-per-pass was not matched either, because  $SO_2$  removals were overpredicted. The cause of the low measured values could be the result of limestone blinding. For coarse grinds at low utilizations, most of the large particles are relatively undissolved. Film thicknesses around these particles are greater and for very reactive limestones the pH drop across this film is greater. Since pH at the limestone surface is higher than the bulk, calcium sulfite saturation is also higher. As a result  $CaSO_3$  could crystallize onto the limestone. This phenomenon is indicated in the slurry scrubber model when

comparing results for low and high utilizations. For Fredonia Extra Coarse with  $U = 41.4\%$ , the model predicts a sulfite saturation of 1.62 at the surface of the limestone in the hold tank. However as the slurry passes through the scrubber, calcium sulfite saturation at the limestone surface increases from 1.90 at the scrubber inlet to 2.34 at the exit. For Fredonia Coarse with  $U = 81.1\%$ , which has a similar  $\text{SO}_2$  removal, the sulfite saturation is predicted to be 2.04 at the limestone surface in the hold tank, but

<b>Table 4.3: Hold Tank Solutions and Scrubber Performance for Fredonia Coarse Limestone</b> <b>Predicted Conditions use <math>k_c = 10^{-11.25}</math></b>								
	U= 87.8%		U= 81.1%		U=77.1%		U=69.6%	
	Meas.	Pred.	Meas.	Pred.	Meas.	Pred.	Meas.	Pred.
% $\text{SO}_2$ Rem.		67.6		73.4		80.5		80.3
Wet	69.2		75.2		81.3		84.1	
UV	70.5		73.7		80.0		82.7	
Mat. Bal.	70.7		77.1		91.2		97.8	
[ $\text{SO}_3^-$ ]	9.8	9.8	5.7	5.4	2.1	2.7	2.6	2.7
[ $\text{CO}_3^-$ ]	4.3	5.2	4.6	5.5	4.7	5.9	4.9	5.9
[ $\text{SO}_4^-$ ]	14.5	15.5	15.2	22.2	7.0	7.9	8.7	15.4
[ $\text{Ca}^{++}$ ]	50.1	44.5	39.2	39.6	27.9	29.0	30.0	29.3
pH	5.55	5.59	5.85	5.85	6.1	5.93	6.15	6.06
CSS	2.60	2.38	2.35	1.98	1.09	1.10	1.38	1.46
% Oxid.	15.9	17.6	24.9	23.4	12.2	14.0	24.7	21.2
mpp	11.5	10.7	12.3	11.8	12.7	11.6	12.0	12.9
% Error	7.0		8.8		0.3		25.4	
% Solids	8.9		8.6		8.4		9.1	
E		1.0		2.5		1.0		2.5
$k_{\text{cry}}$		0.007		0.025		0.80		0.12
$K(\times 10^5)$		2.77		3.03		3.22		3.79

**Table 4.4: Hold Tank Solutions and Scrubber Performance for Fredonia Extra Coarse Limestone**  
**Predicted Conditions use  $k_c = 10^{-11.25}$**

	U= 50.8%		U=41.1%	
	Meas.	Pred.	Meas.	Pred.
% SO <sub>2</sub> Rem.		89.6		90.5
Wet	80.1		76.5	
UV	84.8		79.0	
Mat.Bal.	77.7		---	
[SO <sub>3</sub> <sup>=</sup> ]	3.3	3.2	2.5	2.6
[CO <sub>3</sub> <sup>=</sup> ]	7.1	5.1	5.6	5.5
[SO <sub>4</sub> <sup>=</sup> ]	8.5	13.8	4.8	13.6
[Ca <sup>++</sup> ]	73.9	73.7	74.1	81.2
pH	5.4	5.96	5.5	5.94
CSS	1.07	1.94	0.94	1.61
% Oxid.	26.8	25.5	23.7	24.2
mpp	9.8	11.5	10.0	13.5
% Error	6.8		2.8	
% Solids	9.4		8.0	
E		2.5		3.0
k <sub>cry</sub>		0.03		0.12
K(x 10 <sup>5</sup> )		6.63		4.31

then decreases as the slurry passes through the scrubber. Calcium sulfite saturation at the scrubber inlet is 1.66 dropping to 1.01 at the exit. These predictions along with the observed conditions indicate that limestone blinding occurs in the scrubber rather than in the hold tank where calcium sulfite crystallization is intended to occur.

Another indicator of blinding is the low pH values. Typically since low utilizations indicate high excess limestone, the hold tank pH should be high from the increased limestone dissolution. However, once limestone is blinded, the dissolution

is slowed or stopped. This situation combined with SO<sub>2</sub> absorption causes the bulk pH to drop. Also for a given total solids concentrations, lower limestone utilizations would indicate fewer calcium sulfite seed crystals.

If blinding is modeled as a reduction in active dissolution sites by decreasing the surface rate constant, both SO<sub>2</sub> removal and hold tank pH are more accurately predicted. Using  $k_c = 10^{-12.55}$ , with U=41.4%, the predicted removal is 79.1% compared to the measured average of 80.9%, and the predicted hold tank pH is 5.6 compared to the measured 5.5. When U=50.8%, predicted SO<sub>2</sub> removal is 77.5% compared to 77.8%, and hold tank pH is 5.6 compared to the measured 5.4.

<b>Table 4.5: Hold Tank Solutions and Scrubber Performance for Fredonia Fine Limestone</b> <b>Predicted Conditions use <math>k_c = 10^{-11.25}</math></b>						
	U= 82.8%		U= 76.9%		U=66.7%	
	Meas.	Pred.	Meas.	Pred.	Meas.	Pred.
% SO <sub>2</sub> Rem.		85.5		90.4		96.9
Mat. Bal.	85.7		91.6		93.5	
Wet	86.7		84.4		85.0	
UV	82.3		---		89.6	
[SO <sub>3</sub> <sup>=</sup> ]	3.2	3.3	2.5	2.7	2.5	2.5
[CO <sub>3</sub> <sup>=</sup> ]	6.2	5.7	5.9	5.3	6.5	5.4
[SO <sub>4</sub> <sup>=</sup> ]	4.1	12.4	9.1	14.5	3.5	6.8
[Ca <sup>++</sup> ]	38.4	43.0	77.1	78.9	46.7	47.0
pH	5.5	5.94	4.7	5.88	5.5	5.98
CSS	0.82	1.68	0.23	1.51	0.76	1.34
% Oxid	15.3	17.0	19.4	20.0	7.6	15.4
mpp	11.8	12.8	11.5	12.7	12.0	10.7
% Error	7.6		5.4		6.0	
% Solids	9.2		10.7		8.7	
E		1.7		2.0		1.0
k <sub>cry</sub>		0.03		0.08		0.08
K(x 10 <sup>5</sup> )		10.2		12.1		17.2

The results for Fredonia Fine and Feedbelt grinds are shown in Tables 4.5 and 4.6, respectively. Based on wet analysis, Fredonia Fine and Feedbelt grinds performed the same in the scrubber despite the finer grind of the Feedbelt (Chang and Dempsey, February, 1981). This similarity was also predicted by the scrubber model, however at the lowest utilization of the Feedbelt grind, the model overpredicted the measured removal. For  $U=66.7\%$ , the Fine grind shows a 93.5% removal by material balance which is about 3% less than the predicted value. However for Fredonia

**Table 4.6: Hold Tank Solutions and Scrubber Performance for Fredonia Feedbelt Limestone**  
Predicted Conditions use  $k_c = 10^{-11.25}$

		U= 88.0%		U= 78.7%		U=53.3%	
		Meas.	Pred.	Meas.	Pred.	Meas.	Pred.
% SO <sub>2</sub> Rem.		81.1		91.3		97.9	
Mat. Bal.	82.2			85.9		86.4	
Wet	81.0			84.3		86.0	
UV	80.0			79.6		86.5	
[SO <sub>3</sub> =]	2.6	2.5		2.6	2.3	3.3	2.6
[CO <sub>3</sub> =]	5.0	5.4		5.7	6.1	4.8	6.0
[SO <sub>4</sub> =]	15.5	19.3		4.2	6.5	18.5	21.9
[Ca <sup>++</sup> ]	49.8	53.5		60.3	53.7	44.7	43.0
pH	5.5	6.0		5.6	5.98	5.8	6.13
CSS	0.80	1.01		0.98	1.19	1.26	1.37
% Oxid.	43.9	42.3		13.0	12.0	22.4	21.7
mpp	11.4	12.6		12.2	14.0	12.4	15.4
% Error	10.8			10.3		6.3	
% Solids	9.4			9.5		9.5	
E		6.0			1.0		3.0
k <sub>cry</sub>		0.20			0.20		0.20
K(x 10 <sup>5</sup> )		12.6			15.3		35.0

Feedbelt at  $U = 53.3\%$ , the measured  $\text{SO}_2$  removal was 86% compared to the prediction of 97%. This utilization indicates a large excess of limestone in the system, and it could be that the Fredonia limestone was also blinded in this run. If the surface rate constant for this Feedbelt case is reduced to the same value used to simulate blinding of the Extra Coarse limestone ( $10^{-12.55}$ ), then the predicted removal is 88% and the hold tank pH is 5.89 compared to the measured values of 86.2% removal and pH 5.8.

Using the expected Fredonia rate constant ( $10^{-11.25}$ ), hold tank pH is not accurately predicted for any of the Fine or Feedbelt utilizations. However in many cases the measured pH values are suspect because the measured concentrations and pH yield solutions which are undersaturated to calcium sulfite. This is not possible since these solutions are from the hold tank where  $\text{CaSO}_3$  is crystallizing. Therefore measured pH values would not be matched. This problem was recognized by the researchers for Fredonia Fine (Dempsey, August 1979). They concluded that the measured values of hold tank pH were in error and that the electrode was possibly damaged during a three month shut down of the system for modifications to handle dual alkali studies.

#### Georgia Marble Limestones

The TCA scrubber was tested at two grinds of Georgia Marble Limestone. The wet sieve analysis of these grinds is summarized in Table 4.7. Tables 4.8 and 4.9 show the measured and predicted scrubber performance values for  $\text{SO}_2$  removal and hold tank solutions. Georgia Marble limestones were modeled using  $k_c = 10^{-12.70}$ . This value does an adequate job of predicting removals and hold tank conditions. The results for Georgia Marble fine are shown in Table 4.8. The measured  $\text{SO}_2$  removals for this grind were in error since the removal based on wet gas analysis decreased with an increase in utilization. This result is contrary to expected trends. The material balance method, however, shows the expected trend, and the model predictions of  $\text{SO}_2$  removal compare well with these values. Hold tank conditions are also well matched. These predictions help to confirm that for the fine stones the material balance method does a better job of estimating  $\text{SO}_2$  removal than the UV or gas wet analysis.



**Table 4.7: Wet Sieve Summary for Georgia Marble Grinds**

Grind	% < 325 mesh	% < 200 mesh	% < 70 mesh
Fine	84.1	98.6	99.9
Coarse	48.1	70.1	94.7

**Table 4.8: Hold Tank Solutions and Scrubber Performance  
for Georgia Marble Fine Limestone**  
Predicted Conditions use  $k_c = 10^{-12.70}$

	U= 73.8%		U=61.8%	
	Meas.	Pred.	Meas.	Pred.
% SO <sub>2</sub> Rem.		75.4		70.8
Mat. Bal.	78.0		68.0	
Wet	75.9		79.2	
UV	86.0		86.0	
[SO <sub>3</sub> <sup>=</sup> ]	5.4	5.4	3.2	3.8
[CO <sub>3</sub> <sup>=</sup> ]	4.1	4.4	5.4	4.8
[SO <sub>4</sub> <sup>=</sup> ]	7.7	9.9	2.8	7.8
[Ca <sup>++</sup> ]	52.6	52.7	53.4	49.7
pH	5.2	5.44	5.4	5.56
CSS	0.96	1.24	0.84	1.09
% Oxid.	15.0	15.4	6.4	12.9
mpp	12.7	12.3	12.7	12.6
% Error	2.7		10.5	
% solids	8.1		8.3	
EF		1.0		1.0
k <sub>cry</sub>		0.20		1.20
K(x10 <sup>5</sup> )		7.69		6.47

Table 4.9 shows the measured and predicted values for Georgia Marble coarse. For this grind the material balance method shows the unexpected trend of increased removal with increased utilization. However, both gas analyses show little change in SO<sub>2</sub> removal with changes in utilization. This is also the trend predicted by the slurry scrubber model. In fact, the model predictions are within experimental error for all utilizations when the gas analyses are averaged.

<b>Table 4.9: Hold Tank Solutions and Scrubber Performance for Georgia Marble Coarse Limestone Predicted Conditions use <math>k_c = 10^{-12.70}</math></b>						
	U= 51.6%		U= 46.7%		U=39.9%	
	Meas.	Pred.	Meas.	Pred.	Meas.	Pred.
% SO <sub>2</sub> Rem.		74.4		75.4		78.0
UV	73.0		73.0		76.0	
Wet	71.0		70.0		70.0	
Mat. Bal.	50.0		68.0		65.0	
[SO <sub>3</sub> =]	3.6	3.9	5.9	5.7	1.9	3.4
[CO <sub>3</sub> =]	4.3	4.3	7.3	4.0	6.0	4.4
[SO <sub>4</sub> =]	3.8	8.3	4.4	14.6	4.5	7.7
[Ca <sup>++</sup> ]	59.6	61.8	38.2	43.5	56.1	55.2
pH	5.3	5.49	5.6	5.57	5.4	5.59
CSS	0.84	1.11	1.91	1.84	0.53	1.16
% Oxid.	11.0	15.3	18.6	19.1	16.0	14.7
mpp	10.5	11.3	9.6	10.2	10.9	11.1
% Error	3.0		7.7		7.0	
% Solids	8.8		8.6		8.2	
EF		1.0		1.2		1.0
k <sub>cry</sub>		0.70		0.04		1.10
K(x 10 <sup>5</sup> )		3.78		3.62		3.99

Dempsey et al. (September, 1979) had hypothesized that the gas analyses were in error and used the material balance methods to extrapolate comparisons between limestone types. The scrubber model, however, shows that the gas analyses might not be as inaccurate as thought. Apparently at the low utilizations, there are sufficient numbers of smaller particles that the dissolution flux is relatively constant even though utilization changes. This result is shown by the Slurry Scrubber Model which indicates only a 5% change in reactivity, from  $3.78 \times 10^5$  to  $4.00 \times 10^5 \text{ M}^{-1}\text{cm}^{-2}$ , for a decrease in utilization of Georgia Marble coarse from 51.6% to 39.9%. A similar decrease in utilization for Georgia Marble Fine, from 73.8% to 61.8%, resulted in a 19% increase in limestone reactivity from  $6.47 \times 10^5$  to  $7.69 \times 10^5 \text{ M}^{-1}\text{cm}^{-2}$ . These results show that at low utilizations of this study, the limestone dissolution flux was constant for Georgia Marble coarse limestone.

In addition to the constant reactivity, the usual changes in surface area have been counteracted by the changes in slurry percent solids. As utilization increases, the remaining particles become smaller giving higher surface area per particle. However, the percent solids (and therefore total available  $\text{CaCO}_3$  particles) decreased during these runs as the utilization decreased. This would result in a relatively constant total dissolution area and when combined with a constant flux would give a dissolution rate which did not change with utilization. Therefore  $\text{SO}_2$  removals would be approximately constant. This phenomena was both measured and predicted for Georgia Marble coarse.

#### Longview Limestones

The TCA scrubber was tested at two grinds of Longview limestone. The wet sieve analysis of these grinds is summarized in Table 4.10. Tables 4.11 and 4.12 show the measured and predicted scrubber performance values for  $\text{SO}_2$  removal and hold tank solutions. Longview limestones were modeled using  $k_c = 10^{-12.50}$ . With this value the model does a very good job of predicting removal and hold tank pH for both Longview grinds.

Table 4.10: Wet Sieve Summary for Longview Grinds			
Grind	% < 325 mesh	% < 200 mesh	% < 70 mesh
Fine	84.6	98.1	99.9
Coarse	58.2	70.9	98.4

Table 4.11: Hold Tank Solutions and Scrubber Performance for Longview Fine Limestone Predicted Conditions use $k_c = 10-12.50$						
	U= 81.4%		U= 67.1%		U=55.1%	
	Meas.	Pred.	Meas.	Pred.	Meas.	Pred.
% SO <sub>2</sub> Rem.		73.2		79.2		82.3
Mat.Bal.	72.1		77.6		83.7	
Wet	71.4		76.8		83.4	
UV	70.0		76.3		83.2	
[SO <sub>3</sub> =]	3.8	4.2	2.6	3.0	2.4	2.8
[CO <sub>3</sub> =]	3.7	4.3	5.2	4.6	3.6	5.0
[SO <sub>4</sub> =]	12.9	16.7	10.4	17.3	13.1	19.0
[Ca <sup>++</sup> ]	64.0	68.1	42.8	59.8	59.8	48.3
pH	5.5	5.52	6.32	5.68	6.32	5.83
CSS	1.25	1.28	1.60	1.14	1.71	1.18
% Oxid.	29.4	31.6	27.6	27.7	30.0	29.3
mpp	10.6	11.2	11.1	12.4	11.9	13.1
% Error	-.2		27		4.1	
% Solids	9.6		9.4		9.6	
EF		3.5		3.3		4.0
k <sub>cry</sub>		0.25		1.20		0.80
K(x 10 <sup>5</sup> )		9.55		11.8		14.9

The only problems noted with the Longview stones were the pH values for the two lowest utilizations of the fine grind as shown in Table 4.11. These measurements were apparently erroneous because at pH 6.3 the calcium carbonate saturations for both solutions were greater than one. For  $U = 67.1\%$  and  $U = 55.1\%$ , the calcium carbonate saturations were 1.8 and 1.6 respectively. This condition would not be possible in a hold tank which is designed for limestone dissolution not crystallization. Typically calcium carbonate saturations in scrubbing systems are 0.03 to 0.25 (Rochelle, 1983).

**Table 4.12: Hold Tank Solutions and Scrubber Performance for Longview Coarse Limestone**  
Predicted Conditions use  $k_c = 10^{-12.50}$

	U= 75.3%		U= 74.0%		U=66.7%		U=56.1%	
	Meas.	Pred.	Meas.	Pred.	Meas.	Pred.	Meas.	Pred.
% SO <sub>2</sub> Rem.		70.3		72.3		77.1		79.7
Mat.Bal.	69.9		67.0		69.7		78.2	
Wet	67.9		67.0		70.0		76.0	
UV	70.1		58.0		69.5		76.0	
[SO <sub>3</sub> =]	4.6	4.7	4.0	4.4	3.0	3.5	1.9	2.9
[CO <sub>3</sub> =]	4.1	4.2	4.2	4.3	3.7	4.4	4.3	4.7
[SO <sub>4</sub> =]	11.7	17.0	18.3	18.1	18.1	17.9	14.9	17.0
[Ca <sup>++</sup> ]	61.3	60.5	58.7	54.2	53.7	53.6	58.2	60.3
pH	5.46	5.47	5.4	5.52	5.6	5.64	5.75	5.72
CSS	1.40	1.26	1.05	1.23	1.00	1.19	0.81	1.15
% Oxid.	24.8	25.7	24.0	24.1	28.4	26.5	32.2	31.1
mpp	9.8	11.0	9.7	11.3	10.0	11.3	11.2	12.6
% Error	6.7		9.8		0.3		4.0	
% Solids	9.5		9.2		9.6		9.6	
E		2.5		2.5		3.0		4.0
k <sub>cry</sub>		0.30		0.40		0.60		1.20
K(x 10 <sup>5</sup> )		4.42		5.04		5.59		8.86

Limestone blinding was not observed with either Longview grind at utilizations similar to those resulting in blinding of Fredonia limestones. This is a result of the differences in particle size distributions and the surface rate constants. Both Fredonia Fine and Extra Coarse were coarser than their Longview counterparts (Tables 4.2 and 4.10). More importantly, based on a comparison of surface rate constants, Fredonia limestone is 20 times more reactive than Longview in the presence of sulfite. Therefore for given bulk solution concentrations, pH at the limestone surface of Fredonia would be higher than Longview. These results indicate that it is the more reactive limestones which are potentially susceptible to limestone blinding and that blinding may be related to limestone type rather than grind.

#### Stoneman Limestones

The TCA scrubber was tested at two grinds of Stoneman limestone. The wet sieve analysis of these grinds is summarized in Table 4.13. Tables 4.14 and 4.15 show the measured and predicted scrubber performance values for SO<sub>2</sub> removal and hold tank solutions. Stoneman limestones were modeled using  $k_c = 10^{-12.65}$ . With this value the model does a very good job of predicting removals for both Stoneman grinds.

Table 4.13: Wet Sieve Summary for Stoneman Grinds			
Grind	% < 325 mesh	% < 200 mesh	% < 70 mesh
Fine	82.9	98.7	98.8
Coarse	52.9	71.6	96.4

The results for Stoneman Fine are shown in Table 4.14. Both SO<sub>2</sub> removal and hold tank pH were matched for this grind. Table 4.15 shows the measured and predicted values of Stoneman Coarse. SO<sub>2</sub> removals and make-per-pass were well matched, but hold tank pH and SO<sub>3</sub><sup>=</sup> concentrations were not matched. The large

charge balance errors for this stone show there were significant errors in the measurements of solution composition. Additional indicators of error at all three utilizations of this grind are the very low saturations of calcium sulfite which only varied from 0.15 to 0.61.

<b>Table 4.14: Hold Tank Solutions and Scrubber Performance for Stoneman Fine Limestone</b> <b>Predicted Conditions use <math>k_c = 10^{-12.65}</math></b>				
	U= 76.7%		U=70.4%	
	Meas.	Pred.	Meas.	Pred.
% SO <sub>2</sub> Rem.		72.7		75.5
Mat. Bal.	71.3		81.0	
Wet	66.4		74.2	
[SO <sub>3</sub> <sup>=</sup> ]	3.3	4.2	3.1	3.9
[CO <sub>3</sub> <sup>=</sup> ]	5.3	4.5	5.8	4.8
[SO <sub>4</sub> <sup>=</sup> ]	2.7	10.7	3.1	8.4
[Ca <sup>++</sup> ]	53.4	52.7	45.4	36.6
pH	5.4	5.49	5.6	5.62
CSS	0.84	1.14	1.03	1.13
% Oxid.	12.0	17.0	7.4	14.0
mpp	10.0	11.9	12.5	12.4
% Error	10.5		20.6	
% solids	9.6		8.5	
EF		1.0		1.0
k <sub>cry</sub>		0.60		0.60
K(x 10 <sup>5</sup> )		8.13		8.57

**Table 4.15: Hold Tank Solutions and Scrubber Performance  
for Stoneman Coarse Limestone  
Predicted Conditions use  $k_c = 10^{-12.65}$**

	U= 78.5%		U= 63.4%		U=54.8%	
	Meas.	Pred.	Meas.	Pred.	Meas.	Pred.
% SO <sub>2</sub> Rem.		66.1		71.1		80.5
UV	67.0		71.9		78.5	
Wet	65.0		70.6		78.0	
Mat. Bal.	75.1		77.1		79.5	
[SO <sub>3</sub> <sup>=</sup> ]	3.6	7.1	2.8	4.8	3.5	4.1
[CO <sub>3</sub> <sup>=</sup> ]	1.8	4.4	3.7	4.2	6.3	4.5
[SO <sub>4</sub> <sup>=</sup> ]	8.9	14.2	3.2	11.0	2.2	15.0
[Ca <sup>++</sup> ]	42.9	36.5	26.2	39.7	37.7	31.1
pH	4.6	5.43	5.3	5.57	5.3	5.75
CSS	0.15	1.22	0.36	1.16	0.61	1.27
% Oxid.	11.0	16.0	9.7	16.3	11.7	17.1
mpp	10.9	10.8	11.4	10.6	11.8	10.7
% Error	15.1		12.3		10.9	
% Solids	9.3		7.0		9.3	
EF		1.0		1.0		1.0
k <sub>cry</sub>		0.20		0.60		0.20
K(x 10 <sup>5</sup> )		3.12		3.68		4.15

### General Discussion

The scrubber performance predictions from the Slurry Scrubber Model are summarized in Figure 4.4 where predicted SO<sub>2</sub> removals from all runs are plotted against the measured removals. For most limestone types and utilizations the predicted values are within the  $\pm 4\%$  measurement errors. The three greatest outliers are the Fredonia cases which were determined to have blinded limestones.



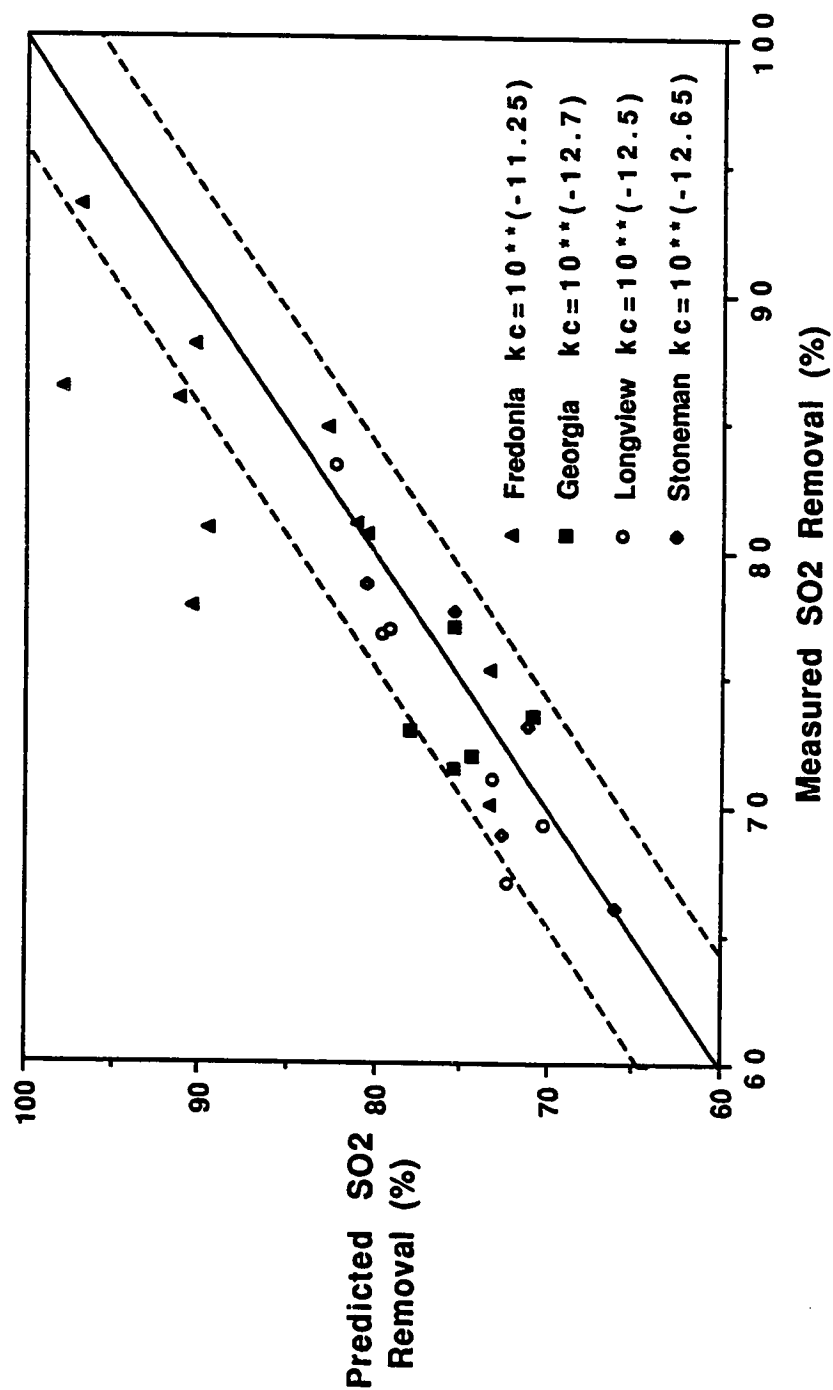


Figure 4.4: SO<sub>2</sub> Parity Plot from Type and Grind Study  
Predicted Removals from the Slurry Scrubber Model

The surface rate constants which were used to model the four limestone types ranged from  $10^{-11.25}$  to  $10^{-12.7}$ . These values slightly extend the region of rate constants determined for the limestone types discussed in Chapter 3. As shown in Table 3.7, those rate constants ranged from  $10^{-11.62}$  to  $10^{-12.66}$ . Apparently Fredonia limestone ( $k_c = 10^{-11.25}$ ) is much more reactive than reagent calcite ( $k_c = 10^{-11.62}$ ). This demonstrates again that reactivity is not necessarily related to limestone purity.

It was observed for all limestone types and utilizations that when the correct limestone surface rate constant is used, solution compositions from the hold tank can, in general, be predicted to within 15%. However, in many cases, there were significant overpredictions of the sulfate concentrations. There are two reasons for these deviations. The first involves measurement errors which were deduced by Dempsey (December, 1980). He noted that in some cases (eg. Longview limestones and Fredonia Extra Coarse) oxidation of the solids was greater than 20%, yet solution compositions indicated undersaturation to gypsum. It has been observed by previous investigators that oxidations greater than 15% will result in solutions which are supersaturated to gypsum.

It can also be concluded that the measurement error must be in the sulfate measurement rather than the pH or calcium. An error in pH can not explain the undersaturation to gypsum because  $pK_2$  for  $H_2SO_4$  is approximately 2.5. Therefore in the scrubber and hold tank which have pH values from 4 to 6, sulfate is largely present as  $SO_4^{=}$  which remains independent of the pH changes. Errors in calcium measurements could not be the cause either, since the calcium concentration is fixed by its soluble salts, and the measured values were well predicted by the model.

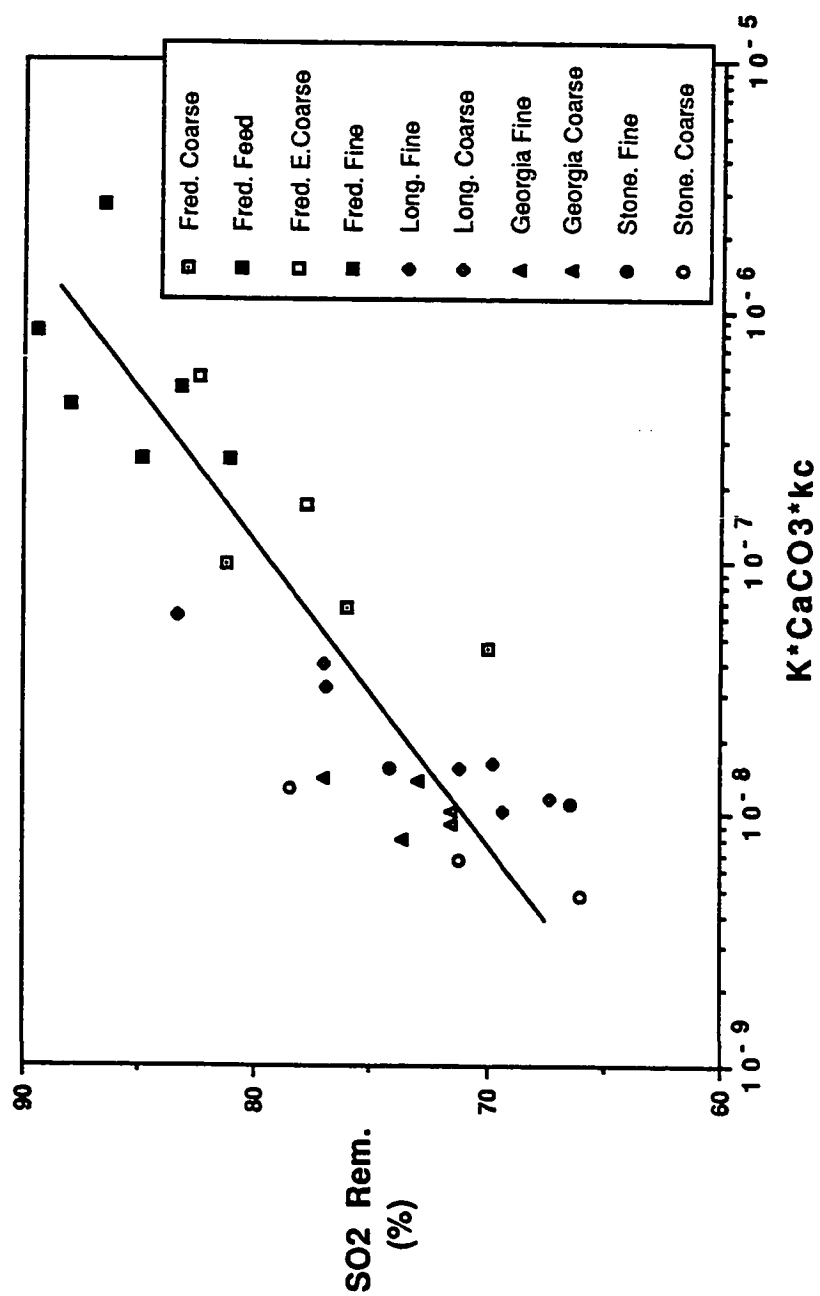
The second explanation for the poor sulfate predictions apply to the limestone cases which had measured oxidations less than 11% (eg. Stoneman limestones), but which had calculated values of approximately 15%. In these cases  $O_2$  absorption was calculated using an enhancement factor of 1.0, equivalent to physical absorption only. In the scrubber physical absorption accounted for 5 to 8% of the total calculated oxidation. This amount of oxidation would be overpredicted if there were known oxygen inhibitors in the solution. The Slurry Scrubber Model is not able to predict cases when the oxidation of sulfite to sulfate will be inhibited.

In the hold tank the model is constrained by the fixed hold tank parameters ( $L/G$  and  $N_I$ ) to give 9% oxidation for all cases. This constraint results from the selection of the hold tank stripping parameters which were fixed for all runs. It would be hoped that for a given hold tank operating under natural oxidation, liquid phase transfer units and  $L/G$  would remain unchanged. The values which were used in the model were selected to give the average carbonate concentration. However, there were large deviations among the measured carbonate concentrations which were not matched by the model. These deviations in the measurements can be explained physically by differences in gas flowrate across the surface of the hold tank which, in turn, would affect the stripping rate. Since these changes could not be quantified, it was decided not to adjust the parameters to match the measured carbonate concentration but to fix them for all runs (See Section 4.3). The fact that stripping rate in the hold tank was not matched also explains why oxidation was not matched. Computer runs which overpredicted stripping (i.e. underpredicted carbonate) would also overpredict oxidation (eg. both Stoneman grinds at the lowest utilizations).

For a given limestone, the utilization is a function of  $k_m\tau$  (Equations 4-7 and 4-8). If two different limestones give the same  $SO_2$  removal, the solution compositions must be the same. If the limestone dependence of  $k_m$  is removed, then the adjusted  $k_m$  is a constant. Within a CSTR system the utilization is inversely proportional to  $\tau$  for a given hold tank volume and constant calcium solids concentration. Figure 4.5 shows the relationship between  $SO_2$  removal and limestone reactivities. In this figure the normalized reactivities, the  $K$  values listed in the results tables, have been corrected for the differences in the total calcium solids by multiplication with the solid calcium carbonate concentration. Mathematically, these values were calculated using Equation (4-22).

$$\text{Adjusted Reactivity} = K[CaCO_3]_s k_c \quad (4-22)$$

The majority of the scatter in this data is a result of the errors in the  $SO_2$  removal measurements. The line drawn through the data is an estimate of the best fit trend. About this line 80% of the data points are within the  $\pm 4\%$  measurement error. One of the outliers is a blinded limestone.

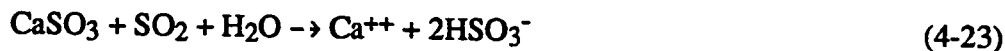
Figure 4.5: SO<sub>2</sub> Dependence on Limestone Reactivity

Although there is scatter in the data, the relationship between limestone reactivity and SO<sub>2</sub> removal is well demonstrated. The reactivities range over three orders of magnitude with a corresponding 30% change in SO<sub>2</sub> removal. At a given reactivity, such as 10<sup>-8</sup> l/gmol-cm, the greatest variation in SO<sub>2</sub> removal is about 12%, of which 8% can be accounted for as measurement errors.

The relationship plotted in Figure 4.5 was based on the assumption that the solution compositions are the same for a given removal. In terms of limestone reactivity this assumption implies that all alkalinity is provided by limestone dissolution. However, some alkalinity is provided by dissolution of calcium sulfite. Since this source has not been accounted for in the abscissa value, this omission will also contribute to some of the scatter in the data.

#### 4.4.3 CaSO<sub>3</sub> Dissolution

In systems with high limestone utilization (low excess limestone), alkalinity in the scrubber can be provided by dissolution of calcium sulfite solids. As shown in Equation (4-23) the stoichiometry of the reaction is one mole calcium sulfite dissolved per mole SO<sub>2</sub> absorbed.



The Slurry Scrubber Model was used to study the effect of dissolving calcium sulfite on SO<sub>2</sub> removal. For the study limestone utilization was fixed at 88% and the calcium sulfite crystallization constant in the hold tank was adjusted to maintain the same scrubber inlet SO<sub>3</sub> concentrations. Figure 4.6 shows the relationship between the dissolved calcium sulfite and the make-per-pass (mpp). Make-per-pass is the moles of SO<sub>2</sub> absorbed per liter of scrubber solution. While the CaSO<sub>3</sub> solids dissolved in the scrubber increases from 1 mM to 5 mM, the make-per-pass only increases from 10.3 mM to 11.25 mM instead of an expected increase of 4 mM. The SO<sub>2</sub> percent removals which corresponded to 10.3 and 11.25 mM were 69.2% and 71.6%.

The reason for the only marginal improvement can be seen in Figure 4.7. In this plot the calcium sulfite and limestone which dissolve in the scrubber are shown against the changes in the calcium sulfite dissolution parameter. An order of magnitude

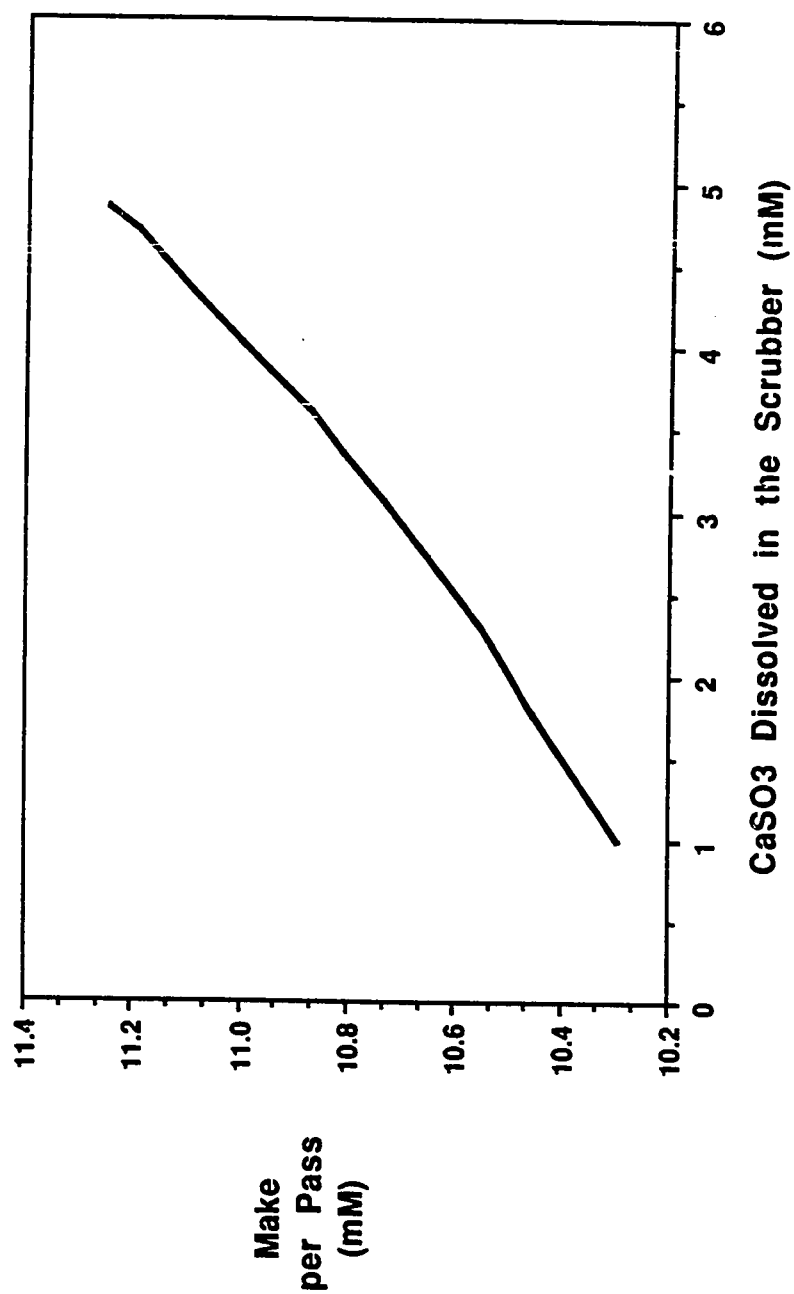


Figure 4.6: Effect of  $\text{CaSO}_3$  Dissolution on Scrubber Performance  
 $U=88\%$ ,  $K(\text{CaCO}_3)=2.77 \times 10^{-5}$  ( $\text{l/gmol-cm}^2$ ), 3170 ppm  $\text{SO}_2$  Inlet

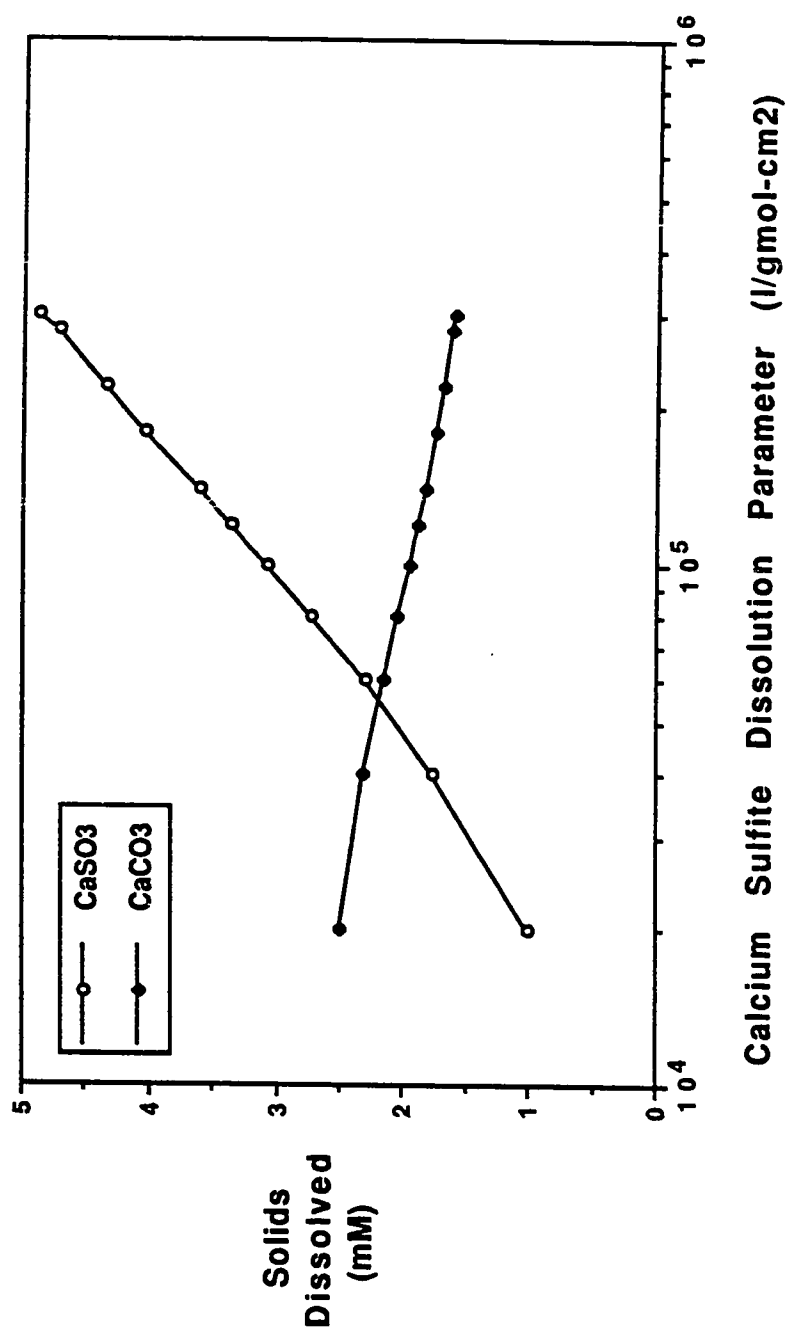


Figure 4.7: Relationship between Dissolved Solids for U=88%,  
 $K(\text{CaCO}_3)=2.77 \times 10^{-5}$  (l/gmol-cm<sup>2</sup>), 3170ppm SO<sub>2</sub> inlet

increase in the dissolution parameter causes a 4 mM increase in sulfite solids dissolved but this increase in sulfite dissolved provides additional inhibiting effect for limestone dissolution. This inhibition results in a decrease of dissolved limestone solids from 2.5mM to 1.5 mM. The stoichiometry for scrubber limestone dissolution is shown in Equation (4-24).



From this equation it is apparent that each mM loss in dissolved limestone results in a loss of two mM absorbed  $\text{SO}_2$ . Therefore calcium sulfite dissolution must compensate for this loss through its 1-1 stoichiometry (Equation 4-23).

The relative contributions of limestone and sulfite reactivities are shown in Figure 4.8. For the study of calcium sulfite reactivity, limestone reactivity was fixed at  $2.8 \times 10^5$  l/gmol-cm<sup>2</sup>. For the study of limestone reactivity, calcium sulfite reactivity was fixed at  $2.0 \times 10^4$  l/gmol-cm<sup>2</sup>. These reactivities have been normalized by their respective solids concentrations. By comparing slopes at the baseline case, this graph demonstrates again that, per gram-mole of solid, limestone is twice as productive as calcium sulfite (Equation 4-24 versus 4-23).

#### 4.4.4 Parameter Analysis

Through a sensitivity analysis on the model parameters the Slurry Scrubber Model can be used to study the implications of limestone type effects on scrubber performance. Although hydrodynamic parameters such as mass transfer coefficients, spray droplet size, and gas phase transfer units have a significant impact on scrubber performance, they will not be discussed here. This study will mainly address those parameters which relate to the chemistry of scrubber performance, especially parameters related to limestone reactivity such as utilization and solid concentrations. The two hydrodynamic parameters which are studied include L/G and scrubber residence time. Changes in these parameters are assumed to be independent of changes in mass transfer coefficients and transfer units. This assumption may not be too bad in a spray tower. An increase in L/G will obviously provide additional area for gas/liquid mass transfer, but the ratio of  $\frac{k_{la}}{k_{ga}}$  should be relatively unchanged. A change in liquor



residence time can be physically simulated by changing liquid hold-up in a tray or packed tower. In addition to these parameters, changes in utilization are studied rather than changes in hold tank residence time.

The comparisons were made using limestone surface rate constants of 10-11.25 and 10-12.5. It was assumed that the desired SO<sub>2</sub> removal was 85% and that the initial inlet SO<sub>2</sub> concentration was 2500 ppm. Longview Fine (85% < 325 mesh) was used to provide a particle size distribution, and calcium sulfite saturation in the hold tank was maintained at approximately 1.15. A sensitivity analysis on the effect of grind was unnecessary since it was well demonstrated by the EPA study that SO<sub>2</sub> removal improves with finer grinds.

For the initial inlet SO<sub>2</sub> concentration, 85% removal was achieved with the more reactive limestone when U = 90%. When the reactivity rate constant is reduced to 10-12.5, simulating a less reactive limestone, removal drops to 72.5%, and the hold tank pH falls from 5.94 to 5.46. In order to achieve 85% removal with the less reactive limestone, one of two changes can be made. Gas/liquid mass transfer can be enhanced by the addition of 280 ppm of adipic acid, or alkalinity can be increased by adding excess limestone to give U = 70%.

The base cases for the sensitivity analysis assumed that utilizations for both stones were set at those values which gave 85% removal without addition of adipic acid. Therefore, the more reactive stone has a base case of U = 90%, and the less reactive stone has a base case of U = 70%. To simulate a typical change in flue gas conditions, SO<sub>2</sub> inlet concentration was increased to 3000 ppm, and the sensitivity analysis was performed to determine which parameters could be used to reestablish 85% removal. The results of the analysis are shown in Table 4.16. This table shows the differential changes of normalized SO<sub>2</sub> removal with differential changes in the normalized parameters. For example, from Table 4.16 the heading of  $\Delta L/G$  represents Equation (4-25).

$$\frac{d \ln \%SO_2}{d \ln L/G} = \frac{(L/G)^0}{(\%SO_2)^0} \frac{d \%SO_2}{d L/G} \quad (4-25)$$

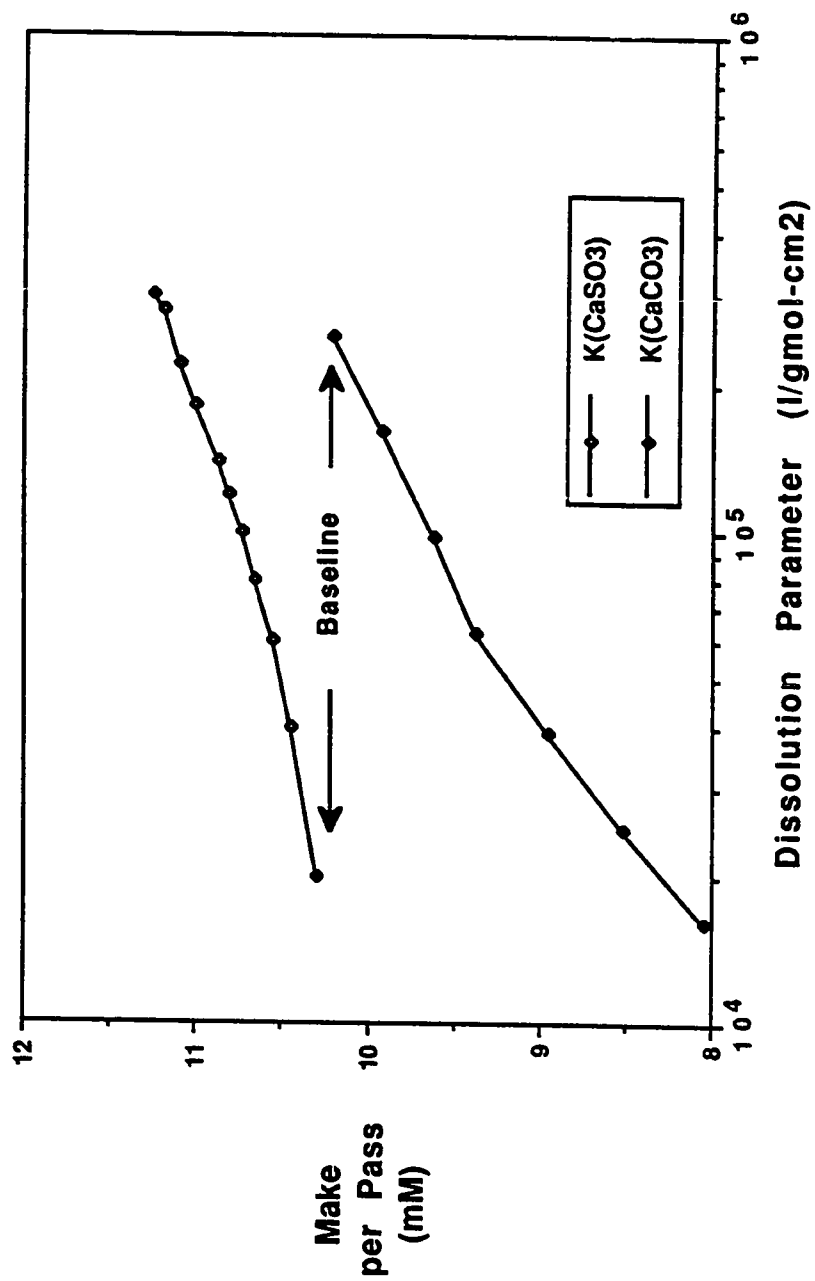


Figure 4.8: Comparison of Solids Reactivities  
U = 88%, 3170 ppm SO<sub>2</sub> Inlet

In this equation the superscript implies the appropriate base case value. Similarly other headings represent the differential changes for those parameters using equations of the form (4-25). Also shown in this table is the absolute effect of adding 50 ppm of adipic acid. This value could not be normalized since both base cases were 0 ppm of adipic acid.

Table 4.16: Slurry Scrubber Model Sensitivities - Effect of Selected Slurry Scrubber Model Parameters on % SO <sub>2</sub> Removal with a Comparison for Two Limestone Reactivities						
	$\frac{d\ln\%Rem}{d\ln ppm^*}$	$\frac{d\ln\%Rem}{d\ln L/G}$	$\frac{d\ln\%Rem}{d\ln U}$	$\frac{d\ln\%Rem}{d\ln\%solids}$	$\frac{d\ln\%Rem}{d\ln\tau_{sc}}$	$\frac{d(\%Rem)}{d(50ppm^{**})}$
$k_c = 10^{-11.25}$	-0.30	0.30	-0.11	0	0.10	+3.4%
$k_c = 10^{-12.5}$	-0.25	0.22	-0.43	0.11	0.09	+4.1%
* ppm refers to inlet gas SO <sub>2</sub> concentration						
** 50 ppm refers to liquid concentration of adipic acid						

It is interesting to note that the more reactive limestone has a greater decrease in SO<sub>2</sub> removal when the inlet concentration is increased. The consequences of the sensitivity study indicate that the best approach which could be taken to compensate for the reduction in SO<sub>2</sub> removal would depend on the reactivity of the stone. For the more reactive stones, loss of SO<sub>2</sub> removal could be counteracted by increasing the liquid flowrate rather than increasing excess limestone (decreasing utilization). However for the less reactive limestone, increasing the excess limestone has a greater effect than increasing liquid flowrate. This result is an outcome of the relationship between dissolution rate and utilization. It can be seen in the slope of the curve in Figure 4.2 that when  $F=0.3$  ( $U=70\%$ ) a small change in utilization gives a faster rate than a small change in utilization at  $F=0.1$  ( $U=90\%$ ).

Additionally, increasing the solids concentrations of the recycled slurry with the original base case utilization would enhance removal for less reactive limestones, but have little or no effect on very reactive limestones. Addition of adipic acid would be helpful in either case. However use of adipic acid has its own set of problems including degradation and coprecipitation with solids which must be considered when deciding a course of action.

#### 4.5 Summary

It was shown through prediction of batch experiments that limestone reactivity can be defined through particle size distributions and the limestone type dependent rate constant. The expanded model was tested against a limestone type and grind study sponsored by the EPA. Batch dissolution measurements of screened limestones in sulfite yielded better estimates of the surface rate constant required for the EPA model than as-ground limestones. The Slurry Scrubber Model was then expanded to predict reactivity from these variables.

The Slurry Scrubber Model was able to predict both SO<sub>2</sub> removal and hold tank compositions of the EPA runs. The effects of limestone type were handled through changes in the surface rate parameter. Within a given type the effects of grind and utilization were well modeled. Additionally the model indicated that for three runs at very low utilizations of the Fredonia stone, the limestone may have partially blinded. This was evidenced by the low removals and hold tank pH values relative to the predictions. When the surface rate constant was reduced to simulate blinding, predicted values approached the observations. The Slurry Scrubber Model was also able to predict the relatively constant removal observed for Georgia Coarse even though utilization changed by 12%.

Based on a parameter sensitivity analysis it was determined that the optimum adjustments to scrubber operations in order to handle system changes may be dependent on the limestone reactivity.

#### 4.6 Notation

$a$  = area of a particle,  $\text{cm}^2$

$B$  = agitation enhancement factor,  $\text{cm}^{-1}$

$C$  = concentration,  $M$  ( $\text{gmol/l}$ )

$C_s$  = concentration of calcium solids,  $M$

$d$  = diameter,  $\text{cm}$

$D$  = diffusivity,  $\text{cm}^2/\text{s}$

$E$  = oxidation enhancement factor, unitless

$f_i$  = fraction remaining of a single particle,  $V_i/V_0$

$F$  = total fraction remaining of all particles given by Equation (4-7) or (4-8)

$k_c$  = limestone surface rate constant,  $M^{5/2}\text{cm/s}$

$k_{\text{cry}}$  = calcium sulfite crystallization parameter, unitless

$k_l$  = solid/liquid mass transfer coefficient,  $\text{cm/s}$

$k_m$  = mass transfer constant defined by Equation (4-4),  $\text{cm}^2/\text{s}$

$K$  = limestone reactivity parameter defined by Equation (4-9),  $\text{sec}/\text{cm}^2/M$

$N_{\text{sc}}$  = Schmidt Number

$t$  = time in a batch reactor,  $\text{sec}$

$U$  = utilization, moles/mole

$V_0$  = initial volume of a particle,  $\text{cm}^3$

$V_t$  = total volume of limestone solids,  $\text{cm}^3$

#### Greek Letters

$\delta$  = film thickness,  $\text{cm}$

$\rho$  = molar density of calcite

$\tau$  = residence time in hold tank,  $\text{sec}$ , or in scrubber,  $\text{sec}/\text{stage}$

#### Subscripts

$i$  indicates a specific size fraction

$o$  indicates initial value

## Chapter 5

### Conclusions and Recommendations

#### 5.1 Particle Size Predictions

The log gamma density function was successfully applied to the prediction of limestone particle size distributions. This model had three unknown parameters:  $\alpha$ ,  $\beta$ , and  $d_{100}$ . The method of moments can be used to regress the parameters for the model when the particle size distributions including  $d_{100}$  were known. Two groups of stones were regressed to find mean values of the log gamma parameters. For limestones ground by a dry roller mill, the values were determined to be 3.75 and 1.81 for  $\alpha$  and  $\beta$  respectively, and for stones ground in a wet ball mill  $\alpha = 6.19$  and  $\beta = 1.23$ . These differences were a result of the variabilities in the fineness of the grinds between the two mill types. Statistical analysis indicated that the  $\alpha$  means could be adequately represented by assuming integer values of 4 and 6.

The prediction of complete distributions from two sieve measurements requires that one of the three parameters is known. By assuming that  $\alpha$  is an integer the log gamma density function can be integrated analytically. Fixing  $\alpha$  as an integer simplifies the analysis and allows the other two parameters to be estimated from the density function itself rather than requiring additional empirical correlations. Sensitivity analysis also supported fixing  $\alpha$  over  $\beta$ . Despite the differences in the means for  $\alpha$ , particle size distributions from both dry roller mills and wet ball mills could be predicted by the log gamma model using sieve data with  $\alpha = 4$ .

The model fit from the sieve data was much better at the coarse end of the distribution. This is a result of the sieve sizes used in the screenings. Since screening of particles smaller than 44 microns (325 mesh) is infeasible, screen sizes are more representative of the coarse end. In a practical sense it is much more important to fit the coarser end since for scrubber systems, it is the coarser particles which remain in the system and determine dissolution rates. For industrial applications where limestones are presently ground to 90% < 325 mesh, this means that careful screening of the larger stones (200 or 140 mesh) is required in order for the Slurry Scrubber model to accurately predict the limestone particle size distributions needed for calculating reactivity.

## 5.2 Effects of Sulfite

In the absence of sulfite, limestone dissolution was controlled solely by mass transfer. For a given stone under mass transfer control, film thickness was found to be independent of pH. Film thicknesses of 16 stones ranged from 3 to 9  $\mu\text{m}$ .

The presence of sulfite in solution was found to have a dual effect on the dissolution of limestone. The sulfite/bisulfite pair acted as a buffer at the limestone interface by providing hydrogen ion consumed during the dissolution reaction. But sulfite also inhibited dissolution by probably adsorbing onto the limestone as calcium sulfite. Using the EDS analyzer on the scanning electron microscope, it was concluded that sulfite was present on the limestone.

The rate of limestone dissolution was determined to be controlled by a combined surface kinetics/mass transfer regime. The sulfite inhibition was accurately modeled in the surface kinetics expression by an inverse dependence on calcium sulfite concentration at the limestone surface. The surface rate expression did a good job of predicting the dissolution of limestone for a variety of stones and over a range of solution compositions. Changes in the pH and the concentrations of calcium, carbonate, sulfite, sulfate, and adipic acid were accurately predicted. While the form of the rate expression was applicable to all stones, the rate constant was stone dependent.

Surface rate constants of 16 limestones were found to range from  $10^{-11.25}$  to  $10^{-12.7}$ . These individual rate constants could not be correlated to physical parameters such as Mg content or BET area. The activation energy for the surface rate reaction was calculated to be between 4 and 10 kcal/gmol.

For application in industrial systems, a sample of the scrubber limestone should be screened and tested in a batch dissolution experiment at conditions which simulate the hold tank solution. Then using the measured rates and the surface rate expression, the specific surface rate constant can be regressed.

### 5.3 Slurry Scrubber Modeling

It was shown through prediction of batch experiments that limestone reactivity can be defined using particle size distributions and the limestone type dependent rate constant. The Slurry Scrubber model was then expanded to predict reactivity from these variables. The estimation of the surface rate constant required for the EPA study was found to be more accurately measured from screened limestones rather than as-ground stones.

The expanded Slurry Scrubber Model was tested against a limestone type and grind study sponsored by the EPA. The model was able to predict both  $\text{SO}_2$  removal and hold tank compositions of the EPA runs. The effects of limestone type were handled through changes in the surface rate parameter. Within a given type the effects of grind and utilization were well modeled. Additionally the model indicated that for three runs at very low utilizations of the Fredonia stone, the limestone may have partially blinded. This was evidenced by the low removals and hold tank pH values relative to the predictions. When the surface rate constant was reduced to simulate blinding, predicted values approached the observations. The Slurry Scrubber model was also able to predict the relatively constant removal observed for Georgia Coarse even though utilization changed by 12%. These results indicate that for industrial applications, the Slurry Scrubber model can be used to identify systems which have



blinded limestones or to clarify systems where observations seem contrary to expectations.

For systems operating at high limestone utilizations, calcium sulfite can provide alkalinity in the scrubber. The reactivity of this solid was also studied using the Slurry Scrubber model. The stoichiometry of alkalinity from calcium sulfite indicates that each additional mM of dissolved  $\text{CaSO}_3$  would result in an additional mM of absorbed  $\text{SO}_2$ . However, four mM of dissolved solid were required for one mM additional  $\text{SO}_2$  because the increase in aqueous sulfite caused reductions in limestone dissolution. On a per mole basis limestone proved to be more productive in  $\text{SO}_2$  removal than dissolved calcium sulfite.

Based on a parameter sensitivity analysis it was determined that the optimum adjustments to scrubber operations in order to handle system changes may be dependent on the limestone reactivity.

## **5.4 Recommendations for Future Work**

### **5.4.1. Experimental Work**

Since many of the newer scrubbers are capable of operating at utilizations greater than 90%, the effect of sulfite on the dissolution rate as a function of conversion should be studied to improve the Slurry Scrubber Model predictions. Since it has been shown that the limestone BET area changes with percent dissolved in the presence sulfite, it may be worth further study. Or it may be sufficient to develop an empirical correlation as proposed by Jarvis et al. (1988), which would require an experimental dissolution measurement of an industrial stone over the complete range from 0 to 100% dissolved. Until this conversion effect is quantified, it may be sufficient to measure the dissolution rate of the industrial stone at the appropriate utilization and regress a surface rate constant which is applicable in that range of dissolution.

If there are large changes in scrubber liquor temperatures, then it would be advisable to study more thoroughly the effect of temperature on the surface rate

constant. If the adsorption of calcium sulfite onto limestone proved to be important step in the process, then experiments should be performed to quantify the adsorption. Auger spectroscopy may prove helpful in this work. This instrument strips the top surface layers off of the sample and determines the elements which are present. Limestone, though, may present a problem in this apparatus since limestone itself is non-conducting and the high beam voltage of the Auger microscope could cause the particles to charge. Charged particles tend to "jump". This phenomena was noted in the SEM microscope for some of the uncoated limestone samples which were not adequately glued to the stage. If Auger spectroscopy can work, it might also be used to demonstrate irreversible limestone blinding.

The limestone surface rate model did not predict measured rates accurately in solutions with high magnesium concentrations. This suggests that the effect of magnesium on limestone dissolution should also be investigated. This study would be important for the few scrubber systems which are magnesia enhanced.

#### 5.4.2 Modeling

As presently written the Slurry Scrubber model uses a simple first order dependence on gypsum saturation to calculate gypsum crystallization. This expression seems adequate in natural oxidation systems, but may not be accurate in forced oxidation systems. Both Tseng (1983) and Gleason (1989) have shown complicated expressions for  $\text{CaSO}_3$  crystallization in scrubber systems. Gypsum crystallization rates should also be studied in solutions representative of scrubber systems to determine the applicable rate expression and the species which might affect the rate.

There are several parameters in the Slurry Scrubber model which are adjustable constants. These include the oxidation enhancement factor, the crystallization constant for calcium sulfite, and the hold tank parameters,  $N_1$  and  $L/G$ . In order to improve the capabilities of the model, these parameters need to be predictable.

Some information is already available for several parameters. The species which enhance the oxidation of sulfite to sulfate are well known (Ulrich, 1981). Additionally there are several factors which are known to affect the calcium sulfite

crystallization parameter. Gleason (1989) has shown that the amount of sulfate present in the sulfite solid will affect the value of the rate constant, and that pH affects the nucleation rate constant of calcium sulfite. It was attempted in this work to develop a correlation for the calcium sulfite crystallization parameter using the values modeled in the EPA study. However, since the pH measurements were erroneous in many cases, the applicable calcium sulfite crystallization parameter could only be estimated. Better measurements would have allowed a more accurate fit of the values, which in turn might have yielded a correlation.

The Slurry Scrubber Model should be tested against data collected from spray scrubbers. This is the most common scrubber in use. Spray scrubbers have very short liquor residence times and it has been commonly assumed that because of this no limestone dissolution occurs in the scrubber. Now that the limestone reactivity model has been verified, the Slurry Scrubber Model could be used to test this assumption.

Forced oxidation studies should also be tested with the Slurry Scrubber Model. The hold tank parameters for these cases would be much better defined than the natural oxidation cases studied in this work. This would allow the hold tank subroutines to be more thoroughly verified.

**Appendix A**  
**Experimental Data**

Table A.1: Reagent 1 Batch Experiments in 0.1M CaCl<sub>2</sub>, 0.85 atm CO<sub>2</sub>,  
and 55°C

		Exp RL-51						Exp RL-53	
Conditions:		pH 5.2	1 mM SO <sub>3</sub>	0 mM SO <sub>4</sub>	Conditions:		pH 4.8	3 mM SO <sub>3</sub>	10 mM SO <sub>4</sub>
mls. Titrated	Frac. Diss.	time (min)	Diff. Rate	mls. Titrated	Frac. Diss.	time (min)	Diff. Rate		
1	0.05	1.08	-4.63E-02	1	0.05	2.55	-1.96E-02		
2	0.1	2.63	-3.23E-02	2	0.1	4.95	-2.08E-02		
3	0.15	4.05	-3.52E-02	3	0.15	7.53	-1.94E-02		
4	0.2	5.63	-3.16E-02	4	0.2	10.17	-1.89E-02		
5	0.25	7.2	-3.18E-02	5	0.25	12.72	-1.96E-02		
6	0.3	8.82	-3.09E-02	6	0.3	15.33	-1.92E-02		
7	0.35	10.5	-2.98E-02	7	0.35	18.15	-1.77E-02		
8	0.4	12.42	-2.60E-02	8	0.4	21.23	-1.62E-02		
9	0.45	14.25	-2.73E-02	9	0.45	24.33	-1.61E-02		
10	0.5	16.47	-2.25E-02	10	0.5	27.45	-1.60E-02		
11	0.55	18.78	-2.16E-02	11	0.55	30.9	-1.45E-02		
12	0.6	20.93	-2.33E-02	12	0.6	34.5	-1.39E-02		
13	0.65	23.55	-1.91E-02						
13.8	0.69	25.95	-1.67E-02						

Table A.1(con't): Reagent 1 Batch Experiments in 0.1M CaCl<sub>2</sub>, 0.85 atm CO<sub>2</sub>, and 55°C

		Exp RL-54		Exp RL-55	
Conditions:	pH 4.8	1 mM SO <sub>3</sub>	10 mM SO <sub>4</sub>	pH 4.8	10 mM SO <sub>4</sub>
mls. Titrated	time(min)	Frac. Dissolve	Diff. Rate	mls. Titrated	time (min)
1	0.9	0.05	-5.56E-02	1	1.65
2	1.8	0.10	-5.56E-02	2	3.15
3	2.7	0.15	-5.56E-02	3	4.65
4	3.75	0.20	-4.77E-02	4	6.28
5	4.73	0.25	-5.11E-02	5	7.77
6	5.85	0.30	-4.47E-02	6	9.27
7	6.93	0.35	-4.64E-02	7	10.65
8	8.07	0.40	-4.39E-02	8	12.2
9	9.23	0.45	-4.32E-02	9	13.8
10	10.5	0.50	-3.94E-02	10	15.35
11	11.85	0.55	-3.71E-02	11	17.03
12	13.2	0.60	-3.71E-02	12	18.72
13	14.78	0.65	-3.17E-02	13	20.4
				14	22.5
				15	24.68
				16	27.27
				17	30.27
					Frac. Dissolved
					Rate
					0.05
					0.10
					0.15
					0.20
					0.25
					0.30
					0.35
					0.40
					0.45
					0.50
					0.55
					0.60
					0.65
					0.70
					0.75
					0.80
					0.85
					-3.03E-02
					-3.34E-02
					-3.34E-02
					-3.07E-02
					-3.36E-02
					-3.34E-02
					-3.63E-02
					-3.23E-02
					-3.13E-02
					-3.23E-02
					-2.98E-02
					-2.96E-02
					-2.98E-02
					-2.38E-02
					-2.30E-02
					-1.93E-02
					-1.67E-02

Table A.1(con't): Reagent 1 Batch Experiments in 0.1M CaCl<sub>2</sub>, 0.85 atm CO<sub>2</sub>, and 55°C

		Exp RL-56					Exp RL-58	
Conditions:	pH 5.3	1 mM SO3	10 mM SO4		Conditions:	pH 5.3	5.6 mM SO3	10 mM SO4
mls. Titrated	time (min)	Frac. Dissolved	Diff. Rate		mls. Titrated	time (min)	Frac. Dissolved	Diff. Rate
1	3	0.05	-1.66E-02		1	10.65	0.05	-4.69E-03
2	6.27	0.10	-1.53E-02		2	23.55	0.1	-3.88E-03
3	9.6	0.15	-1.50E-02		3	31.88	0.15	-6.00E-03
4	12.93	0.20	-1.50E-02		4	40.3	0.2	-5.94E-03
5	16.35	0.25	-1.46E-02		5	49.8	0.25	-5.26E-03
6	20.18	0.30	-1.30E-02		6	58.86	0.3	-5.52E-03
7	24.15	0.35	-1.26E-02		7	68.25	0.35	-5.32E-03
8	27.83	0.40	-1.36E-02		8	78.3	0.4	-4.98E-03
9	32.4	0.45	-1.09E-02		9	88.86	0.45	-4.73E-03
10	36.45	0.50	-1.23E-02		10	101.4	0.5	-3.99E-03
11	41.52	0.55	-9.85E-03		11	114	0.55	-3.97E-03
12	46.65	0.60	-9.73E-03		12	127.8	0.6	-3.62E-03
13	52.8	0.65	-8.12E-03		13	146.7	0.65	-2.65E-03

Table A.1(con't): Reagent 1 Batch Experiments in 0.1M CaCl<sub>2</sub>, 0.85 atm CO<sub>2</sub>, and 55°C

		Exp. RL-60				Exp RL-61	
Conditions:	p H 5.3	7.5 mM SO3	10 mM SO4	Conditions:	pH 5.3	0 mM SO3	10 mM SO4
mls. Titrated	time (min)	Frac. Dissolved	Diff. Rate	mls. Titrated	time (min)	Frac. Dissolved	Diff. Rate
1	15.75	0.05	-3.17E-03	1	5.25	0.05	-9.50E-03
2	32.61	0.10	-2.96E-03	2	10.65	0.10	-9.24E-03
3	48.75	0.15	-3.09E-03	3	15.83	0.15	-9.63E-03
4	63.45	0.20	-3.39E-03	4	21.38	0.20	-8.99E-03
5	78.21	0.25	-3.38E-03	5	27.08	0.25	-8.75E-03
6	92.55	0.30	-3.48E-03	6	32.55	0.30	-9.12E-03
7	107.7	0.35	-3.29E-03	7	38.48	0.35	-8.41E-03
8	121.95	0.40	-3.50E-03	8	44.7	0.40	-8.02E-03
9	137.85	0.45	-3.14E-03	9	51.75	0.45	-7.07E-03
10	153.15	0.50	-3.26E-03	10	58.2	0.50	-7.73E-03
11	169.65	0.55	-3.02E-03	11	65.85	0.55	-6.52E-03
				12	73.65	0.60	-6.39E-03
				13	82.05	0.65	-5.94E-03
				14	91.8	0.70	-5.12E-03
				15	102.45	0.75	-4.68E-03
				16	114.9	0.80	-4.01E-03
				17	130.95	0.85	-3.11E-03



**Table A.1(con't): Reagent 1 Batch Experiments in 0.1M CaCl<sub>2</sub>, 0.85 atm CO<sub>2</sub>, and 55°C**

		Exp RL-62				Exp RL-63	
Conditions:	pH 4.8	0 mM SO <sub>3</sub>	10 mM SO <sub>4</sub>	Conditions:	pH 4.8	20 mM SO <sub>3</sub>	10 mM SO <sub>4</sub>
mls. Titrated	time (min)	Frac. Dissolved	Diff. Rate	mls. Titrated	time (min)	Frac. Dissolved	Diff. Rate
1	1.2	0.05	-4.16E-02	1	2.1	0.05	-0.0238
2	2.25	0.10	-4.76E-02	2	4.65	0.10	-0.0196
3	3.42	0.15	-4.27E-02	3	6.6	0.15	-0.02563
4	4.53	0.20	-4.50E-02	4	8.63	0.20	-0.02462
5	5.7	0.25	-4.27E-02	5	10.38	0.25	-0.02856
6	6.9	0.30	-4.16E-02	6	12.3	0.30	-0.02603
7	8.33	0.35	-3.49E-02	7	14.03	0.35	-0.02889
8	9.6	0.40	-3.93E-02	8	15.9	0.40	-0.02672
9	11.03	0.45	-3.49E-02	9	17.85	0.45	-0.02563
10	12.3	0.50	-3.93E-02	10	19.73	0.50	-0.02658
11	13.88	0.55	-3.16E-02	11	21.75	0.55	-0.02474
				12	24	0.60	-0.02221
				13	26.1	0.65	-0.0238
				14	28.88	0.70	-0.01798
				15	31.8	0.75	-0.01711
				16	34.8	0.80	-0.01666
				17	38.1	0.85	-0.01514

Table A.1(con't): Reagent 1 Batch Experiments in 0.1M  $\text{CaCl}_2$ , 0.85 atm  $\text{CO}_2$ , and 55°C

		Exp RL-64				Exp RL-65	
Conditions:	pH 4.8	4.9 mM SO3	10 mM SO4		Conditions:	pH 5.3	2.3 mM SO3
							10 mM SO4
mls. Titrated	time (min)	Frac. Dissolved	Diff. Rate		mls. Titrated	time(min)	Frac. Dissolved
1	1.05	0.05	-4.75E-02		1	4.17	0.05
2	1.95	0.10	-5.54E-02		2	9.08	0.1
3	2.85	0.15	-5.54E-02		3	13.5	0.15
4	3.83	0.20	-5.09E-02		4	18.45	0.2
5	4.83	0.25	-4.99E-02		5	23.63	0.25
6	5.93	0.30	-4.54E-02		6	29.1	0.3
7	7.13	0.35	-4.16E-02		7	34.65	0.35
8	8.25	0.40	-4.46E-02		8	41.93	0.4
9	9.38	0.45	-4.42E-02		9	47.25	0.45
10	10.65	0.50	-3.93E-02		10	54.45	0.5
11	12	0.55	-3.70E-02		11	62.25	0.55
					12	70.88	0.6

**Table A.1(con't): Reagent 1 Batch Experiments in 0.1M CaCl<sub>2</sub>, 0.85 atm CO<sub>2</sub>, and 55°C**

		Exp RL-66						Exp RL-71		
Conditions:	pH 4.8	9.7 mM SO3	10 mM SO4		Conditions:	pH 5.3	7.3 mM SO3	10 mM SO4		
mls. Titrated	time (min)	Frac. Dissolved	Diff. Rate		mls.titrated	time (min)	Frac.Diss.	Diff. Rate		
1	1.05	0.05	-4.76E-02		1	19.5	0.056	-2.87E-03		
2	2.1	0.1	-4.76E-02		2	40.2	0.113	-2.75E-03		
3	3.3	0.15	-4.17E-02		2.32	44.2	0.131	-4.50E-03		
4	4.53	0.2	-4.07E-02		3	57.8	0.168	-2.72E-03		
5	5.7	0.25	-4.27E-02		4	75.8	0.222	-3.00E-03		
6	6.9	0.3	-4.17E-02		5	95	0.276	-2.81E-03		
7	8.18	0.35	-3.91E-02		5.44	98.4	0.3	-7.06E-03		
8	9.45	0.4	-3.94E-02		6	114.4	0.334	-2.13E-03		
9	10.92	0.45	-3.40E-02		7	132.2	0.391	-3.20E-03		
10	12.23	0.5	-3.82E-02		8	150.2	0.449	-3.22E-03		
11	13.77	0.55	-3.25E-02		8.71	163.8	0.49	-3.01E-03		
12	15.3	0.6	-3.27E-02		9	170.2	0.506	-2.50E-03		
13	16.92	0.65	-3.09E-02		10	187.8	0.561	-3.13E-03		
14	18.75	0.7	-2.73E-02		11	205.6	0.616	-3.09E-03		
15	20.85	0.75	-2.38E-02		11.2	208.8	0.628	-3.75E-03		
16	23.33	0.8	-2.02E-02		12	225	0.672	-2.72E-03		
17	26.03	0.85	-1.85E-02		12.7	239.8	0.771	-6.69E-03		
18	29.7	0.9	-1.36E-02							

Table A.1(con't): Reagent 1 Batch Experiments in 0.1M CaCl<sub>2</sub>, 0.85 atm CO<sub>2</sub>, and 55°C

		Exp RL-73				Exp RL-77	
Conditions:	pH 4.8	14.7 mM SO <sub>4</sub>		Conditions:	pH 5.3	6.1 mM SO <sub>3</sub>	10 mM SO <sub>4</sub>
mls. Titrated	Frac. Diss.	time (min)	Diff. Rate	mls. Titrated	Frac. Diss.	time (min)	Diff. Rate
1	0.05	2.24	-2.23E-02	1	0.05	13.8	-3.62E-03
2	0.1	4.4	-2.31E-02	2	0.1	28.2	-3.47E-03
3	0.15	6.24	-2.72E-02	3	0.15	41.1	-3.88E-03
4	0.2	8.18	-2.58E-02	4	0.2	54.9	-3.62E-03
5	0.25	9.8	-3.09E-02	5	0.25	67.8	-3.88E-03
6	0.3	11.56	-2.84E-02	6	0.3	82.08	-3.50E-03
7	0.35	13.24	-2.98E-02	7	0.35	97.5	-3.24E-03
8	0.4	15	-2.84E-02	8	0.4	112.8	-3.27E-03
9	0.45	16.82	-2.75E-02	9	0.45	130.5	-2.82E-03
10	0.5	18.78	-2.55E-02	10	0.5	149.7	-2.60E-03
11	0.55	20.7	-2.60E-02	11	0.55	171.9	-2.25E-03

Table A.1(con't): Reagent 1 Batch Experiments in 0.1M CaCl<sub>2</sub>, 0.85 atm CO<sub>2</sub>, and 55°C

		Exp RL-76					Exp RL-81	
Conditions:	pH 5.3	6.3 mM SO3	10 mM SO4	Conditions:	pH 4.8	0.63mM SO3	10 mM SO4	
mls. Titrated	Frac.Rem.	time(min)	Diff. Rate	mls. Titrated	Frac.Rem.	time (min)	Diff. Rate	
0	1	0		2	0.9	5.4	-1.67E-01	
1	0.967	14.5	-6.67E-02	3	0.85	8.22	-1.77E-02	
2	0.933	25.3	-3.15E-03	4	0.8	10.92	-1.85E-02	
3	0.9	36.1	-3.06E-03	5	0.75	14.22	-1.52E-02	
4	0.867	44.8	-3.79E-03	6	0.7	17.4	-1.57E-02	
5	0.833	53.5	-3.91E-03	7	0.65	20.7	-1.52E-02	
6	0.8	62.2	-3.79E-03	8	0.6	24	-1.52E-02	
7	0.767	70.9	-3.79E-03	9	0.55	27.72	-1.34E-02	
8	0.733	79.9	-3.78E-03	10	0.5	31.68	-1.26E-02	
9	0.7	88.6	-3.79E-03	11	0.45	35.7	-1.24E-02	
10	0.667	97.6	-3.67E-03	12	0.4	40.26	-1.10E-02	
11	0.633	106.9	-3.66E-03	13	0.35	45	-1.05E-02	
12	0.6	115.9	-3.67E-03	14	0.3	50.1	-9.80E-03	
13	0.567	126.7	-3.06E-03	15	0.25	56.28	-8.09E-03	
14	0.533	136.9	-3.33E-03	15.8	0.21	61.5	-7.66E-03	
15	0.5	148.9	-2.75E-03					
16	0.467	160.9	-2.75E-03					
17	0.433	174.1	-2.58E-03					
18	0.4	189.1	-2.20E-03					
19	0.367	205.9	-1.96E-03					
20	0.333	225.1	-1.77E-03					
21	0.3	247	-1.51E-03					

**Table A.2: Edwards Limestone Batch Experiments in 0.1M CaCl<sub>2</sub>, 0.85 atm CO<sub>2</sub>, and 55°C**

	Edwards	TC-69		Edwards	TC-70
	325-400	Mesh		325-400	
Conditions:	pH 5.3	5.5 mM SO3	10 mM SO4	pH 5.3	0mM SO3 10 mM SO4
mls. Titrated	Frac. Diss.	time (min)	Diff. Rate	Frac. Diss	time(min)
0.88	0.044	14	-3.14E-03	0.05	11.1
1	0.05	17	-2.00E-03	0.101	31.8
2	0.1	54.7	-1.33E-03	0.151	55.2
2.81	0.141	88.4	-1.22E-03	0.201	78
3	0.15	95.6	-1.25E-03	0.252	104.4
4	0.2	145.4	-1.00E-03	0.287	125.4
5	0.25	202.4	-8.77E-04		
6	0.3	277.4	-6.67E-04		

Table A.2(con't): Edwards Limestone Batch Experiments in 0.1M  
CaCl<sub>2</sub>, 0.85 atm CO<sub>2</sub>, and 55°C

Conditions	Edwards 200-325		TC-74 Mesh		Edwards 200-325		TC-75 Mesh	
	pH 5.3		6.1 mM SO <sub>3</sub>	10 mM SO <sub>4</sub>	pH 5.3	0 mM SO <sub>3</sub>	10mM SO <sub>4</sub>	
mls. Titrant	Frac. Diss.	time (min)	Diff. Rate		Frac. Diss.	time(min)	Diff. Rate	
1	0.033	7.6	-4.34E-03		0.025	2	-1.25E-02	
2	0.066	24.8	-1.92E-03		0.05	5.2	-7.81E-03	
3	0.1	46.8	-1.55E-03		0.075	8.8	-6.94E-03	
4	0.133	71.6	-1.33E-03		0.1	13.6	-5.21E-03	
5	0.166	104	-1.02E-03		0.125	19.4	-4.31E-03	
6	0.199	141.6	-8.78E-04		0.15	25.2	-4.31E-03	
7	0.232	189.2	-6.93E-04		0.174	32.6	-3.24E-03	
8	0.265	242.4	-6.20E-04		0.199	40	-3.38E-03	
8.55	0.285	281.2	-5.15E-04		0.224	49	-2.78E-03	
					0.249	57.6	-2.91E-03	
					0.274	67.6	-2.50E-03	
					0.289	73.6	-2.50E-03	

**Table A.3: As-Ground Limestones Batch Experiments: pH 5.8, 5 mM CO<sub>3</sub>, 50mM Ca, 20mM Mg, 11.2mM SO<sub>4</sub>, 127.5mM Cl, and 50°C**

		Georgia Fine	As-Ground	
		3.31mM SO <sub>3</sub>		3.09mM SO <sub>3</sub>
time	dissolved	Meas.F(1)	Dissolved	Meas.F(6)
0	0	1	0	1
2	0.027	0.973	0.0253	0.9747
4	0.0557	0.9443	0.0601	0.9399
6	0.0868	0.9132	0.088	0.912
8	0.1024	0.8976	0.1186	0.8814
14	0.1706	0.8294	0.1928	0.8072
16	0.1853	0.8147	0.205	0.795
22	0.2238	0.7762	0.2541	0.7459
28	0.2568	0.7432	0.3062	0.6938
38	0.304	0.696	0.3647	0.6353
48			0.4131	0.5869
50	0.3479	0.6521	0.4223	0.5777
56	0.3701	0.6299	0.4524	0.5476
68	0.4076	0.5924	0.5025	0.4975
76	0.4286	0.5714	0.53	0.47
90			0.5853	0.4147
92	0.4719	0.5281		
102	0.5028	0.4972	0.6199	0.3801
126	0.55	0.45	0.6808	0.3192
140	0.5825	0.4175	0.7095	0.2905
162			0.7536	0.2464
164	0.6324	0.3676		
168			0.762	0.238
174	0.6429	0.3571	0.7704	0.2296
200			0.8041	0.1959
204	0.6833	0.3167		
224	0.7231	0.2769		
242			0.8544	0.1456
262	0.7595	0.2405		
302			0.9024	0.0976
362	0.8488	0.1512		
380			0.9348	0.0652
444	0.886	0.114	0.96	0.04
518	0.9224	0.0776		
558			0.9771	0.0229
572	0.9316	0.0684		
676	0.9604	0.0396		
892	0.9776	0.0224		



**Table A.3(con't): As-Ground Limestones Batch Experiments: pH 5.8, 5 mM CO<sub>3</sub>, 50mM Ca, 20mM Mg, 11.2mM SO<sub>4</sub>, 127.5mM Cl, and 50°C**

	Stoneman Fine	As-Ground	
	2.62 mM SO <sub>3</sub>	3.05mM SO <sub>3</sub>	2.62mM SO <sub>3</sub>
time(minutes)	Meas. FR(4)	Meas. FR(8)	Meas. FR(13)
0	1	1	1
2	0.9286	0.907	0.9154
4	0.8763	0.8446	0.8567
6	0.8412	0.7966	0.8181
8	0.8153	0.7532	0.7914
10	0.7859	0.7319	0.7712
14	0.7441	0.6922	0.7278
20	0.6911	0.6344	0.6825
28	0.6433	0.5744	0.6325
36	0.5923	0.5255	0.5874
44	0.5634	0.4858	0.5615
56	0.517	0.4457	0.5263
70		0.3933	
76			0.4753
78	0.4639		
94	0.4217	0.3396	
98			0.4334
124	0.3824		
126		0.2849	
128			0.3838
146	0.3528		
152		0.2582	
158			0.3458
166	0.3297		
198		0.2265	
200	0.2969		
212			0.2972
274		0.1781	
290			0.2494
300	0.2346		
368		0.1455	
372	0.1815		
416			0.2086
426	0.1596		
612		0.1017	
664			0.1619
682	0.1013		
1323			0.1012

**Table A.3(con't): As-Ground Limestones Batch Experiments: pH 5.8, 5 mM CO<sub>3</sub>, 50mM Ca, 20mM Mg, 11.2mM SO<sub>4</sub>, 127.5mM Cl, and 50°C**

	Fredonia Fine	As-Ground	
	2.73 mM SO <sub>3</sub>	2.79mM SO <sub>3</sub>	2.97mM SO <sub>3</sub>
time(minutes)	Meas FR(5)	Meas. FR(11)	Meas. FR(9)
0	1	1	1
2	0.9087	0.9095	0.8997
4	0.8328	0.8515	0.8131
6	0.7762	0.8051	0.7486
8	0.7312	0.7571	0.71
10	0.6786	0.7096	0.6775
12	0.6463	0.6691	0.6336
16	0.5979	0.6118	0.5722
18	0.5738	0.5938	0.5526
24	0.5197	0.5278	0.4914
30	0.4683	0.4976	0.4326
38	0.4221	0.4515	0.3909
46	0.3787	0.4073	0.3499
50	0.3703	0.3955	0.3368
58			0.3103
74	0.2962	0.3234	0.2613
82	0.2877		0.2495
92		0.2964	
94	0.2602		0.2248
116		0.2392	
120	0.2252		0.1884
170		0.1826	
206		0.1547	
218	0.126		0.1314
282		0.1132	
322			0.0885
336	0.0754	0.0587	
488			0.0542
530	0.04		
542		0.0314	
666			0.033

**Table A.3(con't): As-Ground Limestones Batch Experiments: pH 5.8, 5 mM CO<sub>3</sub>, 50mM Ca, 20mM Mg, 11.2mM SO<sub>4</sub>, 127.5mM Cl, and 50°C**

	Longview Fine	As-Ground	
	3.43mM SO <sub>3</sub>	3.04mM SO <sub>3</sub>	2.88mM SO <sub>3</sub>
time(minutes)	Meas. FR(3)	Meas. FR(7)	Meas. FR(11)
0	1	1	1
2	0.8653	0.8938	0.8494
4	0.7822	0.826	0.771
6	0.7287	0.7696	0.7273
8	0.6827	0.7218	0.6824
10	0.6413	0.6913	0.6509
12	0.6161	0.6653	0.6229
14	0.594	0.637	0.5902
18	0.5461	0.6125	0.5468
22		0.5555	0.5176
26	0.4917	0.519	0.4818
28	0.48		0.4688
30	0.4679	0.497	0.4579
36	0.444	0.4652	0.426
46	0.4	0.4068	0.392
58	0.3446	0.3661	0.3494
78	0.2908		0.3018
82		0.2994	0.2931
102	0.2522		0.2522
106		0.2528	
126			0.2259
132	0.2139	0.2168	
168		0.1819	
176	0.1688		
192		0.1643	
228			0.127
240	0.1301		
248		0.1394	
280	0.0989		
292			0.0915
302		0.1026	
336		0.0865	
368			0.0655
442		0.0613	
458	0.0515		
506	0.0399		
536			0.0356
590		0.0358	

**Table A.4: Screened Limestones Batch Experiments: pH 5.5, 2 mM CO<sub>3</sub>, 40mM Ca, 15mM Mg, 15mM SO<sub>4</sub>, 96.5mM Cl, and 50°C**

Georgia Marble	Screened (325 400 mesh)	
	5.33mM SO <sub>3</sub>	5.23mM SO <sub>3</sub>
time(min)	Frac.Diss. (15)	Frac.Diss.(19)
5	0.0383	0.0348
10	0.0774	0.0798
15	0.1088	0.1121
20	0.1391	0.1424
25	0.1752	0.1645
30	0.1983	0.1937
35	0.2277	0.2251
40	0.2632	0.2633
45	0.2948	0.2914
50	0.3217	0.3169
55	0.3475	0.3269
60	0.3745	0.3614
65	0.402	0.3887
75	0.45	0.4435
80	0.4826	0.4685
85	0.5123	0.4797
100	0.5796	0.5532
110	0.6253	0.5915
120	0.6627	0.6309
130	0.7092	0.6683
145	0.7548	0.7075
160	0.7957	0.7566
180	0.8586	0.8127
200	0.8965	0.8541
240	0.9425	0.9124
340		0.9774
350	0.9772	

**Table A.4(con't): Screened Limestones Batch Experiments: pH 5.5, 2 mM CO<sub>3</sub>, 40mM Ca, 15mM Mg, 15mM SO<sub>4</sub>, 96.5mM Cl, and 50°C**

Longview	Screened (325 -400 mesh)	
	5.62mM SO <sub>3</sub>	4.99mM SO <sub>3</sub>
time(min)	Frac.Diss.(16)	Frac.Diss.(20)
5	0.0466	0.0718
10	0.0947	0.1423
15	0.1199	0.1961
20	0.1628	0.2401
25	0.193	0.2749
30	0.22	0.3177
35	0.2486	0.3616
40	0.274	0.3901
45	0.03033	0.4246
50	0.3295	0.4601
55	0.3613	0.4875
60	0.3932	0.515
80	0.478	0.6224
95	0.5495	0.6721
110	0.607	0.7132
130	0.6615	0.7675
150	0.7194	0.8218
165	0.7607	0.8539
195	0.8093	0.8877
240	0.8584	0.9201
310	0.9005	0.9423
390	0.9323	0.9532
520	0.9656	0.9644

**Table A.4(con't): Screened Limestones Batch Experiments: pH 5.5, 2 mM CO<sub>3</sub>, 40mM Ca, 15mM Mg, 15mM SO<sub>4</sub>, 96.5mM Cl, and 50°C**

Stoneman	Screened (325 -400 mesh)	
	5.61 mM SO <sub>3</sub>	5.70mM SO <sub>3</sub>
time(min)	Frac.Diss.(21)	Frac.Diss.(17)
5	0.0527	0.0693
10	0.1089	0.1319
15	0.1566	0.1927
20	0.1956	0.2193
25	0.2435	0.2688
30	0.2786	0.317
35	0.3254	0.3503
40	0.3579	0.3968
45	0.3895	0.4243
50	0.4204	0.4528
55	0.4504	0.4833
60	0.4791	0.5182
80	0.5599	0.6108
95	0.6109	0.6569
110	0.6569	0.7024
130	0.714	0.7603
160	0.7696	0.8043
185	0.8017	0.8355
275	0.8567	0.8776
385		0.898
485	0.8782	
705	0.8989	

Fredonia	Screened (325-400 mesh)	
	5.66 mM SO <sub>3</sub>	5.65mM SO <sub>3</sub>
time(min)	Frac.Diss. (18)	Frac.Diss.(14)
5	0.0953	0.0773
10	0.1751	0.1405
15	0.2578	0.1973
20	0.3142	0.2616
25	0.3604	0.3202
30	0.4167	0.3717
35	0.4521	0.4176
40	0.4862	0.4592
45	0.5245	0.4985
50	0.5585	0.5341
55	0.5972	0.5668
60	0.6222	0.5953
65		0.6228
70		0.6506
75	0.6921	0.6742
90	0.7591	0.7336
110	0.8111	0.8006
130	0.8535	0.8449
160	0.8903	0.8871
185	0.9102	0.9116
275	0.9502	0.9526
370		0.9673
405	0.9674	

**Table A.5: Zero Sulfite Batch Experiments: pH 5.5, 2mM CO<sub>3</sub>, 40mM Ca  
15mM Mg, 15 mM SO<sub>4</sub>, 96.5mM Cl, and 50°C**

Frac. Dissolved	Zero Sulfite	Cases	
	As- Ground	Screened	Screened
	Fredonia Fine	Fredonia	Georgia Marble
time(min)	Frac. Diss.(24)	Frac. Diss.(22)	Frac. Diss.(23)
5	0.3141	0.0232	0.035
10	0.3969	0.044	0.074
15	0.4406	0.0646	0.1144
20	0.4703	0.0851	0.1554
25	0.4925	0.1058	0.1902
30	0.5143	0.1228	0.2262
35	0.5316	0.1422	0.2605
40	0.5421	0.1588	0.2904
45	0.5587	0.1785	0.322
50	0.5698	0.1951	0.3501
60	0.5886	0.2271	0.4044
80	0.6206	0.2898	0.4928
95	0.6395	0.3312	0.5479
110	0.6591	0.3723	0.597
130	0.6745	0.4241	
135			0.6631
160	0.6982	0.5085	
170			0.729
185	0.7176	0.5675	
195			0.7589
200		0.6019	
225		0.6568	0.7811
255		0.7107	
275	0.7542		
295		0.7606	
300	0.7819		
370		0.81	
415			0.8289
465	0.8139		
595		0.8759	
750	0.8735		
865			0.8918
915	0.9003		
990		0.931	
1310	0.9674		
1425		0.9674	
1430			0.94

**Report on Reagent 1 Calcite Experiments  
with Aluminum and Flouride  
Progress Report Jan. 1988**

Introduction

The goal of these experiments was to measure the dissolution rate of  $\text{CaCO}_3$  in solution conditions similar to the industrial scrubber and determine the cause of the low pH excursion. The solution concentrations of the scrubber and the experiments are shown in Table A.6.

Experimental Procedure and Analysis

Dissolution rates of 0.20g of reagent  $\text{CaCO}_3$  were measured in 500 ml of solution using the pH stat method. Reaction temperature was maintained at  $56^\circ\text{C}$ , and solutions were sparged with nitrogen. Background solution concentrations were 50mM  $\text{CaCl}_2$  and 10mM  $\text{MgSO}_4$ . Flouride was added as NaF and aluminum was added as  $\text{Al}_2(\text{SO}_4)_3$ .

The dissolution rates were calculated by

$$\text{Rate} = \frac{d(F^{2/3})}{dt}$$

where F = total fraction remaining.

It has been shown that this rate expression is linear when using reagent grade limestone in the range of 5-70% dissolution (95-30% fraction remaining). (See Sept. - Dec. 1987 Progress Report.) In all but one experiment, the rates were calculated between total fraction remainings, F, of 50-45%.

The dissolution rate can be related to the dissolving flux (as reported by Radian) from the following equation



$$\text{Flux} = \frac{1}{4F^{1/3}} d_o \rho_m \text{ Rate}$$

where

$d_o$  = the initial particle diameter, and

$\rho_m = 0.027 \text{ gmole/cm}^3$ , the molar density of the limestone.

### Results

The results of all dissolution experiments are reported in Table A.7. Previous unrelated experiments have shown that for total fraction remaining of  $\text{CaCO}_3$  greater than 30% the reagent limestone can be treated as a monodispersed sample of particle size 11.15 microns. (See Sept. - Dec. 1987 Progress Report).

Initially a base case experiment was performed at pH 5.5 to determine the dissolution rate at the background solution composition. At these conditions there were no problems in measuring a rate.

The next experiment attempted to measure dissolution at pH 5.5 in the presence of 5 mM fluoride. However when the dilute NaF solution was added to the background solution, instantaneous precipitation of  $\text{CaF}_2$  occurred. An attempt to resolve the problem by reducing the pH to less than 3, adding the NaF, and then raising the pH was also unsuccessful. Therefore these experimental conditions could not be tested.

A 2 mM fluoride solution at pH 5.5 was tested next. Again, a small amount of precipitation seemed to occur because a slight clouding of the solution was noticed. However the extent of precipitation was significantly much less than the 5 mM case. A limestone dissolution rate was measured in this solution. The measured rate was on the same order as the rate in the absence of fluoride.

The last set of dissolution rates were measured in a solution containing 5mM and 0.7 mM aluminum. With aluminum present there was no problem holding the

higher fluoride concentration in solution.. Initially pH was set at 5.5, and the limestone was added. Later the pH was reduced to 5.0 and then to 4.5.

Upon initial addition of the limestone approximately 2% dissolved. Acid was added by the pH-stat titrant module to bring the pH back to 5.5. No further dissolution of the limestone occurred at this pH. After 2.5 hours, the pH was dropped to 5.0. At this pH approximately 5% dissolved over 75 minutes. The dissolution rate was measured at pH 5.0 for F of 98-95%. However this rate may not be entirely accurate because this range of F is close to the bound of the rate expression's linearity. The pH was then dropped to 4.5 and dissolution progressed at a rate similar to the pH 5.5 conditions in the absence of fluoride and aluminum. If some sort of blinding phenomenon were not occurring, it would be expected that the dissolution rate at pH 4.5 would be an order of magnitude higher than at pH 5.5. As Table A.7 shows, this was not the case.

### Conclusions

These conclusions are in agreement with the aluminum/fluoride work done by Radian.

1. The scrubber solution is supersaturated to  $\text{CaF}_2$ .
2. Aluminum must be complexing with the fluoride in order to reach the higher concentrations observed in the scrubber.
3. It is the aluminum/fluoride combination which is causing the reduced limestone reactivity.

Table A.6: Scrubber and Experimental Solution Compositions in Flouride Study

	Scrubber	Experimental
Cl <sup>-</sup>	84.5 mM	100 mM
SO <sub>4</sub> <sup>=</sup>	14.4 mM	11.1 mM
NO <sub>3</sub> <sup>-</sup>	11.1 mM	0
Mg <sup>++</sup>	10.2 mM	10 mM
Na <sup>+</sup>	7.0 mM	5 mM
F <sup>-</sup>	4.5 mM	5 mM
Al <sup>+3</sup>	0.7 mM	0.7 mM
Ca <sup>++</sup>	50.8 mM	50 mM

(Calcium calculated by difference.)

Table A.7: Dissolution Rates of Reagent 1 Calcite at 56°C with Nitrogen Sparging.

Exp. Condition	pH	*Rate x 10 <sup>5</sup> (sec <sup>-1</sup> )	*Diss. Flux x 10 <sup>6</sup> (mmoles cm <sup>-2</sup> min <sup>-1</sup> )
50 mM CaCl <sub>2</sub> + 10 mM MgSO <sub>4</sub> (Base Case)	5.5	6.14	35.7
Base + 5 mM NaF	5.5	aborted (CaF <sub>2</sub> precipitation)	
Base + 2 mM NaF	5.5	8.95	46.7
Base + 5 mM NaF + 0.35 mM Al <sub>2</sub> (SO <sub>4</sub> ) <sub>3</sub>	5.5	0	0
	5.0	0.24	1.1
	4.5	9.57	56.7

$$*\text{Rate} = \frac{d(F^{2/3})}{dt}$$

$$*\text{Diss. Flux} = \frac{1}{4F^{1/3}} \text{ doPm Rate}$$

Table A.8: Compositions of Type and Grind Limestone Samples\*

Limestone	Carbonate	CaCO <sub>3</sub>	Dolomite	MgCO <sub>3</sub>	Insolubles
Fredonia	95.0	95.0	3.2	0	1.8
Georgia Marble	95.9	95.9	2.2	0	1.9
Longview	95.0	94.9	3.4	0	1.7
Stoneman	88.0	88.0	9.9	0	2.1

\* All values are weight percents.

Table A.9: Compositions of Other Limestones\*

Limestone	Ca	Mg	CO <sub>3</sub>	% Dolomite	Inerts
Tampa	38.6	0.1	57.8	0	0.8
LaCygne	38.6	0.0	54.7	0.0	6.5
Cholla	40.2	0.19	59.7	0.0	7.5
Gibson	33.7	3.1	----	23.8	5.0
Arapaho	31.6	0.12	----	----	10.5
Iceland Spar	40.0	0.04	60.	----	0.1
Monteagle	38.5	0.6	58.7	< 2	2.7
HSTC	39.5	0.2	59.2	----	0.9
Edwards	39.1	0.1	59.6	< 2	0.2
Maysville	36.8	1.7	59.4	13.1	2.1
Reagent 1	40.0	< 0.01	60.0	0.0	< 0.1

\* All values are weight percents.

## Appendix B

### Analytical Methods

#### B.1 Iodometric Titration

The sulfite concentration of each dissolution experiment was monitored before, during, and at the end of each experiment. The solutions required for titrations were 0.01M iodine, 0.01M sodium thiosulfate, and acetate buffer solution composed of 1M sodium acetate and 0.05 M acetic acid. Starch was used as the endpoint indicator.

Four ml of iodine were added to 5 ml of buffer solution in a 50 ml Erlenmeyer flask. The solution was weighed to  $\pm 0.0001$  g. Approximately 3 ml of dissolution slurry sample were collected in a syringe through a 0.5  $\mu$ m Millipore filter. The clear solution was added to the buffer, and the flask was reweighed to determine the actual grams of clear solution sample. Based on weights of known sample sizes, the density of the solution was estimated to be 0.995 g/ml. Solutions were back titrated with sodium thiosulfate to a clear endpoint. For the blank test, the procedure was repeated using 3 ml of distilled water instead of water. The sulfite concentration of the sample was determined using Equation (B-1).

$$C = \frac{M(B-S)}{2V} \quad \text{B-1}$$

where C = Concentration of sulfite (moles/liter)

M = Concentration of sodium thiosulfate (moles/liter)

B = Volume of thiosulfate used to titrate the blank test (ml)

S = Volume of thiosulfate used to titrate the sample (ml)

V = Volume of sample (ml)

## B.2 EDS Analysis

An important application of the SEM microscope is the Energy Dispersive Spectrographic analyzer(EDS). As the electron beam strikes the sample, x-rays are fluoresced. Two interactions occur: core scattering, which is a continuous background emission; and inner shell ionization which emits sharp peaks within the spectrum. It is the wavelengths of these inner shell x-rays which are characteristic of the elements within the sample. Additionally the intensity of the peak can quantify the elements within the sample.

In order to reduce interference, samples which are analyzed with EDS should not be coated. Limestone, which is a non conductor, must be typically coated with 400 angstroms of gold or palladium in order to produce good microscopic images. Since x-rays are emitted from a shallow depth of about 1 mm, a spectrum from a coated sample would be mainly the coating itself.

A treated sample for EDS analysis was prepared by adding 1 gram of reagent limestone into a 0.1M  $\text{CaCl}_2$  solution at pH 5.3 which contained 6 mM of  $\text{Na}_2\text{SO}_3$ . The sample was allowed to dissolve to equilibrium pH. The limestone was then collected on a filter and rinsed with 0.1M  $\text{CaCl}_2$  solution to remove traces of the sulfite solution from the surface. The sample was then dried in a vacuum oven at 65°C.

The uncoated limestone sample was mounted on a bronze stage with graphite adhesive. The stage was placed in the microscope and the stage depth was set at W.D. 39. The lower objective aperture was set at 600  $\mu\text{m}$  and the gun filament was set at 100 mA. X-rays were collected using the PET crystals which differentiates backscattered electrons from aluminum ( $Z = 13$ ) to krypton ( $Z = 36$ ). The energy window of interest is from 2.0 to 4.5 KeV. Calcium emits x-rays with energies of 3.692 and 4.103 KeV. These x-rays represent  $K\alpha$  and  $K\beta$  emissions within the atomic shell. The corresponding sulfur x-rays occur at 2.308 and 2.464 KeV. Chlorine x-rays are emitted at 2.622 and 2.816 KeV. Beam current was 25KeV and collection time was 180 seconds. The continuous x-ray spectrum (background emission) was subtracted from the final scan in order to differentiate the characteristic peaks.

### B.3. Coulter Counter Procedures and Data

Particle size distributions of the limestone samples were measured using a Coulter Counter Model TAPI analyzer. The measurement obtained from the apparatus are the differential volume percent versus volumetric size. A single aperture can determine 14 fractions from 2 to 40% of the aperture size. When distributions are wide, the samples can be wet sieved into sizes amenable to a particular aperture. The overlapping size fractions can be ratioed and the average scaling factor is used on the smaller distribution. The final distribution is then normalized back to 100%.

The particle size distributions for the limestone samples were measured using the 50, 140 and/or 400  $\mu\text{m}$  apertures. Coulter Counter Type 1-A cationic dispersant was used. Four weight percent  $\text{CaCl}_2$  solution was used as the electrolyte. This solution was prefiltered through a 0.5 mm filter for 12 hours.

The Coulter Counter was calibrated with known particle sizes each day before operating. The 50  $\mu\text{m}$  aperture was calibrated with 2.02  $\mu\text{m}$  particles. For the 140  $\mu\text{m}$  aperture, 19.66  $\mu\text{m}$  particles were used. For the 400  $\mu\text{m}$  aperture, 42.02  $\mu\text{m}$  particles were used. The calibrations resulted in the volume percents being reported with the lower diameter limits of each channel. A few drops of dispersant were placed in a 250 ml beaker with the electrolyte solution, and then a small quantity of limestone was added to produce a concentration index of about 5%. An agitator was used to maintain suspension of the particles. Each sample was collected 3 to 5 times and then averaged to determine the particle size distribution. Measured particle size distributions were reported as volume percents associated with the lower limits of each channel. (i.e. One percent associated with 2  $\mu\text{m}$  implies that one volume (weight) percent of the sample was between 2 and 2.52  $\mu\text{m}$ .)

**Table B.1: Particle Size Distributions**

Diameter	HSTC 1	HSTC 2	L-585	L-587	L-588
( $\mu\text{m}$ )	Diff. Vol. %	Diff. Vol. %	Diff. Vol. %	Diff. Vol. %	Diff. Vol. %
0.63	0	0	0	0	0
0.79	0.9	0.7	0	0	0
1	1.6	1.2	0	0	0
1.26	2.5	2.1	0	0	0
1.59	6.7	3.4	1.6	2	2
2	6.5	5	2.9	3.3	3.1
2.52	7.9	6.5	4.8	5.2	4.6
3.17	9	7.8	7.2	7.1	6.5
4	8.7	7.7	8.7	8.4	7.8
5.04	6.6	7.4	8.4	8.1	7.8
6.35	6.2	6.9	8.1	7.7	7.6
8	5.5	5.8	7.4	6.9	7.1
10.08	5.1	5.6	7.5	7	7.1
12.7	4.8	5	7.2	6.7	6.9
16	4.8	5.2	6.3	6.8	6.7
20.2	4.5	5.1	6.5	6.8	6.4
25.4	4.8	5.4	6.4	6.9	5.6
32	5.2	5.5	6	6.5	4.7
40.3	4.3	4.5	4.3	4.5	7.3
50.8	3.4	3.8	2.8	2.4	6.1
64	1.9	3	1.8	1.7	1.4
80.6	1.3	1.3	1	1.1	0.5
101.6	0.2	1.1	0.6	0.8	0.8
128	0	0	0.3	0	0
161	0	0	0	0	0
203	0	0	0	0	0



**Table B.1(con't): Particle Size Distributions**

	Iceland Spar	Maysville	HSTC	Monteagle
Diameter	325-400 Mesh	325-400 Mesh	325-400 Mesh	325-400 Mesh
(microns)	Diff. Vol. %	Diff. Vol. %	Diff. Vol. %	Diff. Vol. %
4				
5.04				
6.35				
8		0		0
10.08	0	0	0	0.2
12.7	0.3	0.1	0.3	0.2
16	0.5	0.3	0.3	0.3
20.2	0.7	0.5	0.5	0.5
25.4	1	1	0.9	1.3
32	25	17.8	37.3	30
40.3	60.5	66.8	55.8	56.6
50.8	10.2	13.1	3.7	9.7
64	1.2	0.3	0.5	0.8
80.6	0.4	0.1	0.5	0.4
101.6	0.2	0	0.2	0
128	0	0	0	0
161	0	0	0	0

Table B.1(con't): Particle Size Distributions

		Edwards	Limestone Co.	Slurry Sample
Diameter	Limestone Co.	200-325 Mesh	< 325 Mesh	(HSTC-7/86)
(microns)	Diff. Vol. %	Diff. Vol. %	Diff. Vol. %	Diff. Vol. %
0.63				
0.79				
1				
1.26				
1.59	0		0	0
2	3.4		4.5	0.1
2.52	5.4		7	0.2
3.17	7.4		9.6	0.6
4	9		11.7	1
5.04	10.2		13.3	2.3
6.35	9.7		12.6	3.9
8	8.5	0	11	5.4
10.08	6.4	0	8.3	9.5
12.7	4.7	1.3	6.6	12.2
16	4.5	1.7	5.3	14.1
20.2	4.8	3	3.9	14.9
25.4	5.2	5.1	3.2	11.7
32	5.6	8	2.1	9.7
40.3	4.8	16.6	0.9	5.6
50.8	4.4	26.8	0	3.8
64	2.9	23.4	0	1.7
80.6	1.4	8.6	0	1.5
101.6	1.2	3.1	0	0.7
128	0.4	2.2	0	0.8
161	0.1	0.4	0	0.3
203	0	0	0	0

## Appendix C: Scrubber Documentation

### Introduction

The closed loop slurry scrubber model is a composite program which has evolved during 10 years of fundamental research in experimental and modeling efforts. Experimental work contributing to the slurry scrubber model includes submodels for calcium sulfite hemihydrate crystallization (Tseng, 1984),  $\text{SO}_3$  inhibition of limestone dissolution (Gage, 1989), and enhancement of  $\text{SO}_2$  adsorption by sulfite and other buffers (Weems, 1981).

Earlier modeling efforts were applied to the prediction of batch experiment results in the flue gas desulfurization area. Chan and Rochelle(1982) demonstrated that for a 10 micron particle  $\text{CaCO}_3$  dissolution could be accurately modeled by mass transfer with equilibrium reactions using film theory. Toprac measured dissolution rates for limestones of varying particle size distribution (Toprac and Rochelle,1982). He concluded that particle size was the strongest factor affecting the dissolution rate and thus reactivity .

Mehta first modeled slurry scrubbing by integrating  $\text{CaCO}_3$  dissolution and  $\text{SO}_2$  gas/liquid mass transfer as a function of changing gas and solution composition (Mehta and Rochelle, 1983; Mehta, 1982). His model for  $\text{SO}_2$  mass transfer included both gas and liquid phase resistance and simulated liquid phase transfer by approximate surface renewal theory with equilibrium reactions (Chang and Rochelle, 1982; Weems, 1981). Solution equilibria were calculated by the Bechtel-Modified Radian Equilibrium program, BMREP (Epstein, 1975).

Chan and Rochelle extended Mehta's work by adding gas/liquid mass transfer of  $\text{CO}_2$  and  $\text{O}_2$  and  $\text{CaSO}_3$  dissolution enhanced by mass transfer with equilibrium reactions. With appropriate scrubber-specific parameters the extended model correctly predicted reduced  $\text{SO}_2$  removal in the presence of chloride (Chan and Rochelle, 1983).

Later Chan added hold tank submodels to predict scrubber inlet concentrations for a given limestone reactivity. Addition of these routines formed the closed loop of scrubber and hold tank that is the unit operations foundation of the slurry scrubber model.

In the current effort the slurry scrubber model has been adapted to run on a VAX 11/780 mainframe computer. It has also been modified to use either LSODE (Livermore Solver for Ordinary Differential Equations) or IMSL's DGEAR to solve the differential equations. Additional submodels have been developed to predict limestone reactivity from particle size distributions and utilization. When required, particle sizes distributions are modeled using a probability density function and two sieve data measurements. A subroutine has also been added to estimate concentrations required by IMSL's ZSPOW. This subroutine has reduced the number of program halts from ZSPOW and also reduced convergence time. Changes have also been made to the estimation of the boundary condition at the limestone surface. The model is now being tested in simulation of limestone type and grind studies.

### **Model description and theory**

#### **Solution equilibria and diffusivities**

For an initial scrubber inlet composition BMREP is called once to evaluate the rigorous solution equilibria. These results are simplified to eliminate ion pairs and activity coefficients. This is a reasonable approximation since ionic strength and  $\text{Ca}^{++}$  do not vary significantly across the scrubber. Diffusion coefficients are taken from Mehta and Rochelle (1983). Diffusivities for the simplified equilibria are calculated by concentration weighted averages:

$$D_{\text{SO}_3(\text{simplified})} = \frac{\sum D_j^n [C_j]}{\sum [C_j]} \quad (1)$$

where  $j = \text{SO}_3^0, \text{CaSO}_3^0, \text{and MgSO}_3^0$ . The exponent,  $n$ , equals one for solid/liquid mass transfer and one half for gas/liquid mass transfer.

#### Gas/Liquid mass transfer

Absorption of  $\text{SO}_2$  and  $\text{O}_2$  and absorption/desorption of  $\text{CO}_2$  were modeled by two film theory with an approximation to renewal theory to estimate the enhancement of liquid phase diffusion by equilibrium reactions (Chang and Rochelle, 1982; Mehta and Rochelle, 1983). The total flux of a component in the liquid film is given in approximate surface renewal theory by:

$$\text{Flux} = \frac{k_1^0}{\sqrt{D_{\text{SO}_2}}} \sum \sqrt{D_j} \Delta[C_j] \quad (2)$$

The gas flux of  $\text{SO}_2$  must equal the flux of sulfite and sulfate through the liquid film assuming oxidation to sulfate only occurs at the gas/liquid interface. Thus,

$$k_g(P_{\text{SO}_2} - P_{\text{SO}_2,i}) = \frac{k_1^0}{\sqrt{D_{\text{SO}_2}}} (\sum \sqrt{D_j} \Delta[\text{SO}_{3,j}] + \sum \sqrt{D_j} \Delta[\text{SO}_{4,j}]) \quad (3)$$

For  $\text{SO}_2$  absorption both the gas and liquid phase resistance are considered with the interface concentrations related by Henry's constant.

The liquid flux of  $\text{CO}_2$  is found from Equation (2). Gas phase resistance is neglected. Thus,

$$[\text{CO}_2]_i = H P_{\text{CO}_2} \quad (4)$$

The finite-rate reaction of  $\text{CO}_2$ ,  $\text{H}_2\text{O}$ ,  $\text{H}^+$ , and  $\text{HCO}_3^-$  is assumed to be at equilibrium in the liquid film.

Absorption of  $\text{O}_2$  is assumed to be enhanced over physical absorption by a constant factor  $E$  because of the oxidation of sulfite in the gas-liquid interface. Thus  $\text{O}_2$  absorption and sulfite oxidation are given by the flux of the sulfate species:

$$2E \frac{k_1^o}{\sqrt{D_{SO_2}}} \sqrt{D_{O_2}} H_{O_2} P_{O_2} = \frac{k_1^o}{\sqrt{D_{SO_2}}} (\sqrt{D_{SO_4}} \Delta[SO_4^{=}] + \sqrt{D_{HSO_4}} \Delta[HSO_4]) \quad (5)$$

The fluxes of other non-volatile species are taken to be zero.

#### Liquid/solid mass transfer

Limestone and  $CaSO_3$  dissolution are both modeled as steady-state mass transfer between the solid surface and the bulk solution using film theory (Chan and Rochelle, 1982; Mehta and Rochelle, 1983; Tseng and Rochelle, 1983). The flux of a component is proportional to the film thickness,  $\delta$ , and is given by

$$\text{Flux} = \frac{\sum D_i \Delta [C_i]}{\delta} \quad (6)$$

For  $CaCO_3$  dissolution the flux of  $CO_2$  is equal to the flux of  $Ca^{++}$  while the fluxes of sulfite, sulfate, and adipic acid are zero. In the absence of sulfite, limestone dissolution can be modeled by mass transfer (Chan and Rochelle, 1982). When this is true the boundary condition is given by the solubility product of calcite.

$$[Ca^{+2}]_s [CO_3^{=}]_s = K_{sp} \quad (7)$$

Other experimenters have shown that in the presence of inhibitors, dissolution still occurs near equilibrium (Berner and Morse, 1974; Gage, 1989). In the presence of sulfite, limestone dissolution is controlled by a mixed mass transfer/surface kinetics regime. In SSMFGD the surface kinetics rate is given by:

$$\text{Flux} = k \frac{([CaCO_3^o]_{eq} - [CaCO_3^o]_s)^{0.5}}{[CaSO_3^o]_s [CaCO_3^o]_s} \quad (8)$$

where  $k$  is dependent on limestone type.

In the presence of sulfate, calcium sulfite is known to crystallize out as a mixed sulfate/sulfite hemihydrate solid (Jones et al., 1976). Consequently for  $CaSO_3$  dissolution the flux of  $Ca^{++}$  must equal the flux of sulfite and sulfate where the ratio of these fluxes equals the ratio of  $CaSO_3$  to  $CaSO_4$  in the hemihydrate solid.

If the bulk solution composition is given, the flux for limestone or  $\text{CaSO}_3$  dissolution can be found by numerical solution of the set of equations representing the fluxes, solid/liquid equilibria, and acid/base solution equilibria at the solid surface.

### Scrubber Integration

The overall approach to the scrubber is to treat it as a multistage countercurrent contactor with plug flow gas and well mixed liquid. In a given stage the rates of  $\text{CaSO}_3$  and  $\text{CaCO}_3$  dissolution are constant since the liquid is well mixed. However the gas composition changes and the rate of gas/liquid transfer must be numerically integrated.

With guessed outlet solution composition and known outlet gas concentrations for a single stage, the inlet gas concentration is determined by numerical integration of three differential equations:

$$\frac{dP_i}{dN_g} = \frac{k_l^0 (\sum \sqrt{D_j} \Delta [C_j])_i}{k_g \sqrt{D_{\text{SO}_2}}} \quad (9)$$

where  $i = \text{SO}_2, \text{CO}_2, \text{and O}_2$ .  $N_g$  is the number of gas phase transfer units and is defined by:

$$N_g = \frac{k_{ga} Z P}{G} \quad (10)$$

For each stage in the scrubber the following algebraic equations are solved to determine the outlet liquid composition from a given inlet liquid composition and outlet gas composition:

$$\frac{L}{G} ([\text{SO}_4^{2-}]_{T,\text{out}} - [\text{SO}_4^{2-}]_{T,\text{in}}) = 2(P_{\text{O}_2,\text{in}} - P_{\text{O}_2,\text{out}}) - \frac{L}{G} K_{\text{crys1}} (R_{\text{CaSO}_4} - 1) \quad (11)$$

$$\begin{aligned} \frac{L}{G} ([\text{SO}_2]_{T,\text{out}} - [\text{SO}_2]_{T,\text{in}}) &= (P_{\text{SO}_2,\text{in}} - P_{\text{SO}_2,\text{out}}) - 2(P_{\text{O}_2,\text{in}} - P_{\text{O}_2,\text{out}}) \\ &+ \frac{L}{G} K_{\text{CaSO}_3} (\sum D_j \Delta [\text{SO}_{3,j}]) - \frac{L}{G} K_{\text{crys2}} \frac{(R_{\text{CaSO}_3} - 1)^2}{R_{\text{CaSO}_4}} \end{aligned} \quad (12)$$

$$\frac{L}{G}([CO_2]_{T,out} - [CO_2]_{T,in}) = (P_{CO_2,in} - P_{CO_2,out}) + \frac{L}{G}K_{CaCO_3}(\sum D_j \Delta[CO_{3,j}]) \quad (13)$$

$$([Ca^{++}]_{out} - [Ca^{++}]_{in}) = K_{CaSO_3}(\sum D_j \Delta[SO_{3,j}]) - K_{crys2} \frac{(RS_{CaSO_3} - 1)^2}{RS_{CaSO_4}} + K_{CaCO_3}(\sum D_j \Delta[CO_{3,j}]) - K_{crys1}(RS_{CaSO_4} - 1) \quad (14)$$

At each stage an initial guess of outlet composition is generated. Then the gas-phase integration is performed and the non-linear equations (11-14) are solved numerically.

### Hold Tank Treatment

The hold tank is treated as an additional scrubber stage with the assumption that  $SO_2$  stripping is negligible. At the pH of typical hold tanks (5.5 - 6.5) the driving force for desorption of  $SO_2$  is low, therefore gas phase integration is not required. A log-mean driving force is used to describe the change in gas phase concentrations of  $CO_2$  and  $O_2$ . Thus  $N_1$ , the number of liquid phase transfer units, is defined using the log-mean driving force by

$$N_1 = \frac{\Delta[CO_3^{=}] + K_{CaCO_3}(\text{flux } CaCO_3)}{[CO_2^*]_{out} - [CO_2^*]_{in}} \ln \frac{[CO_2]_b - [CO_2^*]_{out}}{[CO_2]_b - [CO_2^*]_{in}} \quad (15)$$

Thus the concentration of outlet  $CO_2$  and  $O_2$  are calculated by the following equation

$$P_{i,out} = H_i[i] \left\{ 1 - \frac{1.0 - \frac{P_{in}}{H_i[i]_b}}{\exp \frac{N_1 L}{H_i G}} \right\} \quad i = CO_2 \text{ and } O_2 \quad (16)$$

The concentration of  $[O_2]_b$  is calculated by assuming the rate of mass transfer equals the rate of sulfite oxidation. Thus



$$[O_2]_b = \frac{[O_2^*]_{in}}{1 + K_{ox}[SO_3=]} \quad (17)$$

### Solids Reactivity

#### Reactivity Parameters

The  $CaSO_3$  and  $CaCO_3$  reactivity parameters used in Equations (12) to (14) are defined such that

$$K_{CaCO_3} = \frac{a\tau}{\delta} \quad (18)$$

These reactivity parameters can be derived from particle size distributions or from batch dissolution data. Since measured reactivity values are seldom available at industrial sites limestone reactivity is predicted from available limestone data. The particle size distribution has been shown to be a significant factor affecting limestone reactivity (Toprac and Rochelle, 1982; Gage, 1989).

The rate of limestone dissolution can be expressed in terms of  $f_p$ , the fraction of undissolved limestone of initial size  $p$ , by the following rate expression:

$$\frac{df_p}{dt} = -\frac{kf_p^{1/3}}{V_p^{2/3}} - \frac{kBf_p^{2/3}}{V_p^{1/3}} \quad (19)$$

When integrated the resulting equation is

$$kt = \frac{3}{B^2} \ln \left[ \frac{1 + BV_p^{1/3}f_p^{1/3}}{1 + BV_p^{1/3}} \right] + BV_p^{1/3} (1 - f_p^{1/3}) \quad (20)$$

Since the liquid recirculation rate is large relative to the limestone feed rate the scrubber stages are treated as a continuous stirred tank reactor. Thus the probability of a limestone particle leaving the scrubber in  $dt$  about  $t$  is given by

$$P(t) = \frac{1}{\tau} e^{-(t/\tau)} \quad (21)$$

The total undissolved limestone ( $F_c$ ) is found by integrating over all possible times for each size fraction and then summing over all size fractions.  $F_c$  is given by

$$F_c = \sum \phi_p \frac{1}{k\tau} \int \frac{e^{-(kt/k\tau)}}{df_p/d(k\tau)} f_p df_p \quad (22)$$

The fraction remaining,  $F_c$ , is related to the utilization,  $U$ , by

$$F_c = 1 - U \quad (23)$$

### Particle Size Distributions

Use of the dissolution model for prediction of limestone reactivity requires the input of the complete range of particle size distributions. However at industrial sites limestones are sized by a few sieve measurements. Typically the distributions are reported as percents less than 200 and 325 mesh (74 and 44 microns, respectively). Therefore a statistical method is required to predict a complete distribution from these sieve measurements.

The log-gamma density function has been used with limestone dissolution experiments to predict fraction remaining versus time (Toprac and Rochelle, 1981; Gage, 1989). The log-gamma probability density function is given by

$$f(Y) = \frac{W^{\alpha-1} e^{-(W/\beta)}}{\beta^{\alpha} \Gamma(\alpha)} \quad (24)$$

where  $W = 3 \ln (d_{100}/d)$ .

Mathematically the parameters  $\alpha$  and  $\beta$  are related to the moments of the distribution. Physically  $\beta$  is related to the mode of breakage and  $\alpha$  increases with increasing breakage frequency. The slurry scrubber model assumes an integer value for  $\alpha$ . Then two sieve measurements are required to calculate the remaining unknowns,  $\beta$  and  $d_{100}$ .

If  $\alpha$  is an integer Equation (24) can be integrated analytically. With the integration limits

$$(1) \text{ for } d = d_{\min}, P(d) = 1, \text{ and}$$

$$(2) \text{ for } d = d_{100}, P(d) = 0$$

The resulting polynomial in  $\alpha$  is

$$P(Y) = \frac{e^{-Y} Y^{\alpha-1}}{(\alpha-1)!} \left[ 1 + \frac{(\alpha-1)}{Y} + \frac{(\alpha-1)(\alpha-2)}{Y^2} + \dots + \frac{(\alpha-1)(\alpha-2)\dots[\alpha-(\alpha-1)]}{Y^{\alpha-1}} \right] \quad (25)$$

$$\text{where } Y = \frac{3}{\beta} \ln \left[ \frac{d_{100}}{d} \right]$$

When complete particle size distributions are available, such as Coulter Counter data, the parameters  $\alpha$  and  $\beta$  can be found by the method of moments. For the log gamma density function the moment generating function is given by

$$\text{Mgf}(t) = [1/(1-\beta t)]^{\alpha} \quad (26)$$

### Model Input Parameters

The following input data and parameters are needed to model a specific scrubber operation:

- 1) Gas, solution, and solids compositions.
- 2) Liquid to gas ratio, L/G.
- 3) Number of contacting stages and gas-phase transfer units.
- 4) Ratio of liquid and gas film mass transfer coefficients,  $k_l^0/k_g$ .

- 5)  $\text{CaSO}_3$  reactivity.
- 6) Oxidation enhancement factor.
- 7) Limestone utilization and either two sieve measurements or a particle size distribution.
- 8) Crystallization constants for  $\text{CaSO}_3$  and  $\text{CaSO}_4$ .
- 9) Liquid residence times in the scrubber and the hold tank.

### References for Appendix C

- Berner, R.A. and J. W. Morse, "Dissolution Kinetics of Calcium Carbonate in Sea Water: IV. Theory of Calcite Dissolution", American Journal Of Science, 265, 45-70, (1974).
- Chan, P.K. and Gary T. Rochelle, "CaCO<sub>3</sub> Dissolution - Effects of pH, CO<sub>2</sub>, and Buffers Modelled by Mass Transfer," ACS Symposium Series, 188, 75 (1982).
- Chan, P.K. and G. T. Rochelle, "Modelling of SO<sub>2</sub> Removal by Limestone Slurry Scrubbers: Effects of Chloride," presented at the EPA/EPRI symposium on Flue Gas Desulfurization , New Orleans, Nov. 1-4, 1983.
- Chang, C.S. and G.T. Rochelle, "Mass Transfer Enhanced by Equilibrium Reactions," Ind. Eng. Chem. Fund., 21, 379-385 (1982).
- Epstein, M., "EPA Alkaline Scrubbing Test Facility: Summary of Testing through October 1974," EPA 650-2-75-047 (1975).
- Gage, C.L. "Limestone Dissolution in Modeling of Slurry Scrubbing for Flue Gas Desulfurization", Ph.D. Dissertation, University of Texas, Austin (1989).
- Jones, B.J., P.S. Lowell, and F.B. Meserole, "Experimental and Theoretical Studies of Solid Solution Formation in Lime and Limestone SO<sub>2</sub> Scrubbers," Radian Corporation, EPA 60012-76-273a, October 1976.
- Lowell, P.S., D.M. Ottmers, K. Schwitzgebel, T.I. Strange, and D.W. Deberry, "A Theoretical Description of the Limestone Injection-Wet Scrubbing Process," U.S. Environmental Protection Agency, APTD 1287, PB 1931-029 (1970).
- Mehta, R.R., and G.T. Rochelle, "Modelling of SO<sub>2</sub> Removal and Limestone Utilization in Slurry Scrubber Systems with Forced Oxidation," presented at the

- AIChE National Meeting, Houston, March 27-31, (1983).
- Mehta, R.R., "Modelling of SO<sub>2</sub> Removal and Limestone Utilization in Slurry Scrubber Systems with Forced Oxidation," M.S. Thesis, University of Texas, Austin (1982).
- Morse, J. W., "Dissolution Kinetics of Calcium Carbonate in Sea Water: V. Effects of Natural Inhibitors and the Position of the Lysocline", American Journal of Science, **274**, 638-647 (1974).
- Rochelle, G.T., and C.J. King , "The Effects of Additives on Mass Transfer in CaCO<sub>3</sub> or CaO Slurry Scrubbing of SO<sub>2</sub> from Waste Gases," Ind. Eng. Chem. Fund., **16**, 67 (1977).
- Rochelle, G.T., P.K. Chan, and A. Toprac, "Limestone Dissolution in Flue Gas Desulfurization Processes", EPA Report, PB 83-252833, (1983).
- Sjoberg, E.Lennart, "Kinetics and Mechanism of Calcite Dissolution in Aqueous Solutions at Low Temperatures," Stockholm Contributions in Geology, **32**, 1-95 (1981).
- Terjeson, S.G. O. Erga, G. Thersen, and A. Ve "Phase Boundary Processes as Rate Determining Steps in Reactions Between Solids and Liquids," Che. Eng. Sci., **14**, 277-289 (1961).
- Toprac, A.J., and G.T. Rochelle, "Limestone Dissolution in Stack Gas Desulfurization Processes - Effect of Type and Grind," Env. Prog., **1** (1), 52 (1982).
- Tseng, P., and G.T. Rochelle, "Dissolution Rates of Calcium Sulfite Hemihydrate in FGD Processes", Env. Prog., **5** (1), 34-40 (1986).
- Weems. W.T., "Enhanced Adsorption of Sulfur Dioxide by Sulfite and Other Buffers," M.S. Thesis, University of Texas, Austin (1981).

**Table C.1: Diffusivity Values at 25°C used in the Slurry Scrubber Model\***

Species	Diffusivity x 10 <sup>5</sup> (cm <sup>2</sup> /s)
H <sup>+</sup>	9.31
OH <sup>-</sup>	5.24
H <sub>2</sub> CO <sub>3</sub>	2.0
HCO <sub>3</sub> <sup>-</sup>	1.18
CO <sub>3</sub> <sup>=</sup>	0.96
H <sub>2</sub> SO <sub>3</sub> <sup>0</sup>	2.0
HSO <sub>3</sub> <sup>-</sup>	1.33
SO <sub>3</sub> <sup>=</sup>	0.96
HSO <sub>4</sub> <sup>-</sup>	1.33
SO <sub>4</sub> <sup>-</sup>	1.06
Ca <sup>++</sup>	0.79
CaOH <sup>+</sup>	0.79
CaHCO <sub>3</sub> <sup>+</sup>	0.72
CaHSO <sub>3</sub> <sup>+</sup>	0.73
CaCO <sub>3</sub> <sup>0</sup>	0.53
CaSO <sub>3</sub> <sup>0</sup>	0.53
CaSO <sub>4</sub> <sup>0</sup>	0.58
Mg <sup>++</sup>	0.70
MgOH <sup>+</sup>	0.70
MgHCO <sub>3</sub> <sup>+</sup>	0.72
MgHSO <sub>3</sub> <sup>+</sup>	0.73
MgCO <sub>3</sub> <sup>0</sup>	0.53
MgSO <sub>3</sub> <sup>0</sup>	0.53
MgSO <sub>4</sub> <sup>0</sup>	0.58
Na <sup>+</sup>	1.35
NaOH <sup>0</sup>	1.35
NaHCO <sub>3</sub> <sup>0</sup>	1.18

**Table C.1(con't): Diffusivity Values at 25°C used in the Slurry Scrubber Model\***

Species	Diffusivity x 10 <sup>5</sup> (cm <sup>2</sup> /s)
NaCO <sub>3</sub> <sup>-</sup>	0.96
NaSO <sub>4</sub> <sup>-</sup>	1.06
Cl <sup>-</sup>	2.03
H <sub>2</sub> Ad <sup>0</sup>	0.736
HAd <sup>-</sup>	0.72
Ad <sup>=</sup>	0.705
CaAd <sup>0</sup>	0.39

\* For the sources of these values see Mehta and Rochelle (1982), Chan and Rochelle (1982), and Tseng and Rochelle (1986).



## Individual Subroutine Documentation

This section contains the individualized subroutine documentation for every subroutine in the Slurry Scrubber Model for Flue Gas Desulfurization. Documentation for each routine uses a four part format with the following form:

- 1) Overview
- 2) Usage
- 3) Algorithmic Techniques
- 4) Programming Details

The Overview section defines the purpose of the subroutine and gives any theoretical or mathematical background necessary to understanding the routine.

The Usage section contains an example of the calling sequence for the routine. All argument variables in the calling statement are defined for both entry and return. If variables are returned or acquired through common blocks, these are also defined as well as their common block locations.

The Algorithmic Technique section discusses any convergence techniques which may be used in the subroutine. If an IMSL routine is used, its calling sequence is detailed but the technique is not discussed.

The Programming Details section gives a step-by-step listing of the programming as it is performed by the subroutine. This should greatly aid when debugging or modifying a routine for specialized use.

The following conventions are used in the Subroutine Documentation section.

1. Capitalized words are variable names as they appear in the subroutine.
2. Underlined words are the names of specific subroutines.
3. Italicized words are the names of common blocks.

## Subroutine Bis

### 1) Overview

**Purpose** - Subroutine Bis is a bisection routine used by subroutine Gvar to find the random variable,  $y$ , of the log-gamma function which satisfies a specified weight fraction.

**Background** - The prediction of a complete particle size distribution is done using the log-gamma function. This function has two parameters,  $\beta$  and  $d_{100}$ , which are specific to the distribution. (See Dist documentation.) These parameters are estimated using the input variables of two sieve weight fractions and their corresponding diameters. Subroutine Gvar sets the bounds on both sides of each weight fraction from an internal database. Subroutine Bis is then called to converge on the specific random variables of the log-gamma function which satisfy the input weight fractions.

### 2) Usage

The calling sequence for Bis is

CALL BIS(PU,PL,P,XU,XL,X)

On entry

P = the input weight fraction,

PU = the upper bound around P,

PL = the lower bound around P,

XU = the random variable corresponding to PU, and

XL = the random variable corresponding to PL.

On return

X = the random variable satisfying P.

### 3) Algorithmic Techniques

Subroutine Bis uses a bisection technique to converge on y. A value of y is assumed halfway between XU and XL. The log-gamma function is evaluated using this y. The resulting cumulative distribution is compared to PU and PL. If either relative error is less than the tolerance, convergence is reached and that value of y is returned to the calling program. If the tolerance is not met, an endpoint is replaced and the halving routine is repeated. The tolerance on the relative error is 0.0001.

### 4) Programming Details

The convergence on X is programming in the following step. Using bounds established in Gvar:

1. Loop 1: Calculate Y at half the random variable interval.
2. Calculate P1, the cumulative fraction at X, using the algebraic expression for the log-gamma function. (Equation (1) in Gvar.)
3. Compare to measured weight fraction for convergence. (Relative error < EPS?)
  - 3.1 True - go to branch 1
  - 3.2 False - continue
4. Replace an endpoint. (P1 < P(input)?)
  - 4.1 True - replace lower bound with P1.
  - 4.2 False - replace the upper bound with P1.
5. Restart loop 1.
6. Branch 1: Return to calling program.

## Subroutine CaSO3di

### 1) Overview

**Purpose** - Subroutine CaSO3di calculates the calcium sulfite dissolution rate.

**Background** - The presence of solids in the scrubber liquor requires the calculation of dissolution rates. These solids include a mixed crystal of  $\text{CaSO}_3/\text{CaSO}_4$  hemihydrate returned from the hold tank. CaSO3di calculates the dissolution rate of the mixed crystal by computing the flux across the solid boundary layer. The two boundary conditions that must be satisfied are: (1) at the edge of the boundary layer the species concentrations must equal the bulk concentrations, (2) at the solid surface the  $K_{sp}$  of the predominate crystal,  $\text{CaSO}_3$ , must be reached.

Once bulk concentrations are known the fluxes of calcium, sulfite, and sulfate can be calculated by iterating on the concentration of  $[\text{H}^+]_s$  at the solid surface. CaSO3di assumes a concentration of  $[\text{H}^+]_s$  and calls subroutine Surface to calculate the concentration of all species at the solid. Control then returns to CaSO3di where the calculated surface concentrations of  $[\text{Ca}^{++}]_s$  and  $[\text{SO}_3^{=}]_s$  are tested for convergence with the  $K_{sp}$  of  $\text{CaSO}_3$ . If the convergence criteria is not met, a new concentration of  $[\text{H}^+]_s$  is assumed and all steps are repeated.

### 2) Usage

The calling sequence for CaSO3di is

Call CaSO3di

On entry

All required variables are accessed through common blocks. These variables (and their common blocks) are the bulk species pseudo-concentrations (*SCONC* and *SCONCI*) and their diffusivities (*DIFF*).

On return

The fluxes of calcium sulfite and calcium sulfate hemihydrate are returned by Surface through common block *DIFLUX*.

### 3) Algorithmic Details

Convergence of the  $K_{sp}$  of  $\text{CaSO}_3$  is reached by iterating on the concentration of  $[\text{H}^+]_s$  at the solid surface. These iterations are done using a bisection technique in two loops. Since the  $[\text{H}^+]_s$  concentration is bounded by zero on the left side and  $[\text{H}^+]_{\text{bulk}}$  on the right side, an initial guess of  $[\text{H}^+]$  equal to the bulk concentration is made. In the first loop the concentration is halved until the calculated product of  $[\text{Ca}^{++}]_s$  and  $[\text{SO}_3^{++}]_s$ ,  $\text{PCaSO}_3$ , is greater than  $K_{sp}$ . Control then drops to the second loop.

In the second loop the assumed  $[\text{H}^+]_s$  concentrations are selected between the end point bounds found in loop 1 which gave  $K_{sp}(\text{calc}) < K_{sp}$  and  $K_{sp}(\text{calc}) > K_{sp}$ . Again the concentrations are halved across the interval with an end point replaced at each step.

Iteration in the second loop continues until one of the following criteria is met:

1.  $|\text{PCaSO}_3 - K_{sp}|/K_{sp} < 0.000001$  or
2.  $|[\text{H}^+]_{\text{new}} - [\text{H}^+]_{\text{old}}|/[\text{H}^+]_{\text{new}} < 0.000001$ .

$\text{CaSO}_3\text{di}$  has one additional restriction. If in either loop the number of iterations exceeds 30, computing stops and an error message is printed which reads "Convergence failed for  $\text{CaSO}_3$  dissolution".

### 4) Programming Details

Convergence to the  $K_{sp}$  of  $\text{CaSO}_3$  is programmed through the following steps. For given bulk species concentrations:

1. Calculate  $\Sigma(D_i C_i)_{\text{bulk}}$  for all species.
2. Assume  $[\text{H}^+] = [\text{H}^+]_{\text{bulk}}$ .
3. Loop 1 : Call Surface and return.
  - 3.1 Compare  $\text{PCaSO}_3$  to  $K_{sp}$ .
  - 3.2 If  $\text{PCaSO}_3 > K_{sp}$ , go to branch 2.
  - 3.3 If  $\text{PCaSO}_3 < K_{sp}$ ,  $[\text{H}^+]_{\text{new}} = 0.5[\text{H}^+]_{\text{old}}$
  - 3.4 Compare iteration number to limit: if  $N = 30$  go to branch 3

- 3.5 Restart loop.
- 4. Branch 2 : establish end points.
  - 4.1  $H1 = [H^+]_{old}$
  - 4.2  $H2 = 2[H^+]_{old}$
- 5. Loop 2 : Assume  $[H^+] = 0.5(H1+H2)$ 
  - 5.1 Call Surface and return.
  - 5.2 Compare iteration number to limit: if  $L = 30$  go to branch 3.
  - 5.3 If  $PCASO3 < K_{sp}$ ,  $H2 = [H^+]$
  - 5.4 If  $PCASO3 > K_{sp}$ ,  $H1 = [H^+]$
  - 5.5 Test for convergence
    - If  $|PCASO3 - K_{sp}|/K_{sp} < 0.000001$ , go to branch 4
    - If  $|H2 - H1|/H2 < 0.000001$ , go to branch 4
  - 5.6 Restart loop
- 6. Branch 3 : Print error message.
  - 6.1 Return to calling program.
- 7. Branch 4 : Return to calling program.

## Subroutine Charbl

### 1) Overview

Purpose - Charbl iterates on the concentration of  $[Ca^{++}]$  to force a zero charge balance in the Bechtel Modified Radian Equilibrium Program, BMREP.

Background - BMREP calculates the equilibrium compositions from activity coefficients estimated using ionic strength. However BMREP does not check to confirm that the electronegativity of the solution is preserved. Since pH is specified at the scrubber inlet, Charbl adjusts the concentration of  $[Ca^{++}]$  in BMREP to satisfy a zero charge balance before the scrubber routines are called.

### 2) Usage

The calling sequence for Charbl is

Call Charbl(X,CM,CHERR)

On entry

X = an array of 50 elements containing the concentrations of the 41 scrubber species.

CM = an array of 8 elements containing concentrations of  $[SO_3^-]$ ,  $[CO_3^-]$ ,  $[SO_4^-]$ ,  $[NO_3^-]$ ,  $[Ca^{++}]$ ,  $[Mg^{++}]$ ,  $[Na^+ + K^+]$ , and  $[Cl^-]$  in that order.

On return

CHERR = the ratio of charge imbalance to the total positive charges.

### 3) Algorithmic Details

There are no special algorithmic techniques in this routine.

### 4) Programming Details

For given bulk species concentrations:

1. Calculate DEL, the difference between positively and negatively charged species.
2. Calculate the sum of the positive charges.
3. Adjust  $[\text{Ca}^{++}]$  when  $\text{DEL} \neq 0$ .
4. Calculate the charge error (CHERR) the ratio of DEL to the positive charges.
5. Return to the calling program.



## Subroutine Conest

### 1) Overview

**Purpose** - Subroutine Conest estimates the first guess for outlet concentrations required by the IMSL routine Zspow.

**Background** - The IMSL routine Zspow uses a modified Powell technique to converge on total bulk outlet concentrations at each stage in the hold tank. This routine is very sensitive to the initial guess for the outlet concentration. Since the overall convergence of SSMFGD typically requires passing through the scrubber/hold tank loop 8 to 12 times, subroutine Conest was written to improve the first estimates for Zspow at each pass through the scrubber and hold tank. Using the previous converged solutions, estimates are calculated by

$$[C_{i+1}]_j = [C_i]_j \left[ 1 + \frac{[C_i]_j - [C_{i-1}]_j}{[C_i]_j} \right] \quad (1)$$

where  $i$  = an iteration counter, and

$j$  =  $[SO_3^-]$ ,  $[CO_3^-]$ ,  $[SO_4^-]$ , and  $[Ca^{++}]$ .

Addition of this routine has reduced the number of program halts from Zspow and has decreased overall convergence time.

### 2) Usage

The calling sequence for subroutine Conest is

CALL CONEST(N,XIN,XOUT,M,L)

On entry

N = a counter indicating the number of calls to Conest.

XIN = an array of four containing converged concentrations at step N,

XOUT = an array of four containing the estimates,

M = a counter indicating whether the scrubber or the hold tank is making the call,

= 1 = hold tank

= 2 = scrubber, and

L = a counter indicating the stage number when M = 2.

### 3) Algorithmic Techniques

There are no special algorithmic techniques in this subroutine.

### 4) Programming Details

The estimation of outlet concentrations is programmed through the following steps.

1. Test counter for calling routine.
  - 1.1 If M = 1, go to branch 1.
  - 1.2 If M = 2, continue
2. Test for iteration number.
  - 2.1 If N = 1, go to branch 2.
  - 2.2 If N > 1, continue.
3. Estimate next guess for scrubber stage L
  - 3.1 Replace stored value of (i-1)th iteration, XS2.
  - 3.2 Replace stored value of (i)th iteration, XS1.
  - 3.3 Estimate next guess, XOUT, using equation 1.
4. Go to branch 4.
5. Branch 2: Store first converged values for scrubber, XS1.
6. Set XOUT = XIN.
7. Go to branch 4.
8. Branch 1: Test for iteration number.
  - 8.1 If N = 1, go to branch 3.
  - 8.2 If N > 1, continue.
9. Estimate next guess for hold tank.

- 9.1 Replace stored value of (i-1)th iteration, XH2.
- 9.2 Replace stored value of (i)th iteration, XH1.
- 9.3 Estimate next guess, XOUT, using equation 1.
- 10. Go to branch 4.
- 11. Branch 3: Store first converged values for hold tank, XH1.
- 12. Set  $XOUT = XIN$ .
- 13. For  $SO_4^{=}$ , set  $XOUT = 1.1XIN$ .
- 14. Branch 4: Return to calling program.

## Subroutine Conopt

### 1) Overview

**Purpose** - Subroutine Conopt is the driver subroutine for predicting multistage scrubber performance given the bulk inlet liquid concentrations.

**Background** - The use of multistage scrubbers requires that the gas and liquid concentrations be studied at each stage. Subroutine Conopt controls calling of the IMSL routine Zspow which determines the exiting liquid concentration at each stage. Conopt also updates gas and liquid concentrations for the next stage.

At each stage Conopt assumes an outlet liquid concentration estimated in Conest and then calls the IMSL routine Zspow. This routine finds the solution to the four non-linear material balance equations by assuming outlet concentrations. Zspow requires an external subroutine (Fcn) to contain these equations. (See Fcn documentation.)

Once Zspow has converged, control then returns to Conopt where values are saved for the output file, Poutput.

### 2) Usage

The calling sequence for Conopt is

CALL CONOPT(NFLAG2)

On entry

NFLAG2 = 12 = cocurrent scrubbing, and  
           < 12 = countercurrent scrubbing.

All other required variables are accessed through common blocks. These variables (and their common blocks) are

BPPI(*PPRESS*) = an array of three containing inlet gas concentrations,

SOLIDIN(*CC3*) = an array of four containing solids concentrations,

NMIX(*INPUT3*) = number of scrubber stages,

RLG(*INPUT2*) = the ratio of gas to liquid flowrates,

CY(*SINGLE*) = an array of three containing outlet gas partial pressures, and

DSOLID(CC3) = an array of four containing the change in solids concentrations.

Liquid concentrations for bulk and individual species are accessed through common blocks *BULKSP* and *BULKI*. Limestone surface concentrations are accessed through *LSURF*.

On return

All values for the output file are returned through common blocks *LAST*, *LAST2*, *CC5*, and *ADD*.

### 3) Algorithmic Details

Subroutine Conopt calls the IMSL routine Zspow to converge on the four non-linear material balance equations. This routine uses a modified Powell method to search for the zero of four equations

$$F(i) = Z(i) - CINSPI \quad i = [SO_3=], [CO_3=], [SO_4=], \text{ and } [Ca^{++}]$$

where

$Z(i)$  = the inlet concentration calculated using the non-linear material balance equation, and

$CINSPI$  = the specified inlet concentration (equal to the exit concentration from the previous stage).

The calling sequence for Zspow is

CALL ZSPOW(FCN,NSIG,N,ITMAX,PAR,X,FNORM,WR,IER)

On entry

FCN = the externally declared subroutine containing the equations to be zeroed,

NSIG = 6, a convergence criteria,

N = 4, the number of equations to be zeroed and the size of array X.

ITMAX = 100, the maximum number of iterations, and

X = the initial guess for the outlet concentration.

On return

X = the converged outlet concentration.

#### 4) Programming Details

The calculations for each stage's exiting concentrations are programmed through the following steps.

1. Initialize values for Zspow.
2. Loop 1 - For stage j, set the exiting liquor concentration equal to the estimate from Conest for a first guess.

- 2.1 Call Zspow to converge on exit liquor concentrations.

- 2.2 Store values for output. (Index j indicates the stage number.)

SOLCON(i,j) = solids concentrations

RS(j,1) = relative saturation of  $\text{CaSO}_3$

RS(j,2) = relative saturation of  $\text{CaSO}_4$

DINV(1,j) = change in concentration of  $\text{SO}_3^{=}$  across stage j

DINV(2,j) = change in concentration of  $\text{CO}_3^{=}$  across stage j

DINV(3,j) = change in concentration of  $\text{SO}_4^{=}$  across stage j

DINV(4,j) = change in concentration of  $\text{Ca}^{++}$  across stage j

DINV(5,j) = make-per-pass on stage j

DINV(6,j) =  $\text{CaSO}_3$  dissolved on stage j

DINV(7,j) =  $\text{CaCO}_3$  dissolved on stage j

BCES(i,j) = bulk liquor concentrations of 17 species

BCG(i,j) = gas partial pressure of 3 species

DISFLUX(j,1) = solid-to-liquid flux of  $\text{CaCO}_3$

DISFLUX(j,2) = solid-to-liquid flux of  $\text{CaSO}_3$

GASFLUX(j,1) = gas-to-liquid flux of  $\text{SO}_2$

GASFLUX(j,2) = gas-to-liquid flux of  $\text{CO}_2$

GASFLUX(j,3) = gas-to-liquid flux of  $\text{O}_2$

BOUND(j) = boundary condition at limestone surface

SFLCA(j) = calcium concentration at limestone surface

SFLCO3(j) = carbonate concentration at limestone surface

SFLSO3(j) = sulfite concentration at limestone surface

- 2.3 Update values for stage j+1.

- 2.3.1 Set inlet solids equal to exit from stage j.

2.3.2 Set inlet liquor concentration of four main species equal to the exit from stage j.

2.3.3 Set outlet gas concentration equal to inlet of stage j.

2.4 Continue this loop through all stages.

3. Calculate the total make-per-pass for the scrubber, TOTMPP.
4. Calculate the percent of  $\text{SO}_3$  oxidized, PEROX.
5. Set the concentrations of the hold tank inlet liquor equal to the exit concentrations from the last stage.
6. Return to calling program.

## Subroutine Conver

### 1) Overview

Purpose - Subroutine Conver iterates on the assumed SO<sub>2</sub> gas driving force at the gas/liquid interface until convergence to a zero charge flux is reached.

Background - The flux of SO<sub>2</sub> across the gas/liquid interface is expressed by:

$$\text{Flux SO}_2 = k_g(P_b - P_i) = k_l\{\sum D_j[\Delta\text{SO}_3^-]_j + \sum D_j[\Delta\text{SO}_4^{=}]_j\}$$

where

$P_b$ ,  $P_i$  = partial pressure of SO<sub>2</sub> in the bulk and at the interface, respectively,

$k_g$ ,  $k_l$  = gas phase and liquid phase mass transfer coefficients, respectively, and

$D_j$  = diffusivity of specie  $j$ .

This flux is limited by the finite boundary layer resistances. Numerically the finite-gas phase resistance is limited by its largest possible driving force which occurs when the gas interface concentration is zero. The liquid phase resistance limit is estimated by setting the SO<sub>2</sub> gas interface concentration equal to its bulk value. Using these limits sets the SO<sub>2</sub> flux bounds in Conver. Subroutine Glmf is then called to solve for the liquid phase interface concentrations based on the assumed gas phase driving force. Once the bounds are established, Conver iterates between them to solve for the SO<sub>2</sub> gas driving force which yields a zero charge flux in the liquid boundary layer.

### 2) Usage

The calling sequence for Conver is

CALL CONVER(DELC)

On entry

All required variables are accessed through common blocks. These variables (and their common blocks) are

SD(DIFF) = an array of 17 containing diffusivities,

BPPPPRESS) = an array of three containing bulk partial pressures,

RKLKG(PPRESS) = the ratio of liquid-to-gas mass transfer coefficients,

RLG(INPUT2) = the ratio of the liquid to gas mass flowrates,



HK(HENRYS) = an array of three containing Henry's constants, and  
 PHIY(*INPUT2*) = the oxygen enhancement factor.

On return

DELCH = the charge flux in the liquid boundary layer.

Other variables are returned through common blocks. These variables (and their common blocks) are

DELFSO2(*RESULT*) = the flux of SO<sub>2</sub> across the interface, and

FFLUX(CONST) = the converged gas driving force of SO<sub>2</sub>.

### 3) Algorithmic Details

Conver uses a regula falsi technique to find the zero charge flux. This convergence technique assumes a linear relationship between the gas driving force, FLUX, and DELCH, the difference in the charge balance across the liquid side boundary layer. Using two end points the slope is calculated and a new value of FLUX is estimated by

$$\text{FLUX}(\text{new}) = \text{FLUX2} + \text{Slope} * \text{DELCH2} \quad (1)$$

where

$$\text{Slope} = \frac{\text{FLUX2} - \text{FLUX1}}{\text{DELCH2} - \text{DELCH1}} \quad (2)$$

A new end point (and thus a new slope) is saved at each step. Since regula falsi techniques can diverge, the technique is modified to use a half-interval guess for FLUX whenever the regula falsi estimate is outside the originals bounds set by finite gas and liquid phase resistances.

Convergence is reached when either of two limits is reached. One limit requires the difference between two driving force estimates to be  $< 0.00001$ . The second limit requires the charge flux in the boundary layer to be  $< 0.00001$ . Additionally an iteration limit stops the program and prints an error message if the number of iterations exceeds 500.

#### 4) Programming Details

Convergence to a zero electrical current in the liquid boundary layer is programmed through the following steps.

1. Calculate the electrical charge in the bulk,  $\sum Z_i D_i C_i$ .
2. Assume liquid phase limit for SO<sub>2</sub> flux (FLUX1).
3. Call Glimt to calculate the interface concentrations and charge flux, DELCH1.
4. Assume gas phase limit for SO<sub>2</sub> flux (FLUX2).
5. Loop 1: Call Glimt to calculate DELCH2.
6. Test (DELCH1\*DELCH2) for negative product.
  - 6.1 True - continue
  - 6.2 False - go to branch 1.
7. Loop 2: Estimate new flux (FLUX<sub>x</sub>) using equation (1).
  - 7.1 Test for convergence,  $0.5|FLUX1-FLUX2|/FLUX1 < 0.0001$ .
    - 7.1.1 False - continue
    - 7.1.2 True - go to branch 2.
  - 7.2 Check that FLUX is between FLUX1 and FLUX2.
    - 7.2.1 True - Continue
    - 7.2.2 False - Set  $FLUX = 1/2(FLUX1 + FLUX2)$
  - 7.3 Call Glimt to calculate interface liquid concentrations and DELCH, liquid charge flux.
  - 7.4 Test for convergence,  $DELCH < 0.0001$ .
    - 7.4.1 False - continue
    - 7.4.2 True - go to branch 3.
  - 7.5 Test (DELCH\*DELCH1) for negative value.
    - 7.5.1 True - go to branch 2.
    - 7.5.2 False - Replace left end point with new values (DELCH1=DELCH, FLUX1=FLUX).
  - 7.6 Restart loop 2.
8. Branch 2: Replace right end point with new values (DELCH2=DELCH, FLUX2=FLUX).
9. Restart loop 2.

10. Branch 1: Compare iteration number to limit: if  $N > 500$  go to branch 4.
11. Estimate new right end flux as one-half the old value.
12. Restart loop 1.
13. Branch 3: Calculate  $\text{SO}_2$  flux based on interface concentrations from Glimt.
14. Store converged FLUX value for next call to Conver, FFLUX.
14. Go to branch 5
15. Branch 4: Print error message.
16. Branch 5: Return to calling program.

## Subroutine Dist

### 1) Overview

**Purpose** - Subroutine Dist calculates a complete particle size distribution using a log-gamma distribution.

**Background** - The prediction of limestone reactivity requires a particle size distribution. If a complete distribution is not available, one can be predicted from two sieve measurements. The density function used in SSMFGD to predict the particle size distribution is the log-gamma function given by

$$f(Y) = \frac{Y^{\alpha-1} e^{-(Y/\beta)}}{\beta^{\alpha} \Gamma(\alpha)} \quad (1)$$

where  $\Gamma$  is the gamma function and  $\alpha$  and  $\beta$  are parameters of the distribution. Mathematically  $\alpha$  and  $\beta$  are related to the moments of the distribution. Physically, they are related to the mode and frequency of breakage.

The random variable,  $Y$ , is a function of the largest particle size in the distribution,  $d_{100}$ , and is given by

$$Y = 3 \ln \left( \frac{d_{100}}{d} \right) \quad (2)$$

When  $\alpha$  is an integer, equation (1) can be integrated analytically. The necessary bounds are (1) for  $d < d_{100}$ ,  $P(d) = 0$  and (2) for  $d = d_{100}$ ,  $P(d) = 1$ . The resulting polynomial in  $\alpha$  is

$$P(Y) = \frac{e^{-Y} Y^{\alpha-1}}{(\alpha-1)!} \left[ 1 + \frac{(\alpha-1)}{Y} + \frac{(\alpha-1)(\alpha-2)}{Y^2} + \dots + \frac{(\alpha-1)(\alpha-2) \dots [\alpha-(\alpha-1)]}{Y^{\alpha-1}} \right] \quad (3)$$

The log-gamma parameters have been fit to nineteen limestones for which complete distributions were measured using a Coulter Counter. This analysis resulted

in a range of  $\alpha$  values from 2.5 to 7.2. Two integer values, 4 and 6, were selected as possible fits for the data. Of these  $\alpha = 4$  resulted in  $d_{100}$  values which were very close to the measured values. This is the  $\alpha$  value used in Dist.

## 2) Usage

The calling sequence for Dist is

CALL DIST(PHI,B,DMAX,IC)

On entry

B = the log-gamma parameter  $\beta$  found in Gvar, and

DMAX = the largest particle,  $d_{100}$ , found in Gvar.

On return

PHI = the complete particle size distribution, and

IC = the number of size intervals calculated.

Additionally the diameters in the distribution are returned through common block *DIAM*.

## 3) Algorithmic Techniques

There are no special algorithmic techniques in this subroutine.

## 4) Programming Details

Subroutine Dist contains a database of 35 diameters ranging between 0.630 and 1680 microns. With this database the particle size distribution is programmed in the following steps using  $\beta$  and DMAX ( $d_{100}$ ) found in subroutine Gvar.

1. Compare each database diameter to DMAX to establish the number of intervals for the distribution, IC.
2. Loop 1: For each diameter, D, calculate the cumulative distribution.
  - 2.1 Ratio D to DMAX.
  - 2.2 Calculate Y from equation (2).
  - 2.3 For  $\alpha = 4$  and Y, calculate equation (3).

3. Calculate the differential distribution,  $\text{PHI}$ , from the cumulative distribution.
4. Return to the calling program.

## Subroutine Equil

### 1) Overview

**Purpose** - Subroutine Equil calculates the slurry liquor composition given total  $[\text{SO}_4^-]$ ,  $[\text{CO}_3^-]$ ,  $[\text{SO}_3^-]$ , and  $[\text{Ca}^{++}]$ .

**Background** - At each stage in the scrubber, liquor compositions must be calculated based on the inlet concentrations and changes within the stage due to absorption and crystallization/dissolution. Non-linear material balance equations solve for total  $[\text{SO}_4^-]$ ,  $[\text{CO}_3^-]$ ,  $[\text{SO}_3^-]$ , and  $[\text{Ca}^{++}]$ , but concentrations of other species are established through equilibrium and charge balances. Subroutine Equil solves for the concentration of these species by assuming a concentration of  $[\text{H}^+]$ , calculating other species concentrations with equilibrium expressions, and converging on  $[\text{H}^+]$  with a charge balance.

The charge balance expression is contained in a function routine called Funct, which is declared external in Equil. Convergence is reached using an IMSL routine, Zfalse. This routine solves for the zero of a function given an interval containing the zero. Zfalse is called in subroutine Equil.

### 2) Usage

The calling sequence for Equil is

```
CALL EQUIL(XR,XL,COUT)
```

On entry

XR = 0.5, the concentration for  $[\text{H}^+]$  known to be on the right side of the zero.

XL = 1.0E-10, the concentration for  $[\text{H}^+]$  known to be on the left side of the zero.

COUT = an array of dimension 4 containing the specified total concentrations of  $[\text{SO}_4^-]$ ,  $[\text{CO}_3^-]$ ,  $[\text{SO}_3^-]$ , and  $[\text{Ca}^{++}]$ .

Other variables which are required by Funct are accessed through common blocks. These variables (and their common blocks) are:

$K(CONST)$  = an array of dimension 50 containing the 41 equilibrium constants calculated in the BMREP,

$SCMG(CATION)$  = the pseudo-concentration of  $[Mg^{++}]$ ,

$SCNA(CATION)$  = the pseudo-concentration of  $[Na^+]$ ,

$KW(EQUILK)$  = the pseudo-equilibrium constant for water,

$KHSO4(EQUILK)$  = the pseudo-constant for  $HSO_4^-$ ,

$KHSO3(EQUILK)$  = the pseudo-constant for  $HSO_3^-$ , and

$KAD(EQUILK)$  = the pseudo-constant for  $HAJ^-$ .

On return the concentrations of 15 species are returned through common block, *BULKSP*. Seven of these are also returned in *SCONC* and seven others in *SCONCI*.

### 3) Algorithmic Details

Convergence to a zero charge balance is reached using the IMSL routine Zfalse. This routine uses a regula falsi technique to search for the zero of the equation:

$$FUNCT = \sum Z_i C_i$$

where  $Z_i$  = the charge of species  $i$ , and

$C_i$  = the concentration, gmol/l.

The calling sequence for Zfalse in subroutine Equil is

CALL ZFALSE(FUNCT, EPS, NSIG, XR, XL, XAPP, ITMAX, IER)

Argument variables not already discussed are defined in Equil with the following values:

Funct = the external function routine containing the equation whose zero is desired.

EPS = 1.0E-6, convergence criteria,

NSIG = 6, the number of significant digits,

ITMAX = 60, the maximum number of iterations,

IER is an output value which indicates an error if convergence can not be reached, and

XAPP, on output, contains the concentration of  $[H^+]$  which caused convergence of FUNCT to zero.



#### 4) Programming Details

Calculation of liquor species are programmed through Equil in the following steps.

For given total concentrations of  $[\text{SO}_4^-]$ ,  $[\text{CO}_3^-]$ ,  $[\text{SO}_3^-]$ , and  $[\text{Ca}^{++}]$ :

1. Initialize values for Zfalse.
2. Call Zfalse.
  - 2.1 Loop : In Zfalse, assume a concentration of  $[\text{H}^+]$  within the interval (XR,XL).
  - 2.2 Branch to real function, Funct.
    - 2.2.1 Calculate the concentrations of other species by equilibrium equations.
    - 2.2.2 Calculate FUNCT, the sum of the charges.
    - 2.2.3 Return to Zfalse.
  - 2.3 Test for convergence,  $\text{FUNCT} < \text{EPS}$ .
    - 2.3.1 False - Restart loop.
    - 2.3.2 True - Return to Equil.
3. On return from Zfalse, if IER = 129, go to branch 1.
4. Go to branch 2.
5. Branch 1 : Print assumed outlet concentrations.
6. Branch 2 : Return to calling program.

## Subroutine Fcn

### 1) Overview

**Purpose** - Subroutine Fcn determines the liquor concentrations entering a scrubber stage based on assumed outlet concentrations at each step in the IMSL routine Zspow.

**Background** - The calling statement for Fcn is contained within the IMSL routine Zspow which was itself called from subroutine Conopt. Therefore Fcn is called at each step of assumed outlet concentrations made by Zspow.

Fcn treats each scrubber stage as a well-mixed regime. Thus exiting conditions are the same as those on the stage. Fcn calls subroutine Intgr to determine exiting gas composition on a stage and then calculates the inlet liquor concentrations of four species ( $[SO_4=]$ ,  $[CO_3=]$ ,  $[SO_3=]$ , and  $[Ca^{++}]$ ) using non-linear material balance equations. In a general form these balances are

$$\text{Inlet} = \text{Outlet} + \text{Absorbed} + \text{Dissolved} - \text{Desorbed} - \text{Crystallized}.$$

The inlet values are then compared to the exit values from the previous stage in order to reach convergence in Zspow.

### 2) Usage

The calling sequence for Fcn is contained within Zspow. Fcn is the first variable in Zspow's argument list and is declared external in subroutine Conopt. Three variables are passed to Fcn from Zspow and one variable is returned. These variables are:

On entry

X = an array containing the assumed outlet concentrations,

N = 4, the number of equations to be converged and the size of the F and X arrays, and

PAR = a dummy parameter not used.

Other required variables are accessed through common blocks. These variables (and their common blocks) are

BPPI(*PPRESS*) = inlet gas partial pressures,

CY(*SINGLE*) = converged outlet gas concentrations,

RLG(*INPUT2*) = the ratio of gas to liquid flowrates,

CINSP(*BULKI*) = an array of four containing the specified inlet liquid concentrations,

DSOLID(*CC3*) = an array of four containing the change in the solid concentrations, and

NFLAG3 (*NFLAG*) = a flag to indicate countercurrent flow.

On return

F = an array containing the difference between the calculated inlet concentrations and the specified inlet concentrations.

### 3) Algorithmic Details

There are no special algorithmic techniques in this subroutine.

### 4) Programming Detail

The calculation of entering liquor concentrations are programmed in the following steps:

1. Check that the assumed liquor concentrations from *Zspow* are positive.
  - 1.1 True - continue
  - 1.2 False - go to branch 1.
2. Set COUT(i) equal to the outlet concentrations assumed by *Zspow*.
3. Call Intgr to calculate the exiting gas concentrations.
4. Set CINSP(i) equal to the exiting concentration from the previous stage.
5. Call Soldbal to calculate the change in solids concentrations on the stage.
6. Calculate Z(i), the inlet concentrations for the four main species.

7. Calculate  $F(i)$ , the difference between the calculated and the specified inlet concentrations.
8. Go to branch 2.
9. Branch 1: Set  $F(i) = 0.1$
10. Go to branch 2.
11. Branch 2: Return to Zspow, the calling program.

These steps are repeated by Zspow until  $F < 0.000001$  or the number of iterations exceeds 100.

## Subroutine Fgktau

### 1) Overview

**Purpose** - Subroutine Fgktau makes a first guess for KTAU in the prediction of limestone reactivity.

**Background** - The prediction of limestone reactivity requires an iteration on the variable KTAU to reach the specified utilization once the particle size distribution is known. Subroutine Fgktau makes a first guess for the value of KTAU based on an empirical correlation from reactivity data on 10 limestones. The correlation is given by:

$$KTAU = (1/NR) UD_{50}/D_{90}$$

where

$$NR = 1.148 \text{ Exp}(-5.116U),$$

U = Utilization, and

D<sub>50</sub> = 50% of all the particles in the limestone sample are smaller than this diameter.

D<sub>90</sub> = 90% of the particles are smaller than this diameter.

### 2) Usage

The calling sequence for Fgktau is

CALL FGKTAU(U,R9050,KTAU)

On entry

U = Utilization, and

R9050 = Ratio of D<sub>90</sub> to D<sub>50</sub>.

On return

KTAU = The estimate for variable KTAU.

### **3) Algorithmic Techniques**

There are no special algorithmic techniques in this subroutine.

### **4) Programming Details**

The calculation for the initial guess of KTAU is programmed in the following steps.

For a given utilization and R9050:

- 1) Calculate NR, the exponential term.
- 2) Calculate KTAU.
- 3) Return to the calling program.

## Subroutine Film

### 1) Overview

**Purpose** - Subroutine Film calculates the average film thickness around the limestone particles which are dissolving in a CSTR system.

**Background** - The use of a surface rate expression in the determination of limestone dissolution rates requires that an estimate of the film thickness is known. Film calculates the thickness for a given particle size distribution and the appropriate fractions remaining in each interval (See React documentation). The averaging factor for the film thickness is derived from the total dissolution rate given by

$$\text{Total rate} = V_T \sum \phi_i \frac{a_i}{V_{oi}} \frac{D \Delta C_i}{\delta_i} \quad (1)$$

The total rate can also be found in terms of an average film thickness and average concentration gradient as shown in Equation (2).

$$\text{Total rate} = \frac{D(\Delta C)_{ave}}{\delta_{ave}} \sum V_T \phi_i \frac{6f_i}{d_i} \quad (2)$$

The summation in this equation is the total area at any time in terms of the fraction remaining. Using Equations (1) and (2),  $\delta_{ave}$  can be found in terms of the individual film thicknesses and for a CSTR system is given by

$$\frac{1}{\delta_{ave}} = \frac{2 \sum \phi_i \int_0^1 IG(f_i) df_i}{\sum \phi_i d_{oi} \int_0^1 f_i^{1/3} IG(f_i) df_i} + 1.612B \quad (3)$$

In this equation the integrand function,  $IG(f_i)$ , is given by

$$IG(f_i) = \frac{e^{-(kt/k\tau)}}{-1 - B V_i^{1/3} f_i^{1/3}} \quad (4)$$

## 2) Usage

The calling sequence for Film is

CALL FILM(N,D,PHI,B,H,KTAU,V)

On entry

N = number of intervals in the particle size distribution,

D = an array containing the particle size diameters,

PHI = an array containing the initial particle size distribution,

B = the agitation enhancement factor,

H = the initial estimate for the integration step size,

KTAU = a factor indicative of utilization which was converged on in React, and

V = an array containing the initial volumes of all the particles in the distribution.

On return

DELAVE = the average film thickness which is returned through common block *RTIME*.

## 3) Algorithmic Details

There are no special algorithmic techniques in this subroutine.

## 4) Programming Details

The convergence for the average film thickness is calculated in the following steps using the value of KTAU converged on in React.

1. Branch 1: Initial variables for calculations.
2. Loop 1: Integrate size fraction, J, from  $f_j = 1$  to  $f_j = 0$ .
  - 2.1 Call Fmint to determine the film thickness at  $f_j = 1$ .
  - 2.2 Determine the integration step size, H.
  - 2.3 Loop 2: Call Fmint to determine the integrand of Equation (4) for three steps.
  - 2.4 Call Simp to evaluate the integral in the numerator of Equation (3).
  - 2.5 Call Simp to evaluate the integral in the denominator of Equation (3).
  - 2.6 Test for complete dissolution of the size fraction.



If  $f_j < 1.0e-15$ , go to branch 2.

If  $f_j > 1.0e-15$ , continue this loop.

2.7 Branch 2: Update numerator and denominator of Equation (3) to include this size fraction.

2.8 Test for  $J = N$

True - go to branch 3.

False - Continue loop 1.

3. Branch 3: Calculate FMAX, the final term in Equation (3).

4. Ratio the numerator and denominator terms to determine DELAVE, the average film thickness.

5. Return to the calling program.

## Subroutine Fint

### 1) Overview

**Purpose** - Subroutine Fint calculates the dissolution rate and the integrand which must be evaluated to calculate utilization.

**Background** - The calculation of limestone reactivity requires the integration over time of each particle size in the distribution with the bounds from  $t = 0$  to  $t = \tau$ , the appropriate residence time. However for most of the particles, complete dissolution occurs before the residence time criteria is met. Thus it becomes wiser to integrate over fraction-of-particle remaining from  $f_p = 1$  to  $f_p = 0$ . The resulting transformed integrand is given by

$$I = \frac{e^{-(kt/k\tau)}}{df_p/d(k\tau)} f_p \quad (1)$$

The denominator is the dissolution rate expression given by

$$\frac{df_p}{dt} = -\frac{kf_p^{1/3}}{V_p^{2/3}} - \frac{kBf_p^{2/3}}{V_p^{1/3}} \quad (2)$$

This equation can be integrated to give

$$kt = \frac{3}{B^2} \ln \left[ \frac{1 + BV_p^{1/3}f_p^{1/3}}{1 + BV_p^{1/3}} \right] + BV_p^{1/3} (1 - f_p^{1/3}) \quad (3)$$

Subroutine Fint evaluates these three expressions for each  $f_p$  assumed in subroutine React. (See React documentation.)

### 2) Usage

The calling sequence for subroutine Fint is

CALL FINT(F,VJ2,VJ3,B,KTAU,FJ)

On entry

F = the fraction-of-particle remaining,  $f_p$ ,

VJ2 =  $V_p^{1/3} f_p^{1/3}$  ( $V_p$  is the initial volume of the particle),

VJ3 =  $V_p^{2/3}$ ,

B = the mass transfer enhancement factor, and

KTAU =  $k\tau$ .

On return

FJ = the value of the integrand.

### 3) Algorithmic Techniques

There are no special algorithmic techniques in this subroutine.

### 4) Programming Details

The calculation of the integrand is programmed in the following steps.

1. If  $f_p < 0$ , set  $f_p = 0$ .
2. Raise  $f_p$  to the  $2/3$  power.
3. Raise  $f_p$  to the  $1/3$  power.
4. Evaluate equation (3).
5. Evaluate equation (2).
6. Evaluate the integrand, equation (1).
7. Return to calling program.

## Subroutine Fmint

### 1) Overview

Purpose - Subroutine Fmint calculates the value of the integrand needed to determine the average film thickness (See Film documentation).

Background - The integrand which is calculated in this subroutine is given by

$$IG(f_i) = \frac{e^{-(kt/kt)}}{-1-BV_i^{1/3}f_i^{1/3}} \quad (1)$$

This variable is calculated both alone (FN) and as a product with  $f_i^{1/3}$  (FD) to give both terms required for the average film thickness integrals.

The value of  $kt$  in the exponential is found using Equation (2) (See Fint documentation).

$$kt = \frac{3}{B^2} \ln \left[ \frac{1 + BV_p^{1/3}f_p^{1/3}}{1 + BV_p^{1/3}} \right] + BV_p^{1/3} (1-f_p^{1/3}) \quad (2)$$

### 2) Usage

The calling sequence for subroutine Fmint is

CALL FMINT(F,VJ2,B,KTAU,FD,FN)

On entry

F = the fraction-of-particle remaining,  $f_i$ ,

VJ2 =  $BV_i^{1/3}$ ,

B = agitation enhancement factor, and

KTAU = a factor indicative of utilization which was converged on in React.

On return

FN = the value of the integrand given by Equation (1), and

FD =  $f_i^{1/3}FN$ .

### 3) Algorithmic Techniques

There are no special algorithmic techniques in this subroutine.

#### 4) Programming Details

The values of the integrands are programmed in the following steps.

1. If  $f_i < 0$ , set  $f_i = 0$ .
2. Calculate  $f_i^{1/3}$ .
3. Calculate  $kt$  using Equation (2).
4. Calculate  $FN$  using Equation (1).
5. Calculate  $FD$  from the product of  $f_i^{1/3}FN$ .

## Subroutine Gktau

### 1) Overview

Purpose - Subroutine Gktau estimates the values of KTAU once a first guess has been made.

Background - The calculation of reactivity requires convergence on a specified utilization. The variable which is iterated on is KTAU. This variable is the product of the dissolution rate constant and the average residence in the vessel. Subroutine Gktau uses a bisection technique to iterate on this variable.

### 2) Usage

The calling sequence for Gktau is

CALL GKTAU(M,KTAU,DIFF,U,R9050)

On entry

M = A counter indicating the number of times Gktau has been called.

KTAU = The old estimate for rate constant times residence time.

DIFF = The difference between the specified utilization and the value of utilization calculated using the old estimate of KTAU.

U = The specified utilization.

R9050 = the ratio of  $D_{90}$  to  $D_{50}$ .

On return

KTAU = the new estimate for rate constant times residence time.

### 3) Algorithmic Techniques

Subroutine Gktau uses a bisection technique to iterate on KTAU. This technique is applied in two stages. When  $M = 1$  (indicating the first call to Gktau), the old estimate for KTAU contains the value calculated in subroutine Fgktau. To establish the bounds for KTAU a second end point is selected dependant on the value of DIFF. If  $DIFF > 0$ , the first end point (KTAU1) is set equal to KTAU and the second end

point (KTAU2) is set equal to 10 times the normalization ratio, NR ( $NR = U/R9050$ ). If  $DIFF < 0$ , KTAU1 is 10,000 times the normalization ratio and KTAU2 is set equal to KTAU. Then the new estimate for KTAU is found by halving the interval KTAU1-KTAU2. If  $M > 1$ , KTAU replaces an end point dependant on the value of DIFF and a new estimate is made.

#### 4) Programming Details

The iteration of KTAU is programmed in the following steps. For given step M

1. If  $M = 1$  go to branch 1.
2. Replace one end point.
  - 2.1 If  $DIFF > 0$ ,  $KTAU1 = KTAU$ .
  - 2.3 If  $DIFF < 0$ ,  $KTAU2 = KTAU$ .
3. Go to branch 2.
4. Branch 1: Establish two end points.
  - 4.1 If  $DIFF > 0$ ,  $KTAU2 = 10NR$  and  $KTAU1 = KTAU$ .
  - 4.2 If  $DIFF < 0$ ,  $KTAU1 = 10,000NR$  and  $KTAU2 = KTAU$ .
  - 4.3 Go to branch 2.
5. Branch 2: Estimate KTAU by halving the interval KTAU1-KTAU2.
6. Return to calling program.

## Subroutine Glmt

### 1) Overview

**Purpose** - Subroutine Glmt calculates the liquid phase interface concentrations from an assumed SO<sub>2</sub> driving force in the gas phase.

**Background** - The calculation of the gas/liquid mass transfer requires the concentrations of gas and liquid species at the interface. For CO<sub>2</sub> and O<sub>2</sub> the gas phase resistance is neglected, but not for SO<sub>2</sub>. Subroutine Conver assumes an SO<sub>2</sub> gas driving force and then calls Glmt to calculate the gas interface concentrations for given bulk gas concentration. Once the three gas concentrations are specified at the interface, the liquid concentrations can be calculated using Henry's constants.

The general expression for the flux of SO<sub>2</sub> is given by

$$\text{Flux SO}_2 = k_g(P_b - P_i) = \frac{k_l}{\sqrt{D_{\text{SO}_2}}} \{ \sum \sqrt{D_j} [\Delta \text{SO}_3^-]_j + \sum \sqrt{D_j} [\Delta \text{SO}_4^{2-}]_j \} \quad (1)$$

The sulfate flux is calculated by assuming that all the absorbed oxygen reacts instantaneously at the interface with sulfite. The total rate of oxygen absorption equals an enhancement factor times the rate from physical absorption. Once the [SO<sub>4</sub><sup>2-</sup>] flux is known, the concentration of [HSO<sub>3</sub><sup>-</sup>]<sub>i</sub> is solved for by rearranging equation (1) to give the quadratic equation

$$\frac{\sqrt{D_{\text{SO}_3}} K_2}{K_1 [\text{H}_2\text{SO}_3]_i} [\text{HSO}_3^-]_i^2 + \sqrt{D_{\text{HSO}_3}} [\text{HSO}_3^-]_i + C = 0 \quad (2)$$

where  $K_1, K_2$  = the first and second acid dissociation constants for H<sub>2</sub>SO<sub>3</sub>.

The constant C is given by

$$C = \sqrt{D_{\text{SO}_2}} [\text{H}_2\text{SO}_3]_i + \text{FLUXSO}_4 - \sum \sqrt{D_j} [C_j] - \frac{k_g}{k_l} \text{FLUX} \sqrt{D_{\text{SO}_2}} \quad (3)$$

where FLUX = the SO<sub>2</sub> gas phase driving force assumed in Conver,



$[H_2SO_3]_i$  = aqueous  $SO_2$  at the interface, and  
 $\sum \sqrt{D_j} [C_j]$  = the sum of sulfite species in the bulk liquid.

Once  $[HSO_3^-]_i$  is known,  $[H^+]_i$  is calculated using  $[H_2SO_3]_i$ . Concentration of other species are then calculated using equilibrium constants.

Since the argument of a quadratic cannot be negative, Glmt checks for a positive value. If the argument is negative, values are printed to aid debugging and the program execution is halted.

## 2) Usage

The calling Sequence for Glmt is  
 CALL GLMT(FLUX,DELCH)

On entry

FLUX = the assumed  $SO_2$  gas driving force.

Other required variables are accessed through common blocks. These variables (and their common blocks) are

HK(HENRYS) = an array of three containing Henry's constants,

BPP(PPRESS) = an array of three containing bulk partial pressures,

PHIY(INPUT2) = the oxygen enhancement factor,

RKLKG(PPRESS) = the ratio of gas-to-liquid mass transfer coefficients, and

SD(DIFF) = an array containing diffusivities.

On return

DELCH = the charge flux in the liquid interface boundary layer.

The interface liquid concentrations are returned through common block *INTERFACE*.

## 3) Algorithmic Details

There are no special algorithmic techniques in this subroutine.

#### 4) Programming Details

The concentration of species in the liquid phase at the interface are calculated in the following steps.

For an assumed gas driving force of  $\text{SO}_2$ ,

1. Calculate interface partial pressure of  $\text{SO}_2$ .
2. Calculate liquid phase concentrations (CGINT) of  $\text{SO}_2$ ,  $\text{CO}_2$ , and  $\text{O}_2$  using interface partial pressures and Henry's constants.
3. Calculate liquid driving force, FLUXSO2.
4. Calculate FLUXSO4 from the  $\text{O}_2$  flux.
5. Calculate term in quadratic, B24AC.
  - 5.1 If  $\text{B24AC} < 0$ , go to branch 1.
  - 5.2 If  $\text{B24AC} > 0$ , continue.
6. Solve quadratic for  $[\text{HSO}_3^-]_i$ .
7. Calculate  $[\text{H}^+]_i$  from  $[\text{HSO}_3^-]_i$  and  $\text{KH}_2\text{SO}_3$ .
8. Calculate concentrations of other species from equilibrium constants.
9. Calculate the flux of  $\text{CO}_2$ .
10. Calculate the total interface charge.
11. Calculate DELCH, the error in the charge flux.
12. Go to branch 2.
13. Branch 1: Print terms to aid debugging.
  - 13.1 Print quadratic terms, A and C.
  - 13.2 Print FLUXSO2, FLUXSO4, and sum of bulk concentrations, ALPH4.
  - 13.3 Stop program.
14. Branch 2: Return to calling program.

## Subroutine Gvar

### 1) Overview

**Purpose** - Subroutine Gvar calculates the log-gamma parameters,  $\beta$  and  $d_{100}$ , from two sieve measurements.

**Background** - The calculation of a complete particle size distribution requires the prediction of the log-gamma parameters. The integrated form of the cumulative log-gamma function is given by the following expression when  $\alpha = 4$ :

$$P(Y) = \frac{e^{-Y}Y^3}{3!} \left[ 1 + \frac{3}{Y} + \frac{6}{Y^2} + \frac{6}{Y^3} \right] \quad (1)$$

where the random variable,  $Y$ , is a function of the largest particle,  $d_{100}$ , and  $\beta$ .  $Y$  is given by

$$Y = \frac{3}{\beta} \ln \frac{d_{100}}{d} \quad (2)$$

### 2) Usage

The calling sequence for Gvar is

CALL GVAR(P1,P2,D1,D2,B,DMAX)

On entry

P1 = the cumulative weight fraction of particles less than D1,

P2 = the cumulative weight fraction of particles less than D2,

D1 = the sieve diameter for P1, and

D2 = the sieve diameter for P2.

On return

B = the log-gamma parameter  $\beta$ , and

DMAX = the largest particle size,  $d_{100}$ .

### 3) Algorithmic Techniques

There are no special algorithmic techniques in this subroutine.

### 4) Programming Details

Subroutine Gvar contains a database of 12 cumulative distributions from equation (1) and their corresponding random variables, Y. A linear relationship is assumed between any two consecutive points. With this database the calculation of the log-gamma parameters are programmed in the following steps.

1. For each weight fraction, P, compare P to the database to find the right and left bounds.
2. Call Bis to converge on the random variable Y1 for the weight fraction P1.
3. Call Bis to converge on the random variable Y2 for the weight fraction P2.
4. Using Y1 and Y2 find the log-gamma parameters from equation (2).
5. Test for reasonable answers: If  $D_{MAX} < 1680$ 
  - False - Print an error message and stop the program.
  - True - Continue
6. Return to the calling program.

## Subroutine Hcomp

### 1) Overview

**Purpose:** - Subroutine Hcomp determines the hold tank liquor composition based on assumed outlet concentration at each step in the IMSL routine Zspow.

**Background** - The calling statement for Hcomp is contained within the IMSL routine Zspow which was itself called from subroutine Holdt. Therefore Hcomp is called at each step of assumed outlet concentrations made by Zspow. Hcomp controls the calling sequence for all subroutines required to determine the solid, liquid, and gas concentrations. Hcomp treats the hold tank as an additional scrubber stage where conditions are such that SO<sub>2</sub> desorption is negligible.

Once Hcomp is called with a set of assumed outlet concentrations, liquid concentrations for 17 species are calculated by subroutine Equil. Hcomp then calls Listone and CaSO3dj to determine the fluxes of CaCO<sub>3</sub> and CaSO<sub>3</sub>. Next subroutine Soldbal is called to determine the crystallization/dissolution rates of CaCO<sub>3</sub>, CaSO<sub>3</sub>, CaSO<sub>4</sub> hemihydrate, and gypsum.

Hcomp determines the CO<sub>2</sub> and O<sub>2</sub> gas concentrations by assuming a log-mean driving force. For example the outlet partial pressure of O<sub>2</sub> is given by:

$$P_{O_2} = H_{O_2}[O_2] \left\{ 1 - \frac{1 - \frac{P_{O_2in}}{H_{O_2}[O_2]}}{\exp \left\{ \frac{N_1 L}{H_{O_2} G} \right\}} \right\} \quad (1)$$

where  $H_{O_2}$  = Henry's constant for oxygen, and

$[O_2]$  = the concentration of dissolved oxygen in the bulk liquid.

Since all the absorbed O<sub>2</sub> reacts with SO<sub>3</sub><sup>=</sup> to form SO<sub>4</sub><sup>=</sup> the O<sub>2</sub> partial pressure must be converged on using two equations. Hcomp calls an IMSL routine Zfalse to find the O<sub>2</sub> partial pressure. Zfalse finds the concentration which gives the zero of function Delin. DELIN (the variable in the function Delin) is the difference between the

O<sub>2</sub> absorbed based on the log-mean driving force expression and the O<sub>2</sub> absorbed based on a material balance for SO<sub>4</sub><sup>=</sup>.

Once outlet gas concentrations are known Hcomp calculates the inlet liquor concentrations. These values are compared to outlet concentrations from the scrubber by Zspow and convergence is reached when the difference between the calculated inlet concentrations and the specified scrubber outlets are less than 0.0001. Hcomp then returns output values to Holdt.

## 2) Usage

The calling sequence for Hcomp is contained within Zspow. Hcomp is the first variable in Zspow's argument list and is declared external in subroutine Holdt. Three variables are passed to Hcomp from Zspow and one variable is returned. These variables are:

On entry

X = an array containing the assumed outlet concentrations,

N = 4, the size of the F and X arrays, and

PAR = a dummy parameter not used.

Other required variables are accessed through common blocks. These variables (and their common blocks) are

L/G(TANKPAR) = the ratio of liquid to gas flowrates in the hold tank,

N<sub>l</sub>(TANKPAR) = the number of liquid phase transfer units in the hold tank,

DSOLID(CC3) = an array of four containing the changes in solids concentrations,

HK(HENRYS) = an array of three containing Henry's constants,

PIN(HTPRINT) = an array of two containing gas partial pressures into the hold tank,

CO2(BULKSP) = the concentration of dissolved CO<sub>2</sub> in the bulk liquid, and

SKSP1 and KSPSO4(EQUKSP) = the pseudo-solubility products for calcium sulfite and gypsum, respectively.

On return

F = an array containing the difference between the calculated hold tank inlet concentrations and the specified concentrations (equivalent to the scrubber outlet).

Other required output variables are accessed through common blocks. These variables (and their common blocks) are

$POUT(HTPRINT)$  = an array of two containing outlet gas partial pressures, and  
 $RSCASO3, RSCASO4(HTPRINT)$  = the relative saturations of  $CaSO_3$  and  $CaSO_4$ .

### 3) Algorithmic Details

Subroutine Hcomp uses the IMSL routine Zfalse to converge on the  $O_2$  partial pressure leaving the hold tank. This routine uses a regula falsi method which requires the right(XR) and left(XL) bounds for the  $O_2$  pressure.

The calling sequence for Zfalse is

CALL ZFALSE(DELIN, EPS, NSIG, XL, XR, XAPP, ITMAX, IER)

On entry

XL =  $0.3P_{O_2}(\text{in})$ , atm,

XR =  $P_{O_2}(\text{in})/1.00001$ , atm,

EPS = 0.0001, convergence criterion,

NSIG = 4, convergence criterion for number of significant digits,

Delin = the externally declared function for which the zero is to be found, and

ITMAX = 200, maximum number of iterations.

On return

XAPP = the partial pressure of  $O_2$  which gave a zero root to DELIN, and

IER = an error parameter if convergence is not reached.

### 4) Programming Details

The inlet liquor concentrations are calculated in the following steps.

For assumed outlet total concentrations

1. Set right (XR) and left (XL) bounds for the hold tank pH.
2. Call Equil to determine pH and liquid concentrations for 17 species.
3. Call Listone to calculate  $CaCO_3$  flux.

4. Call CaSO3di to calculate  $\text{CaSO}_3$  flux.
5. Calculate  $\text{RCASO}_4$  and  $\text{RCASO}_3$ , the relative saturations of gypsum and  $\text{CaSO}_3$  respectively.
6. Call Soldbal to determine dissolution/crystallization rates for solids.
7. Using a log-mean driving force, calculate  $\text{POUT}(1)$ , the outlet gas concentration of  $\text{CO}_2$ .
8. Set right (XR) and left (XL) bounds for  $\text{O}_2$  gas concentration.
9. Branch to Zfalse to converge on the outlet  $\text{O}_2$ .

(In function Delin)

- 9.1 Calculate  $[\text{SO}_4^=]_{\text{bulk}}$  using assumed outlet and the change in solids concentration.
- 9.2 Calculate  $\text{O}_2$  absorbed.
- 9.3 Calculate CIN, the  $[\text{SO}_4^=]$  inlet concentration from  $[\text{SO}_4^=]$  material balance.
- 9.4 Calculate the  $\text{O}_2$  absorbed using the log-mean driving force.
- 9.5 Calculate COLD, the  $[\text{SO}_4^=]$  inlet concentration from the  $\text{O}_2$  absorbed.
- 9.6 Calculate  $\text{DELIN} = \text{CIN} - \text{COLD}$ .
- 9.7 Continue until  $\text{DELIN} < 0.0001$  or the number of iterations exceeds 200.
10. Calculate  $\text{CIN}(I)$ , the inlet liquor concentrations for the four main species.
11. Calculate  $F(I)$ , the difference between calculated and specified inlet liquor concentrations for  $[\text{SO}_3^=]$ ,  $[\text{CO}_3^=]$ ,  $[\text{SO}_4^=]$ , and  $[\text{Ca}^{++}]$ .
12. Return to Zspow, the calling program.

These steps are repeated by Zspow until  $F < 0.000001$  or the number of iterations exceeds 50.



## Subroutine Holdt

### 1) Overview

Purpose - Subroutine Holdt is the driver subroutine for the hold tank.

Background - Subroutine Holdt assumes a hold tank liquor outlet concentration equal to the scrubber inlet and then calls the IMSL routine Zspow where the inlet concentrations are converged on to match the exit conditions from the scrubber. Zspow requires an external subroutine, Hcomp, to contain the four convergence equations. (See Hcomp documentation.) These equations use non-linear material balance expressions for each of the four species,  $\text{SO}_3^-$ ,  $\text{CO}_3^-$ ,  $\text{SO}_4^-$ , and  $\text{Ca}^{++}$ . In a general form these balances are

$$\text{Input} = \text{Output} + \text{Absorbed} + \text{Dissolved} - \text{Desorbed} - \text{Crystallized} \quad (1)$$

For example, since limestone dissolves in the hold tank, the  $\text{CO}_3^-$  balance becomes

$$[\text{CO}_3^-]_{\text{in}} = [\text{CO}_3^-]_{\text{out}} + (\text{PCO}_{2,(\text{out})} - \text{PCO}_{2,(\text{in})}) / (\text{L/G}) - (\text{DAC})_{\text{CaCO}_3} K_{\text{CaCO}_3} \quad (2)$$

where

$K_{\text{CaCO}_3}$  = the limestone reactivity in the hold tank,

$\text{DAC}$  = the flux driving force for the limestone particles, and

$\text{L/G}$  = the ratio of liquid to gas flowrates in the hold tank.

The second term in equation (2) accounts for absorption or desorption of  $\text{CO}_2$ .

Once Zspow converges on the inlet liquor concentrations these values as well as other liquid and solid concentrations are printed to the output file. Finally Holdt updates solid's concentrations for the inlet to the scrubber.

## 2) Usage

The calling sequence for Holdt is

Call Holdt

On entry

All required variables are accessed through common blocks. These variables (and their common blocks) are

RLG2(*TANKPAR*) = ratio of liquid to gas flowrates,

BULK(C(*BULKSP*)) = an array of sixteen containing the individual species concentrations in the hold tank,

RSO3SO4(*DIFLUX*) = the ratio of calcium sulfate to calcium sulfite in the hemihydrate solid,

GAM(*GAMMA*) = activity coefficients,

RSCASO3, RSCASO4(*HTPRINT*) = the relative saturations of calcium sulfite and gypsum

PIN(*HTPRINT*) = gas phase inlet partial pressures of CO<sub>2</sub> and O<sub>2</sub>, and

SOLID(*CC3*) = an array of four containing outlet solids concentrations of CaSO<sub>4</sub>, CaSO<sub>3</sub>, CaCO<sub>3</sub>, and gypsum.

Also accessed through common block *LSURF* are the concentrations of species at the limestone surface.

On return

All required variables are returned through common blocks. These variables (and their common blocks) are

SOLIDIN and SOLIDSP(*CC3*) = an array of four containing the solids concentrations of CaSO<sub>3</sub>, CaCO<sub>3</sub>, CaSO<sub>4</sub>, and gypsum into the scrubber, and

HOUT(*HOLDIN*) = an array of four containing the converged total concentrations.

### 3) Algorithmic Techniques

Subroutine Holdt calls an IMSL routine, Zspow, to converge on the four non-linear material balance equations. This routine uses a modified Powell method to search for the zeros of four equations:

$$F(I) = CIN(I) - CINH(I)$$

where

$CIN(I)$  = the inlet concentration of species  $i$  calculated from the non-linear material balance, and

$CINH(I)$  = the specified inlet concentration which equals the exit concentration from the scrubber.

The calling sequence for Zspow is

CALL ZSPOW(HCOMP,NSIG,N,ITMAX,PAR,X,FNORM,WR,IER)

On entry

Hcomp = the externally declared subroutine containing the equations to be zeroed,

NSIG = 6, a convergence criteria,

N = 4, the number of equations to be solved,

ITMAX = 50, the limit of the number of iterations to be made, and

X = the initial guess for the outlet concentrations.

On return

X = the converged outlet concentrations.

### 4) Programming Details

The hold tank calculations are programmed in the following steps:

1. Set  $X(i)$  equal to the scrubber inlet concentrations.
2. Set  $CINH(i)$  equal to the scrubber outlet concentrations.
3. Call Zspow to calculate the inlet liquor concentrations.
4. Print hold tank concentrations of gas, solids, and liquids to output file.

5. Calculate OXID, the percent of oxidized sulfite from the values of gypsum and calcium sulfate hemihydrate solids concentrations.
6. Calculate the percent oxidation from an  $O_2$  balance.
7. Calculate DELSOL - the difference between the two percent oxidation values.
8. Update solids balance for the scrubber inlet.
  - 8.1 If relative saturation of  $CaSO_4 > 1$ :
    - 8.1.1 Calculate the ratio of sulfate hemihydrate solids to sulfite solids.
    - 8.1.2 Set scrubber inlet solids equal to hold tank solids.
  - 8.2 If relative saturation of  $CaSO_4 < 1$ :
    - 8.2.1 Calculate the dilution factor from addition of water in the limestone slurry.
    - 8.2.2 Calculate the scrubber inlet sulfur solids from the dilution correction.
9. Print scrubber inlet solids concentrations to output file.
10. Return to calling program.

## Subroutine Intgr

### 1) Overview

**Purpose** - Subroutine Intgr determines the changes in gas concentrations of SO<sub>2</sub>, CO<sub>2</sub>, and O<sub>2</sub> across a stage.

**Background** - The scrubber model treats the change in gas concentration as a plug-flow regime. This approach requires the integration of three differential equations given by:

$$\frac{dP_i}{dN_g} = \frac{k_i^0(\sum \sqrt{D_j} \Delta[j])_i}{k_g \sqrt{D_{SO_2}}} \quad (1)$$

where  $i = \text{SO}_2, \text{CO}_2, \text{and O}_2$

$k_l / k_g$  = ratio of mass transfer coefficients,

$N_g$  = number of gas phase transfer units, and

$D$  = diffusivity.

Subroutine Intgr calls LSODE (or DGEAR) an ordinary differential equation solver to integrate the gas concentrations across the stage.

### 2) Usage

The calling sequence for Intgr is

Call Intgr(COUT,NFLAG2)

On entry

NFLAG2 < 12 scrubber operates countercurrently,

= 12 scrubber operates cocurrently, and

COUT = the assumed liquid concentration on the stage.

Other required variables are accessed through common blocks. These variables (and their common blocks) are

BPPI(*PPRESS*) = an array containing the three gas phase partial pressures, and  
 NTSUP(*INPUTSP*) = the number of transfer units per stage.

On return

The inlet gas concentrations (*CY*) are returned through common block *SINGLE*.

### 3) Algorithmic Details

Subroutine *Intgr* uses an ordinary differential equation solver, *LSODE* (or *DGEAR*), to converge on the gas inlet partial pressures. This routine requires an external subroutine (*Fgint*) to contain the differential equations. A discussion of the algorithmic technique for *LSODE* (or *DGEAR*) is not included in this documentation.

### 4) Programming Details

Gas phase concentrations are calculated in the following steps.

For an assumed liquor concentration:

1. Set right (*XR*) and left (*XL*) bounds for pH.
2. Call *Equil* to converge on pH and to calculate the concentration of all 17 species.
3. Call *Listone* to calculate the flux of dissolving limestone.
4. Call *Conver* to set initial bounds for gas flux.
5. Call *CaSO3di* to calculate the flux of dissolving calcium sulfite.
6. Set values for *LSODE* (or *DGEAR*).
7. Call *LSODE* (or *DGEAR*) to converge on the inlet gas concentrations.
  - 7.1 In *Fgint*: Call *Conver* to calculate SO<sub>2</sub> gas flux.
  - 7.2 Integrate gas concentrations for SO<sub>2</sub>, CO<sub>2</sub>, and O<sub>2</sub>.
8. Return to calling program.

### Subroutine Limreac

#### 1) Overview

**Purpose** - Subroutine Limreac calculates the limestone reactivity as needed SSMFGD.

**Background** - In slurry scrubber systems, the liquid recirculation rate is large relative to the limestone feed rate, therefore the hold tank and each stage on the scrubber can be treated as a CSTR for limestone dissolution. Using this approach the rate of change of calcium concentration from limestone dissolution is given by

$$\frac{dCa}{dt} = \frac{C_s U}{\tau} \quad (1)$$

where  $C_s$  = the limestone solids concentration at the inlet,  
 $U$  = utilization, and  
 $\tau$  = residence time.

This can be rewritten in terms of the flux driving force to give

$$\frac{dCa}{dt} = \frac{U}{k\tau \sum D_j \Delta[CO_2]_j} C_s \sum D_j \Delta[CO_2]_j \quad (2)$$

where  $K$  = the dissolution rate constant, and  
 $[CO_2]_j$  = the carbonate species,  $[CO_3^{2-}]$  and  $[HCO_3^-]$ .

From the dissolution rate of a single spherical particle of limestone it can be easily shown that the second term of equation (2) is a constant given by

$$\frac{k}{\sum D_j \Delta[CO_2]_j} = \frac{3.63\pi^{2/3}}{\rho} \quad (3)$$

where  $\rho$  is the limestone molar density.

Using this constant and integrating equation (2) over the residence time yields

$$\Delta C_a = K' \tau C_{CaCO_3} \sum D_j \Delta [CO_2]_j \quad (4)$$

and the constant  $K'$  is given by

$$K' = \frac{U}{k\tau \rho C_s (1-U)} \frac{3.63\pi^{2/3}}{\quad} \quad (5)$$

where  $k\tau = KTAU$ , the variable converged on in subroutine Reac.

To account for the changes in the amount of utilization at each stage, the reactivity parameter is normalized to the initial limestone solids concentration. Then the reactivity at each stage is found by multiplying the reactivity parameter by the concentration of the limestone solids on that stage,  $C_{CaCO_3}$ .

## 2) Usage

The calling sequence for subroutine Limreac is

CALL LIMREAC(U,KTAU)

On entry

U = utilization, and

KTAU = the product of dissolution rate constant times residence time.

Other required variables are accessed through common blocks. These variables (and their common blocks) are

TAUSC, TAUHT(RTIME) = the residence time per stage in the scrubber and hold tank.

Also accessed through comon block *INPUT2* are the dissolution constants for calcium sulfite and gypsum in the scrubber. Crystallization constants for calcium sulfite and gypsum in the hold tank are accessed through *TANKPAR*.

On return



All variables are returned through common blocks. These variables (and their common blocks) are

$XKSP(3,1)(INPUT2)$  = the limestone reactivity parameter in the scrubber,

$XKSP(3,2)(INPUT2)$  = the limestone reactivity parameter in the hold tank,

$XKSP(1,2)(INPUT2)$  = the calcium sulfite dissolution parameter for the hold tank,

$XKSP(2,2)(INPUT2)$  = the gypsum dissolution parameter for the hold tank,

$CXKSP(1,1)(TANKPAR)$  = the crystallization parameter for calcium sulfite in the scrubber, and

$CXKSP(2,1)(TANKPAR)$  = the crystallization parameter for gypsum in the scrubber.

### 3) Algorithmic Techniques

There are no special algorithmic techniques in this subroutine.

### 4) Programming Details

The calculation of reactivity parameters is programmed in the following step.  
For converged KTAU

1. Calculate the constant, equation (3).
2. Calculate reactivity parameter for the scrubber, equation (6).
3. Calculate reactivity parameter for the hold tank.
4. Calculate calcium sulfite and gypsum reactivity parameters for the hold tank using the input values for the scrubber and the residence time ratio.
5. Calculate crystallization parameters for calcium sulfite and gypsum for the scrubber using the input values for the hold tank and the residence time ratio.
6. Return to the calling program.

## Subroutine Listone

### 1) Overview

Purpose - Subroutine Listone calculates the flux of dissolving calcite.

Background - Since the slurry liquor contains limestone solids recycled from the hold tank, the dissolution rate of limestone must be calculated. Subroutine Listone establishes the flux of calcium and carbonate at the solid surface using film theory approximation in the boundary layer. The subroutine assumes a concentration of  $[H^+]$  at the surface. Subroutine Surcone is then called to solve for species concentrations using equilibrium and flux expressions. These values are returned to Listone to test for convergence with the appropriate boundary condition.

### 2) Usage

The calling sequence for Listone is

Call Listone(IFLAG)

On entry

IFLAG = 1, select boundary condition from two choices,  
2, use  $K_{sp}$  of limestone as boundary condition.

Other necessary variables are accessed through common blocks. These variables (and their common blocks) are diffusivities(*DIFF*) and pseudo-concentrations(*SCONC* and *SCONCI*).

On return variables are returned through common blocks. These variables (and their common blocks) are:

FLUXCA (*DIFLUX*) = calcium flux

SFCA,SFCO3,SFSO3,BC (*LSURF*) = surface concentrations of  $[Ca^{++}]$ ,  $[CO_3^{=}]$ , and  $[SO_3^{=}]$ , respectively, and the boundary condition converged on.

### 3) Algorithmic Details

Listone uses a bisection technique on the concentration of  $[H^+]$  to reach convergence with the boundary condition, BC. The boundary condition is either the solubility product of calcite or the continuity of flux at the solis surface. (See Surcone documentation.) The convergence technique is used in two loops.

In the first loop the concentration of  $[H^+]$  at the surface is initially set equal to the bulk concentration. Subroutine Surcone is then called to calculate the concentration of the other species at the surface and to estimate the boundary condition. (The boundary condition which is must be matched depends on the bulk solution conditions. In the presence of sulfite the boundary conditon is the dissolution rate determined by the surface kinetic rate. In the absence of sulfite, the boundary condition is the solubility constant for calcite.) Control then returns to Listone where the calculated surface condition PBC, is compared to the boundary condition. Dependent on the bulk conditions, PBC is either the limestone flux, or the product  $[Ca]_s[CO_3]_s$ . When this value is greater than the boundary condition control falls to the second loop.

In the second loop  $[H^+]$  estimates are bounded between the end point concentrations, H1 and H2, found in loop one which gave PBC on both sides of the boundary condition. As this interval is halved, Surcone is called and a new end point is retained at each step. Convergence is reached when one of the following criteria are met:

- (1)  $|PBC - BC|/|BC| < 0.000001$ , or
- (2)  $|H2 - H1|/|H2| < 0.000001$ .

An additional restriction in Listone is that if the number of iterations in either loop exceeds 30, computation stops and an error message is printed.

### 4) Programming Details

The flux of dissolving limestone is calculated in the following steps:

1. Calculate  $\sum D_i C_i$  in the bulk liquid.
  - 1.1 For all sulfite species,  $SO_3T$ .
  - 1.2 For all acid species,  $AT$ .
  - 1.3 For all sulfate species,  $SO_4T$ .

- 1.4 For calcium and carbonate,  $\text{CaCO}_3\text{T}$ .
2. Calculate  $\sum Z_i D_i C_i$ , the total charge in the bulk liquid.
3. Set  $[\text{H}^+] = [\text{H}^+]_{\text{bulk}}$ .
4. Loop 1 : Call Surcone and return.
  - 4.1 Compare PBC to boundary condition, BC.
    - If  $\text{PBC} < \text{BC}$ , set  $[\text{H}^+] = 0.5[\text{H}^+]_{\text{old}}$
    - If  $\text{PBC} > \text{BC}$ , go to branch 2.
  - 4.2 Compare iteration number to limit: if  $N = 30$  go to branch 3.
  - 4.3 Continue this loop.
5. Branch 2 :  $\text{H1} = [\text{H}^+]_{\text{old}}$ .
6.  $\text{H2} = 2[\text{H}^+]_{\text{old}}$ .
7. Loop 2 :  $[\text{H}^+]_{\text{new}} = 0.5(\text{H1} + \text{H2})$ .
  - 7.1 Call Surcone and return.
  - 7.2 Compare iteration number to limit: if  $L = 30$  go to branch 3.
  - 7.3 Compare PBC to  $K_{\text{sp}}$ .
    - 7.3.1 If  $\text{PBC} < \text{BC}$ ,  $\text{H2} = [\text{H}^+]_{\text{new}}$ .
    - 7.3.2 If  $\text{PBC} > \text{BC}$ ,  $\text{H1} = [\text{H}^+]_{\text{new}}$ .
  - 7.4 Test for convergence.
    - 7.4.1 If  $|\text{PBC} - \text{BC}| / |\text{BC}| < 0.000001$  go to branch 4.
    - 7.4.2 If  $|\text{H2} - \text{H1}| / |\text{H1}| < 0.000001$  go to branch 4.
  - 7.5 Continue this loop.
8. Branch 3 : Print error message, "Convergence failed".
  - 8.1 Return to calling program.
9. Branch 4 : Calculate FLUXCA, the flux of dissolving calcium.
10. Store surface concentrations for output.
11. Return to calling program.

## Subroutine Pseudo

### 1) Overview

**Purpose** - Subroutine Pseudo calculates the pseudo-concentrations of  $[Ca^{++}]$ ,  $[HCO_3^-]$ ,  $[CO_3^{=}]$ ,  $[SO_4^{=}]$ ,  $[SO_3^{=}]$ ,  $[Ad^{=}]$ , and  $[OH^-]$ . Pseudo also calculates diffusivities and pseudo-equilibrium constants with the pseudo-concentrations.

**Background** - The slurry scrubber model uses the Bechtel Modified Radian Equilibrium Program, BMREP, to calculate the activity coefficients, equilibrium constants, and equilibrium concentrations of the inlet liquor. These calculations result in 41 species in the solution. In order to simplify the scrubber calculations, subroutine Pseudo establishes pseudo-concentrations which combine ion pairs of a specie with that specie. Thus, for example,

$$[HCO_3^-](pseudo) = [HCO_3^-] + [CaHCO_3^+] + [MgHCO_3^+]$$

Thus subroutine Pseudo is able to reduce the number of species for the scrubber to 17.

Pseudo also calculates the diffusivities of all 41 species and then uses these to define pseudo-diffusivities. For example,

$$D_{SO_3}(simplified) = \Sigma D_j[j] / \Sigma [j]$$

where  $j = SO_3^{=}$ ,  $CaSO_3^0$ , and  $MgSO_3^0$ .

For gas/liquid mass transfer, the simplified diffusivity is calculated using the weighted average of the square roots.

Three bisulfite equilibrium constants not considered in BMREP are also included in Pseudo. These constants are

$$K_{CaHSO_3} = 0.073$$

$$K_{MgHSO_3} = 0.15$$

$$K_{NaHSO_3} = 2.53$$

These constants are used to find the ion pair concentrations of  $[\text{CaHSO}_3]$ ,  $[\text{MgHSO}_3]$ , and  $[\text{NaHSO}_3]$ . Finally subroutine Pseudo uses the pseudo-concentrations to calculate the pseudo-equilibrium constants.

## 2) Usage

The calling sequence for Pseudo is

Call Pseudo(X,TK,LDIF)

On entry

X = an array containing the concentrations of the 41 species from BMREP,

TK = the temperature,

LDIF = 1, calculate pseudo-diffusivity using diffusivity to the first power,

2, calculate pseudo-diffusivity using diffusivity to the 1/2 power.

On return

All calculated variables are returned through common blocks. These variables (and their common blocks) are:

SD(DIFF) = an array containing diffusivities.

SKSP1, KSPSO4(EQUKSP) = pseudo-solubility constant for calcium sulfite and gypsum, respectively,

KW,KHSO4,KHCO3,KHSO3(EQUILK) = pseudo-equilibrium constants for water, bisulfate, bicarbonate, and bisulfite, respectively.

KAD,K3(EQUILK) = pseudo-equilibrium constants for  $\text{H}_2\text{Ad}$  and  $\text{H}_2\text{CO}_3$ .

K10,K11(EQUILK) = pseudo-equilibrium constants for ion pairs  $\text{CaCO}_3$  and  $\text{CaSO}_3$ .

SKSP(EQUILK) = pseudo-solubility constant for limestone.

BSO2T,BCO2T,BSO4T(BTOT) = total bulk pseudo-concentrations for  $[\text{SO}_3^-]$ ,  $[\text{CO}_3^-]$ , and  $[\text{SO}_4^-]$ .

BH2AT,BCAT,BCLT(BTOT) = total bulk pseudo-concentrations for  $[\text{H}_2\text{Ad}]$ ,  $[\text{Ca}^{++}]$ , and  $[\text{Cl}^-]$ .

Total bulk pseudo-concentrations are also returned through common block *BULK1*. Individual pseudo-concentrations are returned through *SCONC*, *SCONC1*, and *CATION*.

### 3) Algorithmic Details

There are no special algorithmic techniques in this routine.

### 4) Programming Details

The pseudo-constants are calculated in the following steps:

1. Calculate the viscosity of the solution using TK.
2. Calculate diffusivities of all 41 species.
3. Using the added bisulfite equilibrium constants, find the concentrations of their associated ion pairs.
4. Calculate the pseudo-concentration of the 17 SSMFGD species. (SCCA, SCHCO<sub>3</sub>, SCSO<sub>3</sub>, SCSO<sub>4</sub>, SCAD, SCOH, SCH, SCH<sub>2</sub>A, SCHA, SCHSO<sub>4</sub>, SCNA, SCMG, SCSO<sub>2</sub>, SCCO<sub>2</sub>, SCCL, SCCO<sub>3</sub>, and SCHSO<sub>3</sub>).
5. Calculate the pseudo-equilibrium constants from the pseudo-concentrations.
6. Calculate temperature-dependant Henry's constants for CO<sub>2</sub>, SO<sub>2</sub>, and O<sub>2</sub> {HK(1), HK(2), and HK(3), respectively}.
7. Calculate relative saturations of calcium sulfite, gypsum, and limestone (RS1, RS2, and RS3).
8. Return to the calling program.

## Subroutine React

### 1) Overview

**Purpose** - Subroutine React is the driver routine for the prediction of limestone reactivity from utilization and a particle size distribution.

**Background** - The dissolution of limestone in SSMFGD is calculated using the driving force for dissolution ( $D \Delta C$ ) and a reactivity parameter,  $K_{CaCO_3}$ . This parameter is related to the utilization ( $U$ ) and particle size distribution of the limestone as well as the residence time in the scrubber or hold tank. Subroutine React is the driver routine for the prediction of reactivity from these input variables.

The calculation of reactivity begins with an expression for the rate of dissolution of a single particle in terms of  $f_p$ , the fraction of undissolved limestone of initial size  $p$ . This expression for a batch process is given by

$$\frac{df_p}{dt} = -\frac{kf_p^{1/3}}{V_p^{2/3}} - \frac{kBf_p^{2/3}}{V_p^{1/3}} \quad (1)$$

where

$k$  = the dissolution rate constant,

$V_p$  = the volume, and

$B$  = mass transfer enhancement factor from agitation.

This equation and its integrated form are evaluated in subroutine Fint which is called by React.

In order to calculate the total undissolved limestone in a scrubber system, the batch time is transformed to CSTR time. Application of the CSTR process is possible because the liquid recirculation rate is large relative to the limestone feed rate. Thus the total undissolved limestone ( $F_c$ ) is found by integrating each size fraction over all possible times and then summing over all size fractions.  $F_c$  is given by



$$F_c = \sum \phi_p \frac{1}{k\tau} \int \frac{e^{-(kt/k\tau)}}{df_p/d(k\tau)} f_p df_p \quad (2)$$

where  $F_c = 1 - U$

The integral is evaluated by subroutine Simp which is called by React.

As shown by equation (2),  $F_c$  is a function of  $k\tau$  (KTAU). As the driver routine subroutine React assumes a value of KTAU, calls the required subroutines to evaluate the integral, and then checks for convergence with the specified utilization. Once KTAU is known the reactivity parameters are calculated for the specified residence times.

## 2) Usage

The calling sequence for subroutine React is

CALL REACT(U,N,PHI,LA,B1)

On entry

U = utilization,

N = number of intervals in the particle size distribution,

PHI = an array of size N containing the particle size distribution,

LA = a flag indicating whether the particle size distribution is given or should be predicted from seive data, and

B1 = the mass transfer enhancement factor from agitation.

On return

The reactivity parameters are returned through common block *INPUT2*. These parameters are

XKSP(3,1) = the limestone reactivity parameter for the scrubber, and

XKSP(3,2) = the reactivity parameter for the hold tank.

## 3) Algorithmic Techniques

Subroutine React contains no special algorithmic techniques. However convergence on KTAU is done using a bisection technique which is contained in subroutine Gktau.

#### 4) Programming Details

The prediction of limestone reactivity is programmed in the following steps. For specified U, residence times, and some particle size information

1. Test flag for prediction of particle size distribution.
  - 1.1 If  $LA = 1$ , go to branch 1.
  - 1.2 Call Gvar to calculate log gamma parameters.
  - 1.3 Call Dist to calculate complete particle size distribution.
2. Branch 1: Initialize variables for calculations.
3. For each particle size calculate volume (V),  $V^{1/3}$ , and  $V^{2/3}$ .
4. Calculate the ratio, R9050.
5. Call Fgkatu for a first estimate of KTAU using R9050.
6. Loop 1 : Convergence loop on KTAU.
  - 6.1 Initialize values for integrand.
  - 6.2 Loop 2 : Integrate size fraction, J, from  $f_p = 1$  to  $f_p = 0$ .
    - 6.2.1 Call Fint to evaluate integrand for 3 steps.
    - 6.2.2 Call Simp to evaluate the integral.
    - 6.2.3 Determine if function values are close enough to increase step size.
    - 6.2.4 Store solution to integral (SUM).
    - 6.2.5 Test for complete dissolution of size fraction:
      - If integrand  $< 1.0E-6$ , go to branch 2
      - If  $f_p > 0.015$ , continue this loop.
  - 6.3 Branch 2 : Update  $F_c$  to include this size fraction.
  - 6.4 Test for  $J=N$ 
    - 6.4.1 True - go to branch 3.
    - 6.4.2 False - Update to next size and restart loop 2.
7. Branch 3: Check for convergence against specified utilization.
  - 7.1 True - go to branch 4.
  - 7.2 False - continue.
8. Call Gktau for new estimate of KTAU and restart loop 1.
9. Branch 4 : Call Film to determine average film thickness.

11. Call Limreac to predict reactivities as need by scrubber model.
12. Print utilization and reactivity parameters to the output file.
13. Return to calling program.

## Subroutine Scrint

### 1) Overview

**Purpose** - Subroutine Scrint is the driver routine for convergence of the overall scrubber/hold tank loop of SSMFGD.

**Background** - SSMFGD calculates slurry scrubber performance by using a closed-loop operation between the scrubber and hold tank. Overall convergence is reached by passing several times through both scrubber and hold tank until two consecutive hold tank outlet concentrations (which become the scrubber inlet concentrations) are within a relative error bound. The overall driver routine for this convergence is subroutine Scrint. This subroutine also tests for convergence in the scrubber between predicted SO<sub>2</sub> inlet partial pressure and specified inlet partial pressure. If the relative error between these values is greater than 1%, a new outlet partial pressure is assumed using

$$P_{\text{SO}_2(\text{out})\text{new}} = \frac{P_{\text{SO}_2(\text{out})\text{old}} - P_{\text{SO}_2(\text{in})\text{spec}}}{P_{\text{SO}_2(\text{in})\text{calc}}} \quad (1)$$

Inlet scrubber liquid concentrations are reinitialized to their original values (equal to hold tank outlet concentrations) and subroutine Conopt is called to calculate scrubber performance.

When convergence of equation (1) is reached, Scrint sets scrubber outlet concentrations equal to hold tank inlet concentrations and then calls Holdt to calculate hold tank performance. Scrint then tests for overall convergence by

$$\left| \frac{[C_i]_{\text{new}} - [C_i]_{\text{old}}}{[C_i]_{\text{old}}} \right| < \text{DELT} \quad (2)$$

where  $i = \text{SO}_3^=, \text{CO}_3^=, \text{SO}_4^=, \text{and Ca}^{++}$ . DELT is the relative error which depends on the specie. For CO<sub>3</sub><sup>=</sup> and Ca<sup>++</sup> this error is 1% and 10% respectively.

## 2) Usage

The calling sequence for Scrint is

CALL SCRINT(NFLAG,NFLAG2)

On entry

NFLAG = a flag indicating a single or multistage scrubber, and

NFLAG2 = a flag indicating cocurrent or countercurrent contacting.

Other required variables are accessed through common blocks. These variables (and their common blocks) are

FSP(*INPUTSP*) = the inlet SO<sub>2</sub> partial pressure,

NTSUP(*INPUTSP*) = the number of gas phase transfer units per stage.

RLG(*INPUT2*) = the ratio of liquid to gas flowrates in the scrubber,

CY(*SINGLE*) = an array of three containing inlet gas partial pressures (from Intgr),

SOLIDIN(*CC3*) = an array of four containing inlet solids concentrations,

BSO2TI(*BULK1*) = total inlet SO<sub>3</sub>=concentration from Holdt,

BCO2TI(*BULK1*) = total inlet CO<sub>3</sub>= concentration from Holdt,

BSO4TI(*BULK1*) = total inlet SO<sub>4</sub>= concentration from Holdt,

BCATI(*BULK1*) = total inlet Ca<sup>++</sup> concentration from Holdt, and

HOUT(*HOLDIN*) = an array of four containing converged outlet liquor concentrations from Holdt.

On return

No variables are returned to the calling program however some variables are sent from Scrint to other routines through common blocks. These variables (and their common blocks) are

GHT(*ADD*) = an array of four containing initial guesses for the hold tank outlet concentrations, and

ICOUNT(*CC2*) = a counter indicating the number of passes through the scrubber loop.

## 3) Algorithmic Techniques

There are no special algorithmic techniques in this subroutine.

#### 4) Programming Details

The convergence of the overall scrubber/hold tank loop is programmed in the following steps.

1. Test flag for single or multistage scrubber.
  - 1.1 If NFLAG = 11, go to branch 1.
  - 1.2 If NFLAG  $\neq$  11, continue.
2. Calculate crystallization constants from normalized constants and solids concentrations.
3. Calculate bulk inlet concentrations from material balances.
4. Call Equil to calculate individual species concentrations from bulk values.
5. Call Poutput to print output.
6. Go to branch 2.
7. Branch 1: Initialize counters and liquid concentrations for multistage scrubbing.
8. Loop 1: Start scrubber/hold tank loop - Call Conest to estimate bulk outlet concentrations for hold tank.
9. Store scrubber inlet concentrations, CINLET.
10. Loop 2: Start scrubber loop - Assume outlet gas concentrations.
11. Call Conopt to calculate scrubber performance.
12. Check for convergence of SO<sub>2</sub> inlet gas partial pressure.
  - 12.1 If relative error < 1%, go to branch 3.
  - 12.2 If relative error > 1%, continue.
13. Reinitialize liquid and solid concentrations using CINLET and SOLIDIN.
14. Estimate new SO<sub>2</sub> outlet partial pressure using equation (1).
15. Restart loop 2.
16. Branch 3: Call Poutput to print output.
17. Call Holdt to calculate liquid and solids concentrations in the hold tank.
18. Test for overall convergence using equation (2).
  - 18.1 True - go to branch 2.
  - 18.2 False - continue
19. Set scrubber inlet liquid concentrations equal to hold tank outlet concentrations.
20. Store hold tank concentrations as old values.
21. Restart loop 1.

22. Branch 2: Return to calling program (BMREP).

## Subroutine Simp

### 1) Overview

**Purpose** - Subroutine Simp applies Simpson's rule as the integration technique when calculating utilization.

**Background** - The calculation of utilization in a CSTR vessel requires integration over time. Subroutine Simp uses Simpson's rule to evaluate the integral. This technique requires integrand evaluations for three points and has an error related to the cube of the step size. The integral being evaluated is contained in the utilization equation which is given by

$$1 - U = \sum \phi_p \frac{1}{kt} \int \frac{e^{-(kt/kt)}}{df_p/d(k\tau)} f_p df_p$$

A transformation has been performed to convert the integral over time to an integral over fraction remaining. The integral is evaluated for each particle size in the limestone distribution over a range of fraction-of-particle remaining. Each particle is bound between its initial fraction remaining ( $f_p = 1$ ) and complete dissolution ( $f_p = 0$ ).

### 2) Usage

The calling sequence for Simp is

CALL SIMP(FF,PSUM,H)

On entry

FF = An array containing the three integrand evaluations, and

H = The step size.

On return

PSUM = The value of the integral over the step size.

### 3) Algorithmic Techniques

There are no special algorithmic techniques in this subroutine.



#### **4) Programming Details**

The integration over step size,  $H$ , is accomplished in two programming steps:

1. Calculate PSUM by Simpson's rule.
2. Return to calling program.

### Subroutine Soldbal

#### 1) Overview

**Purpose-** Subroutine Soldbal calculates the dissolution and/or crystallization rates of  $\text{CaSO}_3$ ,  $\text{CaSO}_4$  hemihydrate,  $\text{CaCO}_3$ , and gypsum.

**Background -** The presence of solids in the scrubber and hold tank requires the calculation of dissolution/crystallization rates. These rates can then be used to update the solids inventory at each stage in the scrubber or in the hold tank.

The amount of dissolved  $\text{CaCO}_3$  is calculated using the reactivity and the flux of  $\text{CaCO}_3$  determined in subroutine Listone. Soldbal does not allow for the crystallization of  $\text{CaCO}_3$ . However, the other solids are allowed to crystallize if their relative saturation (RS) is greater than one.

For  $\text{CaSO}_3$  the crystallization rates are calculated based on a correlation determined by Phillip Tseng. For  $\text{CaSO}_3$  this rate is given by:

$$\frac{d(\text{CaSO}_3)}{dt} = k_{\text{cry}3} \frac{(\text{RSCaSO}_3 - 1)^2}{\text{RSCaSO}_4} \quad (1)$$

In the presence of calcium sulfate  $\text{CaSO}_3$  will crystallize as a mixed solid with up to 20 percent  $\text{CaSO}_4$  hemihydrate. Thus the crystallization of  $\text{CaSO}_4$  hemihydrate is given by:

$$\frac{d(\text{CaSO}_4)_{\text{hemi}}}{dt} = 0.2(\text{RSCaSO}_4) \frac{d\text{CaSO}_3}{dt} \quad (2)$$

For gypsum the crystallization rate is given by:

$$\frac{d(\text{gypsum})}{dt} = k_{\text{cry}4} (\text{RS}_{\text{gypsum}} - 1) \quad (3)$$

When the relative saturations of  $\text{CaSO}_3$  and  $\text{CaSO}_4$  are less than one, Soldbal calculates the dissolution rates of these solids. These rates take the form:

$$\frac{d(\text{solid})}{dt} = -k(\text{flux}) \quad (4)$$

The values of the flux for calcium sulfite and calcium carbonate are calculated in Listone and CaSO3di and are brought to Soldbal through common blocks.

## 2) Usage

The calling sequence for Soldbal is

Call Soldbal(I)

On entry

I = 1 for scrubber stage, and

2 for hold tank

Other required variables are accessed through common blocks. These variables (and their common blocks) are

SOLIDIN(CC3) = the inlet solids concentrations,

CXKSP(TANKPAR) = the crystallization constants for CaSO<sub>3</sub> and CaSO<sub>4</sub>,

XKSP(INPUT2) = the dissolution constants for CaSO<sub>3</sub>, CaSO<sub>4</sub> hemihydrate, and CaCO<sub>3</sub>, and

FLUXCA,DFCASO3,DFCASO4(DIFLUX) = the flux of limestone, calcium sulfite, and calcium sulfate hemihydrate from the solid to the bulk.

On return

All required variables are returned through common blocks. These variables (and their common blocks) are

SOLID(CC3) = an array of four containing the outlet solids concentrations,

DSOLID(CC3) = an array of four containing the change in solids concentration across the stage,

RSCASO3, RSCASO4(CC4) = the relative saturations of calcium sulfite and gypsum, and

RSO3SO4(DIFLUX) = the ratio of calcium sulfate hemihydrate to calcium sulfite.

### 3) Algorithmic Details

There are no special algorithmic techniques in this subroutine.

### 4) Programming Details

For given inlet solids concentrations

1. Calculate the relative saturations of  $\text{CaSO}_3$  and  $\text{CaSO}_4$  from bulk liquid concentrations.
2. Set ROLD, the ratio of  $\text{CaSO}_4$  hemihydrate to  $\text{CaSO}_3$  equal to 0.2.
3. If  $\text{RSCASO}_3 > 1$ ,
  - 3.1 Calculate the amount of  $\text{CaSO}_3$  crystallized, DSOLID(1), using Equation (1).
  - 3.2 Calculate the outlet concentration, SOLID(1).
  - 3.3 Calculate the amount of  $\text{CaSO}_4$  hemihydrate crystallized in the mixed solid, DSOLID(2), using Equation (2).
  - 3.4 Calculate the outlet concentration of  $\text{CaSO}_4$  hemihydrate, SOLID(2).
4. If  $\text{RSCASO}_4 > 1$ ,
  - 4.1 Calculate the amount of gypsum crystallized, DSOLID(4), using Equation (3).
  - 4.2 Calculate the outlet concentration of gypsum, SOLID(4).
5. Loop 1 - If  $\text{RSCASO}_3 < 1$ ,
  - 5.1 Calculate the amount of dissolved  $\text{CaSO}_3$ , DSOLID(1) using Equation (4).
  - 5.2 Calculate the outlet concentration of  $\text{CaSO}_3$ , SOLID(1).
  - 5.3 Calculate the amount of dissolved calcium sulfate hemihydrate, DSOLID(2) using equation (4).
  - 5.4 Calculate the outlet concentration of calcium sulfate hemihydrate.
6. If  $\text{RSCASO}_4 < 1$ 
  - 6.1  $\text{DSOLID}(4) = 0.0$
  - 6.2  $\text{SOLID}(4) = \text{SOLIDIN}(4)$
7. Calculate the amount of dissolved limestone, DSOLID(3) using Equation (4).
8. Calculate the outlet concentration of limestone, SOLID(3).
9. Calculate  $\text{RSO}_3\text{SO}_4$ , the ratio of calcium sulfate hemihydrate to calcium sulfite.
10. Calculate ERROR, the relative error between  $\text{RSO}_3\text{SO}_4$  and ROLD.

11. Call CaSO3di to determine the flux of  $\text{CaSO}_3$ .
12. If  $\text{ERROR} > 0.01$ , restart loop 1.
13. Return to calling program.

## Subroutine Surcone

### 1) Overview

**Purpose** - Subroutine Surcone calculates species concentrations at the surface of the limestone and determines the boundary condition to be satisfied.

**Background** - Calculation of the calcium and carbonate fluxes requires the concentration of species at the solid surface. Since  $H^+$  is consumed at the surface to form  $HCO_3^-$ , Surcone calculates the species concentrations by assuming a concentration of  $[H^+]$  at the surface. Other concentrations are calculated using equilibrium and flux expressions.

Since neither sulfite, sulfate, or adipic acid are consumed at the surface, the fluxes of these species are zero. These balances, along with equilibrium expressions, provide quick calculations of sulfur and adipic acid species at the surface. The concentration of  $[HCO_3^-]_s$  is then calculated using a zero charge flux. Once  $[HCO_3^-]_s$  is known, the remaining species concentrations are determined.

Subroutine Surcone also estimates the boundary condition at the solid/liquid interface. The boundary condition selected depends on dissolved  $[SO_3^{2-}]$  since this specie affects the dissolution rate of  $CaCO_3$ . In the absence of sulfite, the boundary condition is given by the solubility product of  $CaCO_3$ . When sulfite is present, the boundary condition is the continuity of flux at the solid surface. This is established by setting the mass transfer rate equal to the surface kinetics rate given by

$$\text{Flux} = k \frac{([CaCO_3^o]_{eq} - [CaCO_3^o]_s)^{0.5}}{[CaSO_3^o]_s [CaCO_3^o]_s}$$

Because this model has  $CaSO_3$  ion pair in the denominator, it has the potential of dividing by zero. Therefore this boundary condition is not used if the relative saturation of calcium sulfite at the surface is less than 0.00001.

## 2) Usage

The calling sequence for Surcone is

CALL SURCONE(H,PBC,BC,IFLAG,SCA)

On entry

H = the assumed concentration of  $H^+$  at the surface.

SCA = bulk liquid concentration of calcium.

IFLAG = 1 = select the boundary condition based on sulfite concentration.

2 = use  $K_{sp}(CaCO_3)$  as boundary condition.

Other required variables are accessed through common blocks. These variables (and their common blocks) are:

SD(DIFF) = an array containing diffusivities,

GAMMA(GAM) = an array containing activity coefficients, and

SLP(NEW) = limestone specific surface kinetics constant

Also required are equilibrium constants(CONST) and pseudo-equilibrium constants(EQUILK).

On return

PBC = the predicted surface conditions.

BC = the boundary condition to be met.

Individual species surface concentrations are returned through common block SLIME.

## 3) Algorithmic Details

There are no special algorithmic techniques in this subroutine.

## 4) Programming Details

Calculations of the species concentrations at the surface of limestone are programmed in the following steps:

For given concentration of  $[H^+]_s$

1. Using flux equations and equilibrium constants, calculate the surface concentrations of sulfur and adipic acid species.
2. Calculate  $[HCO_3^-]_s$  using zero-charge flux expression.
3. From the equilibrium constant for  $HCO_3^-$ , find  $[CO_3^{2-}]$ .
4. Calculate  $[CA^{++}]_s$  using CACO3T and surface carbonate species.

5. Calculate PCACO3, the product of  $[Ca^{++}]_s[CO_3^{=}]_s$ .
6. Calculate PCASO3, the product of  $[Ca^{++}]_s[SO_3^{=}]_s$ .
7. Calculate calcium flux, FLUX.
8. Calculate RSSO3, the relative saturation of  $CaSO_3$  at the surface.
9. If IFLAG = 2, go to branch 1.
10. If RSSO3 < 0.00001, go to branch 1.
11. Calculate boundary condition.
  - 11.1 Find DF, the driving force term in the surface rate expression.
  - 11.2 Find SO3IP and CO3IP, the calcium sulfite and calcium carbonate ion pairs at the surface.
  - 11.3 If CO3IP < 0, go to branch 1.
  - 11.4 Find SURFR, the surface kinetics rate.
  - 11.5 Set PBC = FLUX
  - 11.6 Set BC = SURFR
12. Go to branch 2.
13. Branch 1 :
  - 13.1 PBC = PCACO3
  - 13.2 BC =  $K_{sp}(\text{calcite})$
14. Branch 2 : Return to calling program.



## Subroutine Surface

### 1) Overview

**Purpose** - Subroutine Surface calculates species concentrations at the surface of calcium sulfite/sulfate hemihydrate particles.

**Background** - Calculations of the fluxes requires the concentration of species at the solid surface. Since  $H^+$  is consumed at the surface to form  $HSO_3^-$  and  $HSO_4^-$ , Surface calculates species concentrations by assuming a concentration of  $[H^+]$  at the surface. Other concentrations are calculated using equilibrium and flux expressions.

Since neither carbonate nor adipic acid are consumed (or produced) at the calcium sulfite surface, the fluxes of these species are zero. These balances along with equilibrium expressions provide quick calculations of carbonate and adipic acid at the solid surface. The total sulfite flux is calculated assuming a zero-charge flux in the boundary layer. With this value the surface concentration can then be calculated.

The total sulfate flux is established using the sulfite flux and the ratio of  $CaSO_4$  to  $CaSO_3$  in the hemihydrate solid. From this value the sulfate concentration can be calculated with its flux equation. Finally, the flux and thus the surface concentration of  $[Ca^{++}]_s$  is calculated from the sum of the sulfite and sulfate fluxes. Once these surface concentrations are known the product  $[Ca^{++}]_s[SO_3]_s$  is calculated, and the boundary condition is set as the  $K_{sp}$  for  $CaSO_3$ .

### 2) Usage

The calling sequence for Surface is

CALL SURFACE(H,PCASO3,BC)

On entry

H = the assumed concentration of  $[H^+]$  at the surface

On return

PCASO3 = the product of  $[Ca^{++}]_s$  and  $[SO_3]_s$  concentrations at the surface,

BC =  $K_{sp}$  for  $CaSO_3$ .

Other required variables are accessed through common blocks. These variables (and their common blocks) are

$KW, KHSO_4, KHCO_3, KHSO_3, KAD(EQUILK)$  = the pseudo-equilibrium constants for water, bisulfate, bicarbonate, bisulfite, and adipic acid, respectively.

$SD(DIFF)$  = an array containing diffusivities.

$RSO_3SO_4(DIFLUX)$  = the ratio of calcium sulfate to calcium sulfite in the hemihydrate particles.

$K(CONST)$  = an array containing the equilibrium constants.

$SKSP1(EQUKSP)$  = the solubility constant for  $CaSO_3$ .

$CO_3T, SO_3T, AT, SO_4T, (TOTAL)$  = the total bulk concentrations times diffusivities of carbonate, sulfite, acid, and sulfate species, respectively.

$CHARGE(TOTAL)$  = a bulk liquid charge balance using diffusivity times charge concentration.

$CACO_3T(TOTAL)$  = the concentration (times diffusivity) of calcium from limestone dissolution.

$SO_3SO_4(TOTAL)$  = the concentration term containing calcium, sulfate, and sulfite species.

$CAT(TOTALI)$  = the total bulk concentration of  $[Ca^{++}]$ .

On output the surface concentration of 12 species are returned through common block  $SO_3DISS$ .

### 3) Algorithmic Details

There are no special algorithmic techniques in this subroutine.

### 4) Programming Details

Calculation of the species concentrations at the solid surface are programmed in the following steps.

For given  $[H^+]$  at the surface

1. For  $[CO_3^{=}]_{total}$  and  $[A^{=}]_{total}$  with zero fluxes, calculate concentrations using equilibrium and zero flux expressions.
2. Calculate  $FLUXSO_3$  using zero-charge flux ( $\sum Z_i N_i = 0$ , where  $N_i = D_i \Delta C_i$ ).
3. Calculate sulfate flux using  $RSO_3SO_4$  times  $FLUXSO_3$ .
4. Calculate  $[SO_3^{=}]_s$  and  $[SO_4^{=}]_s$  using equilibrium expressions.

5. Calculate  $[\text{Ca}^{++}]_s$  using sulfite flux.
6.  $K_{sp}(\text{calc}) = [\text{Ca}^{++}]_s[\text{SO}_3^{=}]_s$ .
7.  $\text{BC} = \text{SKSP1}$ .
8. Return to calling program.

## SSMFGD Input Requirements

This section discusses the inputs required by the Slurry Scrubber Model for Flue Gas Desulfurization (SSMFGD). Each variable is defined with the required units. Input variables are accessed through four locations:

- 1) The Input file
- 2) The Block Data File
- 3) Subroutine Soldbal
- 4) Subroutine Holdt

The variables which are inputs in the Block Data and Input files will be listed on a line by line basis later in this section. The two subroutines are used to input solids and total calcium concentrations. These inputs are discussed first.

### 1. Subroutine Inputs

Subroutine Soldbal has three data statements through which the solids concentrations are input. All solids are input in gmoles per liter. This is an example of the data statements:

```
DATA RSO3SO4 /0.15/
DATA (SOLIDSP(J),J=1,4) /0.414,0.062,0.177,0.074/
DATA (SOLIDIN(J),J=1,4) /0.414,0.062,0.177,0.074/
```

RSO3SO4 is the ratio of calcium sulfate to calcium sulfite concentrations in the hemihydrate solid. SOLIDSP and SOLIDIN contain identical data which are the solids concentrations of calcium sulfite, calcium sulfate hemihydrate, calcium carbonate, and gypsum in that order. These values can be easily calculated using the solids analysis and the liquor percent solids. Since solids analysis identifies total sulfate and not the specific hemihydrate and dihydrate forms, it is recommended that the concentration of calcium sulfate hemihydrate be set equal to either the total sulfate present OR 15% of the calcium sulfite concentration, whichever is smallest. Gypsum is then found as the

difference between the solids analysis sulfate and the amount accounted for as hemihydrate.

Subroutine Holdt has one data statement through which the total calcium concentration is input in gmoles per liter. An example of that statement is:

DATA TOTCA / 0.722/

TOTCA is the variable name for the total calcium concentration present in the solids. This value is calculated in the same manner as the other solids concentrations.

## 2. The INPUT file

For SSMFGD most of the required input is accessed by the driver routine through read statements. These statements read from a file called INPUT. The following is a line-by-line description of the variables contained in the INPUT file.

Line 1:

IDENT = An identifier for the case study (maximum 80 alphanumeric characters).

Line 2:

INFLAG = A flag indicating whether to use SSMFGD default values for some inputs.

= 1 = Use SSMFGD defaults.

= 2 = All BMREP inputs will be specified.

NDIFF = A flag indicating which differential equation solver to use.

= 1 = Use LSODE

= 2 = Use DGEAR

The next input line (Line 3 only) depends on the value of INFLAG on Input Line 2.

If INFLAG = 1

Line 3:

XK1 = A flag indicating the concentration units for the input species.

= 1 = Input concentrations are in ppm.

= 2 = Input concentrations are in gmole/liter.

TK = Slurry temperature, degrees kelvin.

PH = Scrubber inlet liquor pH.

**If INFLAG = 2**

Line 3:

XPR = A flag indicating the amount of output from BMREP which is to be printed. (SSMFGD default value = 1.)

= 0 = No printout from BMREP.

= 1 = Full printout.

= 2 = Short form printout.

XK1 = A flag indicating the concentration units for the input species.

= 1 = Input concentrations are in ppm.

= 2 = Input concentrations are in gmole/liter.

SJ = A flag indicating whether solids are present. (SSMFGD default value = 0.)

= 0 = No solids present.

= 1 = Solids may be present. Partial pressure of CO<sub>2</sub> will be specified.

TK = Slurry temperature, degrees kelvin.

PP(1) = Partial pressure of SO<sub>2</sub>, atm, above the liquor.

(SSMFGD default value = 0.)

PP(2) = Partial pressure of CO<sub>2</sub>, atm, above the liquor.

(SSMFGD default value = 0.)

SS(1) = Relative saturation of CaSO<sub>3</sub> at which crystallization occurs. Use a value of 1.00 for normal Radian equilibrium.

(SSMFGD default value = 0.55)

SS(2) = Applies to CaCO<sub>3</sub>. (SSMFGD default value = 1.0.)

SS(3) = Applies to CaSO<sub>4</sub>. (SSMFGD default value = 1.0.)

XIPH = A flag indicating whether pH is specified.

(SSMFGD default value = 1.)

= 0 = pH is not specified.

= 1 = pH is specified.

PH = Scrubber inlet liquor pH. (If XIPH = 0, set PH = 0.)

Line 4:

CCM = The input data concentrations of the nine major species in this order: Ca, Mg, Na, K, SO<sub>3</sub>, SO<sub>4</sub>, CO<sub>3</sub>, Cl, and H<sub>2</sub>Ad. H<sub>2</sub>Ad is the concentration of the buffer acid. (If no buffer is added, set CCM(9) = 0.0015 ppm or  $1.0 \times 10^{-8}$  g-mole/liter for SSMFGD.)

Line 5:

BPP = The initial guess for the outlet partial pressures of SO<sub>2</sub>, CO<sub>2</sub>, and O<sub>2</sub>, atm, in that order.

RKLKG = The ratio of liquid-to-gas mass transfer coefficients, atm-ml/gmole.

Line 6:

RLG = The ratio of liquid-to-gas flowrates in the scrubber, liter/gmole.

(Gas flowrate should be calculated on a dry basis at the inlet.)

EF = Oxidation enhancement factor in the scrubber.

Line 7:

XKSP(1,1) = Dissolution rate parameters for CaSO<sub>3</sub> in the scrubber.

XKSP(2,1) = Dissolution rate parameter for gypsum in the scrubber.

Line 8:

FSP = Inlet partial pressure of SO<sub>2</sub>, atm.

NTUSP = Number of gas phase transfer units per stage.

NFLAG = A flag indicating single or multistage contacting,

= 9 = single stage scrubber.

= 11 = multistage scrubber.

NFLAG2 = A flag indicating cocurrent or countercurrent flows.

= 10 = countercurrent gas and liquid flows.

= 12 = cocurrent flows.

Line 9:

NMIX = Number of stages.

CKCAAD = The equilibrium constant at the scrubber temperature for the calcium anion pair formed by addition of an acid buffer.

Line 10:

LA = A flag indicating whether the particle size distribution (PSD) for limestone is to be calculated.

= 0 = PSD is to be predicted from sieve data.

= 1 = PSD is given as input.

U = Limestone utilization, percent.

Line 11:

TAUSC = Liquor residence time per stage in the scrubber, sec.

TAUHT = Liquor residence time in the hold tank, sec.

B = Enhancement to dissolution by agitation.

(For systems with no added buffer, set B = 765.0)

The remaining input lines are dependant on the value of LA in line 10.

If LA = 0, then seive data are required. Thus

Line 12:

P1 = The weight fraction of limestone which is less than size D1, percent.

D1 = A seive mesh diameter, microns.

P2 = The weight fraction of limestone which is less than size D2, percent.

D2 = A seive mesh diameter, microns.

If LA = 1, then the complete PSD is required. Thus

Line 12:

N = The number of diameter/weight fraction pairs.

Lines 13 to 13+N:

D(i) = Diameter, microns.

PHI(i) = The weight (or volume) fraction of particles between sizes  $D_i$  and  $D_{i-1}$ .

### 3. The BLOCK DATA file

Additional SSMFGD inputs are aquired through data statements in the BLOCK DATA file which are accessed by SSMFGD through common blocks. Most of these values are pertinent to the hold tank and solids balance. The following is a line-by-line listing of the required input. (Note: Lines 1-16 contain comment and common block statements.)

Line 17:

PIN(1) = Inlet partial pressure of CO<sub>2</sub>, atm.

PIN(2) = Inlet partial pressure of O<sub>2</sub>, atm.



Line 18:

RLG2 = Ratio of liquid-to-gas flowrates in the hold tank, liter/g-mole.

CXKSP(1,2) = Crystallization constant for calcium sulfite in the hold tank.

CXKSP(2,2) = Crystallization constant for gypsum in the hold tank.

Line 19:

SLP = limestone specific rate constant for surface kinetics

RD = constant by which to reduce limestone reactivity (usually = 1).

Line 20:

E = Oxidation enhancement factor in the hold tank.

NL = Number of liquid phase transfer units in the hold tank.

## Common Block Cross-Reference Sheet

Common Block	Subroutine Locations
ADD	Conopt, Holdt, Scrint
ALPH	Conver, Glmt
BTOT	Equil, Funct, Pseudo
BULKI	Conopt, Fcn, Pseudo, Scrint
BULKSP	Conopt, Delin, Funct, Hcomp, Holdt, Intgr, Soldbal
CATION	Funct, Pseudo
CC1	Holdt, Poutput
CC2	Conopt, Scrint
CC3	Block Data, Conopt, Delin, Fcn, Hcomp, Holdt, Scrint, Soldbal
CC4	Conopt, Soldbal
CC5	Conopt, Poutput
CONST	BMREP, Conver, Funct, Glmt, Listone, Pseudo, Surcone, Surface
DIAM	BMREP, Dist, React
DIFF	CaSO3di, Conver, Fgint, Glmt, Listone, Pseudo, Surcone, Surface
DIFLUX	Block Data, CaSO3di, Conopt, Holdt, Listone, Scrint, Soldbal, Surface
EQUILK	Conver, Funct, Glmt, Listone, Pseudo, Surcone, Surface
EQUKSP	Hcomp, Holdt, Pseudo, Scrint, Soldbal, Surface
GAMMA	BMREP, Conopt, Holdt, Pseudo, Surcone
HENRYS	Conver, Delin, Glmt, Hcomp, Pseudo
HOLDIN	Conopt, Hcomp, Holdt, Scrint
HTPRINT	Block Data, Delin, Hcomp, Holdt
INPUT2	BMREP, Conopt, Conver, Fcn, Glmt, Limreac, React, Scrint, Soldbal
INPUTSP	BMREP, Intgr, Scrint
INTFACE	Conver, Glmt

FLAG	Conopt, Fcn
LIMER	BMREP, React
LAST	Conopt, Holdt, Poutput
LAST2	Conopt, Poutput
LSURF	Conopt, Listone, Holdt
NEW	Block Data, Surcone
PPRESS	BMREP, Conopt, Conver, Fcn, Fgint, Glmt, Intgr, Scrint
RTIME	BMREP, Limreac, Film
RESULT	Conopt, Conver, Fgint, Glmt, Intgr
SCONC	CaSO3di, Conver, Equil, Funct, Listone, Pseudo
SCONC1	CaSO3di, Conver, Equil, Funct, Listone, Pseudo
SINGLE	Conopt, Fcn, Fgint, Intgr, Scrint
SLIME	Listone, Surcone
TANKPAR	Block Data, Delin, Hcomp, Holdt, Limreac, Soldbal
TOTAL	CaSO3di, Listone, Surcone, Surface
TOTAL1	CaSO3di, Surface

## References

- Ando, J. and C. B. Sedman, "Status of Acid Rain and SO<sub>2</sub> and NO<sub>x</sub> Abatement Technology in Japan", Proceedings: Tenth Symposium on Flue Gas Desulfurization EPA-600/9-87-004a, 2:44-65 (1987).
- Barton, P. and T. Vatanatham, "Kinetics of Limestone Neutralization of Acid Waters", Envir. Sci. Tech., 10, 262-266 (1976).
- Baviello, M. A., A. S. Bowie, and L. E. Beerman, The Scrubber Strategy: The How and Why of Flue Gas Desulfurization, Ballinger Publ. Co., Cambridge (1982).
- Berner, R. A. and J. W. Morse, "Dissolution Kinetics of Calcium Carbonate in Sea Water: IV. Theory of Calcite Dissolution", Am. J. Sci., 274, 108-134 (1974).
- Bjerle, I. and G. T. Rochelle, "Limestone Dissolution from a Plane Surface", Chem. Eng. Sci., 39, 183-185 (1984).
- Burgwardt, R. H., T. J. Campbell, J. H. Dempsey, and J. H. Laughlin, "Limestone Type-and-Grind Tests at EPA/IERL-RTP", paper presented at 5th Shawnee Industry Briefing Conference, Raleigh (1980).
- Chan, P. K. "Limestone Dissolution - Effects of pH, CO<sub>2</sub>, and Buffers Modeled by Mass Transfer", M.S. Thesis, University of Texas, Austin (1981).
- Chan, P. K. and G. T. Rochelle, "Limestone Dissolution - Effects of pH, CO<sub>2</sub>, and Buffers Modeled by Mass Transfer", ACS Symp. Ser., 188, 75-97 (1982).
- Chan, P. K. and G. T. Rochelle, "Modeling of SO<sub>2</sub> Removal by Limestone Slurry Scrubbers: Effect of Chloride", Proceedings: Eighth Symposium on Flue Gas Desulfurization EPA-600/9-84-017a, 7:57-78 (1984).
- Chang, J. C. S., T. G. Brna, and N. Kaplan, "Effects of Limestone Type and Grind on Dual Alkali System Performance", Proceedings: Ninth Symposium on Flue Gas Desulfurization EPA-600/9-85-033b, 472-500 (1985).
- Chang, J. C. S. and J. H. Dempsey, "Operation of EPA Owned Pilot SO<sub>2</sub> Scrubber and High Temperature Baghouse", Accurex-RTP Progress Report - 49: EPA Contract 68-02-3648 (December, 1980).
- Chang, J. C. S. and J. H. Dempsey, "Operation of EPA Owned Pilot SO<sub>2</sub> Scrubber and High Temperature Baghouse", Accurex-RTP Progress Report - 50: EPA Contract 68-02-3648 (January, 1981).

Chang, J. C. S., J. H. Dempsey, R. H. Borgwardt, A. J. Toprac, and G. T. Rochelle, "Effects of Limestone Type and Grind on SO<sub>2</sub> Scrubber Performance", Envir. Prog., **1**, 59-64 (1982a).

Chang, J. C. S. and G. T. Rochelle, "Mass Transfer Enhanced by Equilibrium Reactions", Ind. Eng. Chem. Fund., **21**, 379-385 (1982b).

Chen, C-C., H. I. Britt, J. F. Boston, and L. B. Evans, "Local Composition Model for Excess Gibbs Energy of Electrolyte Systems", AIChE J., **28**, 588 (1982).

Clarke, E. T., R. H. Loeppert, and J. M. Ehrman, "Crystallization of Iron oxides on Calcite Surfaces in Static Systems", Clays and Clay Min., **33**, 152-158 (1985).

Compton, R. G. and P. J. Daly, "The Dissolution Kinetics of Iceland Spar Single Crystals", J. Coll. Int. Sci., **101**, 159-166 (1984).

Dempsey, J. H., J. C. S. Chang, and J. A. Mulholland, "Operation of EPA Owned Pilot SO<sub>2</sub> Scrubber and High Temperature Baghouse", Accurex-RTP Progress Report (July, 1983).

Dempsey, J. H., J. C. S. Chang, and J. A. Mulholland, "Operation of EPA Owned Pilot SO<sub>2</sub> Scrubber and High Temperature Baghouse", Accurex-RTP Progress Report - 39: EPA Contract 68-02-3648 (March, 1979).

Dempsey, J. H. and J. A. Mulholland, "Operation of EPA Owned Pilot SO<sub>2</sub> Scrubber and High Temperature Baghouse", Accurex-RTP Progress Report - 40: EPA Contract 68-02-3648 (August, 1979).

Dempsey, J. H. and J. A. Mulholland, "Operation of EPA Owned Pilot SO<sub>2</sub> Scrubber and High Temperature Baghouse", Accurex-RTP Progress Report - 41: EPA Contract 68-02-3648 (September, 1979).

Dempsey, J. H. and J. A. Mulholland, "Operation of EPA Owned Pilot SO<sub>2</sub> Scrubber and High Temperature Baghouse", Accurex-RTP Progress Report - 42: EPA Contract 68-02-3648 (December, 1979).

Dempsey, J. H. and J. A. Mulholland, "Operation of EPA Owned Pilot SO<sub>2</sub> Scrubber and High Temperature Baghouse", Accurex-RTP Progress Report - 48: EPA Contract 68-02-3648 (November, 1980).

Drehmel, D. C., "Limestone Types for Flue Gas Scrubbing", Proceedings of Second International Lime/Limestone Wet-Scrubbing Symposium, EPA-APTD-1161 167-194 (1972).

Ellison, W. and C. B. Sedman, "Assessment of SO<sub>2</sub>/NO<sub>x</sub> Emission Control Technology in Europe", Proceedings: Tenth Symposium on Flue Gas Desulfurization EPA-600/9-87-004a, 2:66-90 (1987).

Epstein, M., C. C. Leivo, and C. H. Rowland, "Mathematical Models for Pressure Drop, Particulate Removal in Venturi, TCA, and Hydro-filter Scrubbers", Proceedings of Second International Lime/Limestone Wet-Scrubbing Symposium, EPA-APTD-1161 45-114 (1972).

Epstein, M., "EPA Alkali Scrubbing Test Facility: Summary of Testing through October 1974", EPA-650/2-75-047, NTIS No. PB-244 901 (1975).

Erga, O. and S. G. Terjesen, "Kinetics of the Heterogeneous Reaction of Calcium Bicarbonate Formation, with Special Reference to Copper Ion Inhibition", Acta Chem. Scand., **10**, 872-875 (1956).

Faist, M. B., C. E. Riese, and L. Gevartzman, Species Distribution Model: A General Computer Program to Calculate the Distribution of Chemical Species Among Multicomponent Phases, DCN 81-213-018-12 (1981).

Faist, M. B., L. Gevartzman, and C. E. Reise, "Development of a Wet Lime/Limestone Flue Gas Desulfurization Process Model - Phase I: Species Distribution Model", paper presented at the Tenth IMACS World Congress on Systems Simulation and Scientific Computation, Montreal (1982).

Farmer, R. W., J. B. Jarvis, and R. Moser, "Effects of Aluminum/Fluoride Chemistry on Wet Limestone Flue Gas Desulfurization", paper presented at Spring National AIChE Meeting, Houston (1987).

Freeman, J. S. and D. L. Rowell, "The Adsorption and Precipitation of Phosphate onto Calcite", J. Soil Sci., **32**, 75-84 (1981).

Giannimaras, E. F. and P. G. Koutsoukos, "The Crystallization of Calcite in the Presence of Orthophosphate", J. Coll. Int. Sci., **116**, 423-430 (1987).

Gleason, C. L., "Nucleation and Crystallization of Calcium Sulfite Hemihydrate", PhD Dissertation, University of Texas (1989).

Henzel, D. S., B. A. Laeske, E. O. Smith, and D.O. Swenson, Handbook for Flue Gas Desulfurization Scrubbing with Limestone, Noyes Data Corp., Park Ridge (1982).

House, W. A. and L. Donaldson, "Adsorption and Coprecipitation of Phosphate on Calcite", J. Coll. Int. Sci., **112**, 309-324 (1986).

Jarvis, J. S., F. B. Messerole, T. J. Selin, G. T. Rochelle, C. L. Gage, and R. E. Moser, "Development of a Predictive Model for Limestone Dissolution in Wet FGD Systems", paper presented at EPA/EPRI Combined FGD and Dry SO<sub>2</sub> Control Symposium, St. Louis (1988).

King, C. V. and C. L. Liu, "The Rate of Solution of Marble in Dilute Acid", Am. Chem. Soc. J., **55**, 1928-1949 (1933).

Kitano, Y., N. Kanamori, and S. Yoshioka, "Adsorption of Zinc and Copper Ions on Calcite and Aragonite and Its Influence on the Transformation of Aragonite to Calcite", Geochim. J., **10**, 175-179 (1976).

Kohl, A. L. and F. C. Riesenfeld, Gas Purification 3rd Ed., Gulf Publ. Co., Houston (1985).

Kyte, W. S., "A Programme for Reducing SO<sub>2</sub> Emissions from U.K. Power Stations - Past and Future", paper presented at the First Combined FGD and Dry SO<sub>2</sub> Control Symposium, St. Louis (1988).

Landolt-Bornstein Physikalisch-Chemische Tabellen, Bd. II-7 225, Springer-Verlag, Berlin (1960).

Laslo, D. and J. C. S. Chang, "Pilot Plant Tests on the Effects of Dissolved Salts on Lime/Limestone FGD Chemistry", Proceedings: Eighth Symposium on Flue Gas Desulfurization EPA-600/9-84-017a, 7:37-56 (1984).

Levich, V. G., Physicochemical Hydrodynamics, Prentice-Hall Inc., Englewood Cliffs (1962).

Lowell, P.S., D. M. Ottmers, K. Schwitzgebel, T. I. Strange, and D. W. Deberry, "A Theoretical Description of the Limestone Injection-Wet Scrubbing Process", USEPA, APID 1287, PB 1931-029 (1970).

Lund, K., H. S. Fogler, C. C. McCune, and J. W. Ault, "Acidization - II. The Dissolution of Calcite in Hydrochloric Acid", Chem. Eng. Sci., **30**, 825-835 (1975).

Mehta, R. R., "Modeling of SO<sub>2</sub> Removal and Limestone Utilization in Slurry Scrubbing Systems with Forced Oxidation", M. S. Thesis, University of Texas, Austin (1982).

Mehta, R. R. and G. T. Rochelle, "Modeling of SO<sub>2</sub> Removal and Limestone Utilization in Slurry Scrubbing Systems with Forced Oxidation", paper presented at the AIChE National Meeting, Houston (1983).

Melia, M. T., R. S. McKibben, and F. M. Jones, "Trends in Commercial Applications of FGD", Proceedings: Tenth Symposium on Flue Gas Desulfurization EPA-600/9-87-004a, 2:23-43 (1987).

Monastersky, R., "Clouds without a Silver Lining", Science News, **134**, 249-251 (1988).

Mori, T., S. Matsuda, F. Nakajima, T. Nishimura, and Y. Arikawa, "Effect of Al<sup>3+</sup> and F<sup>-</sup> on Desulfurization Reaction in the Limestone Slurry Scrubbing Process", Ind. Eng. Chem. Process Des. Dev., **20**, 144-147 (1981).

Morse, J. W., "Dissolution Kinetics of Calcium Carbonate in Sea Water: V. Effects of Natural Inhibitors and the Position of the Chemical Lysocline", Am. J. Sci., **274**, 638-647 (1974).

Morse, J. W., "Dissolution Kinetics of Calcium Carbonate in Sea Water: VI. The Near-Equilibrium Dissolution Kinetics of Calcium Carbonate-Rich Deep Sea Sediments", Am. J. Sci., **278**, 344-353 (1978).

Plummer, L. N. and E. Busenberg, "The Solubilities of Calcite, Aragonite, and Vaterite in CO<sub>2</sub>-H<sub>2</sub>O Solutions between 0 and 90°C, and an Evaluation of the Aqueous Model for the System CaCO<sub>3</sub>-CO<sub>2</sub>-H<sub>2</sub>O", Geochim. Cosmochim. Acta, **46**, 1011-1040 (1982).

Plummer, L.N., T. M. L. Wigley, and D. L. Parkhurst, "The Kinetics of Calcite Dissolution in CO<sub>2</sub>-Water Systems at 5° to 60°C and 0.0 to 1.0 Atm CO<sub>2</sub>", Am. J. Sci., **278**, 179-216 (1978).

Potts, J. M., A. V. Slack, and J. D. Hatfield, "Removal of Sulfur Dioxide from Stack Gases by Scrubbing with Limestone Slurry: Small-Scale Studies at TVA", Proceedings of Second International Lime/Limestone Wet-Scrubbing Symposium, EPA-APTD-1161 195-232 (1972).

Randolph, A. D. and M. A. Larson, Theory of Particulate Processes, New York: Academic Press 1971.

Rickard, D. T. and E. L. Sjoberg, "Mixed Kinetic Control of Calcite Dissolution Rates", Am. J. Sci., **283**, 815-830 (1983).

Rochelle, G. T., Process Synthesis and Innovation in Flue Gas Desulfurization, EPRI FP-463-SR, (1977).

Rochelle, G. T., "Appendix A: Chemistry of Limestone Scrubbers", Handbook for Flue Gas Desulfurization Scrubbing with Limestone, Noyes Data Corp., Park Ridge (1982).

Rochelle, G. T., P. K. Chan, and A. T. Toprac, "Limestone Dissolution in Flue Gas Desulfurization Processes", EPA Cooperative Agreement R806251 (1983).

Rochelle, G. T., and C. J. King, "The Effects of Additives on Mass Transfer in CaCO<sub>3</sub> or CaO Slurry Scrubbing of SO<sub>2</sub> from Waste Gases", Ind. Eng. Chem. Fundam., **16**, 67 (1977).

Shah, I.S., "SO<sub>2</sub> Removal using Calcium Based Alkalies - Pilot Plant Experience", Proceedings of Second International Lime/Limestone Wet-Scrubbing Symposium, EPA-APTD-1161 345-372 (1972).

Shultz, D.M. and C.F. Crouse, "Random Splitting: A Model for a Mass-Size Distribution", South African Stat. J., **7**, 143-152 (1973).



- Sjoberg, E. L., "Kinetics and Mechanism of Calcite Dissolution in Aqueous Solutions at Low Temperatures", Stock. Contr. Geol., **32**, 1-95 (1981).
- Sjoberg, E. L. and D. T. Rickard, "Temperature Dependence of Calcite Dissolution Kinetics between 1 and 62°C at pH 2.7 to 8.4 in Aqueous Solutions", Geochim. Cosmochim. Acta, **48**, 485-493 (1984).
- Sjoberg, E. L. and D. T. Rickard, "The Effect of Added Dissolved Calcium on Calcite Dissolution Kinetics in Aqueous Solutions at 25°C", Chem. Geo., **49**, 405-413 (1985).
- Stewart, D., J. D. Colley, O. W. Hargrove, and A. J. Jones, "Limestone Selection and Preparation for FGD", Proceedings: Ninth Symposium on Flue Gas Desulfurization EPA-600/9-85-033b, 767-784 (1985).
- Sverdrup, H. and Bjerle, I., "Dissolution of Calcite and Other Related Minerals in Acidic Aqueous Solution in a pH-Stat", Vatten, **38**, 59-73 (1982).
- Terjesen, S. G., O. Erga, G. Thorsen, and A. Ve, "II. Phase Boundary Processes as the Rate Determining Steps in Reactions between Solids and Liquids", Chem. Eng. Sci., **14**, 277-288 (1961).
- Toprac, A. J., Limestone Dissolution in Stack Gas Desulfurization Processes, MS thesis, University of Texas, Austin (1981).
- Toprac, A. J. and G. T. Rochelle, "Limestone Dissolution in Stack Gas Desulfurization - Effect of Type and Grind", Envir. Prog., **1**, 52-64 (1982).
- Tseng, P. C. and G. T. Rochelle, "Dissolution Rate of Calcium Sulfite Hemihydrate in Flue Gas Desulfurization Processes", Envir. Prog., **5**, 34-40 (1986).
- Tseng, P. C., "Calcium Sulfite Hemihydrate Dissolution and Crystallization", PhD Dissertation, University of Texas at Austin (1983).
- Uchida, S., C. Y. Wen, and W. J. McMichael, "Dissolution Rate of Limestone into Acid Solution", J. Chin. Inst. Chem. Eng., **5**, 111-114 (1974).
- Ulrich, R. K., "Sulfite Oxidation under Flue Gas Desulfurization Conditions: Enhanced Oxygen Absorption Catalyzed by Transition Metals", PhD Dissertation, University of Texas at Austin (1983).
- Von Tress, M., R.H. Loeppert, and J.H. Matis, "A Calcite Dissolution Model for the Estimation of Particle Size Distribution", Soil Sci. Soc. Am. J., **49**, 302-307 (1985).
- Wallin, M. and I. Bjerle, "A Mass Transfer Model for Limestone Dissolution from a Rotating Cylinder", Chem. Eng. Sci., **44**, 61-67 (1989).
- Weems, W. T., "Enhanced Adsorption of Sulfur Dioxide by Sulfite and Other Buffers", MS Thesis, University of Texas, Austin (1981).

Weiler, H. and W. Ellison, "Progress in European SO<sub>2</sub> and NO<sub>x</sub> Emission Control", paper presented at the First Combined FGD and Dry SO<sub>2</sub> Control Symposium, St. Louis (1988).

Wen, C. Y., and S. Uchida, "Simulation of SO<sub>2</sub> Absorption in a Venturi Scrubber by Alkaline Solutions", Proceedings of Second International Lime/Limestone Wet-Scrubbing Symposium, APTD-1161 (1972).

## VITA

Cynthia Lee Gage was born in Dallas, Texas on September 25, 1950, the daughter of Barbara Lee and Harold Jay Ingham. After graduating from Sherman High School, Sherman, Texas in 1968, she entered Grayson County Junior College for one year. From 1969 to 1978 she worked at different times as a semiconductor assembler, as an auto air conditioning assembler and installer, and as an industrial seamstress. In 1977 she returned to Grayson College and received her Associate of Science Degree in 1978. In the fall of 1978 she entered the University of Texas at Austin and then received her Bachelor of Science degree with honors in Chemical Engineering in May, 1981. The following fall she began graduate studies at the University of Texas in Austin. In December of 1984 she received her Master of Science degree in Chemical Engineering. During 1988 and 1989 while working on her doctorate, she taught mathematics at Austin Community College. After graduating with her Ph.D. from the University of Texas in August of 1989, she will begin working for the Environmental Protection Agency in Research Triangle Park, North Carolina.

### Permanent Address:

c/o H. J. Ingham  
2602 North Turtle Creek  
Sherman, Texas 75090

This dissertation was typed by the author.